ANTIMALARIAL IMIDAZOPYRIDAZINES AND AMINOPYRAZINES: SYNTHESIS, PHYSICOCHEMICAL OPTIMIZATION AND STRUCTURE-ACTIVITY RELATIONSHIPS

Peter Mubanga Cheuka

Supervisor: **Prof. Kelly Chibale**

Department of Chemistry, University of Cape Town

Thesis Submitted for the Degree of

DOCTOR OF PHILOSOPHY

In the Department of Chemistry

UNIVERSITY OF CAPE TOWN

September 2018

TABLE OF CONTENTS

LIST OF FIGURES

Page

LIST OF SCHEMES

Page

LIST OF TABLES

Page

DECLARATION

I, **Peter Mubanga Cheuka**, hereby:

a) grant the University of Cape Town free licence to reproduce this thesis, in whole or in part, for the purpose of research;

b) declare that:

   i. this thesis is my own unaided work, both in concept and execution, and that apart from the normal guidance from my supervisor, I have received no assistance except that which has been acknowledged;

   ii. neither the substance nor any part of this thesis has been in the past, or is being, or is to be submitted for a degree at this University, or any other University.

Signed:…Signed by candidate…… Date: **September 26, 2018**

DEDICATION

To my dear wife Martha Nambela-Cheuka and my two daughters - Merit Taila Cheuka and Lukundo Lutanda Cheuka for your love, support and understanding. You have unconditionally supported me in my life's endeavours, and the completion of this PhD was not going to be possible without your daily words of encouragement.

To my late father Protasio Mwape Cheuka. Although you have no chance to see your dreams materialize, your desire to see me accomplish monumental goals like this one was a source of inspiration to me.

To my mother Angela Chawe for your constant words of encouragement.

To my grandmother Agness Namfukwe. The strong belief you have always held in my capabilities from the time I was a small boy has been instrumental in the successful completion of this PhD degree.

ACKNOWLEDGMENTS

Firstly, I would like to sincerely thank my supervisor Professor Kelly Chibale for providing funding for this PhD project. He is also highly acknowledged for providing guidance from the beginning to the end of this PhD journey. I feel privileged to work with a prolific scientist like you and I am grateful for accepting me into your academic research group. The Drug Discovery and Development Centre (H3D) housed in the Department of Chemistry at University of Cape Town (UCT) and headed by Prof Chibale is also acknowledged for providing access to different research facilities in their laboratories.

I would also like to acknowledge the contributions of our collaborators who provided their expertise in carrying out various biological assays. In this regard, I am grateful to Dr Sergio Wittlin from Swiss Tropical and Public Health Institute (Swiss TPH) in Switzerland for performing all *in vitro* asexual blood stage antiplasmodial assays. The technical support in carrying out *in vitro* liver stage antiplasmodial experiments by Dr Miguel Prudêncio of Instituto de Medicina Molecular (IMM) in Lisbon Portugal is also acknowledged. Additionally, Professor Lyn-Marie Birkholtz (University of Pretoria) and Prof Theresa Coetzer (University of the Witwatersrand) are both acknowledged for the support in carrying out gametocytocidal assays.

Nina Lawrence from the Division of Clinical Pharmacology in the Department of Medicine at University of Cape Town is gratefully acknowledged for carrying out HPLC kinetic solubility and metabolic stability experiments. Dr Dale Taylor of the same division is also acknowledged for carrying out cytotoxicity assays. Furthermore, I would also like to thank Dr Stephen Fienberg, a postdoctoral fellow in Prof Chibale's Research group for carrying out all docking experiments for the synthesized compounds.

Let me also take this opportunity to specially thank Novartis Pharma AG for according me an opportunity to be part of the 2017 Next Generation Scientist (NGS) programme co-administered with the University of Basel in Basel Switzerland. The three-month intensive internship provided me an opportunity to learn drug discovery from a pharma perspective. In this regard, I would like to acknowledge the valuable training I received from the following: My scientific mentors Dr Kenichi Umehara and Dr Joerg Berghausen of the Department of PK Sciences; the NGS core team mentors Dr Marcelo Gutierrez, Ms Akiko Keller and Dr Colin Pillai.

The management of the University of Zambia (UNZA) is also acknowledged for granting me a study leave to pursue this PhD. In particular, the Department of Chemistry at UNZA is gratefully acknowledged for the support.

I would also like to thank Mrs Elaine Rutherfoord-Jones for the effectiveness she has demonstrated in dealing with administrative matters which have been equally important in the smooth progression through my PhD studies.

Let me also extend my gratitude to members of Prof Chibale's Research Group for the friendship and comradeship. The light moments I shared with you made this PhD journey manageable.

Finally, my wife Martha Nambela-Cheuka and my daughters - Merit Taila Cheuka and Lukundo Lutanda Cheuka as well as my extended family members are gratefully acknowledged for understanding my prolonged absence from them. Your support made the completion of this PhD a reality.

PUBLICATIONS AND CONFERENCES

Publications

- Cheuka, P. M.; Lawrence, N.; Taylor, D.; Wittlin, S.; Chibale, K. Antiplasmodial Imidazopyridazines: Structure-Activity Relationship Studies Lead to the Identification of Analogues with Improved Solubility and hERG Profiles. *Med. Chem. Commun*. **2018**, DOI: 10.1039/C8MD00382C.
- Cheuka, P. M.; Mayoka, G.; Mutai, P.; Chibale, K. The Role of Natural Products in Drug Discovery and Development against Neglected Tropical Diseases. *Molecules*. **2017**, *22*, 58.

Conference Presentations: Oral

- Cheuka, P. M. (June 2018). *Antimalarial Imidazopyridazines: Solubility Optimization and Cardiotoxicity De-risking.* The Gordon Research Seminar (GRS) on the Biology of Host-Parasite Interactions. Newport, Rhode Island, USA.

Conference Presentations: Poster

- Cheuka, P. M.; Chibale, K. (July/August 2018). *Antimalarial Imidazopyridazines: Solubility Optimization and Cardiotoxicity De-risking.* 4th Annual Southern African Malaria Research Conference. Johannesburg, South Africa.
- Cheuka, P. M.; Chibale, K. (June 2018). *Antimalarial Imidazopyridazines: Solubility Optimization and Cardiotoxicity De-risking.* The Gordon Research Conference (GRC) on the Biology of Host-Parasite Interactions. Newport, Rhode Island, USA.
- Cheuka, P. M.; Umehara, K.; Berghausen, J.; Lin, W.; Chibale, K.; Heimbach, T.; He, H. (August 2017). *Application of Physiologically-based Pharmacokinetic (PBPK) Modelling to Estimate Pharmacokinetic Profiles of anti-HIV Drugs Efavirenz and Ritonavir in Paediatric Patients – Comparison of Predictability of Clearance to Allometric Scaling*. Next Generation Scientist (NGS) Research Day. Novartis Campus, Basel, Switzerland.
- Cheuka, P. M.; Chibale, K. (November 2016). *Structure-Activity Relationship Studies of Antimalarial 3,6-substituted Imidazopyridazines*. H3D Symposium on Malaria, TB and Neglected Tropical Diseases: Progress in Drug Discovery and Development. Cape Town, South Africa.

- Cheuka, P. M.; Chibale, K. (August/September 2016). *Synthesis and Antiplasmodial Evaluation of Imidazopyridazine Analogues*. XXIV EFMC International Symposium on Medicinal Chemistry. Manchester, UK.
- Cheuka, P. M.; Chibale, K. (August 2016). *Synthesis and Antiplasmodial Evaluation of Imidazopyridazine Analogues*. Gordon Research Seminar (GRS) on Medicinal Chemistry: Understanding Key Concepts for Lead Optimization. Colby-Sawyer College, New London, NH, USA.

ABSTRACT

According to the World Health Organization (WHO) world malaria report released in 2017, about 445,000 malaria deaths were recorded in 2016, a similar mortality as that recorded in the preceding year (446,000 deaths in 2015). Once effective and cheap drugs such as chloroquine and sulfadoxine-pyrimethamine have suffered widespread drug resistance. Additionally, despite the remarkable effectiveness of the currently recommended first line treatment, the artemisinin combination therapies (ACTs), resistance to artemisinin and the partner drugs is beginning to emerge in South East Asia. Furthermore, the current portfolio of medicines, both in clinical use and development has several other shortfalls which need redress. In addition, prevention of transmission and relapse with better safety profiles than current medicines are some of the important features that should be a prioritized characteristic of new medicines. Most importantly, these new regimens should be able to offer chemoprotection and prevent reinfection. Thus, there is need for constant research efforts aimed at identifying and developing novel chemotherapeutic agents for malaria, which are structurally diverse with novel mechanisms of action.

In this PhD thesis, the medicinal chemistry optimization of two antimalarial chemotypes, the imidazopyridazines and aminopyrazines, is reported. In earlier studies, Le Manach and co-workers reported the impressive *in vitro* antiplasmodial activity and *in vivo* antimalarial efficacy of the imidazopyridazine lead compound **19** (Figure 1). However, this compound was plagued by poor solubility and a cardiotoxicity risk as shown from its inhibition of the hERG (human *ether-a-go-go*-related gene)-encoded potassium channel. Further medicinal chemistry optimization led to identification of other derivatives which, albeit exhibiting complete cure of *P. berghei*-infected mice, still displayed poor solubility and hERG inhibition issues. In this project, chemical modification approaches such as the introduction of water solubilizing groups, disruption of molecular planarity and making subtle changes (SAR 1 – 6, Figure 1) were adopted towards improving the solubility and countering hERG inhibition of this class of molecules.

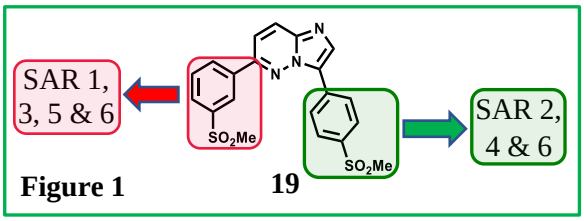

Figure 1 **19**

Through the thesis work undertaken, analogues with a combination of reduced hERG inhibition (IC_{50} = 7.8 – 32 μM) and submicromolar antiplasmodial activity (NF54, IC_{50} = 0.15 – 0.92 μM) were identified. Likewise, the modifications made delivered analogues with moderate to high

solubility (60 – 200 µM) while exhibiting submicromolar antiplasmodial potency (NF54, IC_{50} = 0.14 – 0.99 µM). Furthermore, cytotoxicity assessment of selected analogues against the Chinese Hamster Ovarian (CHO) cell line revealed that most analogues were relatively non-cytotoxic (selectivity indices in the range 72 - > 874). Selected compounds were also screened against gametocyte and liver stage parasites in order to assess transmission blocking and chemoprotection potential, respectively. In this regard, analogues with good gametocytocidal activity (IC_{50} = 0.098 – 0.75 µM) against late stage gametocytes and potent liver stage activity (IC_{50} = 0.045 µM) were identified.

On the other hand, aminopyrazines have also recently shown potential as new antimalarial agents exhibiting promising *in vivo* efficacy in animal models of malaria infection with one analogue having progressed to an optimised late lead stage. However, this aminopyrazine lead compound **24** (Figure 2) as well as the first generation aminopyridine human Phase 2a clinical candidate **MMV390048** showed sub-optimal solubility. In this aspect of the project, chemical modifications mainly focusing on replacing the two aromatic rings with fully and partially saturated heterocyclic systems, hypothesized to potentially disrupt intermolecular π – π stacking thereby improving aqueous solubility, were introduced. The first set of analogues corresponded to the replacement of the trifluoromethylpyridyl ring with partially and fully saturated heterocyclic rings as well as the 4-carboxyphenyl ring while keeping the 4-methylsulfonylphenyl group on the right-hand side portion of the aminopyrazine core scaffold fixed (SAR 1). In SAR 2, the trifluoromethylpyridyl group was fixed on the left-hand side of the aminopyrazine core scaffold while introducing partial and full saturation on the right-hand side of the core. SAR 3 analogues with both aromatic groups simultaneously replaced with partially and fully saturated heterocyclic rings were further generated.

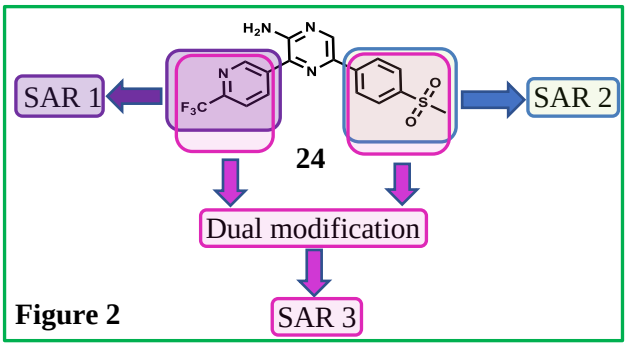

Figure 2

Compared to the lead compound **24** (NF54, IC_{50} = 0.008 µM), the introduced modifications drastically reduced antiplasmodial potency with only one analogue retaining submicromolar activity (NF54, IC_{50} = 0.51 µM). However, the introduced molecular features positively influenced solubility with the new analogues showing 4 - > 20-fold increase in aqueous solubility compared to the lead compound **24**.

For both imidazopyridazines and aminopyrazines, docking studies on a homology model of *Pf*PI4K (*P. falciparum* phosphatidylinositol 4-kinase) were retrospectively undertaken. In both cases, the docking experiments showed that the introduction of the new molecular features was accompanied by loss of key binding interactions to the ATP binding pocket. This was in conformity with the generated parasite-based SAR.

ABBREVIATIONS AND SYMBOLS USED

Å	Angstrom
α	Alpha
δ	Chemical shift
λ	Wave length
a	Axial
ACTs	Artemisinin combination therapies
ADME	Absorption, distribution, metabolism and excretion
AIDS	Acquired immunodeficiency syndrome
APCI	Atmospheric pressure chemical ionization
AR	Analytical reagent
Asp	Aspartic acid
ATP	Adenosine Triphosphate
ATR	Ataxia telangiectasia and Rad3-related
boc	*tert*-Butyloxycarbonyl
BrettPhos	2-(Dicyclohexylphosphino)3,6-dimethoxy-2′,4′,6′-triisopropyl-1,1′-biphenyl
br s	Broad singlet
$CDCl_3$	Deuterated chloroform
CD_3OD	Deuterated methanol
cGMP	cyclic GMP
CHK1	Checkpoint kinase 1
CHO	Chinese Hamster Ovarian
^oC	Degrees celsius

cLog P	Calculated log to base 10 of lipophilicity
^{13}C-NMR	Carbon-13 nuclear magnetic resonance
COSY	Correlation spectroscopy
CYP	Cytochrome P450
d	Doublet
D	Aspartic acid
DAD	Diode array detector
DCM	Dichloromethane
dd	Doublet of doublets
ddd	Doublet of doublets of doublets
ddt	Doublet of doublets of triplets
DDT	Dichlorodiphenyltrichloroethane
DMAP	4-Dimethylaminopyridine
DMEM	Dulbecco's Modified Eagle Medium
DMF	*N*,*N*-Dimethylformamide
DMPK	Drug metabolism and pharmacokinetics
DMSO-d_6	Deuterated dimethylsulfoxide
DNA	Deoxyribonucleic acid
DOT	Directly observed therapy
DPPIV	Dipeptidyl peptidase IV
dt	Doublet of triplets
dtd	Doublet of triplets of doublets
e	Equatorial
EC_{50}	Concentration of a drug that is required for 50% inhibition *in vitro*

ECG	Electrocardiogram
EDCI	1-Ethyl-3-(3-dimethylaminopropyl)carbodiimide
EGFR	Epidermal growth factor receptor
$\boldsymbol{E_H}$	Hepatic extraction ratio
EMA	European Medicines Agency
ESI	Electrospray ionization
Et_3N	Triethylamine
Et_2NH	Diethylamine
EtOAc	Ethyl acetate
EtOH	Ethanol
F	Phenyl alanine
FDA	Food and Drug Administration
FTIs	Farnesyltransferase inhibitors
G6PD	Glucose 6-phosphate1-dehydrogenase
GPR4	G-protein coupled receptor 4
GSEs	General solubility equations
^3H	Tritium
HBA	Hydrogen bond acceptors
HBD	Hydrogen bond donors
H2L	Hit to lead
^1H-NMR	Proton nuclear magnetic resonance
HCV	Hepatitis C virus
HEPES	4-(2-Hydroxyethyl)-1-piperazine-ethanesulphonic acid
hERG	human *ether-a-go-go*-related gene

HIV	Human immunodeficiency virus
HPLC-MS	High pressure liquid chromatography mass spectrometry
HSQC	Heteronuclear Single Quantum Coherence
HTS	High throughput screening
Hz	Hertz
IC_{50}	Concentration of a drug that is required for 50% inhibition *in vitro*
IHME	Institute for Health Metrics and Epidemiology
I_{Kr}	Rapid delayed rectifier current
I_{Ks}	Slow delayed rectifier current
IP	Inflection point
IPTp	Intermittent preventive treatment in pregnancy
IRS	Indoor residual spraying
ITN	Insecticide-treated net
IV	Intravenous
J	Coupling constant
K	Lysine
K1	Drug resistant strain of *Plasmodium falciparum*
µL	Microliter
LHS	Left hand side
L_n	Ligand coordinated to a metal centre, where n = 1, 2, 3., etc
LO	Lead optimization
Lys	Lysine
m	Multiplet
M	Molar

mAU	Milliabsorbance units
MDA	Mass drug administration
$MeSO_2Cl$	Methanesulfonyl chloride
MHz	Megahertz
MIC	Minimum inhibitory concentration
MMV	Medicines for Malaria Venture
m.p.	Melting point
mTOR	Mechanistic target of rapamycin
MTT	3-(4,5-Dimethylthiazol-2-yl)-2,5-diphenyltetrazolium bromide
MW	Molecular weight
mV	Millivolts
m/z	Mass to charge ratio
NADPH	Nicotinamide adenine dinucleotide phosphate
NaO*t*-Bu	Sodium *tert*-butoxide
NBS	*N*-Bromosuccinimide
ND	Not determined
NH_4OAc	Ammonium acetate
NH_4HCO_2	Ammonium formate
NIS	*N*-Iodosuccinimide
nM	Nanomolar
nm	Nanometre
µM	Micromolar
NF54	Drug sensitive strain of *Plasmodium falciparum*
NK_1	Neurokinin-1

P. berghei	*Plasmodium berghei*
PBS	Phosphate buffered saline
$Pd_2(dba)_3$	Tris(dibenzylideneacetone)dipalladium(0)
Pd/C	Palladium on carbon
$Pd(PPh_3)_2Cl_2$	Bis(triphenylphosphine)palladium(II) dichloride
P. f	*Plasmodium falciparum*
P. falciparum	*Plasmodium falciparum*
***Pf*CDPK1**	*Plasmodium falciparum* calcium-dependent protein kinase 1
***Pf*CLK1**	*Plasmodium falciparum* Cdc2-like kinase 1
***Pf*PK7**	*Plasmodium falciparum* protein kinase 7
PGI_2	Prostaglandin I_2
pH	Power of hydrogen or negative log to base 10 of H^+ concentration
Phe	Phenyl alanine
PI3K	Phosphatidylinositol 3-kinase
PI4K	Phosphatidylinositol-4-OH kinase
p*K*a	Negative log to base 10 of the acid dissociation constant
***Pf*PI4K**	*Plasmodium falciparum* phosphatidylinositol-4-OH kinase
P. knowlesi	*Plasmodium knowlesi*
P. malariae	*Plasmodium malariae*
P. ovale	*Plasmodium ovale*
ppm	Parts per million
P. reichenowii	*Plasmodium reichenowii*
prep-TLC	Preparative thin layer chromatography
pSAR	proposed SAR

P. vivax	*Plasmodium vivax*
P. yoelii	*Plasmodium yoelii*
q	Quartet
QSAR	Quantitative structure-activity relationship
QTc	Corrected QT interval
(*R*)-BINAP	(*R*)-(+)-(1,1′-Binaphthalene-2,2′-diyl)bis(diphenylphosphine)
RDT	Rapid diagnostic test
R_f	Retardation factor
RHS	Right hand side
Ro3	Rule of Three
Ro5	Rule of Five
RPM	Revolutions per minute
RT	Reverse transcriptase
rt	Room temperature
s	Singlet
S	Serine
SAR	Structure-activity relationship
SD	Standard deviation
sec	Secondary
Ser	Serine
SERCaP	Single exposure radical cure and prophylaxis
SI	Selectivity index
SMILES	Simplified Molecular Input Line Entry Specification
S_NAr	Nucleophilic aromatic substitution

S_N2	Nucleophilic substitution bimolecular
SOMe	Sulfinylmethyl
SO_2Me	Sulfonylmethyl
SPR	Structure-property relationship
SSR	Structure-solubility relationship
t	Triplet
$t_{1/2}$	Half-life
TB	Tuberculosis
td	Triplet of doublets
TdP	Torsades de pointes
TEA	Triethylamine
tert	Tertiary
THF	Tetrahydrofuran
TLC	Thin layer chromatography
TPP	Target product profile
TPSA	Topological polar surface area
t_r	Retention time
TRK	Tropomyosin receptor kinase
tt	Triplet of triplets
UPLC-MS	Ultra-pressure liquid chromatography mass spectrometry
UV	Ultraviolet
V	Valine
Val	Valine
WHO	World Health Organization

XPhos	2-Dicyclohexylphosphino-2′,4′,6′-triisopropylbiphenyl

CHAPTER 1
INTRODUCTION AND LITERATURE REVIEW

1.1 Chapter Overview

In this chapter, malaria as a disease, is introduced in the context of its brief history, epidemiology and aetiology. The chapter then covers malaria control and prevention strategies such as vector control, chemoprophylaxis, vaccination and mass drug administration (MDA) programmes. The status and challenges of current malaria treatment options as well as antimalarials in the drug development pipeline are also discussed. A survey of the emerging malaria eradication agenda with accompanying newly defined target product profiles (TPPs) for the next generation of antimalarials is presented. Furthermore, the importance of drug solubility and the need to profile drug candidates against drug antitargets such as the human *ether-a-go-go*-related gene (hERG) potassium ion channel is highlighted. Commonly employed strategies to optimize solubility and counter hERG inhibition are also summarised. This is followed by a literature survey of biological properties of imidazopyridazines and aminopyrazines which were a subject of this thesis research. The chapter concludes with an introduction of the overall research programme, detailing the justification of the study, research questions, objective and specific aims.

1.2 Malaria: History and Introduction

There are over 125 different types of malaria parasite species that infect mammals, birds and reptiles. The disease is known to be one of the most ubiquitous and has probably ravaged humanity throughout its evolutionary history.[1] However, the symptoms matching those of malaria were first historically reported around 1550 BC by the ancient Egyptians who noted the association between fevers and wet gounds.[1] The association of malaria with wet ground or stagnant waters later prompted Romans to embark on drainage programmes which marked one of the first preventive measures aimed at halting malaria in the Roman Empire.[2] In Europe and Africa, malaria has been a major public health problem for many centuries, and its spread has been encouraged by travelling tradesmen, settlers and conquering forces. Particularly, the spread of malaria to the New World has been thought to result from the over 400 years of slave trade which also resulted in the deaths of millions of Africans from the disease.[2] Although malaria generally thrives in tropical regions, the early settlers of America suffered a

pronounced impact with incidences peaking in 1875 and more than 600,000 cases being reported in 1914.[2]

Ground-breaking advances in medicine and dedicated efforts of individual scientists have helped in the shift of the understanding of the disease from the ancient mythology-based approach to a clear scientific insight. Malaria parasites in the blood of infected patients were first discovered by Charles Louis Alphonse Laveran, a French Army surgeon.[3] An Italian neurophysiologist, Camillo Golgi, later established a positive correlation between fever symptoms and the rupture and release of merozoites into the blood stream.[3] In 1898-1899, Giovanni Batista Grassi and co-workers showed that the female *Anopheles* mosquito was responsible for the transmission of malaria from one human to the other.[3]

Reports on the origins of malaria, particularly, *Plasmodium falciparum* malaria, the most virulent form of the disease, have been contradictory. *P. falciparum* DNA (deoxyribonucleic acid) has been detected in Egyptian mummified remains dating as far back as 1500 – 500 BC[4] while other studies suggest the disease originated from Gorillas and was probably transmitted to humans from these apes.[5] Still other reports indicate that a bird parasite whose descendants include both the human-infecting *P. falciparum* and the chimpanzee-infecting *P. reichenowii* could have been the origin of *falciparum* malaria.[6]

1.3 Epidemiology of Malaria

Approximately 50% of the world's population was at risk of malaria in 2016.[7] In the same year, ongoing malaria transmission was reported in 91 mainly tropical countries and regions (Figure 1.1). In 2004, malaria deaths were reported to peak at 1.82 million and declined to 1.24 million in 2010 according to the Institute for Health Metrics and Epidemiology (IHME).[8] According to the WHO world malaria report released in 2017, about 445,000 malaria deaths were recorded in 2016, a similar mortality as that recorded in the preceding year (446,000 deaths in 2015). A disproportionately high share of this global malaria burden is carried by the WHO African region (Figure 1.1). In this regard, 90% of malaria cases and 91% of malaria deaths in 2016 occurred in this region. Additionally, 80% of the global malaria burden was accounted for by some 15 countries all of which, except India, are in sub-Saharan Africa.[7]

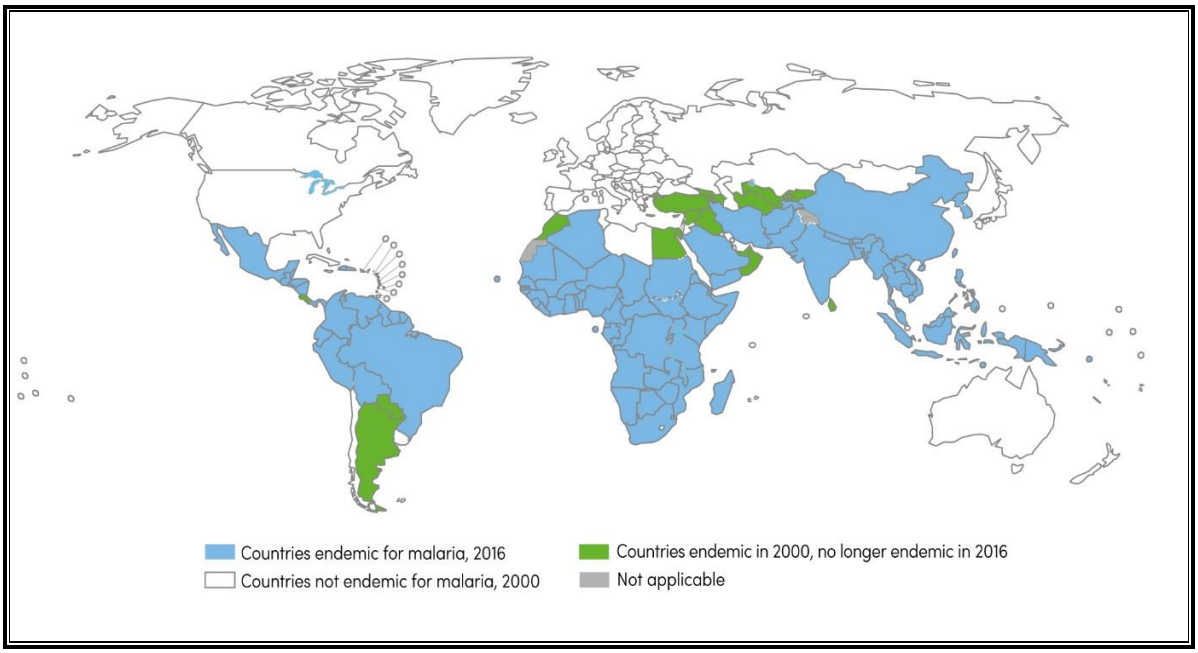

Figure 1.1: Malaria-endemic countries in 2000 and 2016.[7]

Great strides have been made in the fight against malaria in the period between 2000 and 2015. In this period, a 41 and 62% reduction in malaria incidence rates and mortality respectively have been recorded.[7] In 2000, 108 countries were considered malaria endemic while only 91 countries and territories were considered so at the beginning of 2016 (Figure 1.1). The wide-spread deployment of malaria control interventions can partly explain such successes. According to the WHO, malaria is considered to have been eliminated in a particular country if that country registers zero indigenous cases in three consecutive years. Although Tajikistan has not yet had 3 consecutive years of zero indigenous malaria cases, no country in the WHO European region reported indigenous cases in 2015.[7] Unfortunately, for South East Asia, Africa and the Western Pacific, the decline in mortality for all age groups appears to have stalled.[7] However, the understanding of the malaria control programme success is complicated by the uncertainties in the number of cases and deaths reported. In this regard, 31 countries, including the high burden countries like India and Nigeria, out of the 55 countries were the burden was estimated, have a malaria reporting rate of less than 50%.[7]

The risk of contracting and developing severe malaria is considerably higher in some population groups than others. Amongst the high-risk groups are infants, children under 5 years of age, pregnant women, HIV/AIDS patients, non-immune migrants, mobile populations and travellers. Accordingly, such vulnerable population groups need special protection against malaria infection by national malaria control programmes.[7] Children under the age of 5 years

are particularly vulnerable to malaria infections in areas with high transmission with over 70% of all deaths occurring in this age group.[7] Indeed, malaria remains a major cause of morbidity in under 5 children taking the life of a child every two minutes.

1.4 Aetiology of Malaria

1.4.1 Parasite Species Responsible for Malaria

Human malaria is caused by mainly four species of protozoan parasites of the genus Plasmodium which include *P. falciparum, P. vivax, P. malariae* and *P. ovale*.[9] Disturbingly, *P. knowlesi*, a malaria parasite strain known to infect monkeys and occurring in certain forested areas of South East Asia, has recently been shown to infect humans.[10] *P. falciparum* accounts for the largest burden of disease followed by *P. vivax*.[11] Sub-Saharan Africa, New Guinea and Hispaniola are predominated by *P. falciparum* while *P. vivax* affects the Americas and the Western Pacific the most. However, in the Indian sub-continent, Eastern Asia and Oceania, these two species exhibit approximately equal prevalence.[12–14] Endemic sub-Saharan African countries also harbour *P. malariae* the most although it is rare. *P. ovale* accounts for under 1% of isolates and is relatively unusual outside of the African continent.[15] Using molecular methods, the species *P. knowlesi* which is morphologically similar to *P. malariae* has been identified in patients in Malaysia, the Philippines, Thailand and Myanmar. However, human-to-mosquito transmission of *P. knowlesi* has not yet been demonstrated and it appears a monkey reservoir may be required to infect mosquitoes.[10]

1.4.2 Malaria Parasite Life Cycle

As malaria drug discovery efforts evolve, with focus on designing antimalarials that inhibit parasite growth at multiple stages of development,[16] understanding the parasite life cycle becomes important. Of the parasites that infect humans, the life cycle of *P. falciparum* is the most studied and best understood.[17]

Two types of hosts are infected with malaria parasites – the humans and the female *Anopheles* mosquitoes. However, the mosquito vector does not suffer from the presence of the parasites unlike the human host.[18] The parasite life cycle is summarized in figure 1.2.[18] Parasites, in the form of sporozoites, are introduced into the human host during a blood meal of an infected female *Anopheles* mosquito. Sporozoites then invade the liver cells, developing into schizonts which rupture and release merozoites. During the liver stage, particularly in *P. vivax* and *P. ovale* infections, dormant forms of the parasites (hypnozoites) can develop and persist in the

liver resulting in relapses weeks or years later. The initial replication in the liver, also referred to as exo-erythrocytic schizogony, is followed by asexual multiplication in the erythrocytes in a process known as erythrocytic schizogony. It is this blood-stage infection cycle that is associated with the clinical manifestation of malaria.[18] Upon parasitizing red blood cells, merozoites develop into trophozoites, which subsequently mature into schizonts. The rapture of schizonts releases more merozoites, which infect new red blood cells thereby perpetuating the blood-stage infection cycle. Some trophozoites differentiate into sexual erythrocytic forms (gametocytes) which are then ingested by a mosquito during its blood meal.[18]

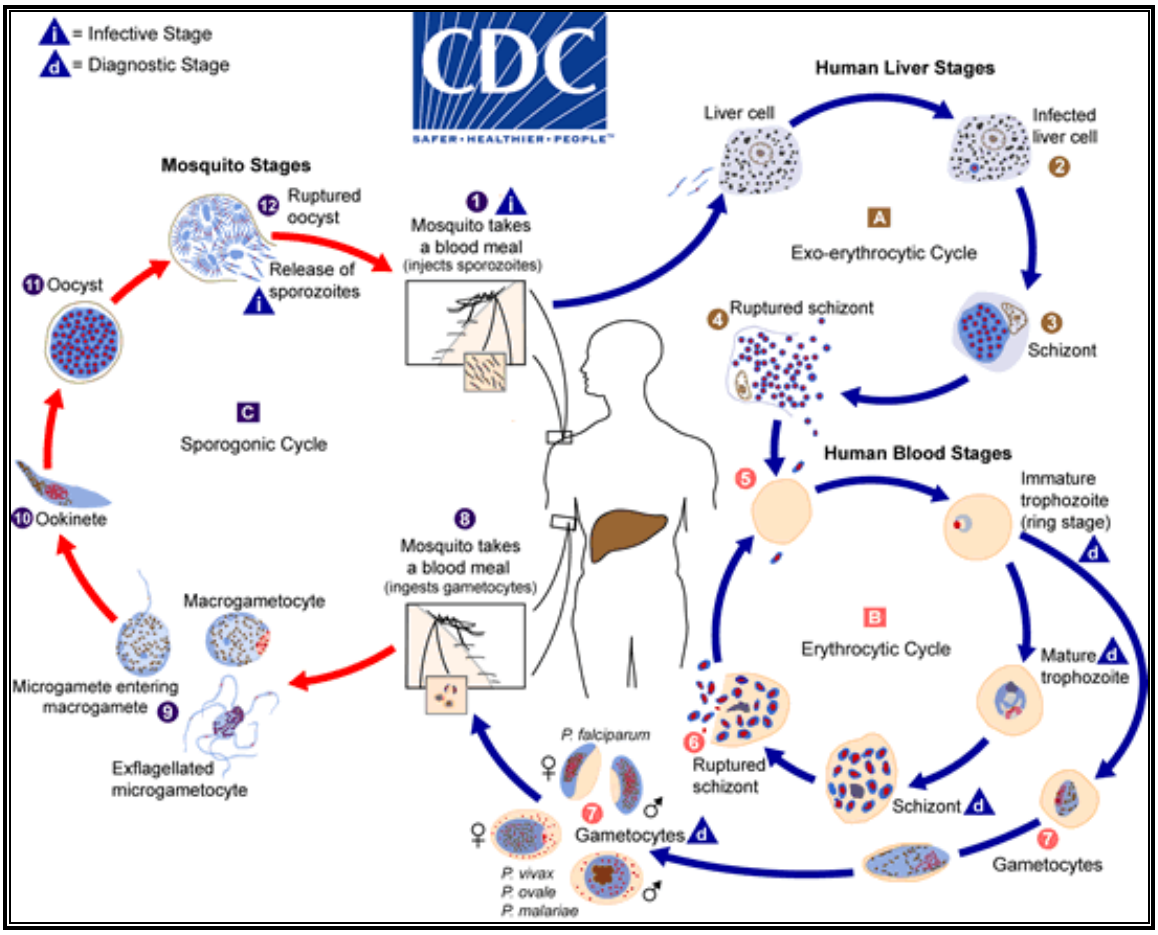

Figure 1.2: Malaria parasite life cycle.[18]

Parasite development in the mosquito, known as the sporogonic cycle, starts with the ingestion of male and female gametocytes during a blood meal by an *Anopheles* mosquito (figure 1.2).[18] In the mosquito's stomach, the male and female gametes fuse together to form zygotes. The zygotes then develop into ookinetes, which are elongated and motile. The ookinetes then migrate to the midgut wall of the mosquito and further develop into oocysts. The oocysts then mature and rupture releasing sporozoites which in turn invade the mosquito's salivary glands.

The malaria life cycle is perpetuated by the inoculation of the sporozoites into the human host during the next blood meal.

1.5 Malaria Control, Prevention and Treatment

Amongst some employed approaches to malaria control include preventive strategies such as vector management and control, chemoprophylaxis, vaccination (ongoing research efforts), and mass drug administration. Most importantly, case management requires the deployment of antimalarial drugs.

1.5.1 Preventive Strategies

1.5.1.1 Vector Management and Control

The focus of mosquito vector control is to reduce the mosquito population. These strategies include the use of household insecticide indoor residual spraying (IRS), insecticide-treated nets (ITNs) and larval control by environmental management.[15] Genetic control methods are still a subject of research. IRS and ITNs have become pivotal in vector control owing to the advent of effective insecticides against adult *Anopheles* mosquitoes.[15]

IRS involves spraying the insecticide on residential walls and ceilings whose effect can last for extended periods depending on the insecticide and surface.[15] Organochlorine insecticides like dichlorodiphenyltrichloroethane (DDT) require only once to twice applications per year while organophosphates like malathion require more frequent application - three or more times per year.[19] Insecticide-treated surfaces are generally lethal to the mosquito upon contact while sub-lethal exposure drives the mosquito outside the house. In an ideal case, the mosquito is killed or repelled before it can feed on humans within the house.[20] Malaria elimination, achieved over half a century ago, in many regions including the Southern United States, most Caribbean islands, Southern Europe, most of the former USSR and Taiwan was facilitated by IRS programmes employing DDT. Malaria prevalence in South Asia, Southern Africa, South America and Zanzibar has also been reduced with IRS programmes involving DDT.[14,21,22] However, environmental and wildlife toxic effects of DDT led the WHO, in mid-2009, to issue a recommendation to phase out DDT while replacing it with other insecticides.[15]

Before insecticides were available for use against adult mosquitoes, vector control efforts were aimed at making potential breeding sites unconducive for *Anopheles* larvae. Such vector control measures are exemplified by two famous historical cases – the fluctuation of the water

levels in the reservoir of the Tennessee Valley Authority and the draining of the Pontine Marshes near Rome.[23] Furthermore, village ponds and wells can be stocked with larvivorous fish species like *Gambusia* and *Poecilia* which are avid feeders on mosquito larvae.[24] In a series of villages in South India, no malaria cases were detected after the implementation of this strategy from 1998 to 2003.[23,25] In another approach, the larva-to-pupa-to-adult metamorphosis can be arrested by treating water-filled pits with insect growth regulators such as pyriproxyfen. In the 1960s, Sri Lanka nearly eradicated malaria when this approach was used. Regrettably, these eradication efforts where frustrated by gem mining which left more pits filled with rain water thereby providing new breeding ground for malaria vectors.[26]

In a genetic control strategy, adult male mosquitoes can be genetically modified by irradiation to carry sterilizing factors such as dominant lethal mutations. Mating such sterile male insects with a population of females produces eggs and larvae incapable of hatching and surviving respectively.[27] Although its application to *Anopheles* mosquitoes is limited, this technique has been successfully used to eradicate other pests.[28]

1.5.1.2 Chemoprophylaxis

Another strategy employed in the prevention of malaria is chemoprophylaxis. In this strategy, development of malaria is prevented by use of antimalarial drugs. Chemoprophylaxis is normally recommended for travellers to malaria-endemic countries and not for residents of such countries.[29] Depending on the malaria parasite species and the drug resistance landscape in a country, the choice of chemoprophylactic agents varies. There are two phases of chemoprophylaxis in the context of malaria prevention – primary and terminal prophylaxis.

In primary prophylaxis, a traveller starts taking antimalarial drugs at recommended doses 2 – 20 days prior to departure for a malarious zone and continues throughout their stay and for 1 – 4 weeks after return. Primary prophylaxis may either be causal or suppressive. Causal prophylaxis involves administration of drugs which inhibit the pre-erythrocytic schizogony thereby disrupting the establishment of liver stage infection. Such causal prophylactic drugs include primaquine and proguanil. However, the use of primaquine for such a purpose has been precluded due to potential adverse effects associated with long term use and its limited availability. On the other hand, suppressive prophylaxis offers protection against clinical illness by administering schizonticidal drugs which inhibit the blood stage forms of the malaria parasites. However, hypnozoites from *P. vivax* and *P. ovale* infections may cause relapse in which case terminal prophylaxis may be necessary.

In order to clear the hypnozoites associated with *P. vivax* and *P. ovale* infections, which can trigger relapses, primaquine is administered for two weeks after returning from a malarious zone in a strategy called terminal prophylaxis.[29]

1.5.1.3 Vaccination

To date and, despite decades of intense research, there is no effective antimalarial vaccine albeit over 20 candidates are under clinical development or are in advanced preclinical development.[30] The most advanced injectable vaccine which is being considered for pilot programmes before full deployment is RTS,S/AS01 (RTS,S) also known as Mosquirix. The vaccine has been developed against the deadliest form of human malaria, *P. falciparum* and is known to partially protect young children against malaria.[9,30] The vaccine is currently undergoing evaluation in sub-Saharan Africa to determine its potential to complement, and not replace, the core preventive, diagnostic and treatment measures recommended by the WHO.[9] In 2015, the European Medicines Agency (EMA), a stringent medicines regulatory body, gave a positive opinion on the vaccine, and three months later in the same year, pilot implementation of the vaccine in a limited number of African countries was recommended by two WHO advisory teams. WHO adopted these recommendations, and in November 2016, announced that the vaccine would be launched in pilot programmes in three sub-Saharan African countries.[9] The initial phase of the programme has secured funding already and vaccinations are scheduled to begin in 2018. If safety and effectiveness are considered acceptable, these pilot programmes could pave way to large-scale deployment of the vaccine.

1.5.1.4 Mass Drug Administration Programmes

In low transmission settings, especially in areas threatened by the emergence of *P. falciparum* resistance, MDA is another tool which can rapidly reduce malaria parasitemia. For instance, in Zambia, an 87% reduction in parasite prevalence was observed in low-transmission areas when dihydroartemisinin – piperaquine was administered in two doses in a randomized controlled trial.[31] However, in high transmission areas, such an effect was not observed. Another variant of MDA involves the identification of asymptomatic individuals via rapid diagnostic tests (RDTs) followed by targeted treatment of such a population. This strategy is exemplified by a recent elimination of nearly 70% of asymptomatic carriers in Zanzibar, a low-transmission area for *P. falciparum*. In this case, all individuals residing within 300 to 1000 meters of individuals with positive RDT also received antimalarial drug treatment.[32]

However, the application of MDA campaigns to eradicate malaria requires caution. This is because the development of drug resistance has been thought to be greatly influenced by the malaria eradication efforts anchored on MDA programmes.[33,34] These programmes are known to exert a considerable degree of drug pressure. Although MDA programmes, such as the use of iodinated salt, have registered remarkable success in contributing to the decline of endemic goitre, chloroquinized salt programmes are thought to have fuelled the emergence of chloroquine-resistant strains of *P. falciparum*.[34] Failure to ensure each individual consumes an adequate dose of salt is one apparent shortfall of such a strategy. Such exposure of the parasite to sub-therapeutic levels of the drug subsequently encouraged the emergence of chloroquine-resistant strains.[35]

1.5.2 The Status and Challenges of Malaria Treatment

1.5.2.1 Current Treatment Regimens and Challenges

Malaria infections are treated and prevented mostly by antimalarial drugs. The erythrocytic stage of malarial infection, a parasite development stage associated with the symptoms of malaria, is the target of most antimalarial drugs. Chloroquine (Figure 1.3), a drug which was the first to be manufactured on a large scale for treatment and prevention of malaria, exhibits activity against the blood stages of *P. ovale*, *P. malariae* and susceptible strains of *P. vivax* and *P. falciparum*.[36] However, although it remains effective in the treatment of *P. ovale*, *P. malariae* and, in most regions, *P. vivax* infections, widespread resistance in most malaria-endemic countries has led to decline in its use for the treatment of *P. falciparum* malaria.[37] Other treatment options have been devised for the treatment of both uncomplicated and complicated malaria. In uncomplicated cases of falciparum malaria, where there is no evidence of vital organ dysfunction and parasitemia is less than 5%,[38] the WHO has recommended artemisinin combination therapies (ACTs) as the first line drugs. Artemisinin derivatives which are administered in combination with other antimalarial drugs (lumefantrine, amodiaquine, mefloquine, sulfadoxine-pyrimethamine and piperaquine) include artesunate, artemether and dihydroartemisinin (Figure 1.3).[38] In cases of complicated falciparum malaria, where advanced signs of organ dysfunction and high levels of parasitemia (> 5%) are evident,[36,39] the cinchona alkaloids (quinine and quinidine) or the artemisinin derivatives (artesunate, artemether and artemotil) (Figure 1.3) are generally considered as treatment options.[36]

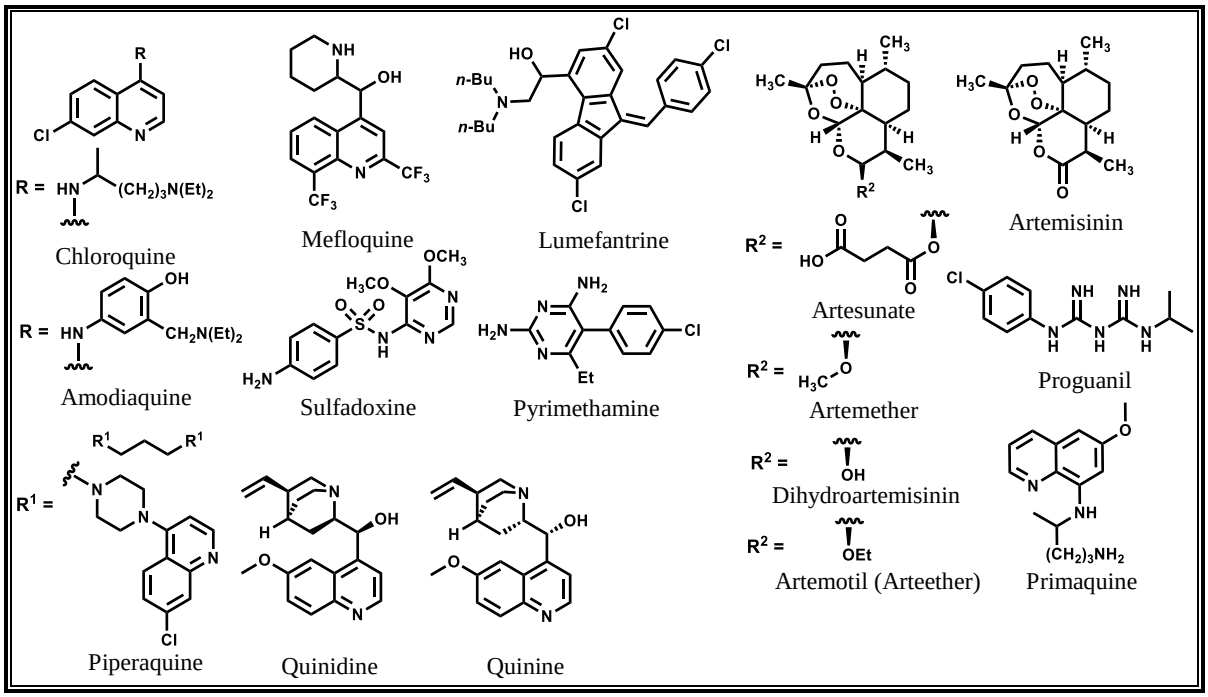

Figure 1.3: Chemical structures of some antimalarial drugs in clinical use.

For pregnant women in areas with medium and high malaria transmission, intermittent preventive treatment in pregnancy (IPTp) with sulfadoxine-pyrimethamine has been recommended. In this strategy, at least three doses of sulfadoxine-pyrimethamine are administered to pregnant women ideally at each of three antenatal care visits during the second and third trimesters.[40,41] Apart from suppressing and clearing asymptomatic infections from the placenta, each dose of sulfadoxine-pyrimethamine provides prophylaxis up to six weeks after treatment. Furthermore, this preventive treatment approach also protects women against adverse birth outcomes associated with sexually transmitted and reproductive tract infections.[42]

Despite the remarkable effectiveness of ACTs, emergence of resistance to artemisinin and the partner drugs is continuously threatening.[43] For instance, resistance to amodiaquine, one of the partner drugs in ACTs, has already been reported in some countries.[44] Moreover, in the Thai-Cambodia and, more recently, the Thai-Myanmar border regions, signs of artemisinin resistance manifested in loss of susceptibility have been documented.[45–47] Furthermore, the current portfolio of medicines, both in clinical use and development, has several other shortfalls which need redress. For instance, single-dose cure regimens as opposed to current three-day treatments are needed. In addition, prevention of transmission and relapse with better safety profiles than current medicines are some of the important features that should be a prioritized characteristic of new medicines. Most importantly, these new regimens should be able to offer

chemoprotection and prevent reinfection.[43] Thus, there is need for constant research efforts aimed at identifying and developing novel chemotherapeutic agents for malaria which are affordable, structurally diverse with novel mechanisms of action.

1.5.2.2 Current Antimalarials: Classification Based on Life Cycle Stage Targeted

Classification of antimalarial drugs can be based on their structure or the parasite life cycle stage targeted. Based on structure, current antimalarials fall into one of these classes of molecules: aryl amino alcohols, 4-aminoquinolines, 8-aminoquinolines, folate synthesis inhibitors, antimicrobials, peroxides, naphthoquinones and iron chelating agents. Respectively, one example of each of these classes is quinine, chloroquine, primaquine, pyrimethamine, doxycycline, artemether, atovaquone and desferrioxamine.[48] The classification based on parasite life cycle stage targeted will be discussed in greater detail in the following sub-sections.

1.5.2.2.1 Tissue Schizontocides

The target stages of this class of drugs are the pre-erythrocytic stages of the parasite in the liver cells. Proguanil and pyrimethamine (Figure 1.3) are the less toxic members of this group and are used as causal prophylactics to prevent infection either alone or in combination with sulphonamides.[49]

1.5.2.2.2 Hypnozoitocides

These drugs, among which, primaquine (Figure 1.3) and some other 8-aminoquinolines are the only examples found to be effective in man, kill the hypnozoites which are the dormant liver stages of the parasite. Therefore, in *P. vivax* and *P. ovale* infections, these drugs are used to prevent relapse associated with infections from these two parasite strains.[49]

1.5.2.2.3 Blood Schizontocides

These antimalarials are generally used in therapy and are quick acting only on the erythrocytic stage of parasite development.[49] Examples include chloroquine and quinine (Figure 1.3) with chloroquine being one of the less toxic members of this family. They are used to prevent the progression of malaria infection to disease by acting as suppressive prophylactics. Although they are not potent on the mature gametocytes of *P. falciparum*, these drugs are potent against gametocytes of *P. vivax*, *P. ovale* and *P. malariae*. In addition to acting at other stages, drugs

such as pyrimethamine, proguanil, sulphonamides, antibiotics, and to a lesser extent, primaquine (Figure 1.3) also possess blood-schizontocidal efficacy.[49]

1.5.2.2.4 Gametocytocides

These drugs kill the blood stage sexual forms of the parasite as well as the mature gametocytes of *P. falciparum*. A typical example of a drug used for this purpose, among other 8-aminoquinoline drugs, is primaquine.[49]

1.5.2.2.5 Sporontocides

Generally, this refers to drugs or their metabolites which interfere with oocyst or sporozoite development in the mosquito following a blood meal. Sporontocidal drugs, exemplified by pyrimethamine, also inhibit oocyst and sporozoite development when fed directly to mosquitoes.[49]

1.6 Current Antimalarials in Clinical Development

The Medicines for Malaria Venture (MMV), a public-private partnership with the goal of fostering development of new malaria treatments archives and updates, every 3 months, a comprehensive list of most of new compounds under development across the globe.[50] Table 1.1, adapted from the MMV's summary, shows antimalarial compounds, including those supported by MMV at different phases of clinical development. Following pre-clinical evaluation, clinical development of a drug candidate constitutes three phases. In phase I trials, the safety, tolerability and dosing in healthy adult volunteers are determined. The drug candidate is then progressed to phase II where it is tested in a limited number of patients to demonstrate the proof-of-concept and further evaluate safety. Phase III trials involve a large cohort of patients in endemic countries and are aimed at comparing efficacy with the standard of care as well as reconfirm safety before the product is licensed.

Table 1.1: Summary of antimalarial drug candidates at different phases of development.[a]

Translational		**Product Development**		
Preclinical	**Human Volunteers**	**Patient Exploratory**	**Patient Confirmatory**	**Regulatory Review**
SAR121 Sanofi	**P218** Janssen (Biotec Thailand)	**Artefenomel-Piperaquine** Sanofi	**Tafenoquine** GSK/MMV GSK/US Army	**Arterolane-piperaquine** Sun Pharma

Table 1.1: Summary of antimalarial drug candidates at different phases of development.[a]

Translational		Product Development		
Preclinical	**Human Volunteers**	**Patient Exploratory**	**Patient Confirmatory**	**Regulatory Review**
AN13762	**SJ733** Kentucky/Eisai	**KAF156-Lumefantrine** Novartis	**Dihydroartemisinin-piperaquine dispersible** Alfasigma/Pierre Fabre	**Rectal artesunate** Strides
UCT943 H3D Cape Town	**ACT-451840** Actelion	**Cipargamin** Novartis	**Co-trimoxazole** ITM Antwerp	
NPC1161B Mississippi	**CDRI 9778** Ipca	**DSM265** Takeda (UTSW)	**Artemisinin-naphthoquine** Kunming Pharma Co	
MK4815 Merck	***N-tert*-butyl Isoquine** LSTM/Liverpool/GSK	**Fosmidomycin-Piperaquine** Jomaa Pharma/GmbH	**Artemether sub-lingual spray** MRC/Suda	
M5717 Merck KGaA		**Methylene Blue-amodiaquine** Heidelberg	**Sulfadoxine-pyrimethamine-Amodiaquine dispersible** S Kant	
MMV253 Zydus Cadila		**SAR97276** Sanofi		
SC83288 Heidelberg University		**Artemisone** UHKST		
DM1157 DesignMedix		**AQ13** Immtech		
		Sevuparin Dilaforette		
		MMV390048 (UCT)		

[a]Adapted from MMV's summary of the global portfolio of antimalarial candidates in clinical development.[50]

Over the past decade, new chemical entities have entered clinical development transforming the portfolio of malaria medicines (Table 1.1).[51] In this section, brief backgrounds for selected drug candidates from table 1.1 are outlined.

Currently, radical cure for *P. vivax* infections relies on primaquine which is administered for fourteen days to completely clear *P. vivax* parasites from the body. Unfortunately, primaquine is incompatible with patients with G6PD (glucose 6-phosphate1-dehydrogenase) deficiency posing a significantly high risk of haemolysis.[52] Although not structurally novel, tafenoquine (structure in figure 1.4), currently in clinical development (Table 1.1), represents a promising alternative to primaquine with clinical studies showing a single dose could clear *P. vivax* parasites.[53,54] This is a significant improvement from primaquine which takes 14 days of treatment. Regrettably, like primaquine, tafenoquine will require a point of care G6PD diagnostic test owing to its haemolytic liabilities.[51]

Although the cornerstone of current antimalarial therapy are artemisinin derivatives like artesunate, the fact that the raw material is still derived from plants still hampers access to such regimens especially in resource-constrained settings. The 1.5 years lead time between demand for the raw material and supply has occasionally led to devastating changes in prices – the past decade has seen a variation in artesunate prices by as much as 4-fold.[51] In response to this supply problem, MMV, in collaboration with other partners, launched a campaign to synthesize endoperoxide derivatives as effective and affordable as artesunate at its best price ($400 per kg). Such efforts have culminated in the synthesis of **OZ277** which was subsequently called **Rbx11160** or arterolane (Figure 1.4). Compared to the high price of artesunate triggered by supply problems, the synthesis was cheaper costing $800 per kg although there is still room for further reduction of this figure to $400 per kg. Comparison of arterolane with the marketed artemether-lumefantrine fixed dose combination (Coartem), in clinical studies demonstrated its non-inferior efficacy.[55] Arterolane, in combination with piperaquine (Table 1.1), under the trade name Synriam, has received approval in India and later in seven African countries following a limited phase III study albeit more stringent regulatory bodies and the WHO are yet to approve the medicine.[51] Efforts to generate a next-generation compound that could solve artesunate price fluctuations with a potentially longer half-life have also delivered **OZ439** (also known as artefenomel, figure 1.4) which is now undergoing evaluation in combination with piperaquine in a phase IIb study (Table 1.1).[51]

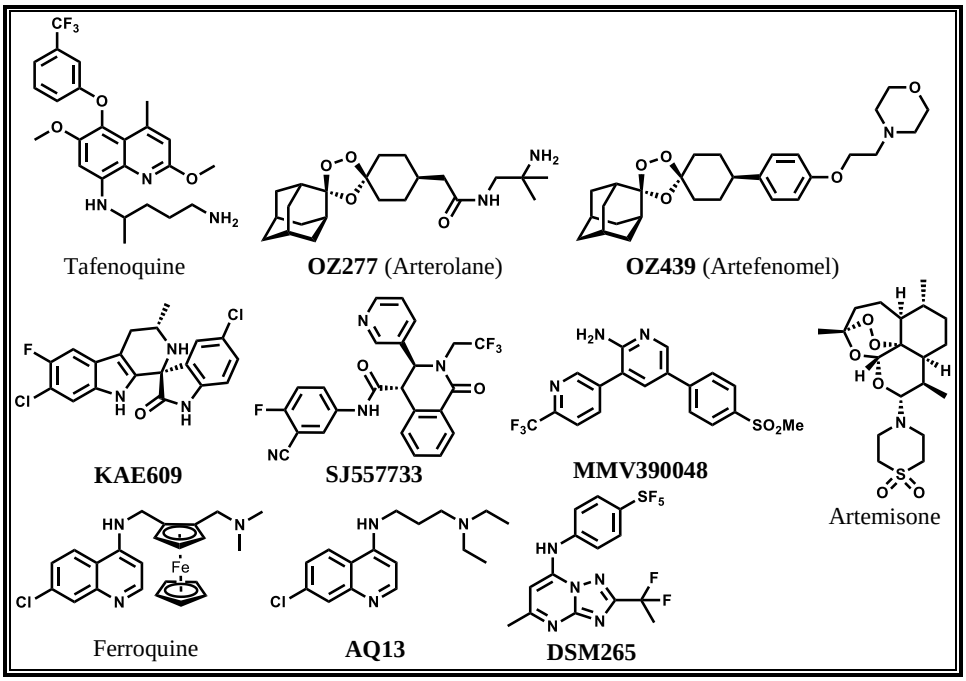

Figure 1.4: Chemical structures of some new antimalarial clinical candidates.

Using target-based approaches, another noteworthy compound **DSM265** (Figure 1.4), belonging to the triazolopyrimidine class, was discovered and commenced phase IIa (Table 1.1) monotherapy studies in Peru at the beginning of 2015. **DSM265** exerts its antimalarial efficacy by inhibiting *Plasmodium falciparum* dihydroorotate dehydrogenase.[56] On the other hand, phenotypic-based approaches have recently furnished **KAE609** (Figure 1.4) also known as cipargamin, a spiroindolone which holds immense promise as a structurally novel antimalarial.[57,58] Medicinal chemistry optimization of the initial hit led to the lead **KAE609** which progressed rapidly through phase I[59] and the first studies in human patients have so far been concluded in Thailand (Table 1.1).[60] Interestingly, apart from maintaining a plasma concentration above the MIC value for several days, **KAE609** kills even faster than artesunate. Furthermore, it is 40- and 7-fold more potent than 4-aminoquinolines and artesunate respectively and required relatively low doses (30 – 75 mg) in total during clinical studies. Therefore, **KAE609** has potential to be cheaper than current therapies and could potentially cure malaria in a single dose. It was anticipated that by 2017, **KAE609** would be submitted for approval.[61] Other notable drug candidates with the same molecular target as **KAE609** include **SJ557733** (also known as **SJ733**) (Figure 1.4) which entered the first-in-human studies in 2016 (Table 1.1) sponsored by St Jude Children's Research Hospital and Rutgers University.[62]

The recent contribution of the African continent in discovering new chemotherapeutic remedies is also worth mentioning. In this regard, a team led by the University of Cape Town in South

Africa have employed phenotypic approaches to develop a clinical candidate **MMV390048** (Figure 1.4) belonging to the aminopyridine class.[63] As the compound progressed to preclinical development, the target was identified to be the lipid *P. falciparum* phosphatidylinositol-4-OH kinase (*Pf*PI4K).[64] **MMV390048** has successfully completed phase I studies[65] and is currently undergoing proof-of-concept studies in *P. vivax*- and *P. falciparum*-infected patients (Table 1.1).[66]

The global antimalarial portfolio also contains other candidates derived from known chemical scaffolds. These include the endoperoxide artemisone,[67] derived from artesunate, the 4-aminoquinolines (ferroquine[68,69] and **AQ13**[70]) (Figure 1.4), **NPC1161B** (an 8-aminoquinoline)[71] and **DM1157** (a chloroquine derivative)[72] (structures for **NPC1161B** and **DM1157** are not shown but developmental status is captured in table 1.1). Additionally, the antimalarial development pipeline also has a significant proportion of new formulations and combinations of existing drugs as captured in table 1.1. Additional new antimalarial clinical candidates at different stages of development (Table 1.1) include **SAR121**, **AN13762**,[73] **UCT943** (an aminopyrazine alternative to **MMV390048**),[74] **MK4815**,[50,75] **M5717**,[76] **MMV253**,[77] **SC83288**,[78] **KAF156**[79] and several others.[80–87]

1.7 Malaria Eradication Agenda

About 10 years ago, the WHO and the Bill and Melinda Gates Foundation announced the long-term goal of malaria eradication. The 60 and 37% significant reduction in mortality and morbidity respectively recorded in the past nearly two decades has been partly driven by the use of existing therapy.[88] The malaria community has now defined clear road maps on the types of new medicines[89] while the WHO has committed to reducing morbidity and mortality by a further 90% by 2030.[90] Clear goals for new therapy have been set by proposals on the types of medicines [target product profiles (TPPs)] needed.[91] During drug discovery and development, TPPs act as strategic tools by providing guidance.[16] In this subsection, the TPPs of new medicines needed to eliminate and eradicate malaria are discussed.

1.7.1 Newly Defined Target Product Profiles for Malaria Elimination and Eradication

1.7.1.1 Antimalarials with Multi-Stage Antimalarial Activity

The blocking of transmission and prevention of relapse is pivotal to the realization of the malaria eradication agenda. In this regard, an ideal combination therapy should contain compounds with activity on hypnozoites and sexual stages in the human host and mosquito

vector in addition to the erythrocytic stage-killing activity.[51,91] Although primaquine remains a gold standard for treating *P. vivax* relapses and transmission blocking, the treatment is lengthy and it is unsafe in G6PD-deficient patients. Therefore, an ideal combination needs to demonstrate a single-dose radical cure and should be devoid of the haemolytic effects associated with primaquine.[91]

1.7.1.2 Resistance-Proof Chemotypes

As much as possible, molecules with pan-activity across the five human-infecting parasite species (*P. falciparum*, *P. vivax*, *P. malariae*, *P. ovale* and *P. knowlesi*) should be prioritized.[91–93] However, due to issues associated with accessibility to parasites and culture conditions, a more realistic approach is to focus on *P. falciparum* and in limited cases *P. vivax*. As a second priority, new antimalarials need to demonstrate lack of cross-resistance against laboratory adapted strains as well as clinical isolates from geographical regions known for antimalarial drug resistance. Such an assessment serves as a measure of the molecule's tendency to develop resistance.[91] Indeed, a number of chemotypes incapable of resistance selection *in vitro* have been identified from recent studies on compounds from the open-access Malaria Box.[94,95] Consequently, optimization and subsequent progress will prioritize interesting scaffolds from within this set.[16]

1.7.1.3 Single Dose Regimens to Simplify Treatment

The ideal medicine needed for eradication of malaria has been termed the SERCaP (single exposure radical cure and prophylaxis). Such a medicine would be critical in eliminating and eradicating malaria in urban or remote rural areas with substandard health systems because only a single encounter with a healthcare provider and the patient would be necessary.[96] Additionally, this ideal medicine could foster compliance since it could easily be administered as directly observed therapy (DOT).[91] A SERCaP treatment should demonstrate a radical cure and must be suitable for MDA programmes. Additionally, such an ideal treatment should offer prophylaxis for a minimum of one month post-treatment. Although the development of a drug with such a stringent TPP would be protracted, chances of malaria eradication could still be drastically improved if new drugs that bear some of these criteria are developed.[96] Admittedly, towards the development of such an ideal medicine, compromises will have to be made.[91]

1.7.1.4 Safe Drugs to Wide Range of Patient Populations

Safe and well tolerated medicines in vulnerable and a wide range of populations will ultimately be required to realize malaria elimination. Such vulnerable populations include pregnant women in their first trimester,[97] asymptomatics,[98] infants,[99] malnourished individuals and patients co-infected with other pathogens such as human immunodeficiency virus (HIV) and tuberculosis (TB).[16] Once again, developing a medicine that meets the needs of all these groups will be a challenge. For instance, due to ethical issues surrounding the recruitment of pregnant women into clinical trials, safety data in pregnant women is currently collected passively. For the artemether-lumefantrine combination, it has taken 20 years after regulatory approval to gather enough safety data to warrant a WHO-recommendation for use in first-trimester pregnancy.[100–104] Above all, the ideal medications need to be affordable to guarantee wide coverage to the many victims of malaria in resource-constrained countries.[91]

1.8 Importance of Solubility in Drug Design and Development

To attain optimal concentration of the drug in systemic circulation for desired therapeutic effect, solubility, the phenomenon of dissolution of a solute in a solvent to give a homogenous system, is a very important factor that needs to be optimised.[105] The low aqueous solubility of a drug candidate can result in low and variable oral bioavailability leading to variability in clinical response. Despite considerable efforts dedicated to improving solubility during lead optimization campaigns, an estimated 40% of drugs on the market and most candidates in the drug development pipeline remain poorly water soluble.[106] For a drug in clinical development, appropriate physical techniques can be employed to address solubility problems[107] although, realistically speaking, enhancement of solubility and absorption through such approaches is severely limited.[108] Thus, it is crucial that drug candidates have their solubility improved upon by chemical-modification means early on at the drug discovery stage.[108] These chemical-modification approaches are presented in subsection 1.8.1 below and, where appropriate, examples cited from literature are illustrated schematically in figure 1.5.

1.8.1 Strategies to Improve Solubility

1.8.1.1 Introduction of Ionizable Groups and Salt Formation

Solubility can be improved upon by the installation of water solubilizing and ionizable groups at a position in the core-scaffold in such a way that does not negatively impact other properties.[109] For instance, the discovery of amlodipine (a calcium channel blocker),[110]

tamoxifen (an estrogen receptor modulator)[111] and farnesoid X receptor (FXR) agonists[112] all involved the introduction of alkoxy amines to the core pharmacophore with concomitant pronounced improvement in solubility compared to the original leads. The latter case is illustrated by an example in figure 1.5. When administered to the mouse using the standard suspension formulation (2% Tween 80 with 0.5% methylcellulose), the lead compound **FXR-450** exhibited low solubility (0.014 mg/mL) in this dosing vehicle which translated to sub-optimal oral bioavailability (21%). By introducing an ionizable centre (a basic amine), a next-generation molecule, candidate (B) was identified which demonstrated a ~ 18- and 423-fold increase in solubility as a free base and hydrochloride salt respectively. The improved solubility in the dosing vehicle along with improved metabolic stability resulted in high oral bioavailability (53%).

Indeed, ionizable groups in new drug molecules, whether cationic or anionic, offer an opportunity to generate salt forms with superior biopharmaceutical properties to the parent molecule.[113] The rate of dissolution and oral absorption can be enhanced by appropriate salt forms. Potential merits of salt formation are evident in drugs like diclofenac whose sodium or potassium salt forms are > 400-fold more water-soluble[114] than the free form.[115] A similar trend also holds true for weakly basic drugs which constitute the largest fraction of ionizable drug molecules. A typical example in this class is enalapril which has inferior aqueous solubility as a free base (~ 0.21 mg/mL) compared to its maleate form (~ 25 mg/mL).[116] Depending on the preferred route of administration, it is wise to prioritise counter ions with prior clinical application when performing salt screening.[109,117,118]

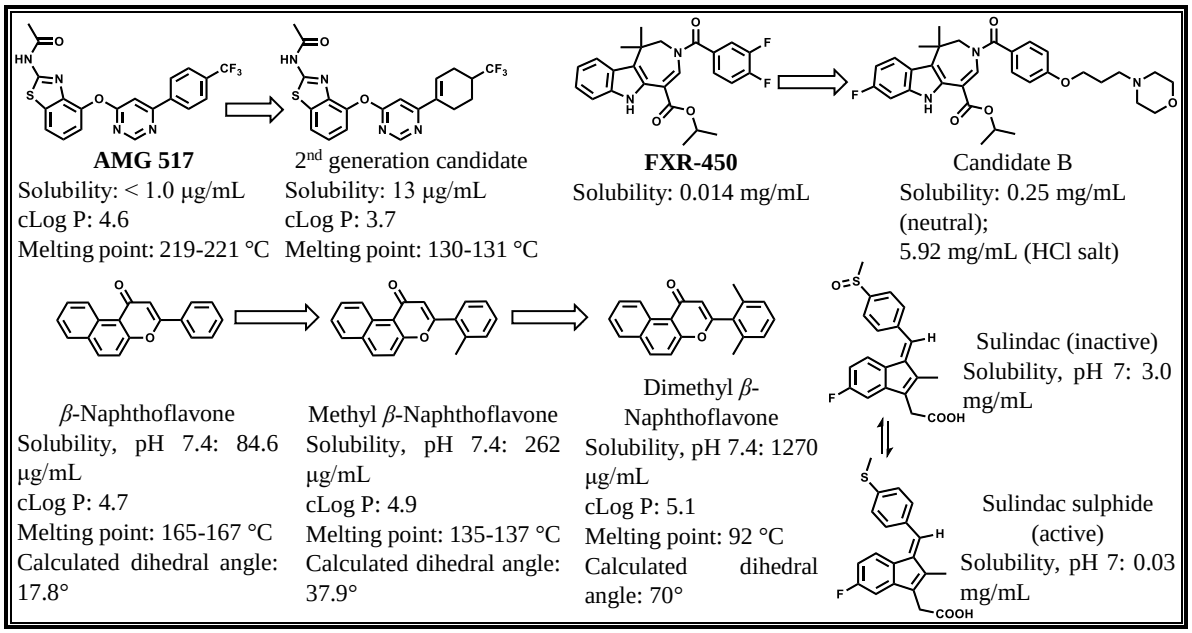

Figure 1.5: Examples of chemical modification approaches to improve solubility.

1.8.1.2 Reduction of Lipophilicity

Reduction of lipophilicity, another approach employed in optimizing solubility, may involve replacing phenyl rings with pyridyl rings and other heteroaromatic rings with hydrogen bonding capability.[119] In addition, structure-property relationship (SPR) investigations on solubility have shown that removing and/or replacing halogen atoms leads to a decrease in lipophilicity and, therefore, enhanced solubility.[120–122] Furthermore, aqueous solubility could significantly be improved upon by decreasing the length of alkyl groups as well as completely eliminating them from the structure.[120,123]

1.8.1.3 Prodrug Approaches

Improving solubility of poorly-soluble drugs, promoting their oral absorption, and enabling safe and effective intravenous (IV) formulations often involves employing prodrug strategies.[124,125] Sulindac is one typical example of a prodrug that achieves better oral delivery due to its water-solubilizing effect of the sulfoxide group which gets metabolized through a reduction to the active sulphide (Figure 1.5).[126] The sulfoxide prodrug exhibits 100-fold higher solubility (3.0 mg/mL) than sulindac sulphide (0.03 mg/mL) at pH 7.[127] Being more polar, the sulfoxide prodrug interacts with aqueous media more effectively than the reduced sulphide. Additionally, sulindac does not inhibit prostaglandin synthetase activity as strongly as sulindac sulphide and, therefore, is less locally irritating.[126]

Other prodrug approaches aimed at increasing solubility involve the linking of the parent molecule to an ionizable promoiety. However, because charged molecules are associated with decreased membrane permeability, there is need to exercise caution to avoid increasing water solubility at the expense of permeability. In particular, phosphate esters introduced at an alcohol functionality of parent molecules have been shown to effectively enhance delivery of water-insoluble parent drug molecules following oral delivery.[125] As the phosphate (R–OPO_3Na_2) prodrug rapidly dissolves in the gastrointestinal fluid, it undergoes enzymatic cleavage mediated by alkaline phosphatase to release the free drug (R-OH). The free drug then crosses the enterocyte membrane ending up in systemic circulation. Such a process functions like a semi-coupled metabolism/transport event.[125] Others have noted some limitations to such an approach including the possibility of precipitation of R-OH following rapid cleavage.[128] Nevertheless, there have been successful examples of the application of this approach as

evident in prodrugs such as fosfluconazole, fosphenytoin and fosamprenavir, which have demonstrated substantially higher solubility compared to parent drugs.[125]

1.8.1.4 Disrupting Molecular Planarity

Generally, improving aqueous solubility involves reduction of lipophilicity by introduction of hydrophilic groups into molecules. However, such a classical and general approach is not universally effective sometimes because interference with the target protein-drug interaction can result from the introduced hydrophilic substituents thereby compromising drug efficacy.[108] It should also be noted that in scenarios where both solubility and hydrophobicity need to be increased, such an approach proves ineffective. The disruption of molecular planarity and symmetry has recently been reviewed as an alternative strategy for improving aqueous solubility.[108] Such a strategy has been rationalized in both quantitative and qualitative terms. In 1980, the general solubility equations (GSEs), derived on the basis of semi-empirical analysis, were presented by Yalkowsky.[129] For instance, solubility, lipophilicity and melting point are related by the following equation:[130]

$$\text{Log[solubility (M)]} = 0.5 - (\log P) - 0.01\{[\text{melting point } (^{o}C)] - 25\}$$

Therefore, from the above equation, the solubility of a solute in water is a function of two factors: the crystallinity of the solute and the ability of the solute to interact with water. In this case, melting point is related to crystallinity and crystal packing energies while log P is a measure of the interaction of the solute with water. Therefore, disruption of crystal packing which results in reduction in melting point would be an alternative approach of enhancing aqueous solubility. Moreover, a concomitant decrease in crystal packing efficiency and melting point would be expected with disruption of molecular planarity and symmetry. A relatively recent survey revealed a decrease in the melting point with an increase in the fraction of sp^3 hybridized carbons in the drug and clinical candidate database.[131]

Specific examples of disruption of planarity/symmetry approach include removal of aromaticity (increasing saturation in the aromatic system).[132] In this case, in their efforts to develop vanilloid receptor 1 antagonists, Wang and co-workers identified the clinical candidate **AMG 517** (Figure 1.5) which exhibited sub-optimal thermodynamic solubility [< 1 μg/mL in phosphate buffered saline (PBS) or 0.01 M HCl]. Partial saturation of the phenyl ring which was hypothesized to reduce structural planarity as well as disrupt crystal stacking potential led to the identification of a second-generation clinical candidate with a 13-fold improved

thermodynamic solubility (13 μg/mL in 0.01 M HCl). Calculated lipophilicity (cLog P) indicates **AMG 517** has a higher lipophilicity than the partially saturated analogue indicating the reduction in lipophilicity, in addition to disruption of planarity, could be contributing to the observed increase in solubility.[108] Moreover, the hypothesis that a reduction in planarity contributes to the enhanced solubility is supported by the fact that **AMG 517** has a higher melting point than the second-generation clinical candidate.[108,132,133]

Molecular planarity can also be reduced by the introduction of substituents in a bicyclic structure in such a way that increases the dihedral angle. Ishikawa *et al*., employed this strategy to substantially increase aqueous solubility (84.6 μg/mL) of the aryl hydrocarbon receptor (AhR) agonist *β*-naphthoflavone (Figure 1.5). Monomethylation at *ortho* position increased thermodynamic aqueous solubility by 4-fold (262 μg/mL) while *ortho* dimethylation increased solubility by an even greater margin (1270 μg/mL, 15-fold improvement).[108] Calculations using density functional theory showed an increase in the dihedral angle in both the monomethylated (37.9°) and dimethylated (70.0°) analogues compared to the unsubstituted parent molecule (17.8°).[108] These derivatizations were also accompanied by increase in hydrophobicity and decrease in melting points. This result demonstrates that, indeed, the introduced substituents led to disruption of planarity with concomitant reduction in crystal packing energy which positively impacts solubility.[108]

Other strategies which have been shown to improve solubility include the introduction of substituents into the benzylic position where feasible;[134] and twisting of fused rings (e.g. subtle positional change of the nitrogen atom within the fused ring system).[135]

In this PhD project, some of these chemical-modification-based approaches were used to improve the aqueous solubility of imidazopyridazine and aminopyrazine analogues.

1.9 Cardiotoxicity: A Major Reason for Drug Withdrawals

Cardiovascular toxicity represents the most encountered serious adverse reaction and is a major contributor to withdrawal of marketed drugs.[136] According to Stevens and Baker,[137] about 45% of total post-approval drug withdrawals from the market are attributed to cardiovascular safety liabilities while hepatic safety liabilities account for 32% of such withdrawals. Cardiotoxicity issues have also prompted severe restrictions on the availability of marketed drugs. Examples of drugs which have suffered complete withdrawals or restrictions in availability include terfenadine, astemizole, grepafloxacin, terodiline, droperidol, lidoflazine, sertindole,

levomethadyl and cisapride.[138] Strangely, of the total drug attrition during phase I clinical development, only 9% is attributed to cardiovascular toxicity.[139] Such a discrepancy highlights the fact that the accuracy of predicting drug-induced cardiotoxicity in preclinical and early clinical stages is highly questionable. As such, in order to avoid delivering drug candidates with a high cardiotoxicity risk into late clinical development and marketing approval phases, there is need to more accurately de-risk projects early on in preclinical and early clinical stages.[136]

1.9.1 Underlying Mechanisms of Cardiotoxicity: Inhibition of the human *ether-a-go-go*-related gene (hERG) K^+ Channel

At cellular level, the efflux of potassium ions (K^+) from the myocytes is mainly responsible for the repolarization phase of the myocytes.[140] The heart harbours various K^+ current subtypes with the delayed rectifier current, I_{Kr} (rapid) and I_{Ks} (slow) being known to play a role in ventricular repolarisation.[140] The action potential may be prolonged by the blockade of either of these two outward potassium currents with I_{Kr} being more prone to pharmacological interference. The pore-forming α subunits of the channel for the I_{Kr} current is encoded by the human *ether-a-go-go*-related gene (hERG).[141] The pro-arrhythmic effects of drugs can be attributed almost exclusively to the blockade of the I_{Kr}. Clinically, the blockade of the I_{Kr} current is manifested in the prolongation of the QT interval and the presence of other T or U wave anomalies on the surface electrocardiogram (ECG).[140] Particularly, torsades de pointes (TdP), a rare but life-threatening form of cardiac arrhythmia arising from QT prolongation has been the main safety issue that has prompted the withdrawal of already marketed drugs.[142]

1.9.2 Strategies to Counter hERG Activity

In 2006, Jamieson *et al*.,[143] conducted a survey of literature on different reports of medicinal chemistry optimization campaigns where hERG/I_{Kr} activity have successfully been detuned. As opposed to developing statistically validated models or 3D pharmacophore information, the authors analysed the literature SAR data on hERG with the aim of devising simplified and user-friendly guidelines on detuning hERG activity that would be useful to a medicinal chemistry practitioner. The authors categorized the optimizations based on similarities in the chemical modification approach employed. These approaches which include discrete structural modifications, formation of zwitterions, control of log P and attenuation of p*K*a will be discussed in greater detail in subsequent sub-sections. However, the authors caution, there is

no such thing as a "one size fits all" solution to minimizing hERG activity and different groups employ different approaches to address this liability.[143]

1.9.2.1 Discreet Structural Modifications

A survey of published SAR information against the hERG channel suggest that π-stacking and hydrophobic interactions between aromatic residues lining the large cavity of the channel and aromatic moieties favourably oriented in a drug molecule are the major determinants of hERG-drug interactions.[144,145] Thus, these putative interactions and affinity for the hERG channel can potentially be disrupted if such molecular features in a drug molecule are subtly or drastically modified.[143] Additionally, introducing constraint in the molecule as well as varying stereochemistry, where pertinent, is one other approach in this category with potential to mitigate hERG activity.[143]

In one approach utilizing subtle modifications, Bell and co-workers have successfully diminished hERG potency of novel pyrrolidinone-based farnesyltransferase inhibitors (FTIs) by varying stereochemistry.[146,147] Although compound **1** (Figure 1.6) was amongst the most potent FTIs (IC_{50} = 0.15 nM) in the series, it was also one of the strongest inhibitors of hERG (IP = 0.08 μM) where IP represents the inflection point in the dose-response hERG inhibition curve. When tested in the anaesthetized dog, at a plasma concentration of 2.4 μM, compound **1** induced a 10% increase in the QTc (corrected QT) interval which was considered unacceptable. Reversing stereochemistry at one chiral centre gave compound **2** with nearly 60-fold reduction in hERG potency (IP = 4.7 μM).[147] Additionally, compound **3**, derived from compound **1** by cyclopentyl-to-cyclohexyl ring expansion (Figure 1.6), exhibited one of the highest potencies and selectivity over hERG (hERG IP = 7 μM; FT IC_{50} < 1 nM).[147] Other examples of structural modifications employed which have successfully diminished hERG activity include positional change of the carbonyl group, removal of the chlorine from the phenyl ring, *N*-methylation,[147] acetylation of the amino functionality, methylsulfonamide-to-ethylsulfonamide change,[148] trifluoromethylation of the phenyl ring,[149] *tert*-butyl-to-*sec*-butyl group conversion,[150] deletion of methyl groups,[151] and *ortho*-to-*para* positional change.[152] For additional examples, the reader is referred to the perspective article by Jamieson *et al*.[143]

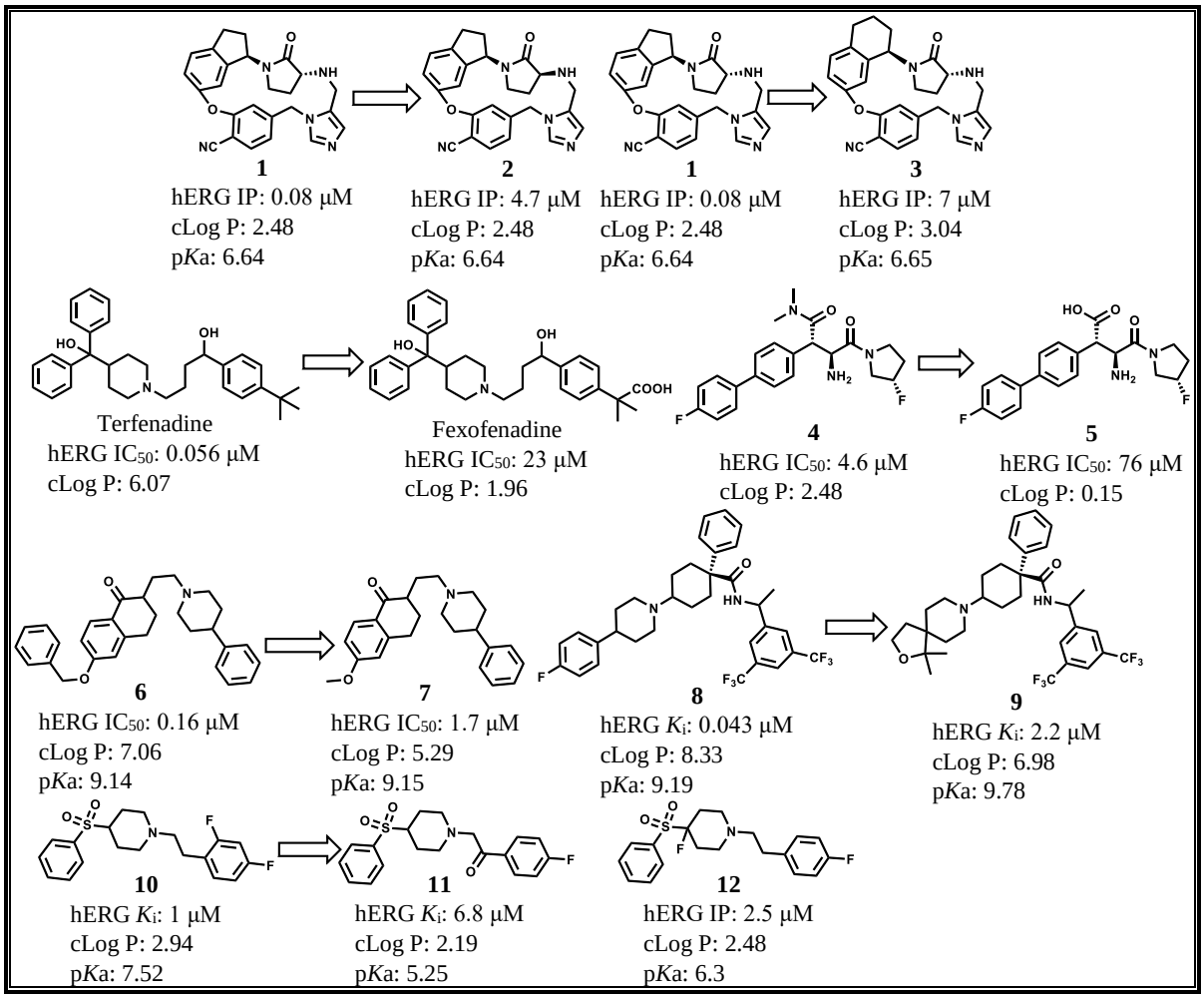

Figure 1.6: Examples of chemical modification approaches to diminish hERG activity.

1.9.2.2 Zwitterion Approach

Formation of zwitterions is also considered another approach to minimizing hERG activity. Such zwitterionic species are physically limited with respect to membrane permeability and, therefore, this prevents access of the drug molecule to the transmembrane binding site. Any potential interactions with hERG are, therefore, minimized. Unfortunately, the zwitterion approach has apparent shortfalls: Suboptimal oral bioavailability attributed to poor absorption.[153,154]

The story of terfenadine (Figure 1.6), a second-generation antihistamine, represents a very good example and one of the earliest applications of the zwitterion approach to minimize hERG activity. After its launch in 1982, post-marketing investigations implicated terfenadine in a few TdP-related cases. The elevated plasma concentrations of terfenadine, when administered concomitantly with food or drugs that inhibit CYP3A4 (cytochrome P450 3A4), were found to cause QT interval prolongation.[155] Although the US Food and Drug Administration (FDA)

issued a black box warning following incidents of cardiac side effects, cases of cardiac arrhythmia continued which led to the eventual withdrawal of terfenadine from the market 15 years after its launch. However, it was discovered that the carboxyl metabolite, which was later marketed as fexofenadine (Figure 1.6), was responsible for the therapeutic efficacy of terfenadine and demonstrated a substantially minimized hERG inhibition (IC_{50} = 23 μM) while displaying no effects on the QT interval. The zwitterionic nature of fexofenadine, which discourages membrane permeability and access to the intracellular cavity of the channel, could explain the reduced hERG binding.[143] Following these observations, the zwitterionic strategy has found application in many studies to detune hERG activity. The difference in hERG activity could also be explained by differences in the conformations of the two compounds as suggested by recent molecular modelling studies.[145]

In another approach, workers at Merck reported the generation of zwitterionic compounds which were virtually inactive on hERG. In their more recent work on biaryl-*β*-methylphenylalanine DPPIV (dipeptidyl peptidase IV) inhibitors,[156] the team generated the carboxylic acid-containing derivative **5** which was 16-fold less potent on hERG compared to the parent carboxamide **4** (Figure 1.6). However, as anticipated, oral bioavailability was compromised by 4-fold (cf. **5**, *F* = 16%; **4**, *F* = 67%). There are other examples, in literature, of the application of the zwitterionic approach where a carboxylic acid[153,157] or its bioisosteres[154] have been incorporated into the amino-containing parent molecule.

1.9.2.3 Control of Log P

Quite often, a positive correlation between hERG blocking and measures of lipophilicity such as log P is evident in SAR data. Such observations have been rationalised by evidence revealing the existence of a lipophilic ligand binding site in the hERG ion channel.[144,158] Therefore, interaction with the lipophilic binding site of the channel can be disrupted when the polarity of a drug molecule is increased. A number of optimization campaigns aimed at decreasing hERG activity have utilized this strategy.[143]

In one approach, workers at Bristol-Myers Squibb reported a significant improvement of selectivity over I_{Kr} following reduction of cLog P by eliminating a phenyl ring from the structure.[159] In this regard, when the phenyl ring in compound **6** (cLog P = 7.06, hERG IC_{50} = 0.16 μM, Figure 1.6) was deleted, the decrease in lipophilicity was accompanied by a nearly 11-fold reduction in hERG activity as shown in compound **7** (cLog P = 5.29, hERG IC_{50} = 1.7

μM, Figure 1.6).[159] A reduction in hERG accompanying such a molecular change is expected since a phenyl ring is considered a key pharmacophore for hERG potency.[143]

In another related strategy, Cooper *et al*.,[160] replaced the terminal fluorinated phenyl ring in an NK_1 (neurokinin-1) receptor antagonist **8** with a saturated spiroether system as shown in analogue **9** (Figure 1.6). Such a reduction in lipophilicity was accompanied by over 50-fold reduction in I_{Kr} activity with preservation of activity at the primary target. Many other studies have utilized the reduction of cLog P to minimize hERG activity. As summarized by Jamieson *et al*.,[143] these include installation of a carboxamide group,[157] introducing polar hydrogen-bonding groups,[150,161] deletion of the phenethyl group, replacing the naphthyl with a pyridyl or cyclohexyl group[162] and replacing the phenyl ring with a methyl group.[163]

1.9.2.4 Attenuation of p*K*a

Attenuation of p*K*a for drug candidates containing basic nitrogens is another approach to address hERG liabilities. A basic nitrogen moiety that is likely to be protonated at physiological pH is a common feature of many ligands that block the hERG channel.[143] The ligand binding affinity for such basic nitrogen-containing compounds is thought to be enhanced by the π-cation interactions between the protonated nitrogen of the amine and aromatic residues within the cavity of the hERG channel.[144,145] Therefore, the proportion of protonated molecules at physiological pH can substantially be reduced by lowering the p*K*a of a basic nitrogen with concomitant disruption of any putative π-cation interactions with the channel. Conversely, introduction of alkoxy/hydroxyl groups at the *β*-position relative to the amine may shield the protonatable centre thereby compromising the π-cation interactions and hence lowering affinity for hERG.[154]

In their attempts to optimize a series of compounds for the primary target (5-HT_{2A} receptor) while trying to improve selectivity over hERG, Fletcher and co-workers[164] identified compound **10** (Figure 1.6) which elicited an over 10% QT interval prolongation at doses of 3 and 10 mg/kg/h in the anesthetised ferret. Among various modifications made to diminish hERG activity, the installation of the ketone at *β* position relative to the amine (compound **11**, Figure 1.6) was accompanied by noteworthy success. A corresponding reduction in I_{Kr} activity was observed with such a p*K*a-reducing structural modification. As anticipated, the hERG optimized analogue was also devoid of QT-prolongation effects when administered at doses up to 10 mg/kg/h in the anesthetized ferret model. However, compound **11** could not be moved forward due to its instability in polar solvents such as methanol which was attributed to the

presence of the ketone moiety.[152] The authors then explored other means of attenuating the basicity without the involvement of the keto group. In this respect, the introduction of the fluorine into the piperidine ring resulted in the reduction of p*K*a and a concomitant reduction in hERG inhibition as reflected in analogue **12** (Figure 1.6) which was also devoid of QT prolongation in anesthetized dogs at plasma concentrations up to 148 μM.

1.10 Pharmacological Properties of Imidazopyridazines and Aminopyrazines

1.10.1 Imidazopyridazines

The imidazopyridazine scaffold is made up of the imidazo and the pyridazine ring systems fused together. This scaffold has been associated with various biological activities (see some examples in figure 1.7). For instance, imidazopyridazine compounds have shown potential application in the treatment of the common cold as demonstrated by their potent activity on a broad spectrum of rhinoviruses,[165] the most important aetiologic agents of the common cold.[166–170]

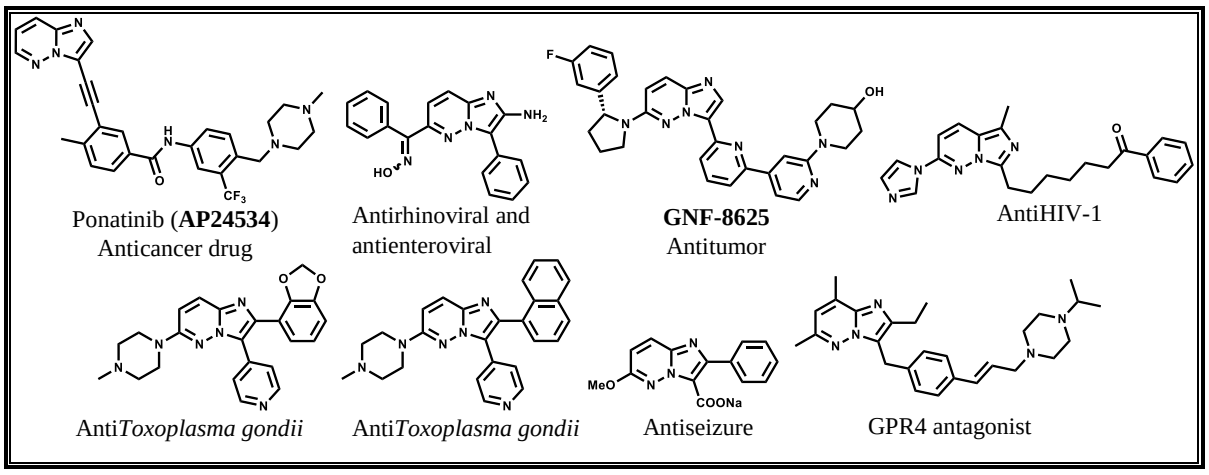

Figure 1.7: Examples of imidazopyridazines with various pharmacological properties.

Recently, five tyrosine kinase inhibitors have been approved for the treatment of cancers by the US FDA.[171] Amongst these new anticancer drugs is an imidazopyridazine-containing compound ponatinib (**AP24534**) which has been approved for the treatment of chronic, accelerated or blast-phase chronic myeloid leukaemia. Additionally, other imidazopyridazine compounds have been found to exhibit potent inhibition of different targets relevant to cancer including mTOR (mechanistic target of rapamycin),[172] PIM kinases,[173] TRK (tropomyosin receptor kinase) receptors,[174] PI3Ks (phosphatidylinositol 3-kinases)[175] and others.[176–181] Imidazopyridazines have also demonstrated promising antiHIV potential with highly potent

activity on the enzyme reverse transcriptase (RT) of HIV-1 as well as excellent potency in cellular assays.[182] Furthermore, imidazopyridazine derivatives possess a range of other pharmacological effects including anti*Toxoplasma gondii*,[183] antialzheimer,[184] antiHCV (hepatitis C virus),[185] antiseizure,[186] and antiinflammatory activities as well as potential to treat pain, autoimmune diseases and angiogenesis [G-protein coupled receptor 4 (GPR4) antagonists].[187]

1.10.2 Aminopyrazines

The aminopyrazine scaffold or its derivative is found in several clinically-established drugs (Figure 1.8). These include sulfalene (an antibacterial sulphonamide),[188] mirfentanil (a fentanyl analogue selective for the μ opioid receptor)[189] and amiloride the diuretic.[190]

A literature survey revealed that aminopyrazines have been extensively explored as anticancer agents. In a recent study, Osborne *et al*.,[191] have identified an oral anticancer pre-clinical candidate (**CCT245737**, Figure 1.8) targeting a kinase responsible for cell growth and division – the checkpoint kinase 1 (CHK1). Moreover, the preclinical candidate exhibited low predicted doses and exposures in humans, a characteristic which could mitigate other off-target activities such as hERG inhibition. In another recent article,[192] workers at AstraZeneca have employed a structure-guided approach to identify an irreversible mutant-EGFR (epidermal growth factor receptor) kinase inhibitor (Figure 1.8) which exhibited *in vivo* antitumor efficacy albeit liabilities with regard to other physical properties remained unresolved. Recently, and in a space of two years only (from 2013 to 2014), over 10 patents[193–200] on the application of aminopyrazines as anticancers targeting the ATR (ataxia telangiectasia and Rad3-related) kinase have been granted to researchers at Vertex Pharmaceuticals, Inc (USA). When tested *in vivo*, the most promising compound, **VE-822** (Figure 1.8), of this class demonstrated effective treatment of non-small cell lung cancer and pancreatic cancer.[201,202] Additionally, other studies have documented the pharmacological effects of aminopyrazines against different types of cancers.[203–207]

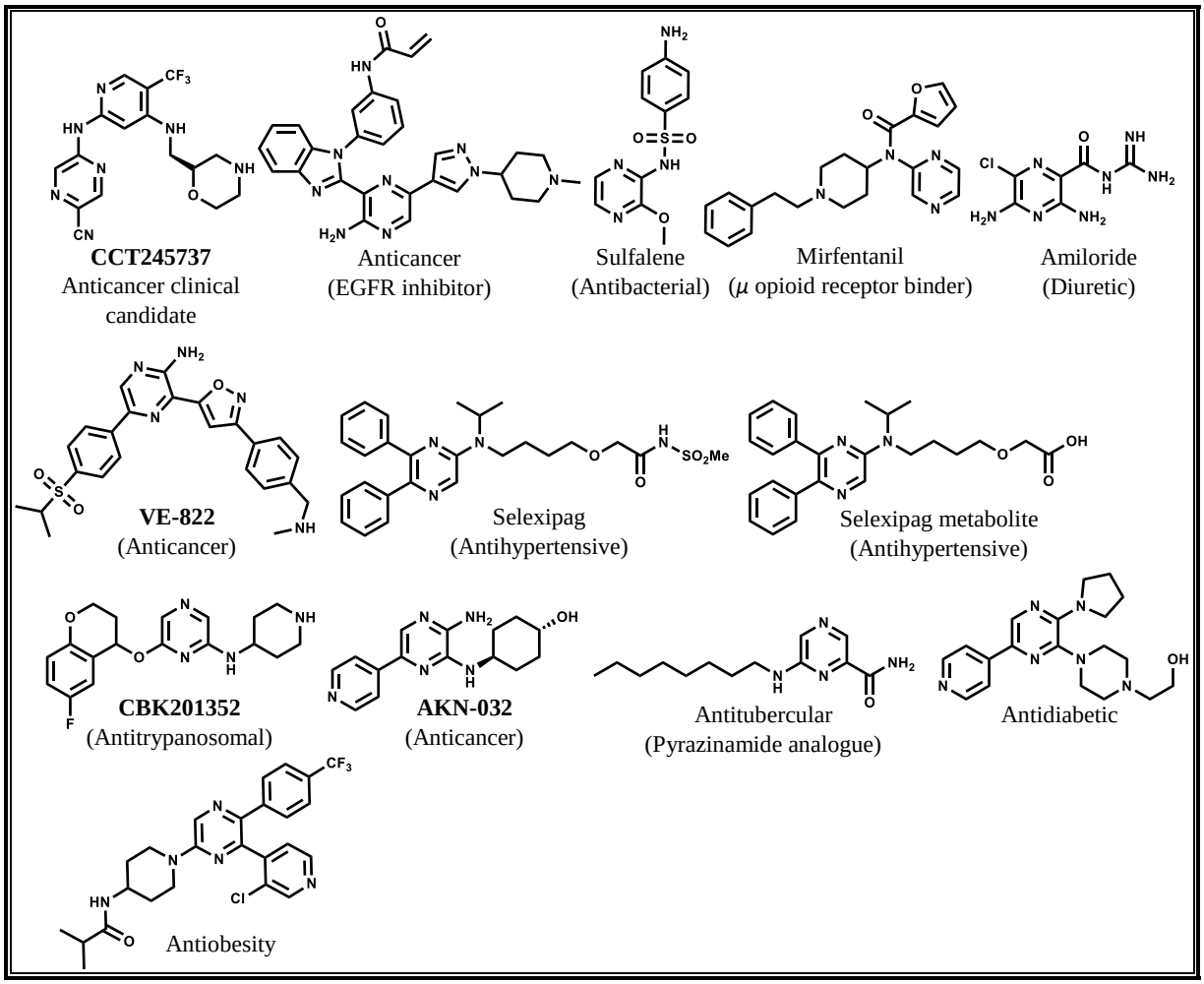

Figure 1.8: Examples of aminopyrazines with various pharmacological properties.

Aminopyrazines have also shown potential for treatment of cardiovascular diseases. Examples in this therapeutic area include the aminopyrazine drug, selexipag, (Figure 1.8) which is currently being developed as a pulmonary arterial antihypertensive.[208] Selexipag and its active metabolite are known to cause vasodilation in the pulmonary circulation by their agonist interaction at the PGI_2 (prostaglandin I2) receptor.[208] Other pharmacological properties exhibited by aminopyrazines include antitrypanosomal,[209] antitubercular,[210] antidiabetic,[211,212] and antiobesity[213] (see examples in figure 1.8). Additional applications of aminopyrazines, both as clinically established drugs and as early phase drug leads or clinical candidates, are documented in recent specialized reviews.[214,215]

1.11 Antimalarial Properties of Imidazopyridazines and Aminopyrazines

1.11.1 Imidazopyridazines

Although imidazopyridazines have been extensively explored in other disease indications such as cancer (see subsection 1.10.1), a literature search revealed only limited exploration of this chemotype with respect to antimalarial therapy. In an article published in 2016, Bhatt *et al.*,[216] have reported the antiplasmodial evaluation of two imidazopyridazine derivatives bearing substituents at positions 2 and 6 of the core-scaffold. The two identified analogues, **13** and **14** (Figure 1.9), only exhibited modest antiplasmodial activity – IC_{50} = 1.57 and 1.87 μM respectively against *P. falciparum* parasites. However, the authors did not state what parasite strain of *P. falciparum* was used in their assays. More recently, Bendjeddou and co-workers[217] have evaluated imidazopyridazines in biochemical assays involving a panel of kinases which included the *Plasmodium falciparum* Cdc2-like kinase 1 (*Pf*CLK1). In this study, the 3,6-disubstituted imidazopyridazine analogue **15** (Figure 1.9) was found to potently inhibit *Pf*CLK1 (IC_{50} = 0.032 μM). Nevertheless, cellular assays to assess the translatability of this potency were not performed.

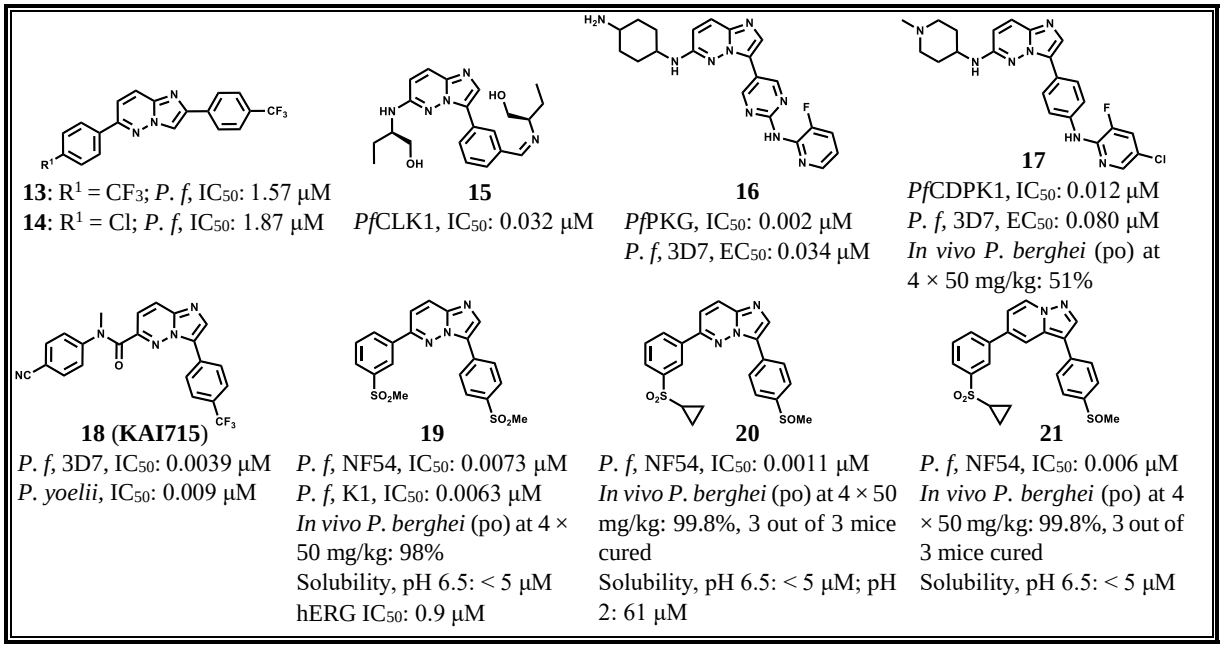

Figure 1.9: Examples of imidazopyridazines with antimalarial properties.

In another recent article, Green *et al.*,[218] have reported the antiplasmodial activity of 3,6-disubstirtuted imidazopyridazines. The authors reported imidazopyridazine analogues with potent activity in both the cyclic GMP (cGMP)-dependent protein kinase (PKG) inhibition assay and cellular assays. The authors further demonstrated that mutations in PKG resulted in

reduced potency of imidazopyridazines on this kinase. Similarly, reduced potency in cellular assays was observed when mutant strains bearing a modified PKG were used, further suggesting this class of molecules exert their activity primarily by inhibition of PKG. Compound **16** (Figure 1.9), a representative example, was highly potent against PKG (IC_{50} = 0.002 μM) and the plasmodium parasites 3D7 (EC_{50} = 0.034 μM).

In a structure-based approach, which employed a homology model of *Plasmodium falciparum* calcium-dependent protein kinase 1 (*Pf*CDPK1), Chapman and co-workers[219] have reported optimization of potency for a series of imidazopyridazines. Although the most promising compound, **17** (Figure 1.9), exhibited potent activity against *Pf*CDPK1 (IC_{50} = 0.012 μM) and whole-cell *P. falciparum* 3D7 parasites (EC_{50} = 0.080 μM), only modest *in vivo* efficacy (51% reduction in parasitemia at 4 × 50 mg/kg) was observed in the *P. berghei*-infected mouse model. Further exploration of imidazopyridazines as potent inhibitors of *Pf*CDPK1 has been reported in two other papers.[220,221]

Imidazopyridazines have also been shown to inhibit the malaria parasite kinase *P. falciparum* protein kinase 7 (*Pf*PK7). *Pf*PK7 represents an emerging malarial drug target which lacks a human homologue and is expressed at several stages of the parasite life cycle including both the sexual and asexual stages in man as well as in the mosquito.[222] Bouloc *et al.*,[223] have reported imidazopyridazine inhibitors of this enzyme whose whole-cell parasite inhibition was only modest. Furthermore, using quantitative structure-activity relationship (QSAR) as well as docking studies, Sahu and co-workers have further shed more light on the structural requirements for inhibitory activity of the imidazopyridazines on *Pf*PK7 and the amino acid residues involved in the imidazopyridazine-*Pf*PK7 enzyme interactions.[224,225]

In another notable study,[226] a group of researchers identified analogues, among them, an imidazopyridazine compound **18** (Figure 1.9) which exhibited activity on *P. falciparum* asexual blood stage 3D7 parasites (IC_{50} = 0.0039 μM) and liver-stage schizonts of the rodent parasite *P. yoelii* (IC_{50} = 0.009 μM). The authors also showed that this class of compounds exert their therapeutic effect by inhibitory interaction with the adenosine triphosphate (ATP)-binding pocket of a lipid kinase, phosphatidylinositol-4-OH kinase (PI4K).

More specifically, work on imidazopyridazines documented in this PhD thesis, was motivated by a series of recent studies undertaken by Le Manach *et al*[119,227,228] where promising diaryl-imidazopyridazines demonstrating *in vivo* efficacy where plagued by poor solubility and a hERG inhibition liability. This series of imidazopyridazines, named SFK52, was identified

from a recent high throughput screening (HTS) campaign of a commercial SoftFocus kinase library.[229] Amongst the 488 diaryl-imidazopyridazines identified, 153 compounds exhibited > 80% inhibition at the screening concentration of 1.82 μM.[227] Medicinal chemistry optimization of the most promising analogues led to the identification of a highly potent lead **19** (Figure 1.9) against both the multidrug resistant, K1 (IC_{50} = 0.0063 μM) and the drug sensitive, NF54 (IC_{50} = 0.0073 μM) strains of *P. falciparum* parasites along with good metabolic stability. In the *in vivo* model of *P. berghei*-infected mice, **19** demonstrated a relatively impressive 98% suppression of parasitemia at an oral dose of 4 × 50 mg/kg. At much lower doses (4 × 1.4 mg/kg and 4 × 15 mg/kg), the lead compound **19** was somewhat ineffective although it exhibited very good potency (90% suppression in parasitemia) in the *P. falciparum* humanised SCID mouse model at a dose of 4 × 1.5 mg/kg. Additionally, compound **19** exhibited poor aqueous solubility (< 5 μM at pH 6.5) and a serious hERG liability (IC_{50} = 0.9 μM).[227]

In an attempt to address the solubility issue and hERG inhibition risk while maintaining potency and metabolic stability, further SAR explorations were undertaken resulting in the identification of analogue **20** (Figure 1.9).[119] This analogue represented the first derivative of this imidazopyridazine series to demonstrate complete cure at an oral dose of 4 × 50 mg/kg. At much lower doses, 4 × 10 mg/kg and 4 × 3 mg/kg, reduction of parasitemia was quite significant, 99.6 and 98% respectively. Regrettably, hERG inhibition studies revealed that the sulfoxide-to-sulfone metabolism of **20** gave a sulfone metabolite which was highly active in the hERG assay (IC_{50} = 0.4 μM). Consequently, the prodrug sulfoxide **20** was considered to carry a potential hERG inhibition risk due to anticipated biotransformation *in vivo*. Moreover, its aqueous solubility remained sub-optimal at pH 6.5 (< 5 μM) albeit a slight improvement was observed at lower pH (61 μM at pH 2).[119] In a more recent paper,[228] analogue **20** was scaffold-hoped to give a pyrazolopyridine lead **21** (Figure 1.9) with the two substituents on the two phenyl rings being retained. It was hoped such a modification would improve selectivity over hERG, pharmacokinetics and *in vivo* efficacy. Unfortunately, the scaffold-hoped analogue still retained a hERG liability and sub-optimal solubility (< 5 μM) despite being able to completely cure *P. berghei*-infected mice at oral doses of 4 × 50 mg/kg.

In this project, other strategies of mitigating hERG liability and improving solubility while trying to maintain good *in vitro* activity, metabolic stability as well as *in vivo* efficacy for this class of molecules were further explored.

1.11.2 Aminopyrazines

Apart from two published papers[74,230], there is no literature precedence with respect to exploration of aminopyrazines as antimalarial agents. Work on aminopyrazines in this thesis was motivated by the impressive antimalarial properties of the 3,5-diaryl-2-aminopyrazines reported in the above mentioned papers. A schematic representation of a series of medicinal chemistry optimization steps which led to the identification of potent aminopyrazines is captured in figure 1.10. Using an image-based assay,[231] a HTS performed on 36,608 compounds from a commercial SoftFocus kinase library[232] identified 442 compounds which exhibited > 50% inhibition of both the 3D7 and Dd2 *P. falciparum* strains at a test concentration of 1.82 μM.[63] The 3,5-diaryl-2-aminopyridine compound, **22** (Figure 1.10), which was amongst the most potent hits exhibiting > 80% inhibition at the screening concentration of 1.82 μM was chosen as a starting point for further medicinal chemistry optimization programmes. Despite being potent *in vitro* against both the NF54 and K1 *P. falciparum* strains (IC_{50} = 0.049 μM), the hit compound only demonstrated moderate metabolic stability with a projected hepatic extraction ratio (E_H) of 0.48 when tested in human liver microsomes. Accordingly, the authors did not anticipate good performance *in vivo* for this metabolically labile compound. In their efforts to address this liability, the authors replaced the methoxyphenyl moiety with the methoxypyridyl group leading to the identification of compound **23** (Figure 1.10) with preserved *in vitro* antiplasmodial potency (NF54 and K1, IC_{50} = 0.051 μM) and improved metabolic stability (E_H = 0.26). Compound **23** also cured animals when administered orally at a dose of 50 mg/kg in a standard Peters test.

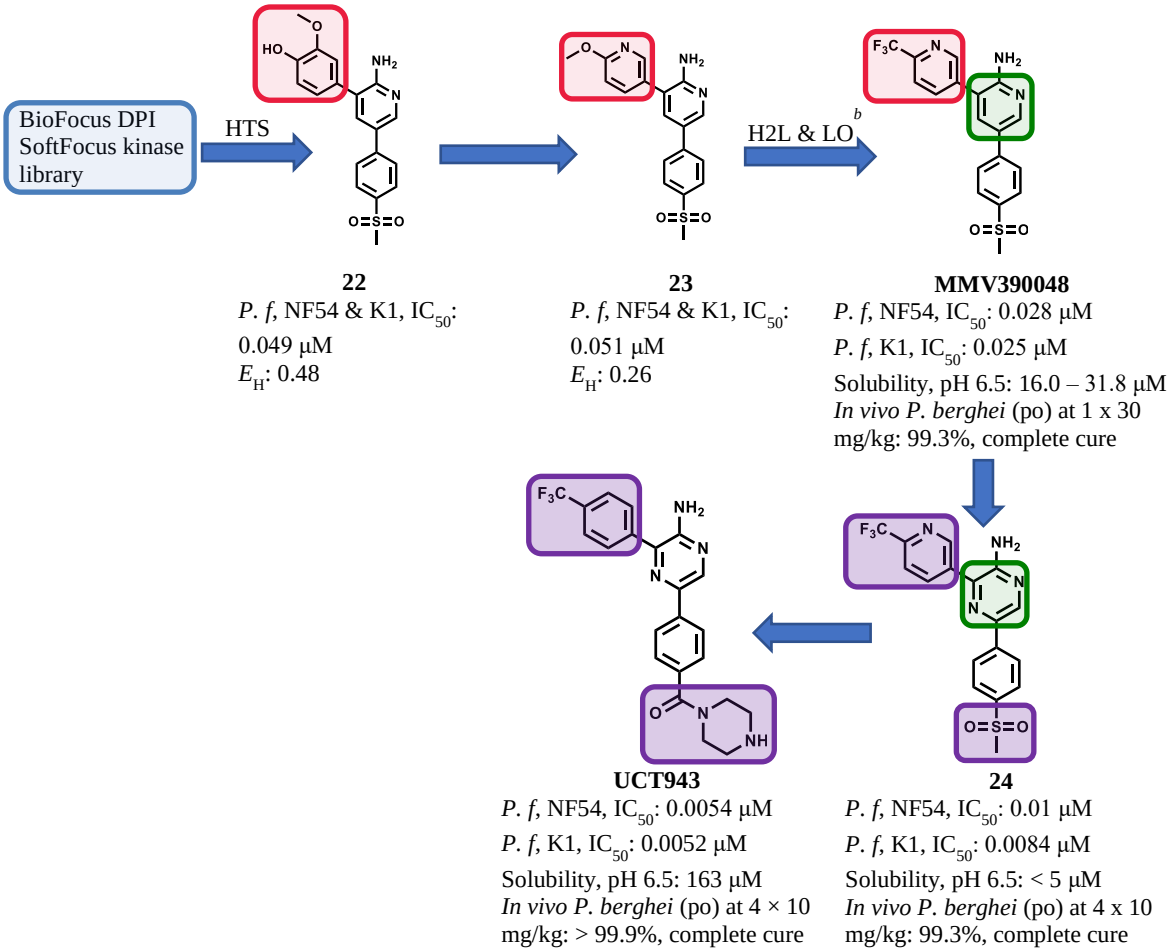

Figure 1.10: A schematic of medicinal chemistry optimization leading to identification of antimalarial aminopyrazines.
[b]H2L, hit to lead; LO, lead optimization.

The encouraging result demonstrated by compound **23** prompted a hit to lead (H2L) and lead optimization (LO) campaign which culminated in the identification of the clinical candidate **MMV390048** (Figure 1.10). This aminopyridine compound was highly potent *in vitro* across the NF54 and K1 parasite strains [IC_{50}: (K1) = 0.025 µM; (NF54) = 0.028 µM] and completely cured *P. berghei*-infected mice with a single oral dose of 30 mg/kg. As pointed out earlier in section 1.6, **MMV390048** successfully completed phase I studies and is currently undergoing phase II proof-of-concept studies in *P. vivax*- and *P. falciparum*-infected patients.[66] Unfortunately, the solubilities of **MMV390048** (16.0 – 31.8 µM, pH 6.5)[63] and an aminopyrazine analogue **24** (< 5 µM, pH 6.5), which was identified in later studies[74,230] via a scaffold-hoping approach, have remained sub-optimal which might pose challenges during development. Interestingly, chemical-modification-based solubility optimization strategies employed in later studies[74] led to the identification of a second-generation pre-clinical candidate **UCT943** with improved aqueous solubility at pH 6.5 (163 µM) (Figure 1.10).

UCT943 has a combination of improved solubility, good efficacy and pharmacokinetics as well as good selectivity over hERG channel inhibition. Preclinical safety assessment of **UCT943** was scheduled to be completed by end of 2017.[233]

1.12 Research Programme

1.12.1 Justification of the Study

The exploration of imidazopyridazines and aminopyrazines as potential novel antimalarial therapies is warranted for several reasons. Firstly, once effective and cheap treatment regimens such as chloroquine and sulfadoxine-pyrimethamine have been beset by emergence of widespread resistance which has hampered malaria control and eradication.[234–237] Secondly, although the current standard of first line malaria treatment, the ACTs, has been remarkably effective, resistance to artemisinin in the Thai-Cambodia and Thai-Myanmar border regions has been reported.[45–47] Additionally, in some countries, resistance to partner drugs such as amodiaquine has already been observed.[44] Therefore, because drug resistance seems an inevitable outcome of antimalarial chemotherapy, there is a critical need to continuously replenish the drug development pipeline with new antimalarial drug candidates with structurally diverse and novel chemical scaffolds.

Thirdly, the malaria eradication agenda requires new therapies which can: deliver a single dose radical cure to simplify treatment; target parasite development at multiple stages; be administered to a wide range of patient populations. The new therapies also need to demonstrate zero propensity to development of resistance. Current treatment options are far from this ideal TPP. Therefore, efforts towards the development of such an ideal medicine need to continue.

Fourthly, imidazopyridazines and aminopyrazines are a new antimalarial chemotype which could offer an opportunity to target the malaria parasite through novel mechanisms of action. Therefore, these chemotypes could potentially be less prone to resistance mechanisms that have rendered current drugs ineffective.

Lastly, as detailed in section 1.10, imidazopyridazines and aminopyrazines have exhibited a wide range of pharmacological properties. Thus, the imidazopyridazine and aminopyrazine scaffolds have proven potential to pharmacologically interfere with a wide range of pathogens as well as non-communicable diseases. Therefore, further investigations into these two classes of chemotypes as novel antimalarial agents is warranted. Investigations into the aminopyrazine

class was motivated by the need to identify second-generation analogues with improved physicochemical properties (mainly solubility). On the other hand, the imidazopyridazine aspect of this project was meant to design analogues devoid of the hERG liability with improved solubility which have been identified as the two major issues in recent studies.[119,227,228]

1.12.2 Research Question

The research question is whether it will be possible to identify antimalarial imidazopyridazine and aminopyrazine analogues with favourable safety, physico-chemical and drug metabolism and pharmacokinetic (DMPK) properties.

1.12.3 Objective

To utilise imidazopyridazines and aminopyrazines as templates for the design and synthesis of potential novel antimalarial agents.

1.12.4 Specific Aims

i) To synthesise various analogues of imidazopyridazines and aminopyrazines and study their *in vitro* antiplasmodial structure-activity relationship.
ii) To profile the synthesized analogues with respect to solubility, cytotoxicity and hERG inhibition *in vitro*.
iii) To investigate factors influencing solubility and deduce relationships.
iv) To evaluate potent, non-cytotoxic, hERG-de-risked and metabolically stable compounds for *in vivo* efficacy and pharmacokinetics.

1.13 References

(1) Fagan, T. When was malaria first discovered and by whom? How is the disease transmitted? What are its effects? https://www.scientificamerican.com/article/when-was-malaria-first-di/. Accessed: 2018-03-23. (Archived by WebCite® at http://www.webcitation.org/6y7zSqwoX).

(2) Malaria: Introduction. https://www.infoplease.com/science/health-and-body/malaria-introduction. Accessed: 2018-03-23. (Archived by WebCite® at http://www.webcitation.org/6y84bwVLk).

(3) The History of Malaria, an Ancient Disease. https://www.cdc.gov/malaria/about/history/. Accessed: 2018-03-23. (Archived by WebCite® at http://www.webcitation.org/6y88vbTkE).

(4) Nerlich, A. G.; Schraut, B.; Dittrich, S.; Jelinek, T.; Zink, A. R. Plasmodium Falciparum in Ancient Egypt. *Emerg. Infect. Dis.* **2008**, *14*, 1317–1319.

(5) Liu, W.; Li, Y.; Learn, G. H.; Rudicell, R. S.; Robertson, J. D.; Keele, B. F.; Ndjango, J.-B. N.; Sanz, C. M.; Morgan, D. B.; Locatelli, S.; Gonder, M. K.; Kranzusch, P. J.; Walsh, P. D.; Delaporte, E.; Mpoudi-Ngole, E.; Georgiev, A. V.; Muller, M. N.; Shaw, G. M.; Peeters, M.; Sharp, P. M.; Rayner, J. C.; Hahn, B. H. Origin of the Human Malaria Parasite Plasmodium Falciparum in Gorillas. *Nature.* **2010**, *467*, 420–425.

(6) Wolfe, N. D.; Dunavan, C. P.; Diamond, J. Origins of Major Human Infectious Diseases. *Nature.* **2007**, *447*, 279–283.

(7) *World Health Organization World Malaria Report*; 2017.

(8) Murray, C. J.; Rosenfeld, L. C.; Lim, S. S.; Andrews, K. G.; Foreman, K. J.; Haring, D.; Fullman, N.; Naghavi, M.; Lozano, R.; Lopez, A. D. Global Malaria Mortality between 1980 and 2010: A Systematic Analysis. *The Lancet.* **2012**, *379*, 413–431.

(9) Malaria. http://www.who.int/mediacentre/factsheets/fs094/en/. Accessed: 2018-03-25. (Archived by WebCite® at http://www.webcitation.org/6yBHHafCR).

(10) White, N. J. Plasmodium Knowlesi: The Fifth Human Malaria Parasite. *Clin. Infect. Dis.* **2008**, *46*, 172–173.

(11) Guerra, C. A.; Gikandi, P. W.; Tatem, A. J.; Noor, A. M.; Smith, D. L.; Hay, S. I.; Snow, R. W. The Limits and Intensity of Plasmodium Falciparum Transmission: Implications for Malaria Control and Elimination Worldwide. *PLoS Med.* **2008**, *5*, e38.

(12) Snow, R. W.; Guerra, C. A.; Noor, A. M.; Myint, H. Y.; Hay, S. I. The Global Distribution of Clinical Episodes of Plasmodium Falciparum Malaria. *Nature.* **2005**, *434*, 214–217.

(13) Price, R. N.; Tjitra, E.; Guerra, C. A.; Yeung, S.; White, N. J.; Anstey, N. M. Vivax Malaria: Neglected and Not Benign. *Am. J. Trop. Med. Hyg.* **2007**, *77*, 79–87.

(14) Breman, J. G. Eradicating Malaria. *Sci. Prog.* **2009**, *92*, 1–38.

(15) Breman, J. G. Malaria: Epidemiology, prevention, and control. https://www.uptodate.com/contents/malaria-epidemiology-prevention-and-control. Accessed: 2018-03-25. (Archived by WebCite® at http://www.webcitation.org/6yBJdd6rp).

(16) Burrows, J. N.; Duparc, S.; Gutteridge, W. E.; Hooft van Huijsduijnen, R.; Kaszubska, W.; Macintyre, F.; Mazzuri, S.; Möhrle, J. J.; Wells, T. N. C. New Developments in Anti-Malarial Target Candidate and Product Profiles. *Malar. J.* **2017**, *16*, 26–29.

(17) Trager, W.; Jensen, J. Human Malaria Parasites in Continuous Culture. *Science.* **1976**, *193*, 673–675.

(18) About Malaria: Biology. https://www.cdc.gov/malaria/about/biology/index.html. Accessed: 2018-03-28. (Archived by WebCite® at http://www.webcitation.org/6yFgts13H).

(19) Sadasivaiah, S.; Tozan, Y.; Breman, J. G. Dichlorodiphenyltrichloroethane (DDT) for Indoor Residual Spraying in Africa: How Can It Be Used for Malaria Control? *Am. J. Trop. Med. Hyg.* **2007**, *77*, 249–263.

(20) Roberts, D. R.; Alecrim, W. D. Behavioral Response of Anopheles Darlingi to DDT-Sprayed House Walls in Amazonia. *Bull. Pan Am. Health Organ.* **1991**, *25*, 210–217.

(21) Giglioli, G. Changes in the Pattern of Mortality Following the Eradication of Hyperendemic Malaria from a Highly Susceptible Community. *Bull. World Health Organ.* **1972**, *46*, 181–202.

(22) Maharaj, R.; Mthembu, D. J.; Sharp, B. L. Impact of DDT Re-Introduction on Malaria Transmission in KwaZulu-Natal. *S. Afr. Med. J.* **2005**, *95*, 871–874.

(23) Curtis, C. F. Integrated Vector Management for Malaria. In *Integrated Pest Management*; Radcliffe, E., Ed.; Cambridge University Press: Cambridge, 2008.

(24) Walshe, D. P.; Garner, P.; Adeel, A. A.; Pyke, G. H.; Burkot, T. R. Larvivorous Fish for Preventing Malaria Transmission. *Cochrane database Syst. Rev.* **2017**, *12*, CD008090.

(25) Ghosh, S. K.; Tiwari, S. N.; Sathyanarayan, T. S.; Sampath, T. R. R.; Sharma, V. P.; Nanda, N.; Joshi, H.; Adak, T.; Subbarao, S. K. Larvivorous Fish in Wells Target the Malaria Vector Sibling Species of the Anopheles Culicifacies Complex in Villages in Karnataka, India. *Trans. R. Soc. Trop. Med. Hyg.* **2005**, *99*, 101–105.

(26) Yapabandara, A. M.; Curtis, C. F.; Wickramasinghe, M. B.; Fernando, W. P. Control of

Malaria Vectors with the Insect Growth Regulator Pyriproxyfen in a Gem-Mining Area in Sri Lanka. *Acta Trop.* **2001**, *80*, 265–276.

(27) Andreasen, M. H.; Curtis, C. F. Optimal Life Stage for Radiation Sterilization of Anopheles Males and Their Fitness for Release. *Med. Vet. Entomol.* **2005**, *19*, 238–244.

(28) Klassen, W.; Curtis, C. F. History of the Sterile Insect Technique (SIT). In *The Sterile Insect Technique: Principles and Practice in Area-wide Integrated Pest Management*; Dyck, V. A., Hendrichs, L., Robinson, A. S., Eds.; Springer: Heidelberg, Germany, 2005; p 3.

(29) Malaria Prophylaxis. https://www.malariasite.com/prophylaxis/. Accessed: 2018-03-31. (Archived by WebCite® at http://www.webcitation.org/6yKXz1mM0).

(30) Malaria vaccine development. http://www.who.int/malaria/areas/vaccine/en/. Accessed: 2018-04-01. (Archived by WebCite® at http://www.webcitation.org/6yLkZtWpq).

(31) Eisele, T. P.; Bennett, A.; Silumbe, K.; Finn, T. P.; Chalwe, V.; Kamuliwo, M.; Hamainza, B.; Moonga, H.; Kooma, E.; Chizema Kawesha, E.; Yukich, J.; Keating, J.; Porter, T.; Conner, R. O.; Earle, D.; Steketee, R. W.; Miller, J. M. Short-Term Impact of Mass Drug Administration With Dihydroartemisinin Plus Piperaquine on Malaria in Southern Province Zambia: A Cluster-Randomized Controlled Trial. *J. Infect. Dis.* **2016**, *214*, 1831–1839.

(32) Björkman, A.; Cook, J.; Sturrock, H.; Msellem, M.; Ali, A.; Xu, W.; Molteni, F.; Gosling, R.; Drakeley, C.; Mårtensson, A. Spatial Distribution of Falciparum Malaria Infections in Zanzibar: Implications for Focal Drug Administration Strategies Targeting Asymptomatic Parasite Carriers. *Clin. Infect. Dis.* **2017**, *64*, 1236–1243.

(33) Wongsrichanalai, C.; Pickard, A. L.; Wernsdorfer, W. H.; Meshnick, S. R. Epidemiology of Drug-Resistant Malaria. *Lancet Infect. Dis.* **2002**, *2*, 209–218.

(34) Payne, D. Did Medicated Salt Hasten the Spread of Chloroquine Resistance in Plasmodium Falciparum? *Parasitol. Today.* **1988**, *4*, 112–115.

(35) Packard, R. M. The Origins of Antimalarial-Drug Resistance. *N. Engl. J. Med.* **2014**, *371*, 397–399.

(36) White, N. J. The Treatment of Malaria. *N. Engl. J. Med.* **1996**, *335*, 800–806.

(37) Daily, J. Treatment of uncomplicated falciparum malaria in nonpregnant adults and children. https://www.uptodate.com/contents/treatment-of-uncomplicated-falciparum-malaria-in-nonpregnant-adults-and-children?topicRef=5702&source=related_link. Accessed: 2018-04-02. (Archived by WebCite® at http://www.webcitation.org/6yNKNTOp8).

(38) WHO Guidelines for the Treatment of Malaria. 2nd Edition, 2010, World Health Organization.

(39) Crawley, J.; Chu, C.; Mtove, G.; Nosten, F. Malaria in Children. *The Lancet.* **2010**, *375*, 1468–1481.

(40) World Health Organization; Global Malaria Program. Updated WHO Policy Recommendation (October 2012): Intermittent Preventive Treatment of Malaria in Pregnancy Using Sulfadoxine-Pyrimethamine (IPTp-SP). Geneva, Switzerland: World Health Organization; 2012.

(41) World Health Organization. Guidelines for the Treatment of Malaria, 3rd Ed, WHO, Geneva 2015.

(42) Chico, R. M.; Chaponda, E. B.; Ariti, C.; Chandramohan, D. Sulfadoxine-Pyrimethamine Exhibits Dose-Response Protection Against Adverse Birth Outcomes Related to Malaria and Sexually Transmitted and Reproductive Tract Infections. *Clin. Infect. Dis.* **2017**, *64*, 1043–1051.

(43) Anthony, M. P.; Burrows, J. N.; Duparc, S.; JMoehrle, J.; Wells, T. N. The Global Pipeline of New Medicines for the Control and Elimination of Malaria. *Malar. J.* **2012**, *11*, 316.

(44) Folarin, O. A.; Bustamante, C.; Gbotosho, G. O.; Sowunmi, A.; Zalis, M. G.; Oduola, A. M. J.; Happi, C. T. In Vitro Amodiaquine Resistance and Its Association with Mutations in Pfcrt and Pfmdr1 Genes of Plasmodium Falciparum Isolates from Nigeria. *Acta Trop.* **2011**, *120*, 224–230.

(45) Dondorp, A. M.; Yeung, S.; White, L.; Nguon, C.; Day, N. P. J.; Socheat, D.; von Seidlein, L. Artemisinin Resistance: Current Status and Scenarios for Containment. *Nat. Rev. Microbiol.* **2010**, *8*, 272–280.

(46) Rueangweerayut, R.; Phyo, A. P.; Uthaisin, C.; Poravuth, Y.; Binh, T. Q.; Tinto, H.; Pénali, L. K.; Valecha, N.; Tien, N. T.; Abdulla, S.; Borghini-Fuhrer, I.; Duparc, S.; Shin, C.-S.; Fleckenstein, L. Pyronaridine–Artesunate versus Mefloquine plus Artesunate for Malaria. *N. Engl. J. Med.* **2012**, *366*, 1298–1309.

(47) Phyo, A. P.; Nkhoma, S.; Stepniewska, K.; Ashley, E. A.; Nair, S.; McGready, R.; ler Moo, C.; Al-Saai, S.; Dondorp, A. M.; Lwin, K. M.; Singhasivanon, P.; Day, N. P.; White, N. J.; Anderson, T. J.; Nosten, F. Emergence of Artemisinin-Resistant Malaria on the Western Border of Thailand: A Longitudinal Study. *The Lancet.* **2012**, *379*, 1960–1966.

(48) Antimalarial Drugs. https://www.malariasite.com/malaria-drugs/. Accessed: 2018-04-

06. (Archived by WebCite® at http://www.webcitation.org/6yTH96GYT).

(49) Warhurst, D. C. Antimalarial Drugs An Update. *Drugs.* **1987**, *33*, 50–65.

(50) Global Portfolio of Antimalarial Medicines. https://www.mmv.org/research-development/mmv-supported-projects. Accessed: 2018-04-07. (Archived by WebCite® at http://www.webcitation.org/6yUyYnxCL).

(51) Wells, T. N. C.; van Huijsduijnen, R. H.; Van Voorhis, W. C. Malaria Medicines: A Glass Half Full? *Nat. Rev. Drug Discov.* **2015**, *14*, 424–442.

(52) Bolchoz, L. J.; Budinsky, R. A.; McMillan, D. C.; Jollow, D. J. Primaquine-Induced Hemolytic Anemia: Formation and Hemotoxicity of the Arylhydroxylamine Metabolite 6-Methoxy-8-Hydroxylaminoquinoline. *J. Pharmacol. Exp. Ther.* **2001**, *297*, 509–515.

(53) Llanos-Cuentas, A.; Lacerda, M. V; Rueangweerayut, R.; Krudsood, S.; Gupta, S. K.; Kochar, S. K.; Arthur, P.; Chuenchom, N.; Möhrle, J. J.; Duparc, S.; Ugwuegbulam, C.; Kleim, J.-P.; Carter, N.; Green, J. A.; Kellam, L. Tafenoquine plus Chloroquine for the Treatment and Relapse Prevention of Plasmodium Vivax Malaria (DETECTIVE): A Multicentre, Double-Blind, Randomised, Phase 2b Dose-Selection Study. *The Lancet.* **2014**, *383*, 1049–1058.

(54) Price, R. N.; Nosten, F. Single-Dose Radical Cure of Plasmodium Vivax : A Step Closer. *The Lancet.* **2014**, *383*, 1020–1021.

(55) Valecha, N.; Krudsood, S.; Tangpukdee, N.; Mohanty, S.; Sharma, S. K.; Tyagi, P. K.; Anvikar, A.; Mohanty, R.; Rao, B. S.; Jha, A. C.; Shahi, B.; Singh, J. P. N.; Roy, A.; Kaur, P.; Kothari, M.; Mehta, S.; Gautam, A.; Paliwal, J. K.; Arora, S.; Saha, N. Arterolane Maleate Plus Piperaquine Phosphate for Treatment of Uncomplicated Plasmodium Falciparum Malaria: A Comparative, Multicenter, Randomized Clinical Trial. *Clin. Infect. Dis.* **2012**, *55*, 663–671.

(56) Coteron, J. M.; Marco, M.; Esquivias, J.; Deng, X.; White, K. L.; White, J.; Koltun, M.; El Mazouni, F.; Kokkonda, S.; Katneni, K.; Bhamidipati, R.; Shackleford, D. M.; Angulo-Barturen, I.; Ferrer, S. B.; Jiménez-Díaz, M. B.; Gamo, F.-J.; Goldsmith, E. J.; Charman, W. N.; Bathurst, I.; Floyd, D.; Matthews, D.; Burrows, J. N.; Rathod, P. K.; Charman, S. A.; Phillips, M. A. Structure-Guided Lead Optimization of Triazolopyrimidine-Ring Substituents Identifies Potent Plasmodium Falciparum Dihydroorotate Dehydrogenase Inhibitors with Clinical Candidate Potential. *J. Med. Chem.* **2011**, *54*, 5540–5561.

(57) Rottmann, M.; McNamara, C.; Yeung, B. K. S.; Lee, M. C. S.; Zou, B.; Russell, B.; Seitz, P.; Plouffe, D. M.; Dharia, N. V.; Tan, J.; Cohen, S. B.; Spencer, K. R.; Gonzalez-

Paez, G. E.; Lakshminarayana, S. B.; Goh, A.; Suwanarusk, R.; Jegla, T.; Schmitt, E. K.; Beck, H.-P.; Brun, R.; Nosten, F.; Renia, L.; Dartois, V.; Keller, T. H.; Fidock, D. A.; Winzeler, E. A.; Diagana, T. T. Spiroindolones, a Potent Compound Class for the Treatment of Malaria. *Science.* **2010**, *329*, 1175–1180.

(58) Yeung, B. K. S.; Zou, B.; Rottmann, M.; Lakshminarayana, S. B.; Ang, S. H.; Leong, S. Y.; Tan, J.; Wong, J.; Keller-Maerki, S.; Fischli, C.; Goh, A.; Schmitt, E. K.; Krastel, P.; Francotte, E.; Kuhen, K.; Plouffe, D.; Henson, K.; Wagner, T.; Winzeler, E. A.; Petersen, F.; Brun, R.; Dartois, V.; Diagana, T. T.; Keller, T. H. Spirotetrahydro β-Carbolines (Spiroindolones): A New Class of Potent and Orally Efficacious Compounds for the Treatment of Malaria. *J. Med. Chem.* **2010**, *53*, 5155–5164.

(59) Leong, F. J.; Li, R.; Jain, J. P.; Lefèvre, G.; Magnusson, B.; Diagana, T. T.; Pertel, P. A First-in-Human Randomized, Double-Blind, Placebo-Controlled, Single- and Multiple-Ascending Oral Dose Study of Novel Antimalarial Spiroindolone KAE609 (Cipargamin) To Assess Its Safety, Tolerability, and Pharmacokinetics in Healthy Adult Volunteers. *Antimicrob. Agents Chemother.* **2014**, *58*, 6209–6214.

(60) White, N. J.; Pukrittayakamee, S.; Phyo, A. P.; Rueangweerayut, R.; Nosten, F.; Jittamala, P.; Jeeyapant, A.; Jain, J. P.; Lefèvre, G.; Li, R.; Magnusson, B.; Diagana, T. T.; Leong, F. J. Spiroindolone KAE609 for Falciparum and Vivax Malaria. *N. Engl. J. Med.* **2014**, *371*, 403–410.

(61) Cully, M. Next-Generation Antimalarial from Phenotypic Screen Shows Clinical Promise. *Nat. Rev. Drug Discov.* **2014**, *13*, 717–717.

(62) First-in-Human Study of an Oral Plasmodium Falciparum Plasma Membrane Protein Inhibitor. https://clinicaltrials.gov/ct2/show/NCT02661373. Accessed: 2018-04-11. (Archived by WebCite® at http://www.webcitation.org/6ybD7MnCN).

(63) Younis, Y.; Douelle, F.; Feng, T.-S.; Cabrera, D. G.; Le Manach, C.; Nchinda, A. T.; Duffy, S.; White, K. L.; Shackleford, D. M.; Morizzi, J.; Mannila, J.; Katneni, K.; Bhamidipati, R.; Zabiulla, K. M.; Joseph, J. T.; Bashyam, S.; Waterson, D.; Witty, M. J.; Hardick, D.; Wittlin, S.; Avery, V.; Charman, S. A.; Chibale, K. 3,5-Diaryl-2-Aminopyridines as a Novel Class of Orally Active Antimalarials Demonstrating Single Dose Cure in Mice and Clinical Candidate Potential. *J. Med. Chem.* **2012**, *55*, 3479–3487.

(64) Ghidelli-Disse, S.; Lafuente-Monasterio, M.; Waterson, D.; Witty, M.; Younis, Y.; Paquet, T.; Street, L. J.; Chibale, K.; Gamo-Benito, F.; Bantscheff, M.; Drewes, G. Identification of Plasmodium PI4 Kinase as Target of MMV390048 by

Chemoproteomics. *Malar. J.* **2014**, *13*, 38.

(65) MMV390048 and Its Antimalarial Activity Against Plasmodium Falciparum in Healthy Adult Subjects, Part B. https://clinicaltrials.gov/ct2/show/NCT02783833. Accessed: 2018-04-11. (Archived by WebCite® at http://www.webcitation.org/6ybGxA7Ev).

(66) MMV390048 POC in Patients With P. Vivax and P. Falciparum Malaria. Https://Clinicaltrials.Gov/Ct2/Show/NCT02880241. Accessed: 2018-05-09. (Archived by WebCite® at Http://Www.Webcitation.Org/6zICn3pDh).

(67) Nagelschmitz, J.; Voith, B.; Wensing, G.; Roemer, A.; Fugmann, B.; Haynes, R. K.; Kotecka, B. M.; Rieckmann, K. H.; Edstein, M. D. First Assessment in Humans of the Safety, Tolerability, Pharmacokinetics, and Ex Vivo Pharmacodynamic Antimalarial Activity of the New Artemisinin Derivative Artemisone. *Antimicrob. Agents Chemother.* **2008**, *52*, 3085–3091.

(68) Biot, C.; Nosten, F.; Fraisse, L.; Ter-Minassian, D.; Khalife, J.; Dive, D. The Antimalarial Ferroquine: From Bench to Clinic. *Parasite.* **2011**, *18*, 207–214.

(69) Supan, C.; Mombo-Ngoma, G.; Dal-Bianco, M. P.; Ospina Salazar, C. L.; Issifou, S.; Mazuir, F.; Filali-Ansary, A.; Biot, C.; Ter-Minassian, D.; Ramharter, M.; Kremsner, P. G.; Lell, B. Pharmacokinetics of Ferroquine, a Novel 4-Aminoquinoline, in Asymptomatic Carriers of Plasmodium Falciparum Infections. *Antimicrob. Agents Chemother.* **2012**, *56*, 3165–3173.

(70) Mzayek, F.; Deng, H.; Mather, F. J.; Wasilevich, E. C.; Liu, H.; Hadi, C. M.; Chansolme, D. H.; Murphy, H. A.; Melek, B. H.; Tenaglia, A. N.; Mushatt, D. M.; Dreisbach, A. W.; Lertora, J. J. L.; Krogstad, D. J. Randomized Dose-Ranging Controlled Trial of AQ-13, a Candidate Antimalarial, and Chloroquine in Healthy Volunteers. *PLoS Clin. Trials.* **2007**, *2*, e6.

(71) Nanayakkara, N. P. D.; Ager, A. L.; Bartlett, M. S.; Yardley, V.; Croft, S. L.; Khan, I. A.; McChesney, J. D.; Walker, L. A. Antiparasitic Activities and Toxicities of Individual Enantiomers of the 8-Aminoquinoline 8-[(4-Amino-1-Methylbutyl)Amino]-6-Methoxy-4-Methyl-5-[3,4-Dichlorophenoxy]Quinoline Succinate. *Antimicrob. Agents Chemother.* **2008**, *52*, 2130–2137.

(72) Peyton, D. Latter-Stage Preclinical Developmental Work on PL69/DM1157. *Malar. J.* **2014**, *13*, 70.

(73) Zhang, Y.-K.; Plattner, J. J.; Freund, Y. R.; Easom, E. E.; Zhou, Y.; Gut, J.; Rosenthal, P. J.; Waterson, D.; Gamo, F.-J.; Angulo-Barturen, I.; Ge, M.; Li, Z.; Li, L.; Jian, Y.; Cui, H.; Wang, H.; Yang, J. Synthesis and Structure–activity Relationships of Novel

Benzoxaboroles as a New Class of Antimalarial Agents. *Bioorg. Med. Chem. Lett.* **2011**, *21*, 644–651.

(74) Le Manach, C.; Nchinda, A. T.; Paquet, T.; Gonzàlez Cabrera, D.; Younis, Y.; Han, Z.; Bashyam, S.; Zabiulla, M.; Taylor, D.; Lawrence, N.; White, K. L.; Charman, S. A.; Waterson, D.; Witty, M. J.; Wittlin, S.; Botha, M. E.; Nondaba, S. H.; Reader, J.; Birkholtz, L.-M.; Jiménez-Díaz, M. B.; Martínez, M. S.; Ferrer, S.; Angulo-Barturen, I.; Meister, S.; Antonova-Koch, Y.; Winzeler, E. A.; Street, L. J.; Chibale, K. Identification of a Potential Antimalarial Drug Candidate from a Series of 2-Aminopyrazines by Optimization of Aqueous Solubility and Potency across the Parasite Life Cycle. *J. Med. Chem.* **2016**, *59*, 9890–9905.

(75) Powles, M. A.; Allocco, J.; Yeung, L.; Nare, B.; Liberator, P.; Schmatz, D. MK-4815, a Potential New Oral Agent for Treatment of Malaria. *Antimicrob. Agents Chemother.* **2012**, *56*, 2414–2419.

(76) First-in-Human Trial of Single Ascending Dose, Multiple Ascending Dose and Malaria Challenge Model in Healthy Subjects. https://clinicaltrials.gov/ct2/show/NCT03261401. . 2018-04-12. URL:https://clinicaltrials.gov/ct2/show/NCT03261401. Accessed: 2018-04-12. (Archived by WebCite® at http://www.webcitation.org/6ycykHu2X).

(77) Hameed, S.; Solapure, S.; Patil, V.; Henrich, P. P.; Magistrado, P. A.; Bharath, S.; Murugan, K.; Viswanath, P.; Puttur, J.; Srivastava, A.; Bellale, E.; Panduga, V.; Shanbag, G.; Awasthy, D.; Landge, S.; Morayya, S.; Koushik, K.; Saralaya, R.; Raichurkar, A.; Rautela, N.; Roy Choudhury, N.; Ambady, A.; Nandishaiah, R.; Reddy, J.; Prabhakar, K. R.; Menasinakai, S.; Rudrapatna, S.; Chatterji, M.; Jiménez-Díaz, M. B.; Martínez, M. S.; Sanz, L. M.; Coburn-Flynn, O.; Fidock, D. A.; Lukens, A. K.; Wirth, D. F.; Bandodkar, B.; Mukherjee, K.; McLaughlin, R. E.; Waterson, D.; Rosenbrier-Ribeiro, L.; Hickling, K.; Balasubramanian, V.; Warner, P.; Hosagrahara, V.; Dudley, A.; Iyer, P. S.; Narayanan, S.; Kavanagh, S.; Sambandamurthy, V. K. Triaminopyrimidine Is a Fast-Killing and Long-Acting Antimalarial Clinical Candidate. *Nat. Commun.* **2015**, *6*, 6715.

(78) Pegoraro, S.; Duffey, M.; Otto, T. D.; Wang, Y.; Rösemann, R.; Baumgartner, R.; Fehler, S. K.; Lucantoni, L.; Avery, V. M.; Moreno-Sabater, A.; Mazier, D.; Vial, H. J.; Strobl, S.; Sanchez, C. P.; Lanzer, M. SC83288 Is a Clinical Development Candidate for the Treatment of Severe Malaria. *Nat. Commun.* **2017**, *8*, 14193.

(79) Leong, F. J.; Zhao, R.; Zeng, S.; Magnusson, B.; Diagana, T. T.; Pertel, P. A First-in-

Human Randomized, Double-Blind, Placebo-Controlled, Single- and Multiple-Ascending Oral Dose Study of Novel Imidazolopiperazine KAF156 To Assess Its Safety, Tolerability, and Pharmacokinetics in Healthy Adult Volunteers. *Antimicrob. Agents Chemother.* **2014**, *58*, 6437–6443.

(80) Abbat, S.; Jain, V.; Bharatam, P. V. Origins of the Specificity of Inhibitor P218 toward Wild-Type and Mutant Pf DHFR: A Molecular Dynamics Analysis. *J. Biomol. Struct. Dyn.* **2015**, *33*, 1913–1928.

(81) Le Bihan, A.; de Kanter, R.; Angulo-Barturen, I.; Binkert, C.; Boss, C.; Brun, R.; Brunner, R.; Buchmann, S.; Burrows, J.; Dechering, K. J.; Delves, M.; Ewerling, S.; Ferrer, S.; Fischli, C.; Gamo–Benito, F. J.; Gnädig, N. F.; Heidmann, B.; Jiménez-Díaz, M. B.; Leroy, D.; Martínez, M. S.; Meyer, S.; Moehrle, J. J.; Ng, C. L.; Noviyanti, R.; Ruecker, A.; Sanz, L. M.; Sauerwein, R. W.; Scheurer, C.; Schleiferboeck, S.; Sinden, R.; Snyder, C.; Straimer, J.; Wirjanata, G.; Marfurt, J.; Price, R. N.; Weller, T.; Fischli, W.; Fidock, D. A.; Clozel, M.; Wittlin, S. Characterization of Novel Antimalarial Compound ACT-451840: Preclinical Assessment of Activity and Dose–Efficacy Modeling. *PLOS Med.* **2016**, *13*, e1002138.

(82) Shafiq, N.; Rajagopalan, S.; Kushwaha, H. N.; Mittal, N.; Chandurkar, N.; Bhalla, A.; Kaur, S.; Pandhi, P.; Puri, G. D.; Achuthan, S.; Pareek, A.; Singh, S. K.; Srivastava, J. S.; Gaur, S. P. S.; Malhotra, S. Single Ascending Dose Safety and Pharmacokinetics of CDRI-97/78: First-in-Human Study of a Novel Antimalarial Drug. *Malar. Res. Treat.* **2014**, *2014*, 1–10.

(83) O'Neill, P. M.; Park, B. K.; Shone, A. E.; Maggs, J. L.; Roberts, P.; Stocks, P. A.; Biagini, G. A.; Bray, P. G.; Gibbons, P.; Berry, N.; Winstanley, P. A.; Mukhtar, A.; Bonar-Law, R.; Hindley, S.; Bambal, R. B.; Davis, C. B.; Bates, M.; Hart, T. K.; Gresham, S. L.; Lawrence, R. M.; Brigandi, R. A.; Gomez-delas-Heras, F. M.; Gargallo, D. V.; Ward, S. A. Candidate Selection and Preclinical Evaluation of N - Tert -Butyl Isoquine (GSK369796), An Affordable and Effective 4-Aminoquinoline Antimalarial for the 21st Century. *J. Med. Chem.* **2009**, *52*, 1408–1415.

(84) Lell, B.; Ruangweerayut, R.; Wiesner, J.; Missinou, M. A.; Schindler, A.; Baranek, T.; Hintz, M.; Hutchinson, D.; Jomaa, H.; Kremsner, P. G. Fosmidomycin, a Novel Chemotherapeutic Agent for Malaria. *Antimicrob. Agents Chemother.* **2003**, *47*, 735–738.

(85) Taudon, N.; Margout, D.; Wein, S.; Calas, M.; Vial, H. J.; Bressolle, F. M. M. Quantitative Analysis of a Bis-Thiazolium Antimalarial Compound, SAR97276, in

Mouse Plasma and Red Blood Cell Samples, Using Liquid Chromatography Mass Spectrometry. *J. Pharm. Biomed. Anal.* **2008**, *46*, 148–156.

(86) Nde, P.; Cho-Ngwa, F.; Titanji, V.; Samje, M.; Leitgeb, A. M.; Blomqvist, K.; Wahlgren, M. Low Anticoagulant Heparin Disrupts Plasmodium Falciparum Rosettes in Fresh Clinical Isolates. *Am. J. Trop. Med. Hyg.* **2011**, *84*, 390–396.

(87) Sandison, T. G.; Homsy, J.; Arinaitwe, E.; Wanzira, H.; Kakuru, A.; Bigira, V.; Kalamya, J.; Vora, N.; Kublin, J.; Kamya, M. R.; Dorsey, G.; Tappero, J. W. Protective Efficacy of Co-Trimoxazole Prophylaxis against Malaria in HIV Exposed Children in Rural Uganda: A Randomised Clinical Trial. *BMJ.* **2011**, *342*, d1617.

(88) Fact Sheet: World Malaria Report 2015. http://www.who.int/malaria/media/world-malaria-report-2015/en/. Accessed: 2018-04-13. (Archived by WebCite® at http://www.webcitation.org/6ydvFMRe7).

(89) A Research Agenda for Malaria Eradication: Drugs. *PLoS Med.* **2011**, *8*, e1000402.

(90) Global Technical Strategy for Malaria 2016-2030. http://www.who.int/malaria/areas/global_technical_strategy/en/. Accessed: 2018-04-13. (Archived by WebCite® at http://www.webcitation.org/6ydwaatcd).

(91) Burrows, J. N.; Hooft van Huijsduijnen, R.; Möhrle, J. J.; Oeuvray, C.; Wells, T. N. Designing the next Generation of Medicines for Malaria Control and Eradication. *Malar. J.* **2013**, *12*, 187.

(92) Bruce, M. C.; Day, K. P. Cross-Species Regulation of Malaria Parasitaemia in the Human Host. *Curr. Opin. Microbiol.* **2002**, *5*, 431–437.

(93) Cox-Singh, J.; Singh, B. Knowlesi Malaria: Newly Emergent and of Public Health Importance? *Trends Parasitol.* **2008**, *24*, 406–410.

(94) Corey, V. C.; Lukens, A. K.; Istvan, E. S.; Lee, M. C. S.; Franco, V.; Magistrado, P.; Coburn-Flynn, O.; Sakata-Kato, T.; Fuchs, O.; Gnädig, N. F.; Goldgof, G.; Linares, M.; Gomez-Lorenzo, M. G.; De Cózar, C.; Lafuente-Monasterio, M. J.; Prats, S.; Meister, S.; Tanaseichuk, O.; Wree, M.; Zhou, Y.; Willis, P. A.; Gamo, F.-J.; Goldberg, D. E.; Fidock, D. A.; Wirth, D. F.; Winzeler, E. A. A Broad Analysis of Resistance Development in the Malaria Parasite. *Nat. Commun.* **2016**, *7*, 11901.

(95) Spangenberg, T.; Burrows, J. N.; Kowalczyk, P.; McDonald, S.; Wells, T. N. C.; Willis, P. The Open Access Malaria Box: A Drug Discovery Catalyst for Neglected Diseases. *PLoS ONE.* **2013**, *8*, e62906.

(96) Alonso, P. L.; Brown, G.; Arevalo-Herrera, M.; Binka, F.; Chitnis, C.; Collins, F.; Doumbo, O. K.; Greenwood, B.; Hall, B. F.; Levine, M. M.; Mendis, K.; Newman, R.

D.; Plowe, C. V.; Rodríguez, M. H.; Sinden, R.; Slutsker, L.; Tanner, M. A Research Agenda to Underpin Malaria Eradication. *PLoS Med.* **2011**, *8*, e1000406.

(97) Griffin, J. B.; Lokomba, V.; Landis, S. H.; Thorp, J. M.; Herring, A. H.; Tshefu, A. K.; Rogerson, S. J.; Meshnick, S. R. Plasmodium Falciparum Parasitaemia in the First Half of Pregnancy, Uterine and Umbilical Artery Blood Flow, and Foetal Growth: A Longitudinal Doppler Ultrasound Study. *Malar. J.* **2012**, *11*, 319.

(98) Chen, I.; Clarke, S. E.; Gosling, R.; Hamainza, B.; Killeen, G.; Magill, A.; O'Meara, W.; Price, R. N.; Riley, E. M. "Asymptomatic" Malaria: A Chronic and Debilitating Infection That Should Be Treated. *PLOS Med.* **2016**, *13*, e1001942.

(99) Nambozi, M.; Van Geertruyden, J.-P.; Hachizovu, S.; Chaponda, M.; Mukwamataba, D.; Mulenga, M.; Ubben, D.; D'Alessandro, U. Safety and Efficacy of Dihydroartemisinin-Piperaquine versus Artemether-Lumefantrine in the Treatment of Uncomplicated Plasmodium Falciparum Malaria in Zambian Children. *Malar. J.* **2011**, *10*, 50.

(100) Malaria in pregnancy: WHO Evidence Review Group meeting report. http://www.who.int/malaria/mpac/mpac-sept2015-erg-mip-report.pdf. Accessed: 2018-04-14. (Archived by WebCite® at http://www.webcitation.org/6yfZVBkeh).

(101) Manyando, C.; Mkandawire, R.; Puma, L.; Sinkala, M.; Mpabalwani, E.; Njunju, E.; Gomes, M.; Ribeiro, I.; Walter, V.; Virtanen, M.; Schlienger, R.; Cousin, M.; Chipimo, M.; Sullivan, F. M. Safety of Artemether-Lumefantrine in Pregnant Women with Malaria: Results of a Prospective Cohort Study in Zambia. *Malar. J.* **2010**, *9*, 249.

(102) Moore, B. R.; Salman, S.; Davis, T. M. E. Treatment Regimens for Pregnant Women with Falciparum Malaria. *Expert Rev. Anti. Infect. Ther.* **2016**, *14*, 691–704.

(103) Mosha, D.; Mazuguni, F.; Mrema, S.; Sevene, E.; Abdulla, S.; Genton, B. Safety of Artemether-Lumefantrine Exposure in First Trimester of Pregnancy: An Observational Cohort. *Malar. J.* **2014**, *13*, 197.

(104) Piola, P.; Nabasumba, C.; Turyakira, E.; Dhorda, M.; Lindegardh, N.; Nyehangane, D.; Snounou, G.; Ashley, E. A.; McGready, R.; Nosten, F.; Guerin, P. J. Efficacy and Safety of Artemether–lumefantrine Compared with Quinine in Pregnant Women with Uncomplicated Plasmodium Falciparum Malaria: An Open-Label, Randomised, Non-Inferiority Trial. *Lancet Infect. Dis.* **2010**, *10*, 762–769.

(105) Savjani, K. T.; Gajjar, A. K.; Savjani, J. K. Drug Solubility: Importance and Enhancement Techniques. *ISRN Pharm.* **2012**, *2012*, 1–10.

(106) Williams, H. D.; Trevaskis, N. L.; Charman, S. A.; Shanker, R. M.; Charman, W. N.;

Pouton, C. W.; Porter, C. J. H. Strategies to Address Low Drug Solubility in Discovery and Development. *Pharmacol. Rev.* **2013**, *65*, 315–499.

(107) Palucki, M.; Higgins, J. D.; Kwong, E.; Templeton, A. C. Strategies at the Interface of Drug Discovery and Development: Early Optimization of the Solid State Phase and Preclinical Toxicology Formulation for Potential Drug Candidates. *J. Med. Chem.* **2010**, *53*, 5897–5905.

(108) Ishikawa, M.; Hashimoto, Y. Improvement in Aqueous Solubility in Small Molecule Drug Discovery Programs by Disruption of Molecular Planarity and Symmetry. *J. Med. Chem.* **2011**, *54*, 1539–1554.

(109) Kerns, E. H.; Di, L. *Drug-like Properties: Concepts, Structure Design and Methods: From ADME to Toxicity Optimization*, 2nd ed.; 2008.

(110) Arrowsmith, J. E.; Campbell, S. F.; Cross, P. E.; Stubbs, J. K.; Burges, R. A.; Gardiner, D. G.; Blackburn, K. J. Long-Acting Dihydropyridine Calcium Antagonists. 1. 2-Alkoxymethyl Derivatives Incorporating Basic Substituents. *J. Med. Chem.* **1986**, *29*, 1696–1702.

(111) Jordan, V. C. Tamoxifen: A Most Unlikely Pioneering Medicine. *Nat. Rev. Drug Discov.* **2003**, *2*, 205–213.

(112) Lundquist, J. T.; Harnish, D. C.; Kim, C. Y.; Mehlmann, J. F.; Unwalla, R. J.; Phipps, K. M.; Crawley, M. L.; Commons, T.; Green, D. M.; Xu, W.; Hum, W.-T.; Eta, J. E.; Feingold, I.; Patel, V.; Evans, M. J.; Lai, K.; Borges-Marcucci, L.; Mahaney, P. E.; Wrobel, J. E. Improvement of Physiochemical Properties of the Tetrahydroazepinoindole Series of Farnesoid X Receptor (FXR) Agonists: Beneficial Modulation of Lipids in Primates. *J. Med. Chem.* **2010**, *53*, 1774–1787.

(113) Di, L.; Fish, P. V.; Mano, T. Bridging Solubility between Drug Discovery and Development. *Drug Discov. Today.* **2012**, *17*, 486–495.

(114) Fini, A.; Fazio, G.; Hervás, M.-J. F.; Holgado, M. A.; Rabasco, A. M. Factors Governing the Dissolution of Diclofenac Salts. *Eur. J. Pharm. Sci.* **1996**, *4*, 231–238.

(115) Fini, A.; Fazio, G.; Gonzalez-Rodriguez, M.; Cavallari, C.; Passerini, N.; Rodriguez, L. Formation of Ion-Pairs in Aqueous Solutions of Diclofenac Salts. *Int. J. Pharm.* **1999**, *187*, 163–173.

(116) Kasim, N. A.; Whitehouse, M.; Ramachandran, C.; Bermejo, M.; Lennernäs, H.; Hussain, A. S.; Junginger, H. E.; Stavchansky, S. A.; Midha, K. K.; Shah, V. P.; Amidon, G. L. Molecular Properties of WHO Essential Drugs and Provisional Biopharmaceutical Classification. *Mol. Pharm.* **2004**, *1*, 85–96.

(117) Paulekuhn, G. S.; Dressman, J. B.; Saal, C. Trends in Active Pharmaceutical Ingredient Salt Selection Based on Analysis of the Orange Book Database. *J. Med. Chem.* **2007**, *50*, 6665–6672.

(118) Bighley, L. D. et al. Salt Forms of Drugs and Absorption. In *Encyclopedia of Pharmaceutical Technology*; Swarbrick, J., Boylan, J. C., Eds.; Marcel Dekker, Inc, 1995; pp 453–499.

(119) Le Manach, C.; Paquet, T.; Gonzàlez Cabrera, D.; Younis, Y.; Taylor, D.; Wiesner, L.; Lawrence, N.; Schwager, S.; Waterson, D.; Witty, M. J.; Wittlin, S.; Street, L. J.; Chibale, K. Medicinal Chemistry Optimization of Antiplasmodial Imidazopyridazine Hits from High Throughput Screening of a SoftFocus Kinase Library: Part 2. *J. Med. Chem.* **2014**, *57*, 8839–8848.

(120) Zhang, L.; Zhu, H.; Mathiowetz, A.; Gao, H. Deep Understanding of Structure–solubility Relationship for a Diverse Set of Organic Compounds Using Matched Molecular Pairs. *Bioorg. Med. Chem.* **2011**, *19*, 5763–5770.

(121) Leach, A. G.; Jones, H. D.; Cosgrove, D. A.; Kenny, P. W.; Ruston, L.; MacFaul, P.; Wood, J. M.; Colclough, N.; Law, B. Matched Molecular Pairs as a Guide in the Optimization of Pharmaceutical Properties; a Study of Aqueous Solubility, Plasma Protein Binding and Oral Exposure. *J. Med. Chem.* **2006**, *49*, 6672–6682.

(122) Warner, D. J.; Griffen, E. J.; St-Gallay, S. A. WizePairZ: A Novel Algorithm to Identify, Encode, and Exploit Matched Molecular Pairs with Unspecified Cores in Medicinal Chemistry. *J. Chem. Inf. Model.* **2010**, *50*, 1350–1357.

(123) Forster, S.; Buckton, G.; Beezer, A. E. The Importance of Chain Length on the Wettability and Solubility of Organic Homologs. *Int. J. Pharm.* **1991**, *72*, 29–34.

(124) Rautio, J.; Kumpulainen, H.; Heimbach, T.; Oliyai, R.; Oh, D.; Järvinen, T.; Savolainen, J. Prodrugs: Design and Clinical Applications. *Nat. Rev. Drug Discov.* **2008**, *7*, 255–270.

(125) Stella, V. J.; Nti-Addae, K. W. Prodrug Strategies to Overcome Poor Water Solubility. *Adv. Drug Deliv. Rev.* **2007**, *59*, 677–694.

(126) Duggan, D. E.; Hooke, K. F.; Hwang, S. S. Kinetics of the Tissue Distributions of Sulindac and Metabolites. Relevance to Sites and Rates of Bioactivation. *Drug Metab. Dispos.* **1980**, *8*, 241–246.

(127) Graham, D. Y.; Smith, J. L.; Holmes, G. I.; Davies, R. O. Nonsteroidal Anti-Inflammatory Effect of Sulindac Sulfoxide and Sulfide on Gastric Mucosa. *Clin. Pharmacol. Ther.* **1985**, *38*, 65–70.

(128) Heimbach, T. Absorption Rate Limit Considerations for Oral Phosphate Prodrugs. *Pharm. Res.* **2003**, *20*, 848–856.

(129) Banerjee, S.; Yalkowsky, S. H.; Valvani, C. Water Solubility and Octanol/Water Partition Coefficients of Organics. Limitations of the Solubility-Partition Coefficient Correlation. *Environ. Sci. Technol.* **1980**, *14*, 1227–1229.

(130) Jain, N.; Yalkowsky, S. H. Estimation of the Aqueous Solubility I: Application to Organic Nonelectrolytes. *J. Pharm. Sci.* **2001**, *90*, 234–252.

(131) Lovering, F.; Bikker, J.; Humblet, C. Escape from Flatland: Increasing Saturation as an Approach to Improving Clinical Success. *J. Med. Chem.* **2009**, *52*, 6752–6756.

(132) Wang, H.-L.; Katon, J.; Balan, C.; Bannon, A. W.; Bernard, C.; Doherty, E. M.; Dominguez, C.; Gavva, N. R.; Gore, V.; Ma, V.; Nishimura, N.; Surapaneni, S.; Tang, P.; Tamir, R.; Thiel, O.; Treanor, J. J. S.; Norman, M. H. Novel Vanilloid Receptor-1 Antagonists: 3. The Identification of a Second-Generation Clinical Candidate with Improved Physicochemical and Pharmacokinetic Properties. *J. Med. Chem.* **2007**, *50*, 3528–3539.

(133) Doherty, E. M.; Fotsch, C.; Bannon, A. W.; Bo, Y.; Chen, N.; Dominguez, C.; Falsey, J.; Gavva, N. R.; Katon, J.; Nixey, T.; Ognyanov, V. I.; Pettus, L.; Rzasa, R. M.; Stec, M.; Surapaneni, S.; Tamir, R.; Zhu, J.; Treanor, J. J. S.; Norman, M. H. Novel Vanilloid Receptor-1 Antagonists: 2. Structure−Activity Relationships of 4-Oxopyrimidines Leading to the Selection of a Clinical Candidate. *J. Med. Chem.* **2007**, *50*, 3515–3527.

(134) Bare, T. M.; Brown, D. G.; Horchler, C. L.; Murphy, M.; Urbanek, R. A.; Alford, V.; Barlaam, C.; Dyroff, M. C.; Empfield, J. B.; Forst, J. M.; Herzog, K. J.; Keith, R. A.; Kirschner, A. S.; Lee, C.-M. C.; Lewis, J.; McLaren, F. M.; Neilson, K. L.; Steelman, G. B.; Trivedi, S.; Vacek, E. P.; Xiao, W. Pyridazinoquinolinetriones as NMDA Glycine-Site Antagonists with Oral Antinociceptive Activity in a Model of Neuropathic Pain. *J. Med. Chem.* **2007**, *50*, 3113–3131.

(135) Li, Q.; Wang, W.; Berst, K. B.; Claiborne, A.; Hasvold, L.; Raye, K.; Tufano, M.; Nilius, A.; Shen, L. L.; Flamm, R.; Alder, J.; Marsh, K.; Crowell, D.; Chu, D. T. W.; Plattner, J. J. Synthesis and Structure-Activity Relationships of 2-Pyridones: II. 8-(Fluoro-Substituted Pyrrolidinyl)-2-Pyridones as Antibacterial Agents. *Bioorg. Med. Chem. Lett.* **1998**, *8*, 1953–1958.

(136) Ferri, N.; Siegl, P.; Corsini, A.; Herrmann, J.; Lerman, A.; Benghozi, R. Drug Attrition during Pre-Clinical and Clinical Development: Understanding and Managing Drug-Induced Cardiotoxicity. *Pharmacol. Ther.* **2013**, *138*, 470–484.

(137) Stevens, J. L.; Baker, T. K. The Future of Drug Safety Testing: Expanding the View and Narrowing the Focus. *Drug Discov. Today.* **2009**, *14*, 162–167.

(138) Roden, D. M. Drug-Induced Prolongation of the QT Interval. *N. Engl. J. Med.* **2004**, *350*, 1013–1022.

(139) Sibille, M.; Deigat, N.; Janin, A.; Kirkesseli, S.; Vital Durand, D. Adverse Events in Phase-I Studies: A Report in 1015 Healthy Volunteers. *Eur. J. Clin. Pharmacol.* **1998**, *54*, 13–20.

(140) Yap, Y. G. Drug Induced QT Prolongation and Torsades de Pointes. *Heart.* **2003**, *89*, 1363–1372.

(141) Sanguinetti, M. C.; Jiang, C.; Curran, M. E.; Keating, M. T. A Mechanistic Link between an Inherited and an Acquird Cardiac Arrthytmia: HERG Encodes the IKr Potassium Channel. *Cell.* **1995**, *81*, 299–307.

(142) Valentin, J.-P. Reducing QT Liability and Proarrhythmic Risk in Drug Discovery and Development. *Br. J. Pharmacol.* **2010**, *159*, 5–11.

(143) Jamieson, C.; Moir, E. M.; Rankovic, Z.; Wishart, G. Medicinal Chemistry of HERG Optimizations: Highlights and Hang-Ups. *J. Med. Chem.* **2006**, *49*, 5029–5046.

(144) Mitcheson, J. S.; Chen, J.; Lin, M.; Culberson, C.; Sanguinetti, M. C. A Structural Basis for Drug-Induced Long QT Syndrome. *Proc. Natl. Acad. Sci.* **2000**, *97*, 12329–12333.

(145) Pearlstein, R. A.; Vaz, R. J.; Kang, J.; Chen, X.-L.; Preobrazhenskaya, M.; Shchekotikhin, A. E.; Korolev, A. M.; Lysenkova, L. N.; Miroshnikova, O. V; Hendrix, J.; Rampe, D. Characterization of HERG Potassium Channel Inhibition Using CoMSiA 3D QSAR and Homology Modeling Approaches. *Bioorg. Med. Chem. Lett.* **2003**, *13*, 1829–1835.

(146) Bell, I. M.; Gallicchio, S. N.; Abrams, M.; Beshore, D. C.; Buser, C. A.; Culberson, J. C.; Davide, J.; Ellis-Hutchings, M.; Fernandes, C.; Gibbs, J. B.; Graham, S. L.; Hartman, G. D.; Heimbrook, D. C.; Homnick, C. F.; Huff, J. R.; Kassahun, K.; Koblan, K. S.; Kohl, N. E.; Lobell, R. B.; Lynch, J. J.; Miller, P. A.; Omer, C. A.; Rodrigues, A. D.; Walsh, E. S.; Williams, T. M. Design and Biological Activity of (S)-4-(5-{[1-(3-Chlorobenzyl)-2- Oxopyrrolidin-3-Ylamino]Methyl}imidazol-1-Ylmethyl)Benzonitrile, a 3-Aminopyrrolidinone Farnesyltransferase Inhibitor with Excellent Cell Potency. *J. Med. Chem.* **2001**, *44*, 2933–2949.

(147) Bell, I. M.; Gallicchio, S. N.; Abrams, M.; Beese, L. S.; Beshore, D. C.; Bhimnathwala, H.; Bogusky, M. J.; Buser, C. A.; Culberson, J. C.; Davide, J.; Ellis-Hutchings, M.; Fernandes, C.; Gibbs, J. B.; Graham, S. L.; Hamilton, K. A.; Hartman, G. D.;

Heimbrook, D. C.; Homnick, C. F.; Huber, H. E.; Huff, J. R.; Kassahun, K.; Koblan, K. S.; Kohl, N. E.; Lobell, R. B.; Lynch, J. J.; Robinson, R.; Rodrigues, A. D.; Taylor, J. S.; Walsh, E. S.; Williams, T. M.; Zartman, C. B. 3-Aminopyrrolidinone Farnesyltransferase Inhibitors: Design of Macrocyclic Compounds with Improved Pharmacokinetics and Excellent Cell Potency. *J. Med. Chem.* **2002**, *45*, 2388–2409.

(148) McCauley, J. A.; Theberge, C. R.; Romano, J. J.; Billings, S. B.; Anderson, K. D.; Claremon, D. A.; Freidinger, R. M.; Bednar, R. A.; Mosser, S. D.; Gaul, S. L.; Connolly, T. M.; Condra, C. L.; Xia, M.; Cunningham, M. E.; Bednar, B.; Stump, G. L.; Lynch, J. J.; Macaulay, A.; Wafford, K. A.; Koblan, K. S.; Liverton, N. J. NR2B-Selective N -Methyl- d -Aspartate Antagonists: Synthesis and Evaluation of 5-Substituted Benzimidazoles. *J. Med. Chem.* **2004**, *47*, 2089–2096.

(149) Kim, D.; Wang, L.; Hale, J. J.; Lynch, C. L.; Budhu, R. J.; MacCoss, M.; Mills, S. G.; Malkowitz, L.; Gould, S. L.; DeMartino, J. A.; Springer, M. S.; Hazuda, D.; Miller, M.; Kessler, J.; Hrin, R. C.; Carver, G.; Carella, A.; Henry, K.; Lineberger, J.; Schleif, W. A.; Emini, E. A. Potent 1,3,4-Trisubstituted Pyrrolidine CCR5 Receptor Antagonists: Effects of Fused Heterocycles on Antiviral Activity and Pharmacokinetic Properties. *Bioorg. Med. Chem. Lett.* **2005**, *15*, 2129–2134.

(150) Shu, M.; Loebach, J. L.; Parker, K. A.; Mills, S. G.; Chapman, K. T.; Shen, D.-M.; Malkowitz, L.; Springer, M. S.; Gould, S. L.; DeMartino, J. A.; Siciliano, S. J.; Salvo, J. D.; Lyons, K.; Pivnichny, J. V.; Kwei, G. Y.; Carella, A.; Carver, G.; Holmes, K.; Schleif, W. A.; Danzeisen, R.; Hazuda, D.; Kessler, J.; Lineberger, J.; Miller, M. D.; Emini, E. A. Antagonists of Human CCR5 Receptor Containing 4-(Pyrazolyl)Piperidine Side Chains. Part 3: SAR Studies on the Benzylpyrazole Segment. *Bioorg. Med. Chem. Lett.* **2004**, *14*, 947–952.

(151) Kang, J.; Wang, L.; Chen, X.-L.; Triggle, D. J.; Rampe, D. Interactions of a Series of Fluoroquinolone Antibacterial Drugs with the Human Cardiac K^+ Channel hERG. *Mol. Pharmacol.* **2001**, *59*, 122–126.

(152) Fish, L. R.; Gilligan, M. T.; Humphries, A. C.; Ivarsson, M.; Ladduwahetty, T.; Merchant, K. J.; O'Connor, D.; Patel, S.; Philipps, E.; Vargas, H. M.; Hutson, P. H.; MacLeod, A. M. 4-Fluorosulfonylpiperidines: Selective 5-HT2A Ligands for the Treatment of Insomnia. *Bioorg. Med. Chem. Lett.* **2005**, *15*, 3665–3669.

(153) Xu, J.; Wei, L.; Mathvink, R.; He, J.; Park, Y.-J.; He, H.; Leiting, B.; Lyons, K. A.; Marsilio, F.; Patel, R. A.; Wu, J. K.; Thornberry, N. A.; Weber, A. E. Discovery of Potent and Selective Phenylalanine Based Dipeptidyl Peptidase IV Inhibitors. *Bioorg.*

Med. Chem. Lett. **2005**, *15*, 2533–2536.

(154) Edmondson, S. D.; Mastracchio, A.; Duffy, J. L.; Eiermann, G. J.; He, H.; Ita, I.; Leiting, B.; Leone, J. F.; Lyons, K. A.; Makarewicz, A. M.; Patel, R. A.; Petrov, A.; Wu, J. K.; Thornberry, N. A.; Weber, A. E. Discovery of Potent and Selective Orally Bioavailable β-Substituted Phenylalanine Derived Dipeptidyl Peptidase IV Inhibitors. *Bioorg. Med. Chem. Lett.* **2005**, *15*, 3048–3052.

(155) Woosley, R. L. Cardiac Actions of Antihistamines. *Annu. Rev. Pharmacol. Toxicol.* **1996**, *36*, 233–252.

(156) Edmondson, S. D.; Mastracchio, A.; Beconi, M.; Colwell, L. F.; Habulihaz, B.; He, H.; Kumar, S.; Leiting, B.; Lyons, K. A.; Mao, A.; Marsilio, F.; Patel, R. A.; Wu, J. K.; Zhu, L.; Thornberry, N. A.; Weber, A. E.; Parmee, E. R. Potent and Selective Proline Derived Dipeptidyl Peptidase IV Inhibitors. *Bioorg. Med. Chem. Lett.* **2004**, *14*, 5151–5155.

(157) Vaz, R. J.; Gao, Z.; Pribish, J.; Chen, X.; Levell, J.; Davis, L.; Albert, E.; Brollo, M.; Ugolini, A.; Cramer, D. M.; Cairns, J.; Sides, K.; Liu, F.; Kwong, J.; Kang, J.; Rebello, S.; Elliot, M.; Lim, H.; Chellaraj, V.; Singleton, R. W.; Li, Y. Design of Bivalent Ligands Using Hydrogen Bond Linkers: Synthesis and Evaluation of Inhibitors for Human β-Tryptase. *Bioorg. Med. Chem. Lett.* **2004**, *14*, 6053–6056.

(158) Fernandez, D.; Ghanta, A.; Kauffman, G. W.; Sanguinetti, M. C. Physicochemical Features of the HERG Channel Drug Binding Site. *J. Biol. Chem.* **2004**, *279*, 10120–10127.

(159) Ahmad, S.; Doweyko, L.; Ashfaq, A.; Ferrara, F. N.; Bisaha, S. N.; Schmidt, J. B.; DiMarco, J.; Conder, M. L.; Jenkins-West, T.; Normandin, D. E.; Russell, A. D.; Smith, M. A.; Levesque, P. C.; Lodge, N. J.; Lloyd, J.; Stein, P. D.; Atwal, K. S. Tetrahydronaphthalene-Derived Amino Alcohols and Amino Ketones as Potent and Selective Inhibitors of the Delayed Rectifier Potassium Current I_{Ks}. *Bioorg. Med. Chem. Lett.* **2004**, *14*, 99–102.

(160) Cooper, L. C.; Carlson, E. J.; Castro, J. L.; Chicchi, G. G.; Dinnell, K.; Di Salvo, J.; Elliott, J. M.; Hollingworth, G. J.; Kurtz, M. M.; Ridgill, M. P.; Rycroft, W.; Tsao, K.-L.; Swain, C. J. 4,4-Disubstituted Cyclohexylamine NK1 Receptor Antagonists II. *Bioorg. Med. Chem. Lett.* **2002**, *12*, 1759–1762.

(161) Fraley, M. E.; Arrington, K. L.; Buser, C. A.; Ciecko, P. A.; Coll, K. E.; Fernandes, C.; Hartman, G. D.; Hoffman, W. F.; Lynch, J. J.; McFall, R. C.; Rickert, K.; Singh, R.; Smith, S.; Thomas, K. A.; Wong, B. K. Optimization of the Indolyl Quinolinone Class of KDR (VEGFR-2) Kinase Inhibitors. *Bioorg. Med. Chem. Lett.* **2004**, *14*, 351–355.

(162) Rowley, M.; Hallett, D. J.; Goodacre, S.; Moyes, C.; Crawforth, J.; Sparey, T. J.; Patel, S.; Marwood, R.; Patel, S.; Thomas, S.; Hitzel, L.; O'Connor, D.; Szeto, N.; Castro, J. L.; Hutson, P. H.; MacLeod, A. M. 3-(4-Fluoropiperidin-3-yl)-2-Phenylindoles as High Affinity, Selective, and Orally Bioavailable H5-HT 2A Receptor Antagonists. *J. Med. Chem.* **2001**, *44*, 1603–1614.

(163) Friesen, R. W.; Ducharme, Y.; Ball, R. G.; Blouin, M.; Boulet, L.; Côté, B.; Frenette, R.; Girard, M.; Guay, D.; Huang, Z.; Jones, T. R.; Laliberté, F.; Lynch, J. J.; Mancini, J.; Martins, E.; Masson, P.; Muise, E.; Pon, D. J.; Siegl, P. K. S.; Styhler, A.; Tsou, N. N.; Turner, M. J.; Young, R. N.; Girard, Y. Optimization of a Tertiary Alcohol Series of Phosphodiesterase-4 (PDE4) Inhibitors: Structure−Activity Relationship Related to PDE4 Inhibition and Human Ether-a-Go-Go Related Gene Potassium Channel Binding Affinity. *J. Med. Chem.* **2003**, *46*, 2413–2426.

(164) Fletcher, S. R.; Burkamp, F.; Blurton, P.; Cheng, S. K. F.; Clarkson, R.; O'Connor, D.; Spinks, D.; Tudge, M.; van Niel, M. B.; Patel, S.; Chapman, K.; Marwood, R.; Shepheard, S.; Bentley, G.; Cook, G. P.; Bristow, L. J.; Castro, J. L.; Hutson, P. H.; MacLeod, A. M. 4-(Phenylsulfonyl)Piperidines: Novel, Selective, and Bioavailable 5-HT 2A Receptor Antagonists. *J. Med. Chem.* **2002**, *45*, 492–503.

(165) Hamdouchi, C.; Sanchez-Martinez, C.; Gruber, J.; del Prado, M.; Lopez, J.; Rubio, A.; Heinz, B. A. Imidazo[1,2-*b*]Pyridazines, Novel Nucleus with Potent and Broad Spectrum Activity against Human Picornaviruses: Design, Synthesis, and Biological Evaluation. *J. Med. Chem.* **2003**, *46*, 4333–4341.

(166) Couch, R. B. Rhinoviruses. In *Virology*; Fields, B. N., Ed.; Raven Press: New York, 1990; pp 607–629.

(167) Rueckert, R. R. Picornaviruses and Their Replication. In *Virology*; Fields, B. N., Ed.; Raven Press: New York, 1985; pp 705–738.

(168) Monto, A. S.; Bryan, E. R.; Ohmit, S. Rhinovirus Infections in Tecumseh, Michigan: Frequency of Illness and Number of Serotypes. *J. Infect. Dis.* **1987**, *156*, 43–49.

(169) Blaas, D.; Hofer, F.; Gruenberger, M.; Kowalski, H.; Machat, H.; Kuechler, E.; Huettinger, M. Entry of Minor Group Human Rhinoviruses into the Cell. In *Cellular Receptors for Animal Viruses*; Wimmer, E., Ed.; Cold Spring Harbor Laboratory Press: New York, 1994; pp 129–140.

(170) Chapman, M. S.; Rossmann, M. G. Comparison of Surface Properties of Picornaviruses: Strategies for Hiding the Receptor Site from Immune Surveillance. *Virology.* **1993**, *195*, 745–756.

(171) Mullard, A. 2012 FDA Drug Approvals. *Nat. Rev. Drug Discov.* **2013**, *12*, 87–90.

(172) Peterson, E. A.; Boezio, A. A.; Andrews, P. S.; Boezio, C. M.; Bush, T. L.; Cheng, A. C.; Choquette, D.; Coats, J. R.; Colletti, A. E.; Copeland, K. W.; DuPont, M.; Graceffa, R.; Grubinska, B.; Kim, J. L.; Lewis, R. T.; Liu, J.; Mullady, E. L.; Potashman, M. H.; Romero, K.; Shaffer, P. L.; Stanton, M. K.; Stellwagen, J. C.; Teffera, Y.; Yi, S.; Cai, T.; La, D. S. Discovery and Optimization of Potent and Selective Imidazopyridine and Imidazopyridazine MTOR Inhibitors. *Bioorg. Med. Chem. Lett.* **2012**, *22*, 4967–4974.

(173) Pogacic, V.; Bullock, A. N.; Fedorov, O.; Filippakopoulos, P.; Gasser, C.; Biondi, A.; Meyer-Monard, S.; Knapp, S.; Schwaller, J. Structural Analysis Identifies Imidazo[1,2-*b*]Pyridazines as PIM Kinase Inhibitors with In Vitro Antileukemic Activity. *Cancer Res.* **2007**, *67*, 6916–6924.

(174) Choi, H.-S.; Rucker, P. V.; Wang, Z.; Fan, Y.; Albaugh, P.; Chopiuk, G.; Gessier, F.; Sun, F.; Adrian, F.; Liu, G.; Hood, T.; Li, N.; Jia, Y.; Che, J.; McCormack, S.; Li, A.; Li, J.; Steffy, A.; Culazzo, A.; Tompkins, C.; Phung, V.; Kreusch, A.; Lu, M.; Hu, B.; Chaudhary, A.; Prashad, M.; Tuntland, T.; Liu, B.; Harris, J.; Seidel, H. M.; Loren, J.; Molteni, V. (*R*)-2-Phenylpyrrolidine Substituted Imidazopyridazines: A New Class of Potent and Selective Pan-TRK Inhibitors. *ACS Med. Chem. Lett.* **2015**, *6*, 562–567.

(175) Han, W.; Menezes, D. L.; Xu, Y.; Knapp, M. S.; Elling, R.; Burger, M. T.; Ni, Z.-J.; Smith, A.; Lan, J.; Williams, T. E.; Verhagen, J.; Huh, K.; Merritt, H.; Chan, J.; Kaufman, S.; Voliva, C. F.; Pecchi, S. Discovery of Imidazo[1,2-*a*]-Pyridine Inhibitors of Pan-PI3 Kinases That Are Efficacious in a Mouse Xenograft Model. *Bioorg. Med. Chem. Lett.* **2016**, *26*, 742–746.

(176) Yang, B. V; Brown, G. D.; Gupta, S. V. S. A. K.; Pitts, W. J. Imidazopyridazine JAK-3 Inhibitors and Their Use for the Treatment of Inflammatory and Autoimmune Diseases. WO2014039595, 2014.

(177) Yao, W.; Zhang, C.; Xu, M.; Zhuo, J.; He, C. Substituted Imidazopridazines and Benzimidazoles as Inhibitors of FGFR3. USO09533954B2, 2017.

(178) Oguro, Y.; Cary, D. R.; Miyamoto, N.; Tawada, M.; Iwata, H.; Miki, H.; Hori, A.; Imamura, S. Design, Synthesis, and Evaluation of Novel VEGFR2 Kinase Inhibitors: Discovery of [1,2,4]Triazolo[1,5-*a*]Pyridine Derivatives with Slow Dissociation Kinetics. *Bioorg. Med. Chem.* **2013**, *21*, 4714–4729.

(179) Miyamoto, N.; Oguro, Y.; Takagi, T.; Iwata, H.; Miki, H.; Hori, A.; Imamura, S. Design, Synthesis, and Evaluation of Imidazo[1,2-*b*]Pyridazine Derivatives Having a Benzamide Unit as Novel VEGFR2 Kinase Inhibitors. *Bioorg. Med. Chem.* **2012**, *20*,

7051–7058.

(180) Bärfacker, L.; Scott, W.; Hägebarth, A.; Ince, S.; Rehwinkel, H.; Politz, O.; Neuhaus, R.; Briem, H.; Bömer, U. Imidazopyridazines as AKT Kinase Inhibitors. USOO9604989B2, 2017.

(181) Santag, S.; Siegel, F.; Wengner, A. M.; Lange, C.; Bömer, U.; Eis, K.; Pühler, F.; Lienau, P.; Bergemann, L.; Michels, M.; von Nussbaum, F.; Mumberg, D.; Petersen, K. BAY 1143269, a Novel MNK1 Inhibitor, Targets Oncogenic Protein Expression and Shows Potent Anti-Tumor Activity. *Cancer Lett.* **2017**, *390*, 21–29.

(182) Livermore, D. G.; Bethell, R. C.; Cammack, N.; Hancock, A. P.; Hann, M. M.; Green, D. V.; Lamont, R. B.; Noble, S. A.; Orr, D. C.; Payne, J. J. Synthesis and Anti-HIV-1 Activity of a Series of Imidazo[1,5-*b*]Pyridazines. *J. Med. Chem.* **1993**, *36*, 3784–3794.

(183) Moine, E.; Dimier-Poisson, I.; Enguehard-Gueiffier, C.; Logé, C.; Pénichon, M.; Moiré, N.; Delehouzé, C.; Foll-Josselin, B.; Ruchaud, S.; Bach, S.; Gueiffier, A.; Debierre-Grockiego, F.; Denevault-Sabourin, C. Development of New Highly Potent Imidazo[1,2-*b*]Pyridazines Targeting Toxoplasma Gondii Calcium-Dependent Protein Kinase 1. *Eur. J. Med. Chem.* **2015**, *105*, 80–105.

(184) Jain, P.; Karthikeyan, C.; Moorthy, N. S.; Waiker, D.; Jain, A.; Trivedi, P. Human CDC2-Like Kinase 1 (CLK1): A Novel Target for Alzheimer's Disease. *Curr. Drug Targets.* **2014**, *15*, 539–550.

(185) Leivers, M.; Miller, J. F.; Chan, S. A.; Lauchli, R.; Liehr, S.; Mo, W.; Ton, T.; Turner, E. M.; Youngman, M.; Falls, J. G.; Long, S.; Mathis, A.; Walker, J. Imidazopyridazine Hepatitis C Virus Polymerase Inhibitors. Structure–Activity Relationship Studies and the Discovery of a Novel, Traceless Prodrug Mechanism. *J. Med. Chem.* **2014**, *57*, 1964–1975.

(186) Rimoli, M. G.; Russo, E.; Cataldi, M.; Citraro, R.; Ambrosino, P.; Melisi, D.; Curcio, A.; De Lucia, S.; Patrignani, P.; De Sarro, G.; Abignente, E. T-Type Channel Blocking Properties and Antiabsence Activity of Two Imidazo[1,2-b]Pyridazine Derivatives Structurally Related to Indomethacin. *Neuropharmacology.* **2009**, *56*, 637–646.

(187) Velcicky, J.; Miltz, W.; Oberhauser, B.; Orain, D.; Vaupel, A.; Weigand, K.; Dawson King, J.; Littlewood-Evans, A.; Nash, M.; Feifel, R.; Loetscher, P. Development of Selective, Orally Active GPR4 Antagonists with Modulatory Effects on Nociception, Inflammation, and Angiogenesis. *J. Med. Chem.* **2017**, *60*, 3672–3683.

(188) Roblin, R. O.; Williams, J. H.; Winnek, P. S.; English, J. P. Chemotherapy. II. Some Sulfanilamido Heterocycles 1. *J. Am. Chem. Soc.* **1940**, *62*, 2002–2005.

(189) France, C. P.; Winger, G.; Medzihradsky, F.; Seggel, M. R.; Rice, K. C.; Woods, J. H. Mirfentanil: Pharmacological Profile of a Novel Fentanyl Derivative with Opioid and Nonopioid Effects. *J. Pharmacol. Exp. Ther.* **1991**, *258*, 502–510.

(190) Cragoe, E. J. (3-Amino-5,6-Disubstituted-Pyrazinoyl) Guanidines. US3313813A, 1964.

(191) Osborne, J. D.; Matthews, T. P.; McHardy, T.; Proisy, N.; Cheung, K.-M. J.; Lainchbury, M.; Brown, N.; Walton, M. I.; Eve, P. D.; Boxall, K. J.; Hayes, A.; Henley, A. T.; Valenti, M. R.; De Haven Brandon, A. K.; Box, G.; Jamin, Y.; Robinson, S. P.; Westwood, I. M.; van Montfort, R. L. M.; Leonard, P. M.; Lamers, M. B. A. C.; Reader, J. C.; Aherne, G. W.; Raynaud, F. I.; Eccles, S. A.; Garrett, M. D.; Collins, I. Multiparameter Lead Optimization to Give an Oral Checkpoint Kinase 1 (CHK1) Inhibitor Clinical Candidate: (*R*)-5-((4-((Morpholin-2-ylmethyl)Amino)-5-(Trifluoromethyl)Pyridin-2-yl)Amino)Pyrazine-2-Carbonitrile (CCT245737). *J. Med. Chem.* **2016**, *59*, 5221–5237.

(192) Hennessy, E. J.; Chuaqui, C.; Ashton, S.; Colclough, N.; Cross, D. A. E.; Debreczeni, J. É.; Eberlein, C.; Gingipalli, L.; Klinowska, T. C. M.; Orme, J. P.; Sha, L.; Wu, X. Utilization of Structure-Based Design to Identify Novel, Irreversible Inhibitors of EGFR Harboring the T790M Mutation. *ACS Med. Chem. Lett.* **2016**, *7*, 514–519.

(193) Charrier, J.-D.; Durrant, S. J.; Kay, D.; O'Donnell, M.; Knegtel, R. M. A.; MacCormick, S.; Pinder, J.; Young, S. C.; Binch, H. M.; Cleveland, T.; Fanning, L. T. D.; Hurley, D. J.; Joshi, P.; Sheth, U. J.; Silina, A.; Reaper, P. M.; Virani, A. N. Compounds Useful as Inhibitors of ATR Kinase. US8410112B2, 2013.

(194) Charrier, J. D.; Durrant, S. J.; Knegtel, R. Preparation of Pyrazine Derivatives Useful as Inhibitors of ATR Kinase. US20130115310, 2013.

(195) Charrier, J. D.; Durrant, S. J.; Shaw, D. M. Preparation of Pyrazine Derivatives Useful as Inhibitors of ATR Kinase. US0115311, 2013.

(196) Charrier, J. D.; Storck, P. H.; Pinder, J.; Studley, J. R. Preparation of Pyrazine Derivatives Useful as Inhibitors of ATR Kinase. US0115312, 2013.

(197) Charrier, J. D.; O'Donnell, M. E.; Everitt, S. R. Preparation of Pyrazine Derivatives Useful as Inhibitors of ATR Kinase. US0115313, 2013.

(198) Charrier, J. D.; Kay, D. Preparation of Pyrazine Derivatives Useful as Inhibitors of ATR Kinase. Vertex Pharmaceuticals Inc, 2013.

(199) Charrier, J. D.; Pinder, J.; Storck, P. H. Preparation of Substituted Isoxazolylpyrazinamines as Inhibitors of ATR Kinase. US0107093, 2014.

(200) Charrier, J. D.; Durrant, S. J.; Kay, D.; Al, E. Compounds Useful as Inhibitors of ATR

Kinase. US113005, 2014.

(201) Pollard, J. R.; Reaper, P. M. Treating Pancreatic Cancer and Non-Small Cell Lung Cancer with ATR Kinase Inhibitors. WO049859, 2013.

(202) Fokas, E.; Prevo, R.; Pollard, J. R.; Reaper, P. M.; Charlton, P. A.; Cornelissen, B.; Vallis, K. A.; Hammond, E. M.; Olcina, M. M.; Gillies McKenna, W.; Muschel, R. J.; Brunner, T. B. Targeting ATR in Vivo Using the Novel Inhibitor VE-822 Results in Selective Sensitization of Pancreatic Tumors to Radiation. *Cell Death Dis.* **2012**, *3*, e441.

(203) Terstiege, I.; Perry, M.; Petersen, J.; Tyrchan, C.; Svensson, T.; Lindmark, H.; Öster, L. Discovery of Triazole Aminopyrazines as a Highly Potent and Selective Series of PI3Kδ Inhibitors. *Bioorg. Med. Chem. Lett.* **2017**, *27*, 679–687.

(204) Barlaam, B.; Cosulich, S.; Fitzek, M.; Green, S.; Harris, C. S.; Hudson, K.; Lambert-van der Brempt, C.; Ouvry, G.; Page, K.; Ruston, L.; Ward, L.; Delouvrié, B. Design of Selective PI3Kα Inhibitors Starting from a Promiscuous Pan Kinase Scaffold. *Bioorg. Med. Chem. Lett.* **2015**, *25*, 2679–2685.

(205) Eriksson, A.; Höglund, M.; Lindhagen, E.; Åleskog, A.; Hassan, S. B.; Ekholm, C.; Fhölenhag, K.; Jensen, A. J.; Löthgren, A.; Scobie, M.; Larsson, R.; Parrow, V. Identification of AKN-032, a Novel 2-Aminopyrazine Tyrosine Kinase Inhibitor, with Significant Preclinical Activity in Acute Myeloid Leukemia. *Biochem. Pharmacol.* **2010**, *80*, 1507–1516.

(206) Whelligan, D. K.; Solanki, S.; Taylor, D.; Thomson, D. W.; Cheung, K.-M. J.; Boxall, K.; Mas-Droux, C.; Barillari, C.; Burns, S.; Grummitt, C. G.; Collins, I.; van Montfort, R. L. M.; Aherne, G. W.; Bayliss, R.; Hoelder, S. Aminopyrazine Inhibitors Binding to an Unusual Inactive Conformation of the Mitotic Kinase Nek2: SAR and Structural Characterization. *J. Med. Chem.* **2010**, *53*, 7682–7698.

(207) Fauber, B. P.; Dragovich, P. S.; Chen, J.; Corson, L. B.; Ding, C. Z.; Eigenbrot, C.; Giannetti, A. M.; Hunsaker, T.; Labadie, S.; Liu, Y.; Liu, Y.; Malek, S.; Peterson, D.; Pitts, K.; Sideris, S.; Ultsch, M.; VanderPorten, E.; Wang, J.; Wei, B.; Yen, I.; Yue, Q. Identification of 2-Amino-5-Aryl-Pyrazines as Inhibitors of Human Lactate Dehydrogenase. *Bioorg. Med. Chem. Lett.* **2013**, *23*, 5533–5539.

(208) Sitbon, O.; Morrell, N. Pathways in Pulmonary Arterial Hypertension: The Future Is Here. *Eur. Respir. Rev.* **2012**, *21*, 321–327.

(209) Vodnala, S. K.; Lundback, T.; Sjoberg, B.; Svensson, R.; Rottenberg, M. E.; Hammarstrom, L. G. J. In Vitro and In Vivo Activities of 2-Aminopyrazines and 2-

Aminopyridines in Experimental Models of Human African Trypanosomiasis. *Antimicrob. Agents Chemother.* **2013**, *57*, 1012–1018.

(210) Servusová, B.; Paterová, P.; Mandíková, J.; Kubíček, V.; Kučera, R.; Kuneš, J.; Doležal, M.; Zitko, J. Alkylamino Derivatives of Pyrazinamide: Synthesis and Antimycobacterial Evaluation. *Bioorg. Med. Chem. Lett.* **2014**, *24*, 450–453.

(211) Henderson, A. J.; Hadden, M.; Guo, C.; Douglas, N.; Decornez, H.; Hellberg, M. R.; Rusinko, A.; McLaughlin, M.; Sharif, N.; Drace, C.; Patil, R. 2,3-Diaminopyrazines as Rho Kinase Inhibitors. *Bioorg. Med. Chem. Lett.* **2010**, *20*, 1137–1140.

(212) Shen, W.; Taylor, B.; Jin, Q.; Nguyen-Tran, V.; Meeusen, S.; Zhang, Y.-Q.; Kamireddy, A.; Swafford, A.; Powers, A. F.; Walker, J.; Lamb, J.; Bursalaya, B.; DiDonato, M.; Harb, G.; Qiu, M.; Filippi, C. M.; Deaton, L.; Turk, C. N.; Suarez-Pinzon, W. L.; Liu, Y.; Hao, X.; Mo, T.; Yan, S.; Li, J.; Herman, A. E.; Hering, B. J.; Wu, T.; Martin Seidel, H.; McNamara, P.; Glynne, R.; Laffitte, B. Inhibition of DYRK1A and GSK3B Induces Human β-Cell Proliferation. *Nat. Commun.* **2015**, *6*, 8372.

(213) Wustrow, D. J.; Maynard, G. D.; Yuan, J.; Zhao, H.; Mao, J.; Guo, Q.; Kershaw, M.; Hammer, J.; Brodbeck, R. M.; Near, K. E.; Zhou, D.; Beers, D. S.; Chenard, B. L.; Krause, J. E.; Hutchison, A. J. Aminopyrazine CB1 Receptor Inverse Agonists. *Bioorg. Med. Chem. Lett.* **2008**, *18*, 3376–3381.

(214) Miniyar, P. B.; Murumkar, P. R.; Patil, P. S.; Barmade, M. A.; Bothara, K. G. Unequivocal Role of Pyrazine Ring in Medicinally Important Compounds: A Review. *Mini Rev. Med. Chem.* **2013**, *13*, 1607–1625.

(215) Dolezal, M.; Zitko, J. Pyrazine Derivatives: A Patent Review (June 2012 - Present). *Expert Opin. Ther. Pat.* **2015**, *25*, 33–47.

(216) Bhatt, A.; Singh, R. K.; Kant, R. Synthesis of Novel Imidazo [1,2-b] Pyridazine Derivatives and Study of Their Biomedicinal Efficacy. *Chem. Biol. Lett.* **2016**, *3*, 38–43.

(217) Bendjeddou, L. Z.; Loaëc, N.; Villiers, B.; Prina, E.; Späth, G. F.; Galons, H.; Meijer, L.; Oumata, N. Exploration of the Imidazo[1,2-*b*]Pyridazine Scaffold as a Protein Kinase Inhibitor. *Eur. J. Med. Chem.* **2017**, *125*, 696–709.

(218) Green, J. L.; Moon, R. W.; Whalley, D.; Bowyer, P. W.; Wallace, C.; Rochani, A.; Nageshan, R. K.; Howell, S. A.; Grainger, M.; Jones, H. M.; Ansell, K. H.; Chapman, T. M.; Taylor, D. L.; Osborne, S. A.; Baker, D. A.; Tatu, U.; Holder, A. A. Imidazopyridazine Inhibitors of Plasmodium Falciparum Calcium-Dependent Protein Kinase 1 Also Target Cyclic GMP-Dependent Protein Kinase and Heat Shock Protein

90 To Kill the Parasite at Different Stages of Intracellular Development. *Antimicrob. Agents Chemother.* **2016**, *60*, 1464–1475.

(219) Chapman, T. M.; Osborne, S. A.; Wallace, C.; Birchall, K.; Bouloc, N.; Jones, H. M.; Ansell, K. H.; Taylor, D. L.; Clough, B.; Green, J. L.; Holder, A. A. Optimization of an Imidazopyridazine Series of Inhibitors of Plasmodium Falciparum Calcium-Dependent Protein Kinase 1 (Pf CDPK1). *J. Med. Chem.* **2014**, *57*, 3570–3587.

(220) Large, J. M.; Osborne, S. A.; Smiljanic-Hurley, E.; Ansell, K. H.; Jones, H. M.; Taylor, D. L.; Clough, B.; Green, J. L.; Holder, A. A. Imidazopyridazines as Potent Inhibitors of Plasmodium Falciparum Calcium-Dependent Protein Kinase 1 (PfCDPK1): Preparation and Evaluation of Pyrazole Linked Analogues. *Bioorg. Med. Chem. Lett.* **2013**, *23*, 6019–6024.

(221) Chapman, T. M.; Osborne, S. A.; Bouloc, N.; Large, J. M.; Wallace, C.; Birchall, K.; Ansell, K. H.; Jones, H. M.; Taylor, D.; Clough, B.; Green, J. L.; Holder, A. A. Substituted Imidazopyridazines Are Potent and Selective Inhibitors of Plasmodium Falciparum Calcium-Dependent Protein Kinase 1 (PfCDPK1). *Bioorg. Med. Chem. Lett.* **2013**, *23*, 3064–3069.

(222) Ward, P.; Equinet, L.; Packer, J.; Doerig, C. Protein Kinases of the Human Malaria Parasite Plasmodium Falciparum: The Kinome of a Divergent Eukaryote. *BMC Genomics.* **2004**, *5*, 79.

(223) Bouloc, N.; Large, J. M.; Smiljanic, E.; Whalley, D.; Ansell, K. H.; Edlin, C. D.; Bryans, J. S. Synthesis and in Vitro Evaluation of Imidazopyridazines as Novel Inhibitors of the Malarial Kinase PfPK7. *Bioorg. Med. Chem. Lett.* **2008**, *18*, 5294–5298.

(224) Sahu, N. K.; Shahi, S.; Sharma, M. C.; Kohli, D. V. QSAR Studies on Imidazopyridazine Derivatives as PfPK7 Inhibitors. *Mol. Simul.* **2011**, *37*, 752–765.

(225) Sahu, N. K.; Kohli, D. V. Structural Insight for Imidazopyridazines as Malarial Kinase PfPK7 Inhibitors Using QSAR Techniques. *Med. Chem. (Los. Angeles).* **2012**, *8*, 636–648.

(226) McNamara, C. W.; Lee, M. C. S.; Lim, C. S.; Lim, S. H.; Roland, J.; Nagle, A.; Simon, O.; Yeung, B. K. S.; Chatterjee, A. K.; McCormack, S. L.; Manary, M. J.; Zeeman, A.-M.; Dechering, K. J.; Kumar, T. R. S.; Henrich, P. P.; Gagaring, K.; Ibanez, M.; Kato, N.; Kuhen, K. L.; Fischli, C.; Rottmann, M.; Plouffe, D. M.; Bursulaya, B.; Meister, S.; Rameh, L.; Trappe, J.; Haasen, D.; Timmerman, M.; Sauerwein, R. W.; Suwanarusk, R.; Russell, B.; Renia, L.; Nosten, F.; Tully, D. C.; Kocken, C. H. M.; Glynne, R. J.; Bodenreider, C.; Fidock, D. A.; Diagana, T. T.; Winzeler, E. A. Targeting Plasmodium

PI(4)K to Eliminate Malaria. *Nature.* **2013**, *504*, 248–253.

(227) Le Manach, C.; Gonzàlez Cabrera, D.; Douelle, F.; Nchinda, A. T.; Younis, Y.; Taylor, D.; Wiesner, L.; White, K. L.; Ryan, E.; March, C.; Duffy, S.; Avery, V. M.; Waterson, D.; Witty, M. J.; Wittlin, S.; Charman, S. A.; Street, L. J.; Chibale, K. Medicinal Chemistry Optimization of Antiplasmodial Imidazopyridazine Hits from High Throughput Screening of a SoftFocus Kinase Library: Part 1. *J. Med. Chem.* **2014**, *57*, 2789–2798.

(228) Le Manach, C.; Paquet, T.; Brunschwig, C.; Njoroge, M.; Han, Z.; Gonzàlez Cabrera, D.; Bashyam, S.; Dhinakaran, R.; Taylor, D.; Reader, J.; Botha, M.; Churchyard, A.; Lauterbach, S.; Coetzer, T. L.; Birkholtz, L.-M.; Meister, S.; Winzeler, E. A.; Waterson, D.; Witty, M. J.; Wittlin, S.; Jiménez-Díaz, M.-B.; Santos Martínez, M.; Ferrer, S.; Angulo-Barturen, I.; Street, L. J.; Chibale, K. A Novel Pyrazolopyridine with in Vivo Activity in Plasmodium Berghei - and Plasmodium Falciparum - Infected Mouse Models from Structure–Activity Relationship Studies around the Core of Recently Identified Antimalarial Imidazopyridazines. *J. Med. Chem.* **2015**, *58*, 8713–8722.

(229) González Cabrera, D.; Douelle, F.; Feng, T.-S.; Nchinda, A. T.; Younis, Y.; White, K. L.; Wu, Q.; Ryan, E.; Burrows, J. N.; Waterson, D.; Witty, M. J.; Wittlin, S.; Charman, S. A.; Chibale, K. Novel Orally Active Antimalarial Thiazoles. *J. Med. Chem.* **2011**, *54*, 7713–7719.

(230) Younis, Y.; Douelle, F.; González Cabrera, D.; Le Manach, C.; Nchinda, A. T.; Paquet, T.; Street, L. J.; White, K. L.; Zabiulla, K. M.; Joseph, J. T.; Bashyam, S.; Waterson, D.; Witty, M. J.; Wittlin, S.; Charman, S. A.; Chibale, K. Structure–Activity-Relationship Studies around the 2-Amino Group and Pyridine Core of Antimalarial 3,5-Diarylaminopyridines Lead to a Novel Series of Pyrazine Analogues with Oral in Vivo Activity. *J. Med. Chem.* **2013**, *56*, 8860–8871.

(231) Duffy, S.; Avery, V. M. Development and Optimization of a Novel 384-Well Anti-Malarial Imaging Assay Validated for High-Throughput Screening. *Am. J. Trop. Med. Hyg.* **2012**, *86*, 84–92.

(232) John, H. C.; Hill, R. D.; Sheppard, D. W.; Slater, M. J.; Stouten, P. F. W. The Design and Application of Target-Focused Compound Libraries. *Comb. Chem. High Throughput Screen.* **2011**, *14*, 521–531.

(233) New candidate UCT 943. https://www.mmv.org/newsroom/interviews/new-candidate-uct-943. Accessed: 2018-05-03. (Archived by WebCite® at http://www.webcitation.org/6z8xsnkzz).

(234) White, N. J. Antimalarial Drug Resistance. *J. Clin. Invest.* **2004**, *113*, 1084–1092.

(235) Sibley, C. H.; Hyde, J. E.; Sims, P. F. G.; Plowe, C. V.; Kublin, J. G.; Mberu, E. K.; Cowman, A. F.; Winstanley, P. A.; Watkins, W. M.; Nzila, A. M. Pyrimethamine–sulfadoxine Resistance in Plasmodium Falciparum: What Next? *Trends Parasitol.* **2001**, *17*, 582–588.

(236) Terlouw, D. J.; Nahlen, B. L.; Courval, J. M.; Kariuki, S. K.; Rosenberg, O. S.; Oloo, A. J.; Kolczak, M. S.; Hawley, W. A.; Lal, A. A.; Kuile, F. O. T. Sulfadoxine-Pyrimethamine in Treatment of Malaria in Western Kenya: Increasing Resistance and Underdosing. *Antimicrob. Agents Chemother.* **2003**, *47*, 2929–2932.

(237) Warhurst, D. C. Resistance to Antifolates in Plasmodium Falciparum, the Causative Agent of Tropical Malaria. *Sci. Prog.* **2002**, *85*, 89–111.

CHAPTER 2
DESIGN, SYNTHESIS AND CHARACTERIZATION OF TARGET COMPOUNDS

2.1 Chapter Overview

In this chapter, the rationale behind the design of target compounds is presented. This is followed by brief descriptions of the chemistry employed, mechanisms of the reactions (some mechanisms the author considers trivial have been left out) and characterization of intermediates as well as target compounds. The two chemotypes, the imidazopyridazines and aminopyrazines, covered in this thesis are dealt with in separate sub-sections.

2.2 Rationale for Design of Target Compounds

2.2.1 Imidazopyridazines

As noted in subsection 1.11.1 of the preceding chapter, imidazopyridazines have recently been recognized to possess *in vitro* antiplasmodial activity in the low nanomolar range and impressive *in vivo* efficacy.[1–3] Despite the impressive antimalarial activity, frontline compounds were associated with poor solubility and hERG inhibition liabilities. In this project, various chemical modification strategies aimed at generating analogues with potentially improved aqueous solubility and hERG inhibition profiles were employed.

Figure 2.1 shows a summary of the target compounds classed according to the chemical modification approach used. In designing the target compounds, the right-hand side portion of the molecule was fixed as a 4-methylsulfinylphenyl group (SARs 1 and 3) since such a sulfoxide-containing group is characterized by enhanced solubility relative to the sulfone counterpart.[2] Such sulfoxide analogues would also act as prodrugs by being metabolized to corresponding sulfones *in vivo*. Le Manach and co-workers have recently employed such a prodrug strategy by synthesizing solubility-enhancing sulfoxides that were shown to be metabolized to the corresponding sulfones.[2]

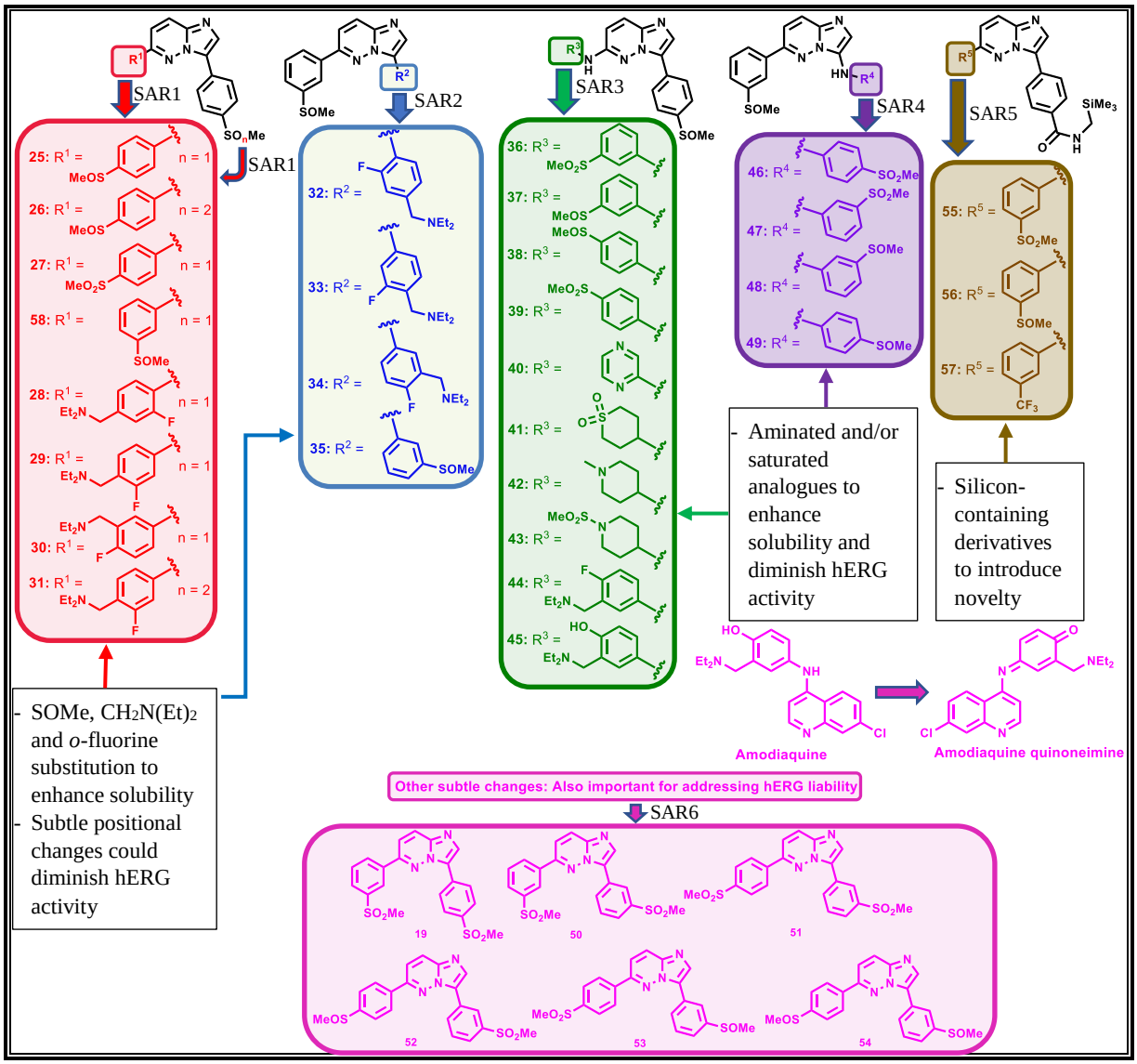

Figure 2.1: Chemical structures of target imidazopyridazine compounds.

By fixing the right-hand portion of the imidazopyridazine core scaffold as 4-methylsulfinylphenyl moiety, analogues **25**, **27 - 30**, **36** – **45** and **58** (SARs 1 and 3) were synthesized. For comparison purposes, two sulfone analogues (**26** and **31**) bearing a 4-methylsulfonylphenyl substructure on the right-hand side portion were synthesized. The first generation imidazopyridazines, **19** and **58**, possessed a sulfone and sulfoxide group respectively at the *meta* position of the left-hand side phenyl ring. A positional change of these two groups on the left-hand side phenyl ring resulted in analogues **25** – **27**. While substitution with a sulfoxide in **25** and **26** served to enhance solubility,[2] the accompanying *meta*-to-*para* positional changes in the two analogues as well as that in **27** have potential to attenuate hERG inhibition. Such subtle modifications have been applied by different research groups to successfully diminish hERG binding.[4,5] Additional analogues such as **35**, and **50** – **54** (SARs 2

and 6), resulting from subtle peripheral changes, were also designed to exploit such a hERG-attenuating strategy. Comparison among the different positional isomers generated would also shed more light on the importance of substituent position on antiplasmodial activity. Furthermore, **19**, the lead compound previously reported[1,2] to possess impressive antimalarial properties but marred by poor aqueous solubility and hERG inhibition liabilities, was resynthesized to serve as a control in biological assays.

The regioisomeric analogues (**28** – **30**) were designed to explore the effect of relative positions of substituents on the aromatic ring. Moreover, the incorporation of the basic side chain in compound **45** was also motivated by the presence of such molecular features in clinically established antimalarial drugs exemplified by amodiaquine (Figure 2.1). Incorporation of such basic side chains was also envisaged to facilitate salt formation in formulation efforts meant to improve physico-chemical properties. Analogues **32** – **34** (SAR2), with basic side chains on the right-hand side phenyl ring, were also inspired by the same rationale. Another important approach employed to improve aqueous solubility of drug molecules containing biaryl systems is the introduction of groups at the *ortho* or 2 position to increase the dihedral angle. This has the potential to disrupt molecular planarity and, therefore, discourage crystal packing which may result in improved aqueous solubility.[6] In designing compounds **28** and **32** with substitution in the *ortho* position, this strategy was employed.

Because lipophilic binding pockets in the hERG K^+ ion channel are known to be crucial to drug binding via interaction with the suitably positioned lipophilic substructures in drug molecules, increasing the polarity of the molecule can potentially disrupt such lipophilic interactions.[7,8] Capitalizing on this strategy, the hydrophilic aminated analogues **36** – **45** (SAR3) were designed and synthesized. It was also hypothesized that introduction of an amino linker into the analogues could also potentially result in improved aqueous solubility – the NH linker could facilitate hydrogen bonding interactions with water molecules. In another set of molecules synthesised by amination on the imidazole ring (**46 - 49**) (SAR4), this strategy was also utilized. Indeed, such a strategy, anchored on changes in lipophilicity, has been successfully employed to minimize hERG inhibition by a number of medicinal chemistry optimization programs.[9–14]

Amodiaquine, a Mannich-base 4-aminoquinoline drug was once actively used prophylactically.[15] Unfortunately, the hepatotoxicity and agranulocytosis associated with its chronic use has led to its withdrawal.[16–20] However, amodiaquine still finds use as a partner drug in artemisinin-based combination therapies for treatment of uncomplicated malaria,

particularly in Africa. It is also a drug of choice for treatment of acute malaria if the potential for drug toxicity is considered less important compared to the risk of infection.[21] The bioactivation of amodiaquine to its quinoneimine reactive metabolite (Figure 2.1) has been implicated in amodiaquine-induced hepatotoxicity.[22] Its disruption of cell functions has been thought to arise from the irreversible binding of such electrophilic reactive metabolites to proteins.[23] Comfortingly, subsequent studies have circumvented the formation of amodiaquine reactive metabolites by replacing the hydroxyl with a fluoro group as well as designing isoquine, an isomer of amodiaquine resulting from interchanging the positions of the hydroxyl and the Mannich base side chain.[24,25] In this regard, analogue **44** (a fluoro version of the Mannich base side chain) was designed to avoid the opportunity for formation of such reactive metabolites. However, the Mannich base analogue, **45**, was also included for comparison purposes. It is also possible that **45** may not form reactive metabolites. Thus, evaluation through metabolite trapping experiments would be necessary. The derivative **44**, differing from **30**, only in the presence of an NH linker between two aryl systems was designed to evaluate the influence of such a hydrophilic spacer on pharmacological properties. The non-basic NH spacer would also shed more light on its influence of physico-chemical parameters and hERG potency.

Furthermore, because phenyl rings are known to be pharmacophoric moieties for hERG binding,[26,27] three analogues (**41** - **43**), with saturated cyclic substituents were also designed. These could potentially discourage π - π interactions with phenyl-containing amino acid residues in the hERG channel. Replacement of phenyl rings with saturated molecular features also has the potential to discourage intermolecular π - π stacking and, thereby, potentially enhancing solubility.[6]

Within the context of introducing novelty to the new target compounds, selected silicon-containing derivatives **55** – **57** (SAR5) were generated. This bio-organosilicon chemistry approach also has potential to generate novel silicon-containing bioisosteres with pharmacologically relevant properties.[28] Once again, compounds **56** (sulfoxide) and **55** (sulfone) will bring to the fore any significant influence of the sulfone and sulfoxide groups on pharmacological and physico-chemical properties. Such a comparison of sulfoxide and sulfone groups also inspired the design of other pairs of analogues bearing the sulfoxide and sulfone at the point of variation (e.g., analogues **25** vs **27**, **36** vs **37**, **38** vs **39**, **46** vs **49** and **47** vs **48**). Lastly, the design of the target compounds in figure 2.1 was also inspired by the need to expand the scope of SAR around imidazopyridazines.

2.2.2 Aminopyrazines

SAR explorations aimed at improving solubility of the antimalarial aminopyrazines have led to the identification of the preclinical candidate **UCT943**[29] (see subsection 1.11.2 of chapter 1). However, the modifications pursued in this initial SAR where, to a large extent, peripheral in nature – i.e., involving the introduction of water solubilizing substituents on the phenyl ring at position 5 of the aminopyrazine core-scaffold. In this PhD project, the disruption-of-molecular-planarity approach, by replacing the two aromatic rings at positions 3 and 5 with saturated ring systems was adopted (Figure 2.2). In SAR1, the trifluoromethylpyridyl ring was replaced with partially as well as fully saturated heterocyclic ring systems while fixing a methylsulfonylphenyl ring at position 5. Similar modifications were made in SAR2 while keeping the trifluoromethylpyridyl ring fixed at position 3. In SAR3, both aromatic rings were replaced with partially and fully saturated heterocyclic ring systems. These modifications have potential to improve aqueous solubility by discouraging intermolecular $\pi - \pi$ stacking interactions.[6] Using this approach, analogues **59** – **68** and **70** – **72** were designed. It was also envisaged that the basic piperidine and piperazine moieties introduced would facilitate hydrogen bonding thereby improving aqueous solubility. Such basic molecular features would also act as sites for potential salt formation in formulation efforts. A lone analogue **69** bearing a water-solubilizing benzoic acid moiety was also synthesized. The analogues were also designed in such a way that would probe the effect of partial saturation on both antiplasmodial activity and solubility (e.g., **59** vs **60**, **63** vs **64** and **70** vs **71**). Additionally, while some analogues served to draw comparisons between the pharmacological activity of *N*-boc-protected derivatives and free amines (**60** vs **61** and **64** vs **65**), others were designed to give insight into the pharmacological effect of *N*-mesylation (**61** vs **62**, **65** vs **66** and **67** vs **68**).

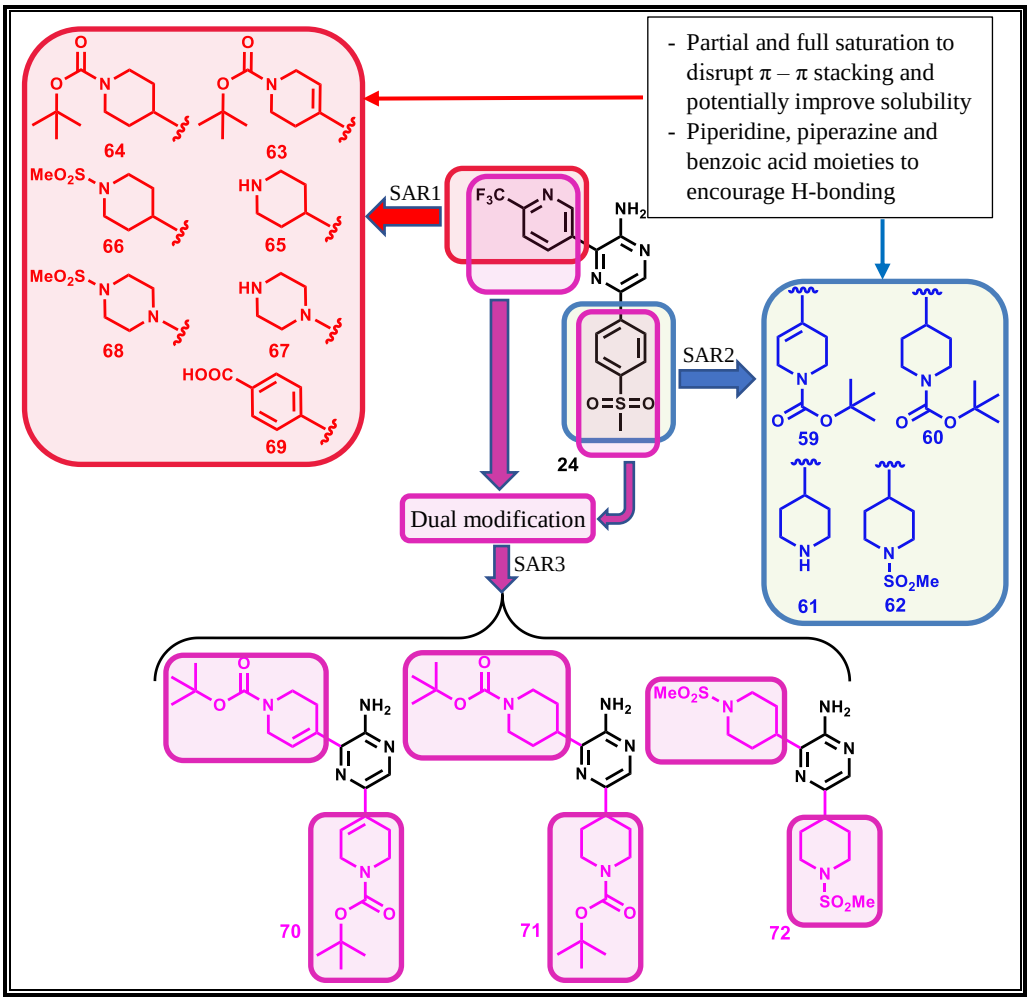

Figure 2.2: Chemical structures of target aminopyrazine compounds.

2.3 Chemistry: Imidazopyridazine Analogues

2.3.1 Synthesis of Imidazopyridazine Analogues

2.3.1.1 Synthesis of Analogues 19, 26 – 34, 36 – 45, 51 – 54 and 58

Compounds **19**, **26** – **34**, **36** – **45**, **51** – **54** and **58** (Figure 2.1) were synthesized following a generic synthetic approach outlined in scheme 2.1. A condensation/cyclization of commercially available 6-chloropyridazin-3-amine (**1a**) with bromoacetaldehyde diethylacetal in presence of hydrobromic acid (HBr) gave the chloroimidazopyridazine intermediate **2a**.[1] Regioselective electrophilic aromatic iodination, with *N*-iodosuccinimide (NIS) being the source of electrophilic iodine, afforded the iodinated intermediate, **3a**, in 81% yield.[1,30,31] The intermediate, **3a**, was then subjected to sequential Suzuki-Miyaura cross coupling reactions[32,33] to deliver the diaryl-imidazopyridazines (**19**, **26** – **34**, **51** – **54** and **58**) in 13 – 80% yield. Finally, a palladium-mediated Buchwald-Hartwig amination[34,35] of the chloro-bearing intermediate **4a** afforded the aminated analogues **36** – **45** in low yields (8 - 30%).

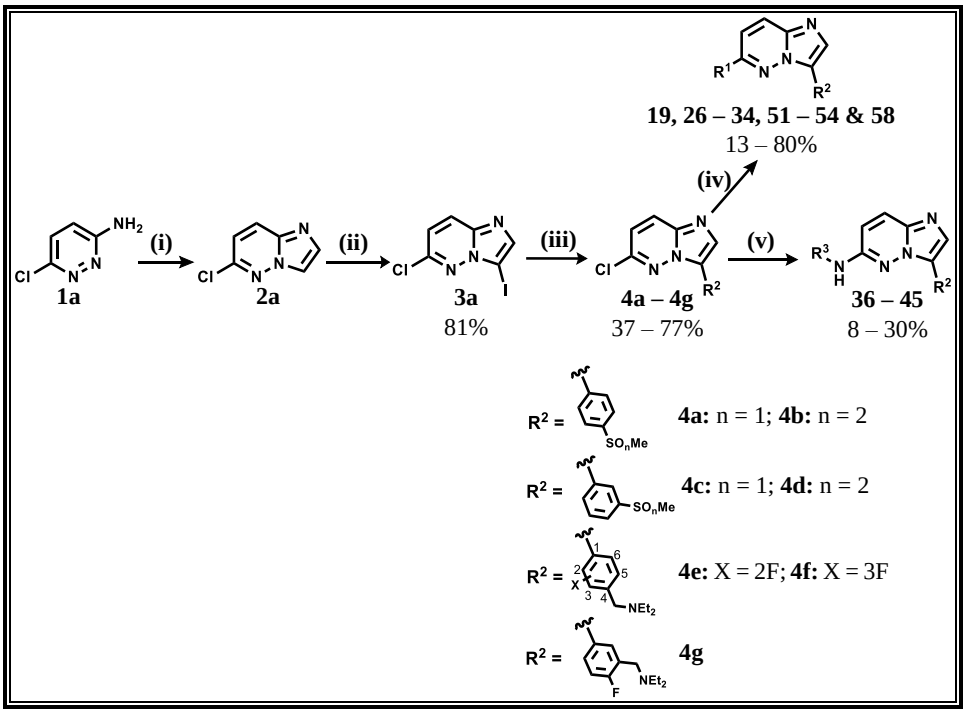

Scheme 2.1: General synthetic approach for analogues **19**, **26** – **34**, **36** – **45**, **51** – **54** and **58**.

Reagents and reaction conditions: (i) $BrCH_2CH(OEt)_2$, aq HBr, EtOH/H_2O, reflux, 103 ºC, 22 h; (ii) NIS, DMF, rt (21 ºC), 5 d; (iii) appropriate boronic acid or boronic acid pinacol ester, $Pd(PPh_3)_2Cl_2$, 1 M aq K_2CO_3, DMF, 80 ºC, 3.5 - 46 h; (iv) appropriate boronic acid or boronic acid pinacol ester, $Pd(PPh_3)_2Cl_2$, 1 M aq K_2CO_3, DMF, 100 ºC, 4 – 21 h; (v) R^3NH_2, $Pd_2(dba)_3$, (*R*)-BINAP for **39**, BrettPhos for **36**, **44** & **45**, XPhos for **37**, **38** & **40 – 43**, K_2CO_3 for **39**, Cs_2CO_3 for **36**, **44** & **45**, NaO*t*-Bu for **37**, **38** & **40 - 43**, toluene/1,4-dioxane for **39**, 1,4-dioxane for all other analogues, 100 °C for **42**, 120 ºC for all other analogues, sealed tube, inert atmosphere (N_2), 6 – 43 h.

Table 2.1 summarizes the target compounds and isolated yields obtained via scheme 2.1.

Table 2.1: Isolated yields for compounds obtained via scheme 2.1

Code	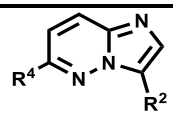		% Yield
	R^4	R^2	
19	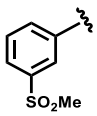	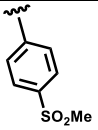	57
26	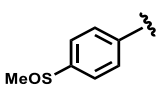	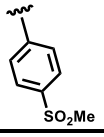	57

Table 2.1: Isolated yields for compounds obtained via scheme 2.1

Code	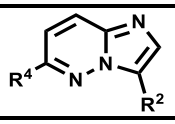		% Yield
	R^4	R^2	
27	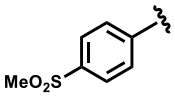	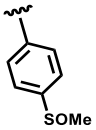	60
28	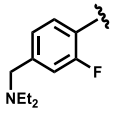	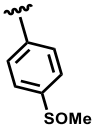	59
29	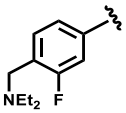	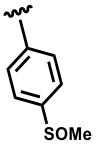	57
30	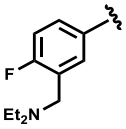	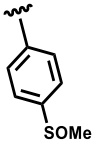	80
31	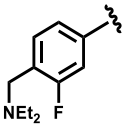	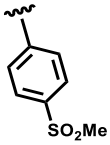	13
32	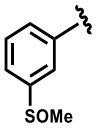	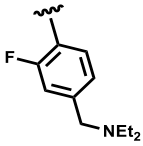	38
33	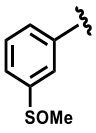	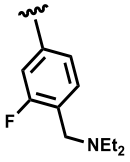	27
34	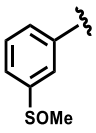	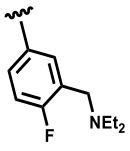	42
51	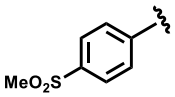	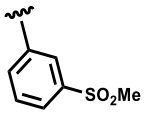	20
52	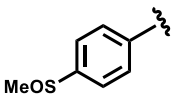	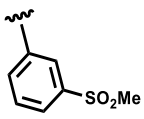	45
53	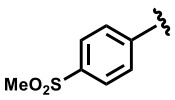	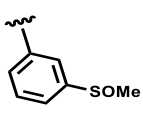	37

Table 2.1: Isolated yields for compounds obtained via scheme 2.1

Code	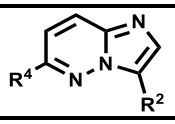		% Yield
	R^4	R^2	
54	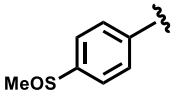	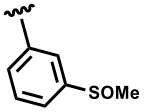	58
58	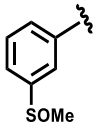	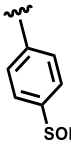	51
36	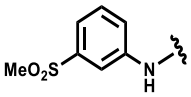	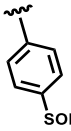	16
37	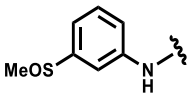	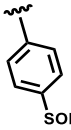	18
38	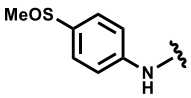	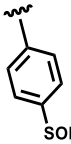	8
39	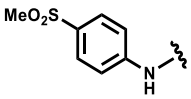	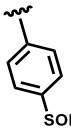	13
40	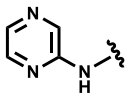	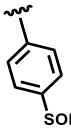	29
41	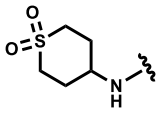	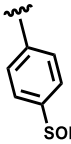	15
42	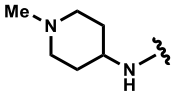	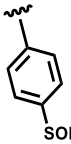	14
43	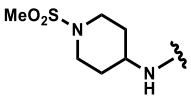	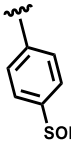	30
44	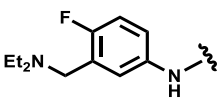	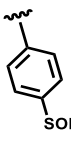	10

Table 2.1: Isolated yields for compounds obtained via scheme 2.1

Code			% Yield
	R^4	R^2	
45	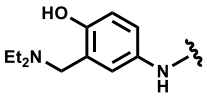	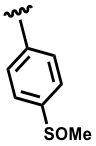	18

2.3.1.2 Synthesis of the Aniline Precursor 5d Required for Synthesis of Analogue 44

The aniline precursor, **5d**, required for the synthesis of analogue **44** (table 2.1), could not be sourced commercially and, therefore, was prepared in-house according to scheme 2.2. The commercially available alcohol starting material (**5a**) was tosylated in the presence of sodium hydroxide. The obtained tosylated intermediate (**5b**) was then treated with diethylamine to afford the amino-substituted intermediate **5c** in 87% yield.[36] The aniline precursor, **5d**, was then realized in quantitative yield following reduction of the nitro group to the amino functionality in presence of acidified stannous chloride ($SnCl_2$).[36]

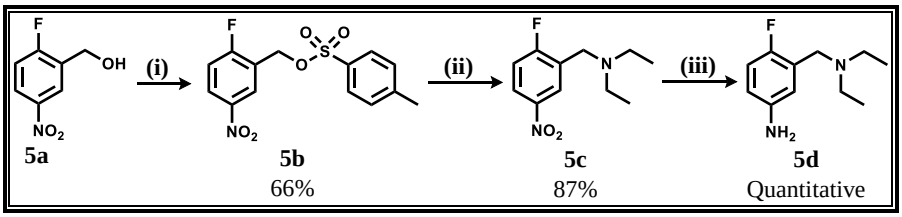

Scheme 2.2: Synthetic approach for aniline starting material **5d**.

Reagents and reaction conditions: (i) aq NaOH, *p*-toluenesulfonyl chloride, THF, 0 - 11 ºC, 2 h; (ii) Et_2NH, Et_3N, 1,4-dioxane, 55 ºC, 5 h; (iii) $SnCl_2$, aq HCl, THF, reflux, 66 ºC, 29 h.

2.3.1.3 Synthesis of the Phenolic Precursor 5h Required for Synthesis of Analogue 45

The phenolic starting material (**5h**), a precursor for the Buchwald-Hartwig amination towards analogue **45**, was realized via a three-step synthetic sequence from commercially available 4-aminophenol (**5e**) as captured in scheme 2.3. Anilines are extremely reactive towards electrophilic aromatic substitution reactions, leading to undesirable polysubstitution side products.[37,38] Such side reactions are considerably circumvented by acetylating the amino group to form the acetanilide derivative. In this regard, the acetylated intermediate (**5f**) was synthesized by reacting the commercially available 4-aminophenol (**5e**) with acetic anhydride under reflux. A Mannich base side chain was then introduced via electrophilic aromatic substitution in the presence of formaldehyde and diethylamine. The amino group was

subsequently deacetylated by refluxing in aqueous HCl to afford the Mannich base intermediate **5h** in 43% yield, which was later utilized in a Buchwald-Hartwig amination reaction.

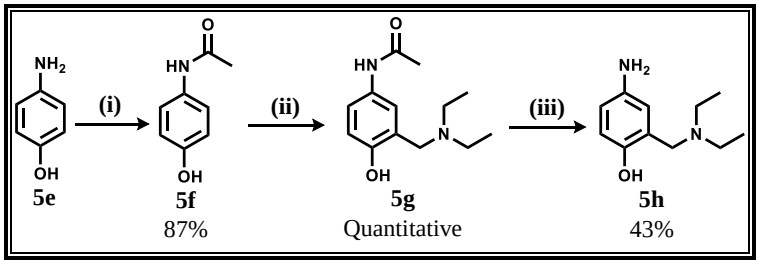

Scheme 2.3: Synthetic approach for phenolic starting material **5h**.

Reagents and reaction conditions: (i) Acetic anhydride, THF, reflux, 60 ºC, 1.75 h; (ii) aq HCHO, Et_2NH, ethanol, microwave irradiation, 80 ºC, 1.5 h; (iii) aq HCl, reflux, 80 ºC, 2 h.

2.3.1.4 Synthesis of Analogues 25, 35 and 46 – 50

Analogues **25**, **35** and **46 – 50** (see structures in figure 2.1) were realized using the synthetic approach shown in scheme 2.4. Analogues **50** and **25** have the same nature and pattern of substitution on their two phenyl rings. While analogue **50** is *meta*-substituted with a sulfone on both phenyl rings, analogue **25** bears sulfoxide substituents at the *para* position of both phenyl rings. Since the same boronic acid was required for the coupling reaction on both reaction sites of the dihalogenated intermediate **3a**, the two analogues were realized by a simple one pot Suzuki-Miyaura cross coupling[32,33] using an excess (2.2 eq) of the respective boronic acids (Scheme 2.4A). Although another analogue, **35**, could have been obtained using the same one pot synthetic approach, it was synthesized from a different available bromo-intermediate (**6b**) in a single step Suzuki-Miyaura cross coupling[32,33] reaction (Scheme 2.4B).

Analogues **46** – **49** were synthesised according to scheme 2.4B. The previously synthesized chlorinated intermediate **2a** was subjected to a Suzuki-Miyaura cross coupling[32,33] to afford the phenylated intermediate **6a** in low yield (48%). Regioselective electrophilic aromatic bromination using *N*-bromosuccinimide (NBS) afforded the brominated intermediate **6b** in moderate yield (59%).[2] The aminated analogues **46** – **49** were then obtained in poor yields (9 – 17%) via a Buchwald-Hartwig amination reaction.[34,35]

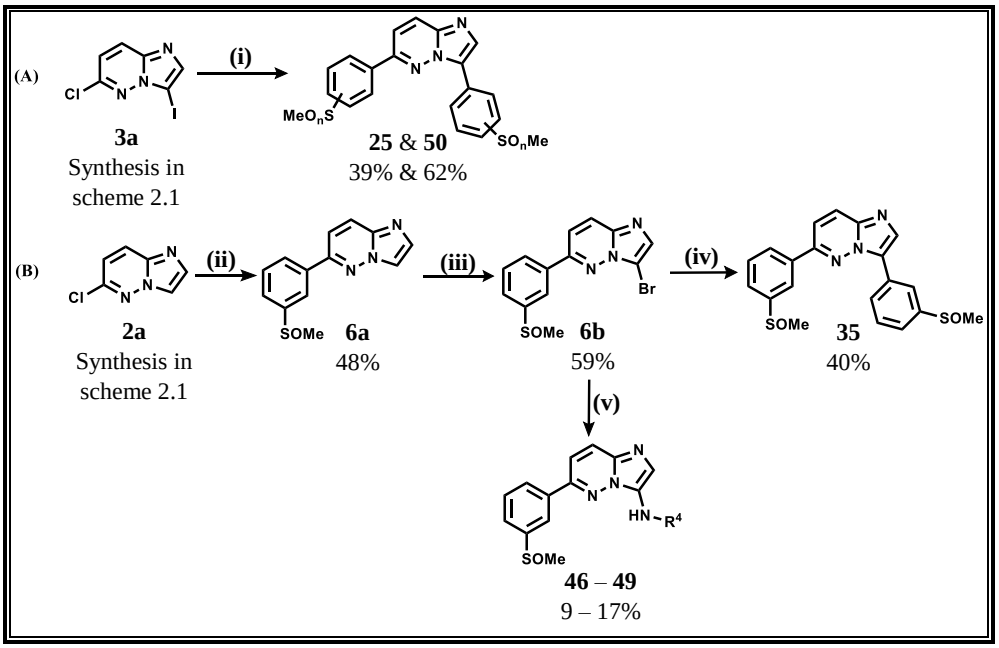

Scheme 2.4: General synthetic approach for analogues **25, 35** and **46 – 50**.

Reagents and reaction conditions: (i) appropriate boronic acid (excess, 2.2 eq), $Pd(PPh_3)_2Cl_2$, 1 M aq K_2CO_3, DMF, 100 ºC, 15 h for **25** and 24 h for **50**; (ii) 3-methylsulfinylphenylboronic acid, $Pd(PPh_3)_2Cl_2$, 1 M aq K_2CO_3, DMF, 100 ºC, 3.25 h; (iii) NBS, DMF, rt (23 ºC), 22 h; (iv) 3-methylsulfinylphenylboronic acid, $Pd(PPh_3)_2Cl_2$, 1 M aq K_2CO_3, DMF, 100 ºC, 20 h; (v) R^4-NH_2, $Pd_2(dba)_3$, BrettPhos, Cs_2CO_3, 1,4-dioxane, 120 ºC, sealed tube, 5 – 39 h.

The synthesized analogues are summarized in table 2.2 below.

Table 2.2: Isolated yields for compounds obtained via scheme 2.4

Code	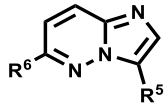		% Yield
	R^6	R^5	
25	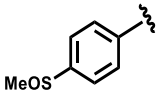	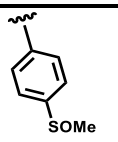	39
35	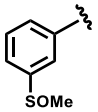	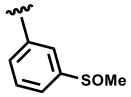	40
50	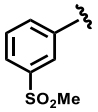	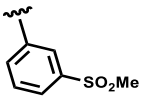	62
46	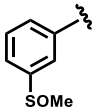	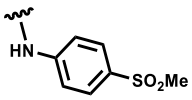	9

Table 2.2: Isolated yields for compounds obtained via scheme 2.4

Code	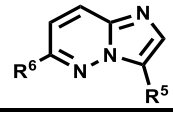		% Yield
	R^6	R^5	
47	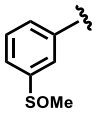	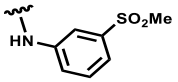	10
48	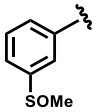	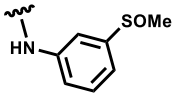	15
49	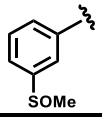	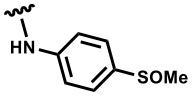	17

2.3.1.5 Synthesis of Silylamide Analogues 55 – 57

The silylamide imidazopyridazine derivatives were synthesized via a synthetic protocol involving carboxylic acid intermediates (Scheme 2.5). The chloroiodoimidazopyridazine intermediate **3a** was regioselectively coupled with the commercially available 4-carboxyphenylboronic acid in a Suzuki-Miyaura cross coupling[32,33] step to afford intermediate **7a** in 56% yield. A subsequent Suzuki-Miyaura cross coupling[32,33] of intermediate **7a** with appropriate arylboronic acids furnished the carboxylic acid intermediates **7b** and **7c** in 95 and 54% yields respectively. Intermediate **7d** was obtained in a low 39% yield following a Suzuki-Miyaura cross coupling using a different intermediate **7e** (**7e** synthesized by Le Manach *et al*[2]). The target compounds (**55** – **57**) were realized by an EDCI (1-ethyl-3-(3-dimethylaminopropyl)carbodiimide)- and DMAP (4-dimethylaminopyridine)-mediated acid-amine coupling.[39]

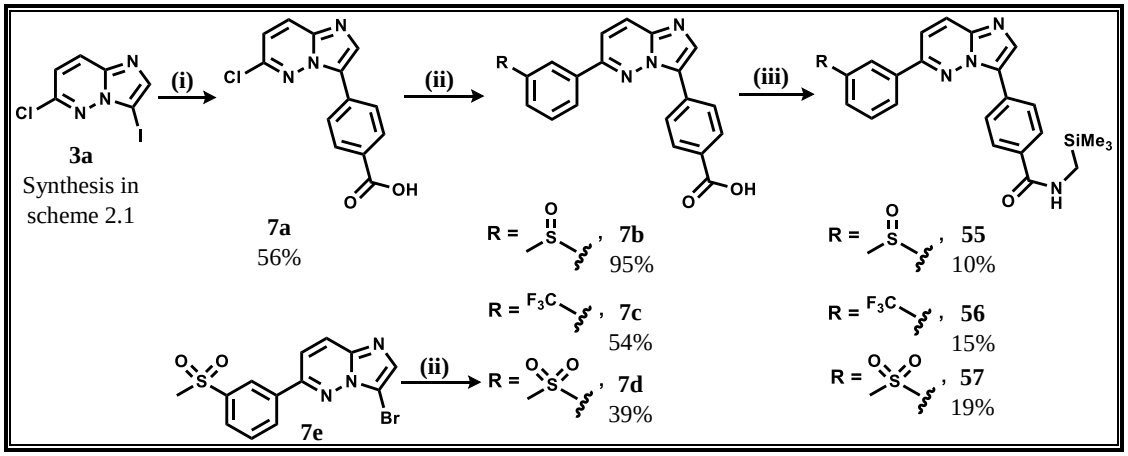

Scheme 2.5: General synthetic approach to silicon-containing imidazopyridazines **55** – **57**.

Reagents and reaction conditions: (i) 4-Carboxyphenylboronic acid, $Pd(PPh_3)_2Cl_2$, 1 M aq K_2CO_3, DMF, 80 ºC, 27 h; (ii) arylboronic acid, $Pd(PPh_3)_2Cl_2$, 1 M aq K_2CO_3, DMF, 100 ºC, 22 – 30 h; (iii) (trimethylsilyl)methylamine, EDCI.HCl, DMAP, DCM/DMF for **55**, DCM for **57**, DMF for **56**, rt for **55** and **56**, 36 ºC for **57**, 20 – 60 h.

2.3.2 Proposed Mechanistic Details and Characterization

In this subsection, mechanisms accompanying the reactions carried out are proposed with an attempt being made to back up such mechanisms with literature information. Once again, mechanisms considered trivial are left out. Intermediate compounds were characterised using ^{1}H-NMR (proton nuclear magnetic resonance) and/or HPLC-MS (high pressure liquid chromatography mass spectrometry) while final target compounds were fully characterised by these two techniques as well as ^{13}C-NMR (carbon-13 NMR). For compounds **30** and **57**, the ^{13}C-NMR spectra could not be acquired due to insufficient material. In addition to the ^{1}H-NMR and ^{13}C-NMR spectra, which are presented for representative compounds, the HPLC chromatograms and mass spectra showing the observed quasi-molecular ion peaks are also presented for final compounds.

2.3.2.1 Ring Closure and Aromatization: Step (i), Scheme 2.1

Acetals are deprotected in presence of catalytic amounts of BrØnsted acids to afford their carbonyl versions.[40,41] Therefore, the formation of intermediate **2a**, most likely, commences with the deprotection of bromoacetaldehyde diethylacetal (Scheme 2.6). A protonation step followed by an intramolecular elimination gives a resonance-stabilized oxonium ion.

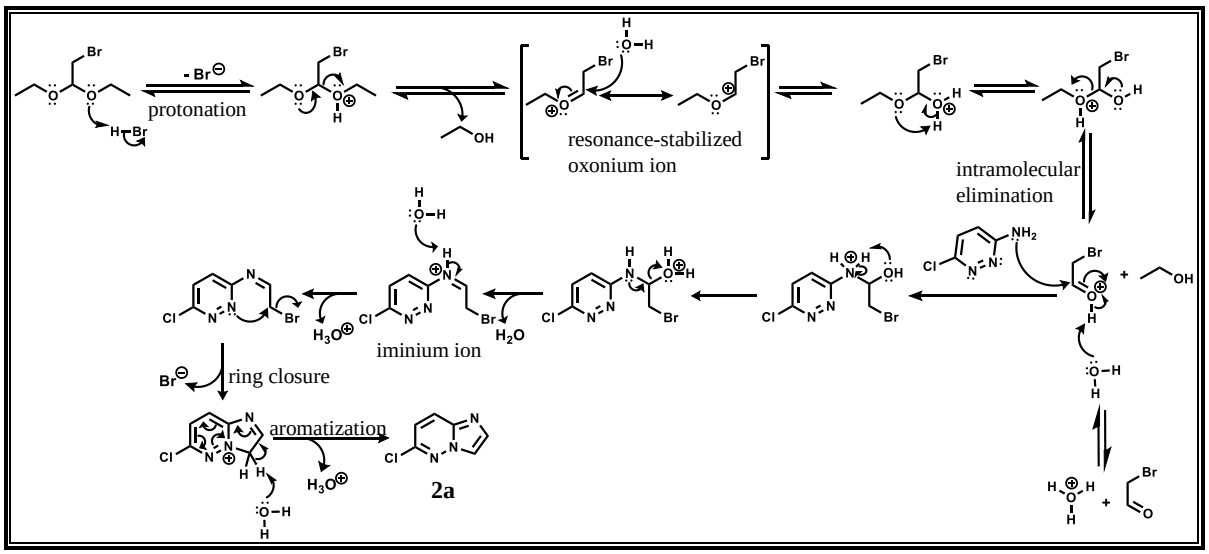

Scheme 2.6: Proposed reaction mechanism for condensation/cyclization and aromatization.

The relatively more electrophilic oxonium ion is then attacked by a water molecule giving a protonated intermediate, which further undergoes intramolecular elimination after internal proton transfer to give the protonated aldehyde. A deprotonation step gives the free aldehyde, in the process, regenerating the acid catalyst in form of a hydronium ion. A nucleophilic addition of 6-chloropyridazin-3-amine to the protonated aldehyde gives the hydroxyl intermediate which, upon intramolecular proton transfer, undergoes elimination to form the iminium ion. A neutral imine is subsequently formed via a deprotonation step. A nucleophilic substitution reaction involving a pyridazine nitrogen leads to a cyclized ionic intermediate. A final aromatization step leads to the formation of intermediate **2a** while the BrØnsted acid is regenerated. This intermediate was confirmed by HPLC-MS: $APCI^+/ESI^+$-*m/z* found 154.0 $[M + H]^+$ (calculated exact mass = 153.0094), t_r = 1.1 min.

2.3.2.2 Electrophilic Aromatic Iodination: Step (ii), Scheme 2.1

The formation of the dihalogenated intermediate **3a** involves electrophilic aromatic iodination mediated by NIS (Scheme 2.7). The π electrons of the imidazo ring system attack the iodine in NIS with the succinimide anion acting as a leaving group.[42,43] The succinimide anion deprotonates the heteroarenium ion intermediate giving the iodinated heteroaromatic compound **3a** with succimide being formed as a by-product.

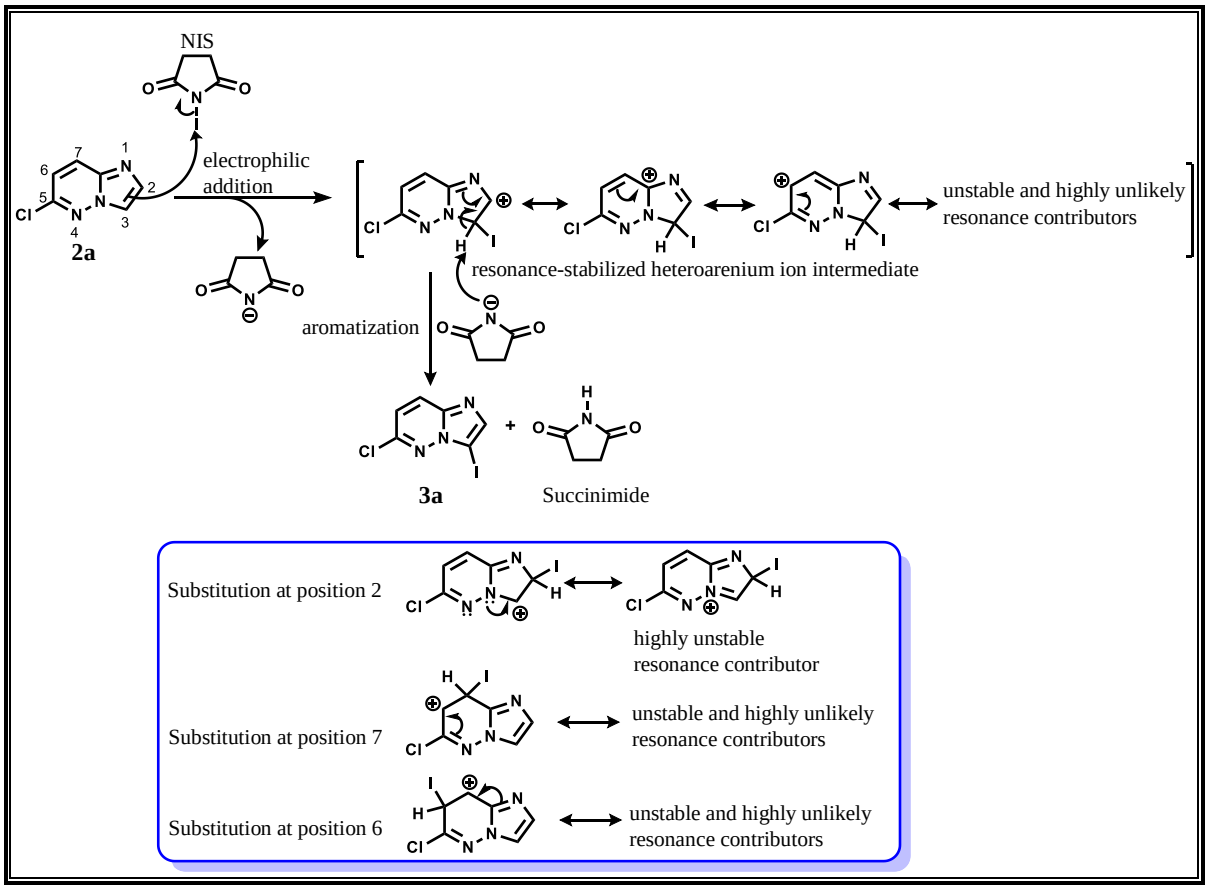

Scheme 2.7: Reaction mechanism for electrophilic aromatic iodination.

The regioselectivity of this reaction can be explained by careful examination of the heteroarenium ion intermediates that would form from potential electrophilic attack at various positions. Electrophilic attack at position 3 is the most favoured because it gives rise to a heteroarenium ion intermediate with the largest number of resonance contributors (Scheme 2.7). With the positive charge resident on carbon atoms, which can better accommodate it, these resonance contributors are also the most stable. On the contrary, electrophilic attack at positions 2, 6 or 7 gives rise to heteroarenium ion intermediates with a limited number of resonance contributors. In these cases, highly unstable resonance contributors with the positive charge residing on the electronegative nitrogen renders substitution at these positions not feasible.

Successful synthesis of the dihalogenated intermediate **3a** was confirmed by HPLC-MS ($ESI^+/APCI^+$: *m/z* $[M + H]^+ = 279.8$, calculated exact mass = 278.9060, $t_r = 3.0$ min). ^{1}H-NMR spectroscopy also confirmed the successful synthesis of **3a** (Figure 2.3) with protons H2 and H3 coupling to each other and appearing as doublets at chemical shifts δ 7.92 and 7.14 ppm respectively. As anticipated, proton H1 resonated as a singlet at δ 7.88 ppm.

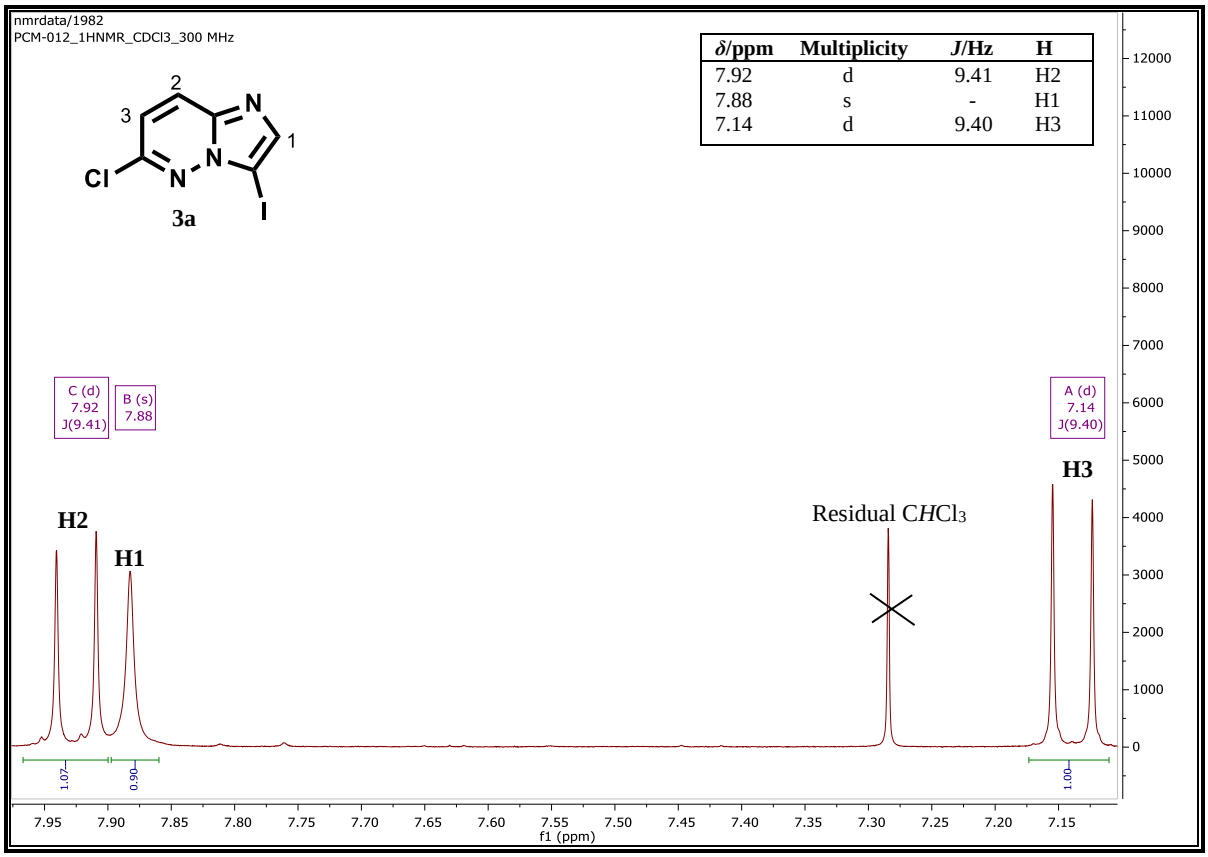

Figure 2.3: ^{1}H-NMR spectrum of **3a** at 300 MHz in $CDCl_3$.

2.3.2.3 Suzuki-Miyaura Cross-coupling: Step (iii), Scheme 2.1

The next step in the synthetic protocol in scheme 2.1 involved a Suzuki-Miyaura cross coupling of the dihalogenated precursor **3a** with various arylboronic acids as well as arylboronic acid pinacol esters. The reaction mechanism has been postulated to occur as outlined in scheme 2.8.[43,44] The first step involves the oxidative addition of the heteroarylhalide (**3a**) to the Pd^0 catalyst to form the Pd^{2+} complex. The halide (in this case iodine) is then replaced by a nucleophilic attack of one carbonate (CO_3^{2-}) ion on the palladium complex. The boronic acid or the pinacol ester equivalent is also activated or rendered more nucleophilic by the nucleophilic addition of a carbonate anion on the electrophilic boron atom. A transmetalation step follows in which the now more nucleophilic Ar group bonds to the palladium complex while the eliminated carbonate anion bonds to the boronic centre. The biaryl bond is then formed in a reductive elimination step, which also regenerates the Pd^0 catalytic species for the next catalytic cycle.

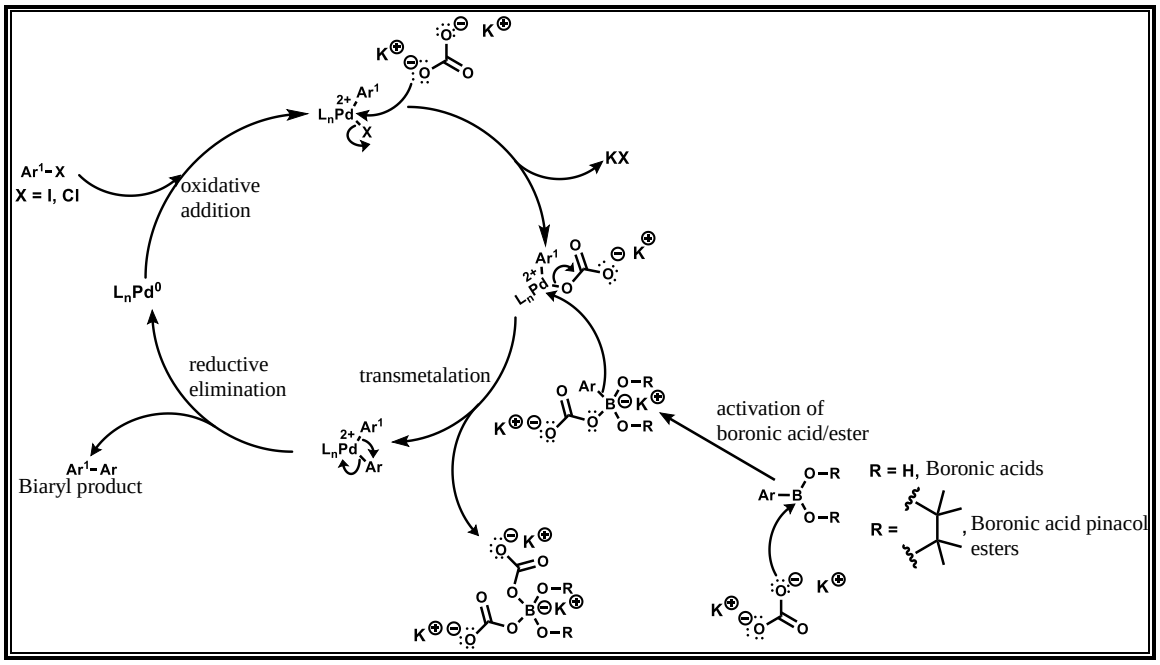

Scheme 2.8: Reaction mechanism for the Suzuki-Miyaura cross-coupling reaction.[43,44]

The intermediates arising from the first Suzuki-Miyaura cross-coupling reaction, as captured in step (iii) of scheme 2.1, were characterized by ^{1}H-NMR and, in most cases, HPLC-MS. For each class of intermediates, a representative ^{1}H-NMR spectrum is shown.

For the sulfoxide-containing intermediate **4a**, characterization by HPLC-MS revealed a characteristic quasi-molecular ion peak $[M + H]^{+}$ at *m/z* 292.0 (calculated exact mass = 291.0233). The successful incorporation of the 4-methylsulfinylphenyl moiety was also evident in the ^{1}H-NMR spectrum (Figure 2.4) with an upfield singlet signal (δ = 2.81 ppm) corresponding to the relatively shielded three methyl protons (H4) of the methylsulfinyl group. The two sets of protons, H2 and H3, were observed as two doublets, integrating for two protons each, in the downfield aromatic region. Two other doublets, integrating for one proton each, were attributed to protons H5 and H6, while proton H1 corresponded to a one-proton singlet signal in the aromatic region of the spectrum.

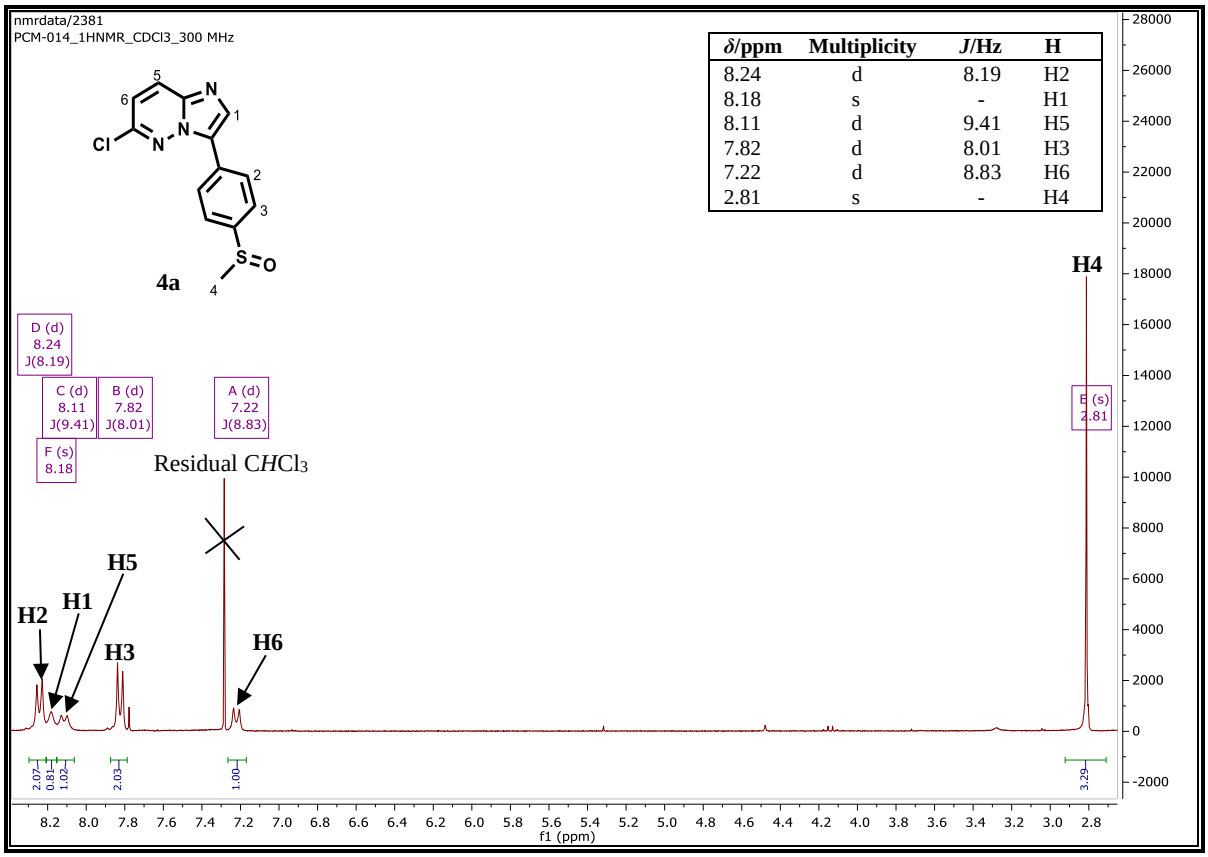

Figure 2.4: ^{1}H-NMR spectrum of **4a** at 300 MHz in $CDCl_3$.

The first Suzuki-Miyaura cross-coupling reaction [step (iii) in scheme 2.1] also gave rise to regioisomeric biaryl intermediates with basic side chains on the phenyl ring (**4e** – **g**). As expected, two of these regioisomeric intermediates, whose formation was monitored by HPLC-MS, exhibited the same quasi-molecular ion peak $[M + H]^+$ at *m/z* 333.1 (calculated exact mass = 332.1204). Common to all three regioisomeric intermediates is the diethylaminomethyl group attached to the benzene ring. As anticipated, in addition to aromatic protons resonating in the aromatic region (δ = 7.00 – 8.25 ppm), the ^{1}H-NMR spectra of these intermediates were characterized by three signals in the aliphatic region (see representative spectrum in figure 2.5). The highly shielded methyl protons resonated upfield giving a triplet at around δ = 1.13 ppm which integrated for 6 protons of the two methyl groups of the basic side chain. A 4-proton quartet signal, corresponding to the 4 hydrogens on the two methylene groups adjacent to the methyl groups, was also observed at approximately δ = 2.65 ppm. The non-coupled aliphatic protons of the comparatively deshielded methylene carbon bonded to the nitrogen and the benzene ring resonated as a singlet at around δ = 3.70 ppm. A representative ^{1}H-NMR spectrum for this class of intermediates is shown in figure 2.5.

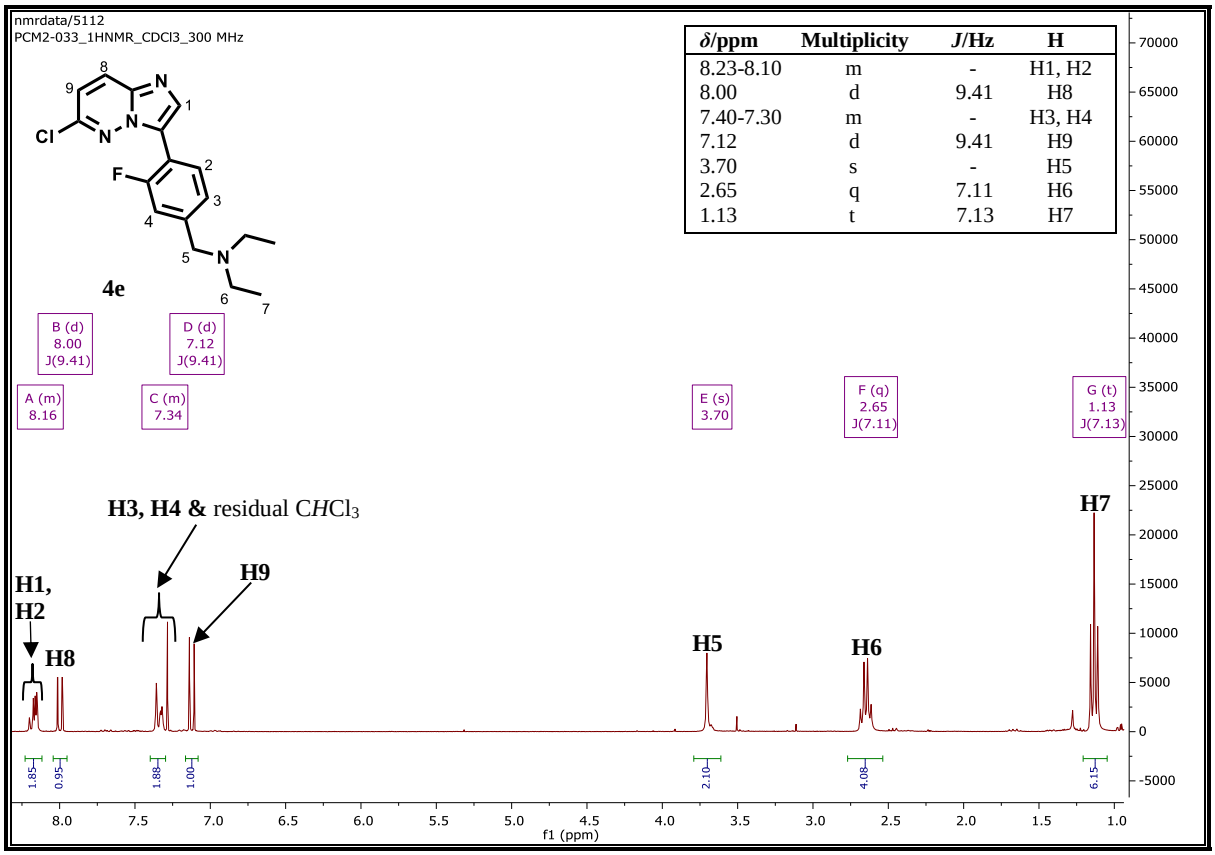

Figure 2.5: ^{1}H-NMR spectrum of **4e** at 300 MHz in $CDCl_3$.

2.3.2.4 Suzuki-Miyaura Cross-coupling: Step (iv), Scheme 2.1

Diaryl-imidazopyridazine analogues were obtained following a second Suzuki-Miyaura cross coupling as captured in scheme 2.1. For the reaction mechanism of this and other Suzuki-Miyaura cross-coupling reactions in this thesis, refer to scheme 2.8. The final target compounds representing this class are shown in table 2.1. For all diphenylated analogues containing either the sulfone or sulfoxide groups on both phenyl rings (**19**, **26**, **27**, **50** – **54** and **58**), the number of aromatic protons was constant. This was consistent with all the corresponding ^{1}H-NMR spectra which exhibited aromatic signals integrating for 11 protons in total. The ^{1}H-NMR spectrum for the representative analogue **26** is shown in figure 2.6.

A well resolved ^{1}H-NMR multiplicity pattern was observed. As anticipated, the more shielded sulfinylmethyl protons (H9) resonated as a singlet relatively upfield (δ = 2.84 ppm) while the less shielded sulfonylmethyl protons (H4) resonated as a singlet relatively downfield at δ = 3.15 ppm. The splitting pattern of the protons attached to the imidazopyridazine core (H1, H5 and H6) was similar to that observed for the intermediate **4e** (Figure 2.5). Four distinct doublets corresponding to the four pairs of phenyl protons were observed. In this regard, protons H2 resonated at δ = 8.41 ppm integrating for two protons while showing coupling to a two-proton

signal for H3 (J ~ 8.8 Hz). In like manner, coupling was observed for protons H7 and H8 which were associated with the same coupling constant (J ~ 8.7 Hz) at chemical shifts δ = 8.19 and 7.88 ppm respectively.

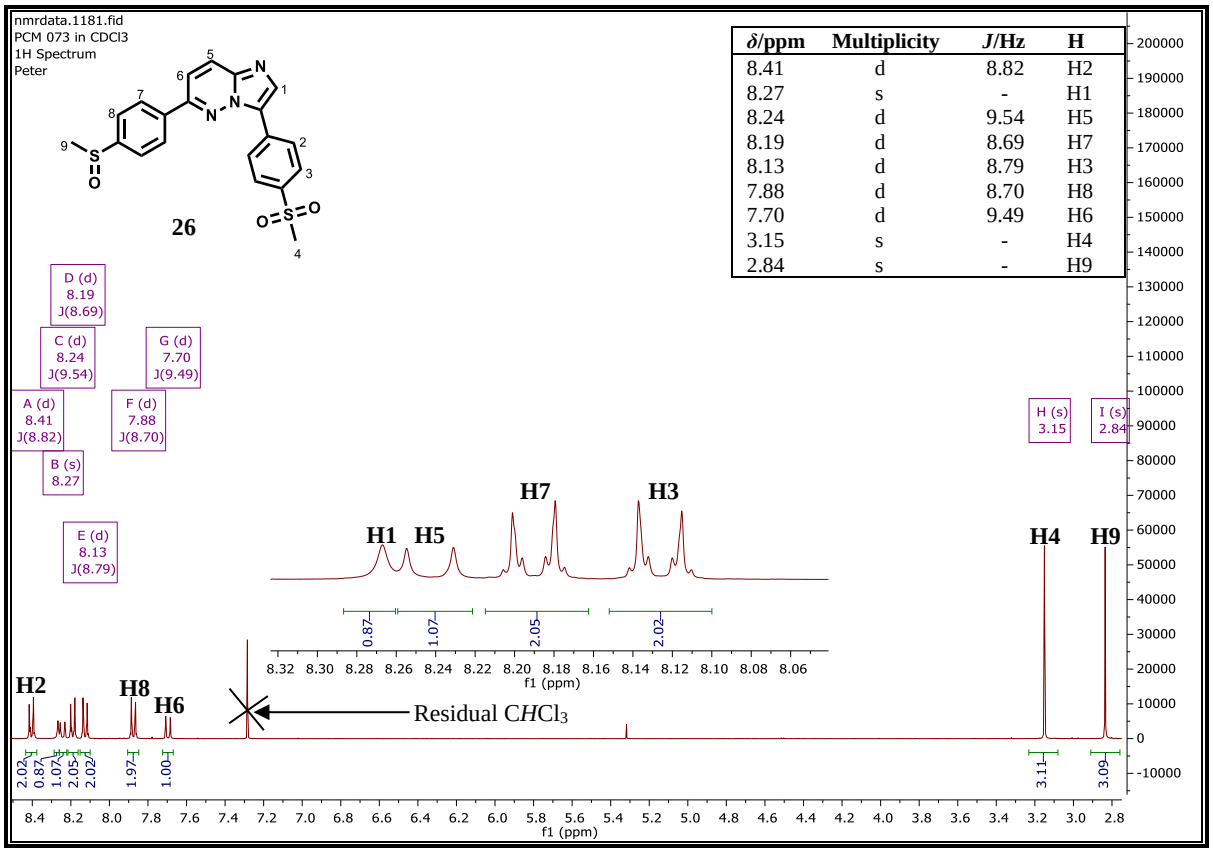

Figure 2.6: ^{1}H-NMR spectrum of **26** at 400 MHz in $CDCl_3$.

The ^{13}C-NMR spectrum for the representative compound **26** is shown in figure 2.7. Heteronuclear Single Quantum Coherence (HSQC) spectroscopy, a 2-D NMR technique facilitated the unambiguous assignment of signals arising from carbons attached to protons. As anticipated, two signals appearing in the aliphatic region at δ = 44.00 and 44.58 ppm corresponded to C9 and C4 respectively. Also notable are signals corresponding to C5 and C6 which resonated at δ = 126.65 and 116.66 ppm respectively with virtually the same peak intensity. As expected, chemically equivalent phenyl carbons such as C2, C3, C7 and C8 gave relatively intense signals in the range δ = 128.08 - 124.49 ppm. Carbon C1 was also unambiguously assigned to a signal at δ = 134.52 ppm. The relatively weak signals observed in the range δ = 151.23 - 137.92 ppm and at δ = 133.74 ppm, in addition to intense signals, were attributed to quaternary carbons. Additionally, two other quaternary carbons resonated together with C7 (128.08 ppm) and C3 (127.97 ppm) as is evident from the pronounced peak intensity of signals at these two chemical shifts.

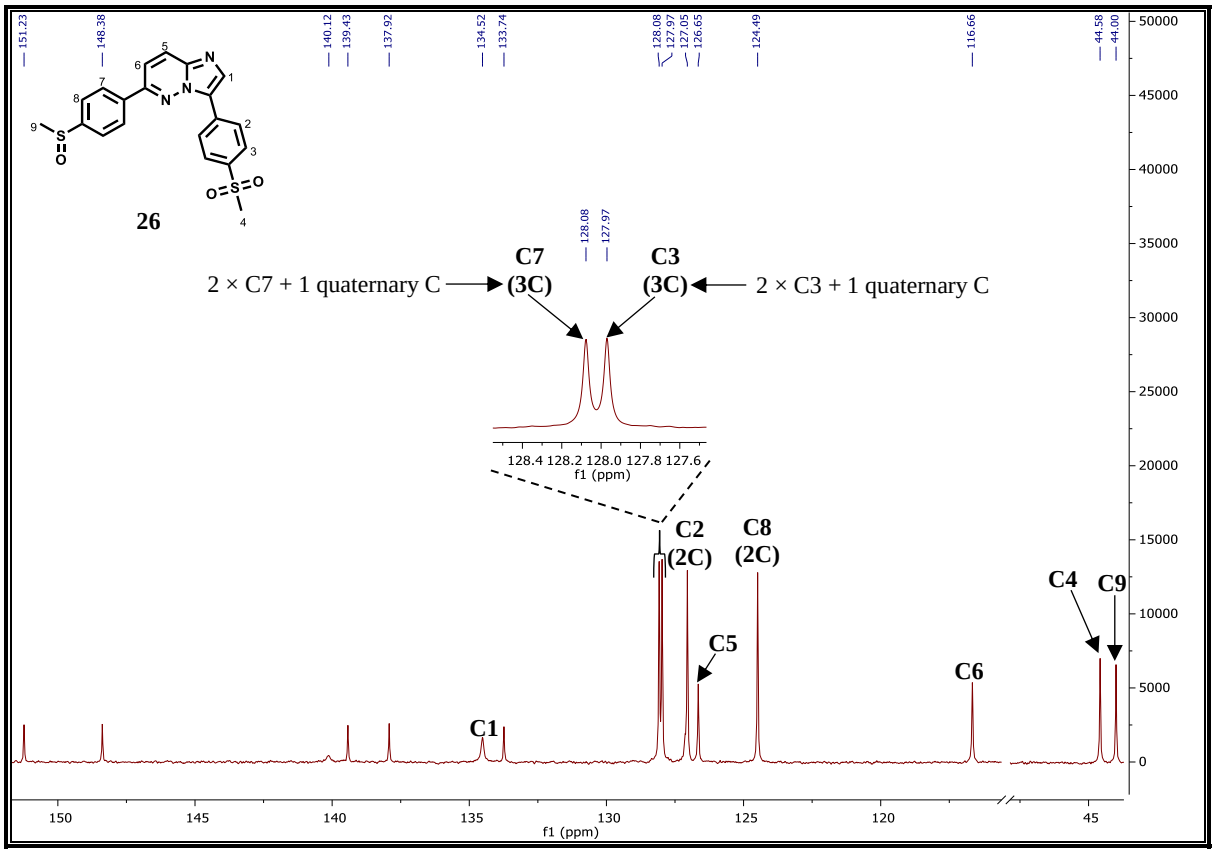

Figure 2.7: ^{13}C-NMR spectrum of **26** at 101 MHz in $CDCl_3$.

HPLC-MS analysis of these analogues further confirmed their successful synthesis with pseudo-molecular ion $[M + H]^+$ *m/z* peaks observed for all the compounds. For a representative analogue **26** (calculated exact mass = 411.0711), a pseudo-molecular ion $[M + H]^+$ was observed at *m/z* = 412.1 at a retention time, t_r = 2.518 min (Figure 2.8).

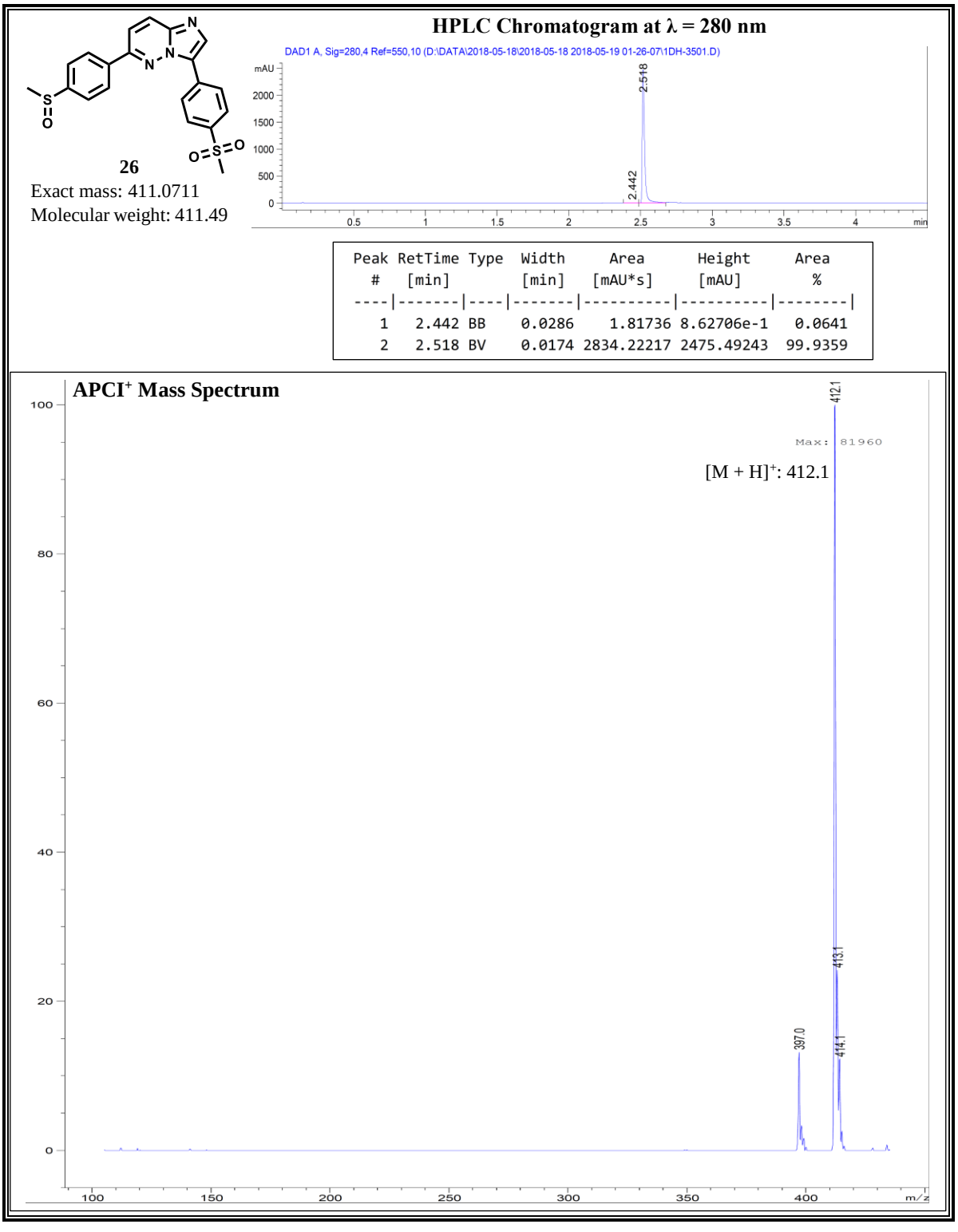

Figure 2.8: HPLC Chromatogram and APCI$^+$ mass spectrum of **26**.

The second Suzuki-Miyaura cross-coupling reaction on the chloro-substituted intermediates (step iv, scheme 2.1) also delivered other biaryl analogues such as the regioisomeric analogues **28** – **30** (Table 2.1). Additionally, **31** (Table 2.1), an analogue with a pro-drug-like relationship

with compound **29**, was also synthesized. The ^{1}H-NMR spectra of these analogues were generally of a similar pattern with 4 characteristic signals in the aliphatic region corresponding to the four different classes of aliphatic protons. The spectrum for analogue **30** (Figure 2.9) is shown as a representative example. The relatively highly shielded methyl protons H12 were observed as a triplet at δ = 1.14 ppm and coupled to the neighbouring H11 protons. The slightly more deshielded four H11 protons resonated as a quartet at δ = 2.67 ppm and, as expected, exhibiting the same coupling constant (J = 7.07 Hz) as that of the H12 triplet. However, for analogues **28** and **31**, the expected quartet at around the same chemical shift was not well resolved, and all attempts at manipulating the samples to get the desired multiplicity proved futile. Very sharp singlet peaks corresponding to the uncoupled H4 and H10 protons were also observed at δ = 2.81 and 3.78 ppm respectively. Notable multiplicity patterns in the aromatic region include the unusual multiplet at δ = 7.20 ppm. Although this peak, corresponding to proton H8, has a typical triplet appearance, attempts to calculate the corresponding coupling constant were unsuccessful. Furthermore, ^{1}H-NMR-processing software also recognized this signal as a multiplet. This is hardly surprizing because proton H8 could be experiencing unequal coupling from proton H7 and the adjacent fluorine. Similarly, a signal that appears as a doublet of doublet of doublets (ddd) at δ = 7.92 ppm could not be recognized as such due to unequal long-range couplings between proton H9 and the fluorine atom. More sophisticated NMR experiments, such as the two-dimensional Correlation Spectroscopy (COSY) and HSQC also gave insight into such fluorine-coupling behaviour. On the other hand, protons H2 and H3 were observed as two doublets at δ = 8.37 and 7.80 ppm respectively with exactly equal coupling constants (J = 8.65 Hz). As expected, the other regioisomeric analogues, including the sulfone **31**, gave different aromatic multiplicity patterns attributable to the different positions of the fluoro and diethylaminomethyl groups on the phenyl ring.

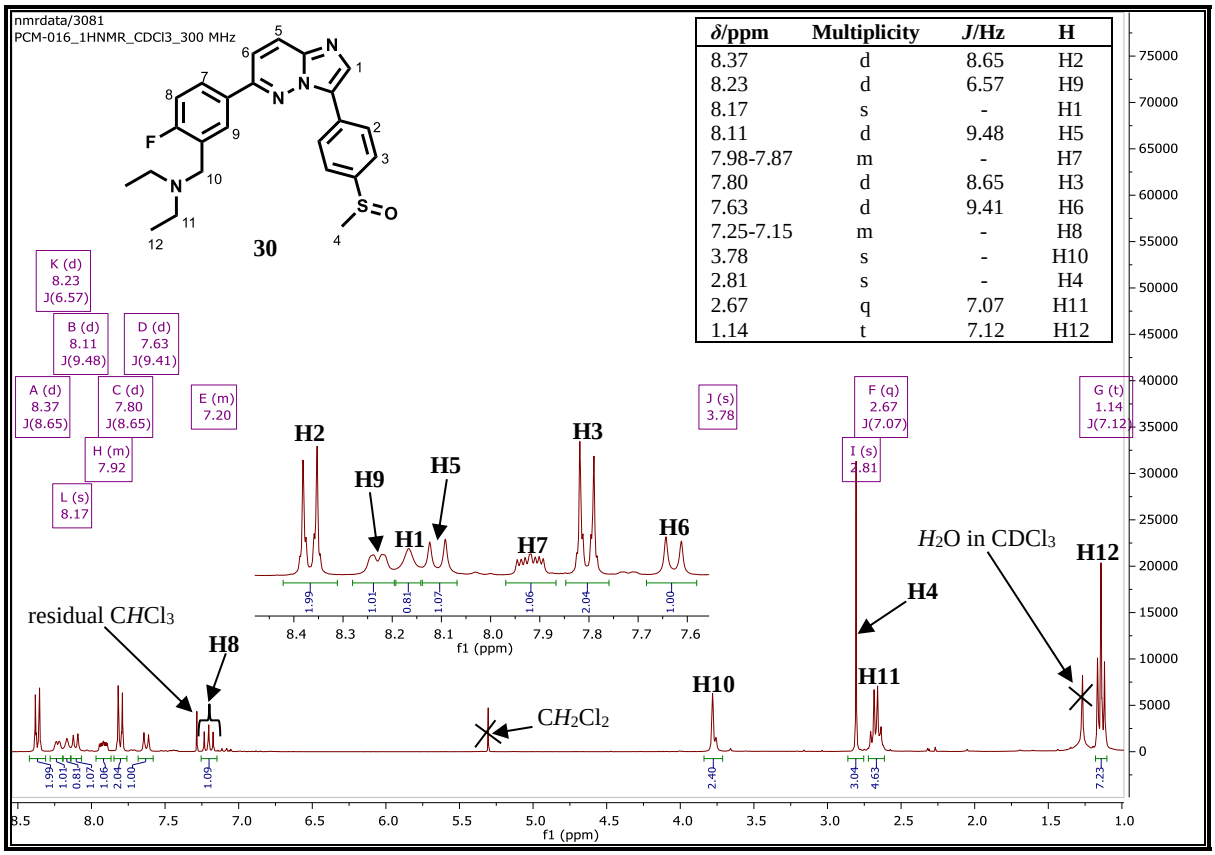

Figure 2.9: ^{1}H-NMR spectrum of **30** at 300 MHz in $CDCl_3$.

Further characterization by HPLC-MS of these analogues confirmed their molecular weights. The isomeric analogues exhibited the same *m/z* values corresponding to their quasi-molecular ions $[M + H]^+$ (**30**: *m/z* = 437.1, calculated exact mass = 436.1733; **28**: *m/z* = 437.1, calculated exact mass = 436.1733 and **29**: *m/z* = 437.2, calculated exact mass = 436.1733). With a calculated exact mass of 452.1682, the sulfone, **31**, also exhibited a quasi-molecular ion at *m/z* = 453.1. For the representative analogue **30**, the HPLC chromatogram and mass spectrum are shown in figure 2.10.

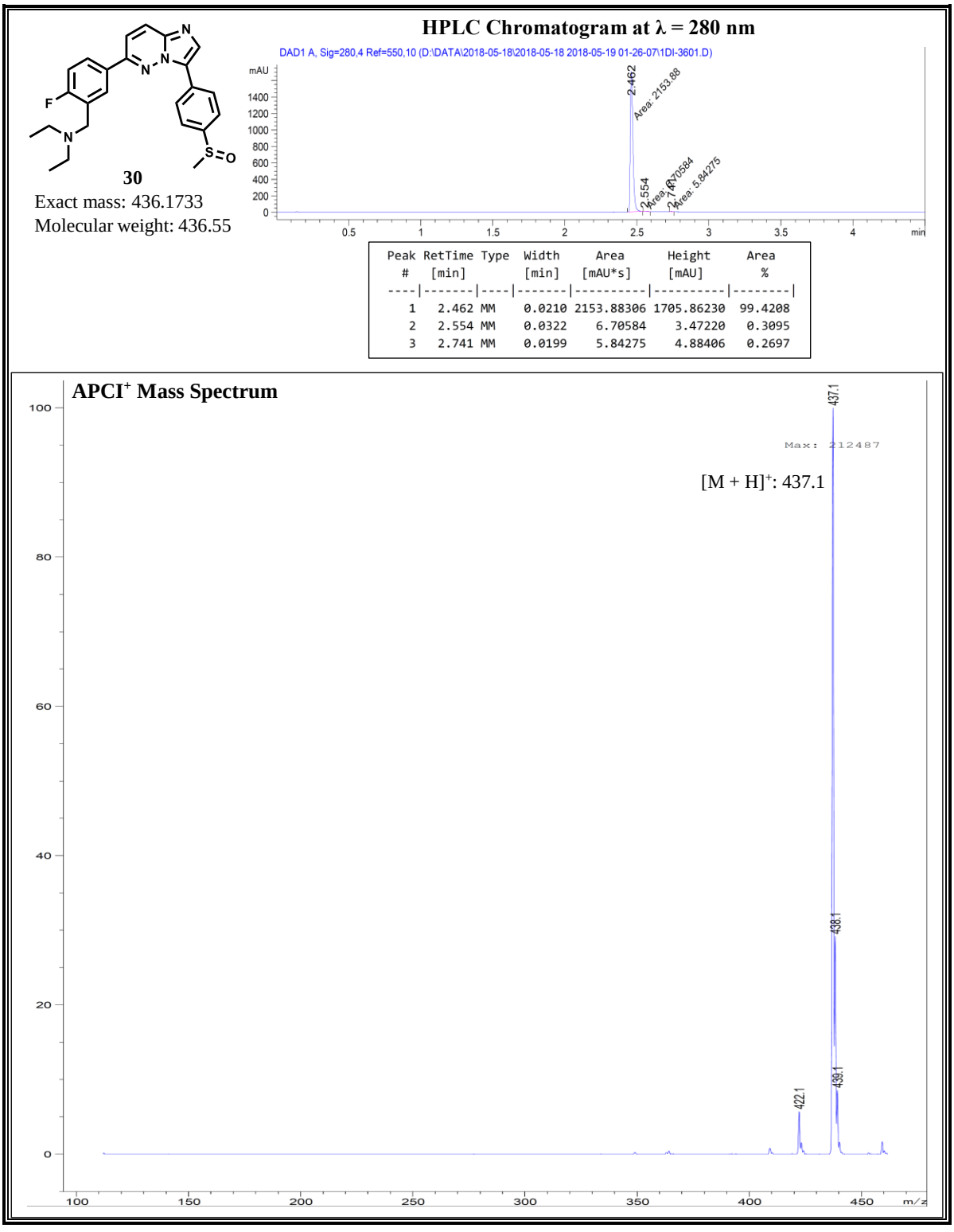

Figure 2.10: HPLC Chromatogram and APCI$^+$ mass spectrum of **30**.

Keeping the left-hand portion of the imidazopyridazine core-scaffold as 3-methylsulfinylphenyl moiety while introducing basic side chains on the right portion gave rise to analogues **32 - 34** (Table 2.1). These derivatives are also regioisomeric to one another and

so are they to derivatives **28 - 30** (Table 2.1). Therefore, the ^{1}H-NMR signal pattern remained essentially the same for these sets of regioisomers. As observed for the other regioisomers, the expected splitting pattern for two of these analogues (**32** and **33**) was not observed. In this regard, the expected 4-proton quartet signal for the 4 methylene protons of the two carbons directly bonded to the nitrogen atom of the basic side chain was not observed. Compound **32** gave a broad singlet while **33** gave a broad doublet for these protons. On the contrary, a well resolved multiplicity was observed for **34** and the solved ^{1}H-NMR spectrum for this representative compound is shown in figure 2.11 below.

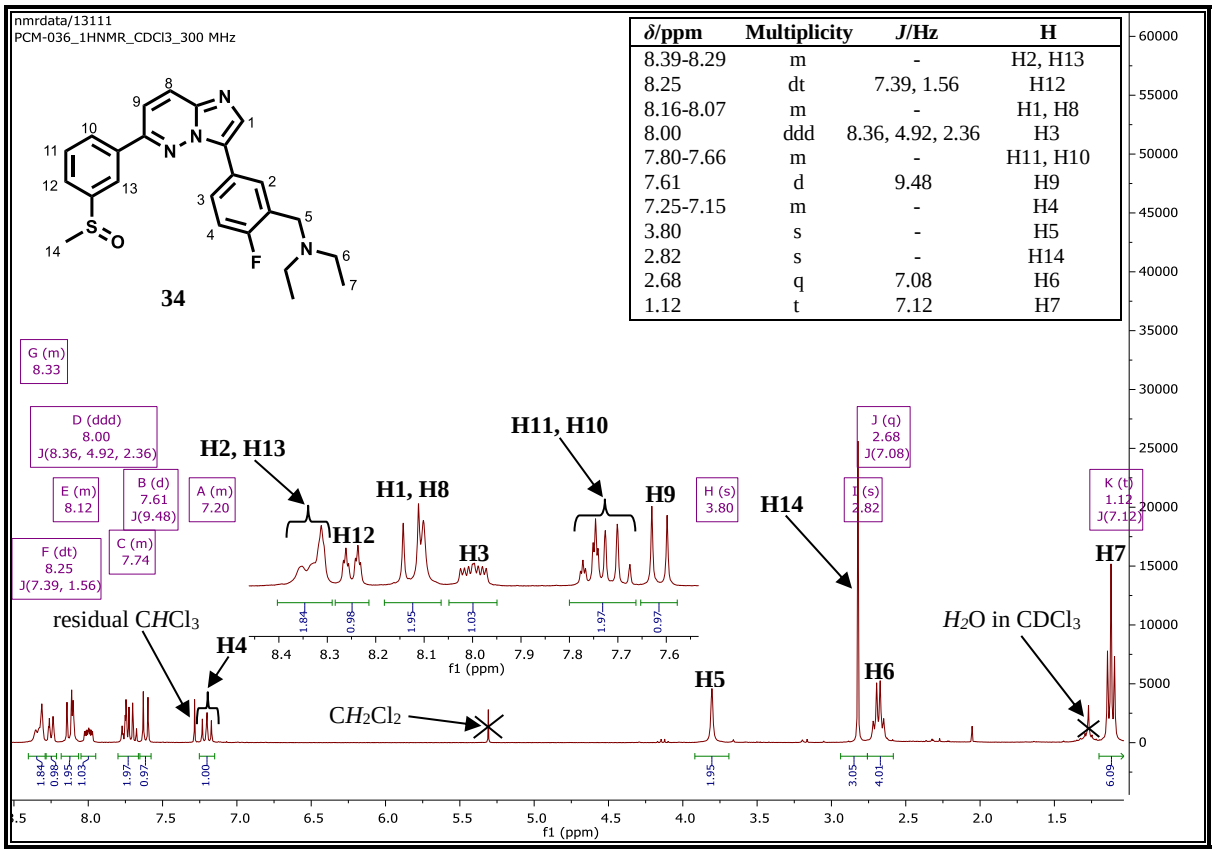

Figure 2.11: ^{1}H-NMR spectrum of **34** at 300 MHz in $CDCl_3$.

Noteworthy splitting patterns in the ^{1}H-NMR spectrum is the doublet of triplets (dt) at δ = 8.25 ppm. This signal was attributed to proton H12 whose short range (J^3) coupling to H11 accounts for one large coupling constant (J = 7.39 Hz). The second, and relatively smaller coupling constant (J = 1.56 Hz), arises from long range coupling (J^4) to H10 and H13. COSY and HSQC NMR correlation experiments were employed to gain insight into such coupling behaviour. Again, employing such correlation experiments, the well resolved 1-proton signal splitting as a doublet of doublet of doublets (ddd) was attributed to proton H3. In this regard, a short-range coupling to H4, and two unequal long-range couplings to fluorine and H2 resulted in such a

splitting pattern. As observed previously for analogue **30**, H4 was recognized as a multiplet albeit exhibiting an appearance of a triplet. This, once again, may be attributed to unequal couplings to H3 and the adjacent fluorine atom.

Furthermore, all the 24 carbon atoms in compound **34** were accounted for in the ^{13}C-NMR spectrum shown in figure 2.12. The two highly shielded equivalent carbon atoms, C11, resonated at the most upfield chemical shift (δ = 11.58 ppm). C22 connected to a less electronegative atom (sulfur) resonated relatively upfield (δ = 44.13 ppm) compared to C10 (δ = 46.97 ppm) and C9 (δ = 49.88 ppm) carbons which are directly connected to a more electronegative atom (nitrogen). The aromatic C14 resonated at δ = 115.04 ppm which is consistent with the chemical shift (δ = 116.66 ppm) observed for the same carbon in compound **26** (see figure 2.7). However, the neighbouring carbon (C13) resonates significantly downfield (δ = 133.60 ppm) compared to the same carbon in analogue **26** (δ = 126.65 ppm). Interestingly, C7 resonated as a doublet at δ = 115.61 ppm with a large coupling constant (J = 22.94 Hz) which is typical of J^2 coupling to the fluorine attached to the adjacent carbon atom, C6.[45] As expected, the quaternary carbon C6 directly attached to the fluorine atom was highly deshielded resonating as a weak signal at δ = 162.23 ppm. It is also worth noting that, for aromatic carbons bonded to hydrogens, those on the sulfoxide-substituted phenyl ring (C17 – C19 and C21) including the imidazo C1 all resonated as strong signals. On the contrary, C4, C7 and C8 attached to the fluoro- and diethylaminomethyl-substituted phenyl ring were relatively weaker. As expected, all the remaining seven quaternary carbons resonated as seven weak signals (see unassigned signals).

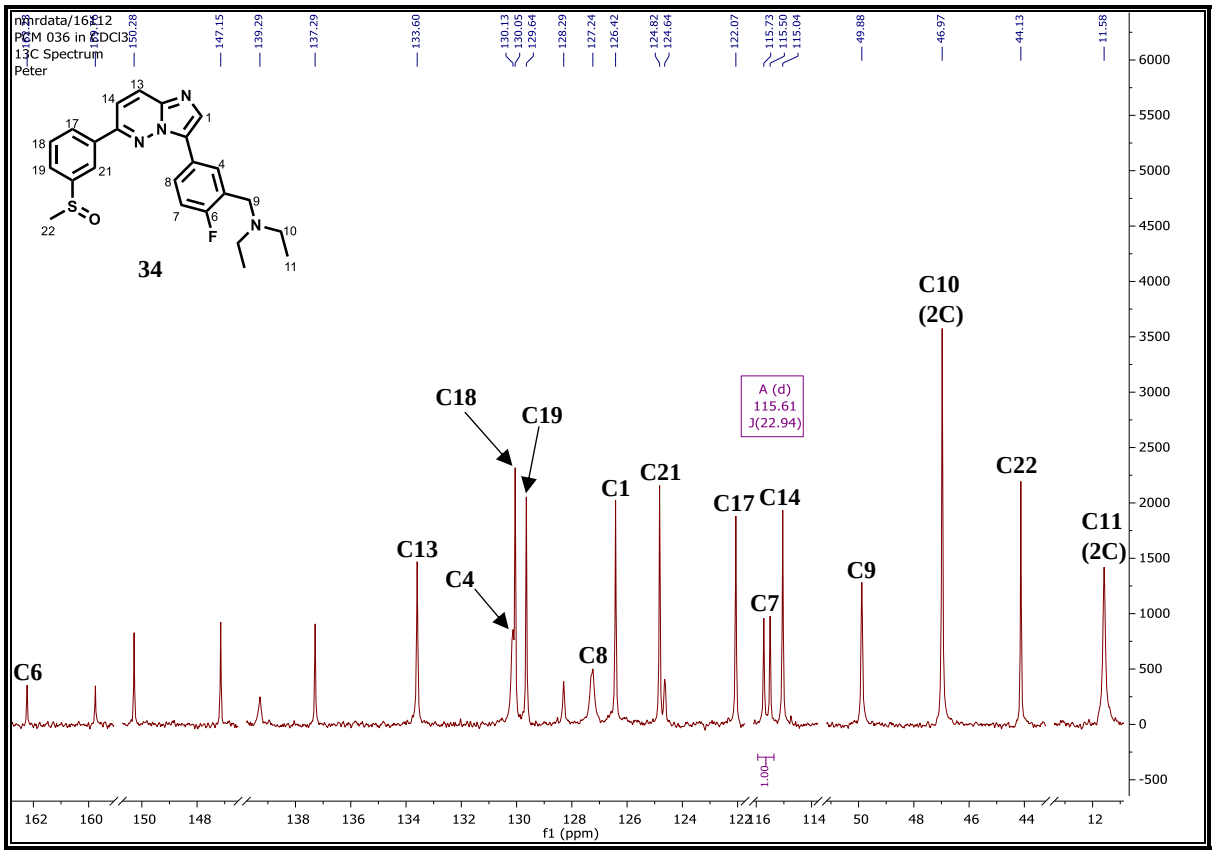

Figure 2.12: ^{13}C-NMR spectrum of **34** at 101 MHz in $CDCl_3$.

When further subjected to molecular weight confirmation by HPLC-MS, the three analogues (**32 - 34**) exhibited the same quasi-molecular ion $[M + H]^+$ at *m/z* = 437.2, calculated exact mass = 436.1733. The three regioisomers also exhibited almost the same retention times (t_r ~ 2.5 min). The HPLC chromatogram and the mass spectrum of the representative analogue **34** is shown in figure 2.13 below.

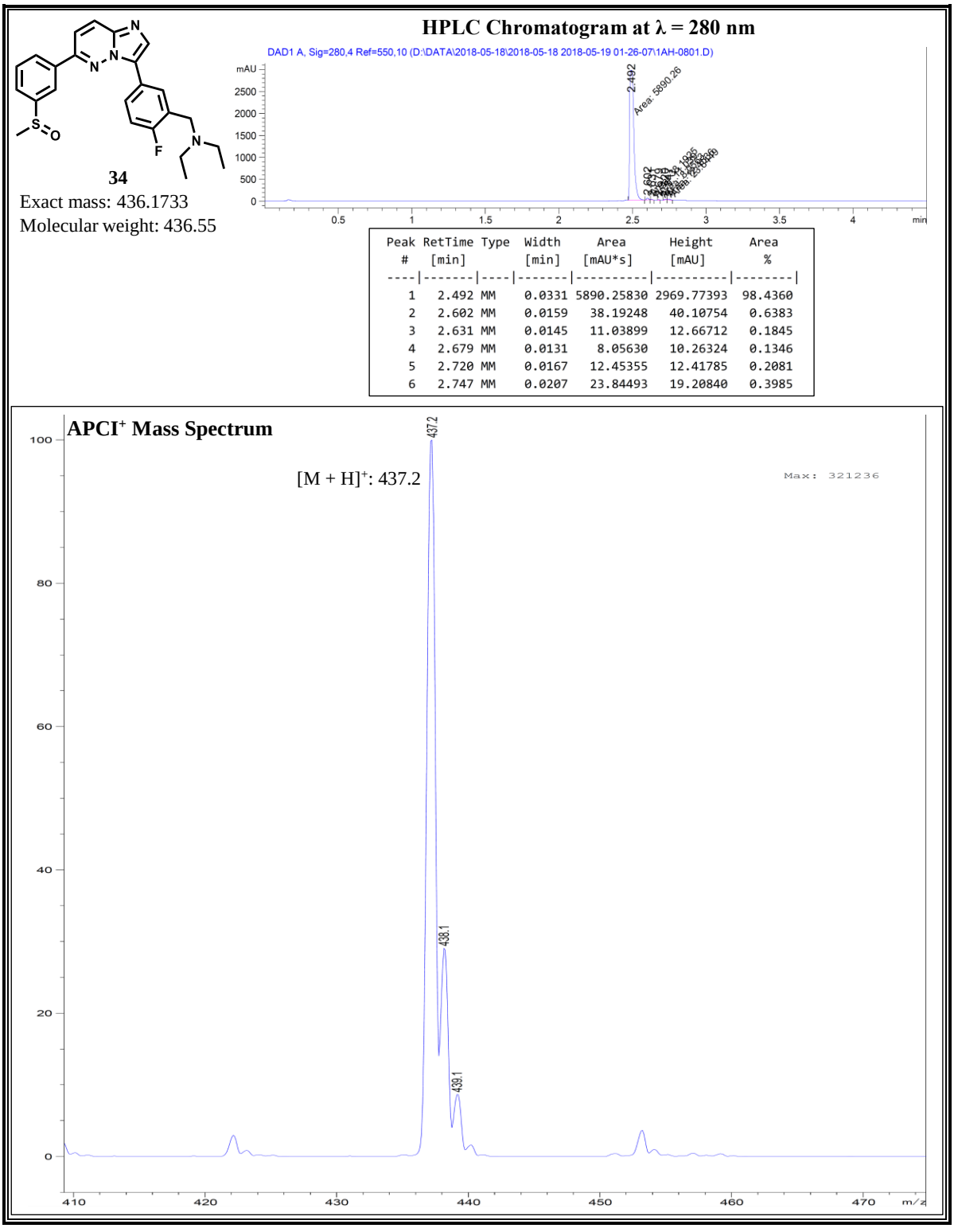

Figure 2.13: HPLC Chromatogram and APCI$^+$ mass spectrum of **34**.

2.3.2.5 Buchwald-Hartwig Amination: Step (v), Scheme 2.1

As opposed to the Suzuki-Miyaura cross-coupling, which leads to carbon-carbon bond formation, the Buchwald-Hartwig amination furnishes compounds containing carbon-nitrogen

bonds. In some aspects, the catalytic cycle by which this reaction occurs is similar to that for the Suzuki-Miyaura cross-coupling. In this reaction, an aryl halide is cross-coupled with an amine in presence of a palladium catalyst and a base. The reaction's catalytic cycle is depicted in scheme 2.9.[46–48] In the first step, the aryl halide oxidatively adds to the palladium after which the amine coordinates to the palladium metal centre. Deprotonation of the amine by the base (e.g., Cs_2CO_3), generates the highly nucleophilic amide ion, which then substitutes the chloro group. The final aminated product is then formed via a reductive elimination step with the palladium catalyst being regenerated.

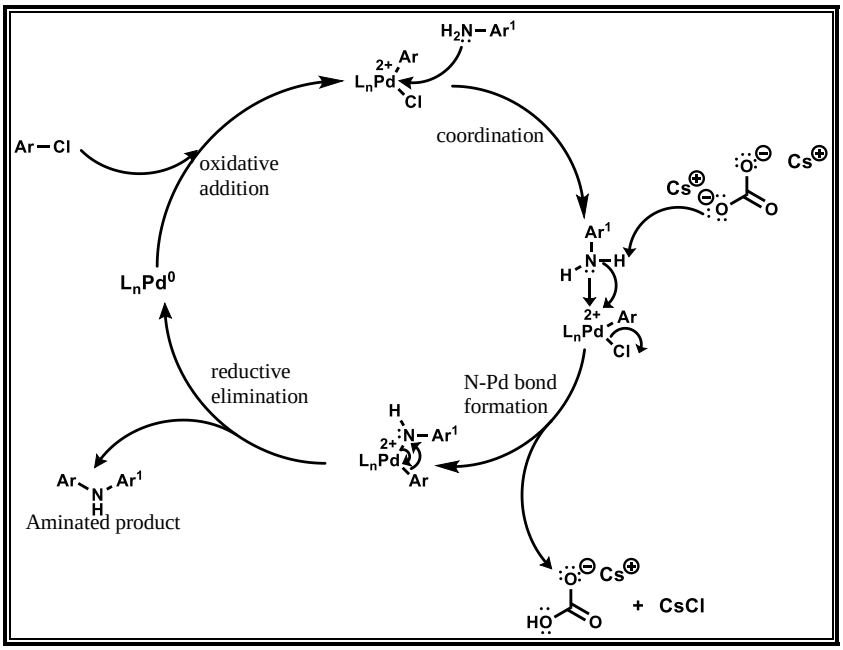

Scheme 2.9: Catalytic cycle for the Buchwald-Hartwig amination.[46–48]

This reaction afforded analogues with an amino (NH) linker between the core imidazopyridazine scaffold and the aromatic/aliphatic substituents (**36** – **45**, Table 2.1). Consistent with the newly introduced NH linker, the ^{1}H-NMR spectra of all the analogues, save for **45**, showed a diagnostic signal corresponding to the N*H* proton. Except for analogue **45** whose ^{1}H-NMR spectrum was acquired in deuterated methanol (CD_3OD), all ^{1}H-NMR spectra for the remainder of the aminated analogues were acquired in deuterated dimethylsulfoxide (DMSO-d_6) and chloroform ($CDCl_3$) in the case of **44**. Therefore, the absence of an N*H* signal in the spectrum for **45** could be, most likely, due to protium-deuterium (H-D) isotopic exchange which is common[48] when ^{1}H-NMR spectra are acquired in CD_3OD for compounds containing exchangeable hydrogens. For analogues appended with aromatic amines (**36** - **40**, **44** and **45**), the N*H* proton resonated relatively downfield at around δ = 10 ppm while the N*H* proton on

the aliphatic-attached nitrogen in the remainder of the analogues resonated relatively upfield at around δ = 7.0 ppm. In the case of **44** and **45**, such a coupling reaction was accompanied by the appearance of aliphatic-region ^{1}H-NMR signals corresponding to the basic side chain in these compounds.

A representative ^{1}H-NMR spectrum for analogue **37** is captured in figure 2.14. Two diagnostic signals were observed. These include a signal arising from the highly deshielded N*H* (H7) proton which appears as a singlet at δ = 9.81 ppm. Successful installation of a methylsulfinylaniline moiety was also accompanied by the appearance of an extra signal at δ = 2.73 ppm integrating for three protons of the methylsulfinyl group. Some other noteworthy splitting patterns arising from the newly introduced group include a singlet with a triplet-like appearance which was not well resolved at δ = 8.11 ppm. This corresponded to proton H11 whose triplet-like shape could be arising from long range J^4 coupling to protons H8 and H10. Proton H8 resonated as a doublet of doublets signal at δ = 7.77 ppm integrating for one proton. Short range coupling (J^3 = 8.09 Hz) to H9 as well as long range coupling (J^4 = 1.30 Hz) to H10 explains this splitting pattern. A well-defined one-proton triplet signal (δ = 7.57 ppm, J = 7.89 Hz) and doublet (δ = 7.31 ppm, J = 7.66 Hz) were attributed to protons H9 and H10 respectively. Short range coupling to two neighbours (H8 and H10) accounts for the splitting pattern of the H9 signal while coupling to H9 accounts for the H10 doublet.

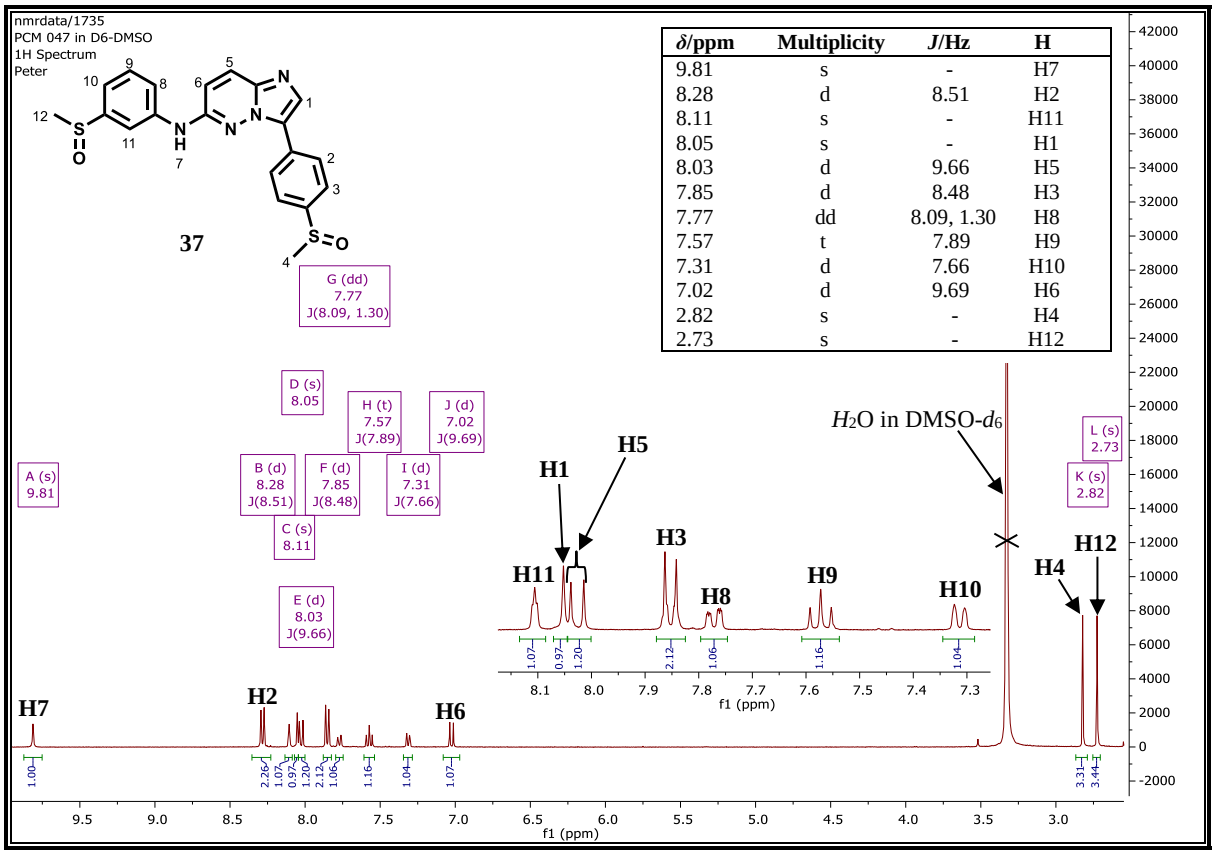

Figure 2.14: ^{1}H-NMR spectrum of **37** at 400 MHz in DMSO-d_6.

The aminated analogues were also confirmed by ^{13}C-NMR and figure 2.15 shows a representative spectrum for the aniline analogue **37**. The signals in the spectrum were generally well resolved with minimal overlap. Notable chemical shift values arising from the introduced aniline motif include those from the hydrogen-containing carbons such as 43.83 ppm (C18); 113.50 ppm (C17); 117.01 ppm (C15); 121.14 ppm (C13) and 130.32 ppm (C14) which were, as expected, more pronounced than the seven unassigned quaternary carbon signals.

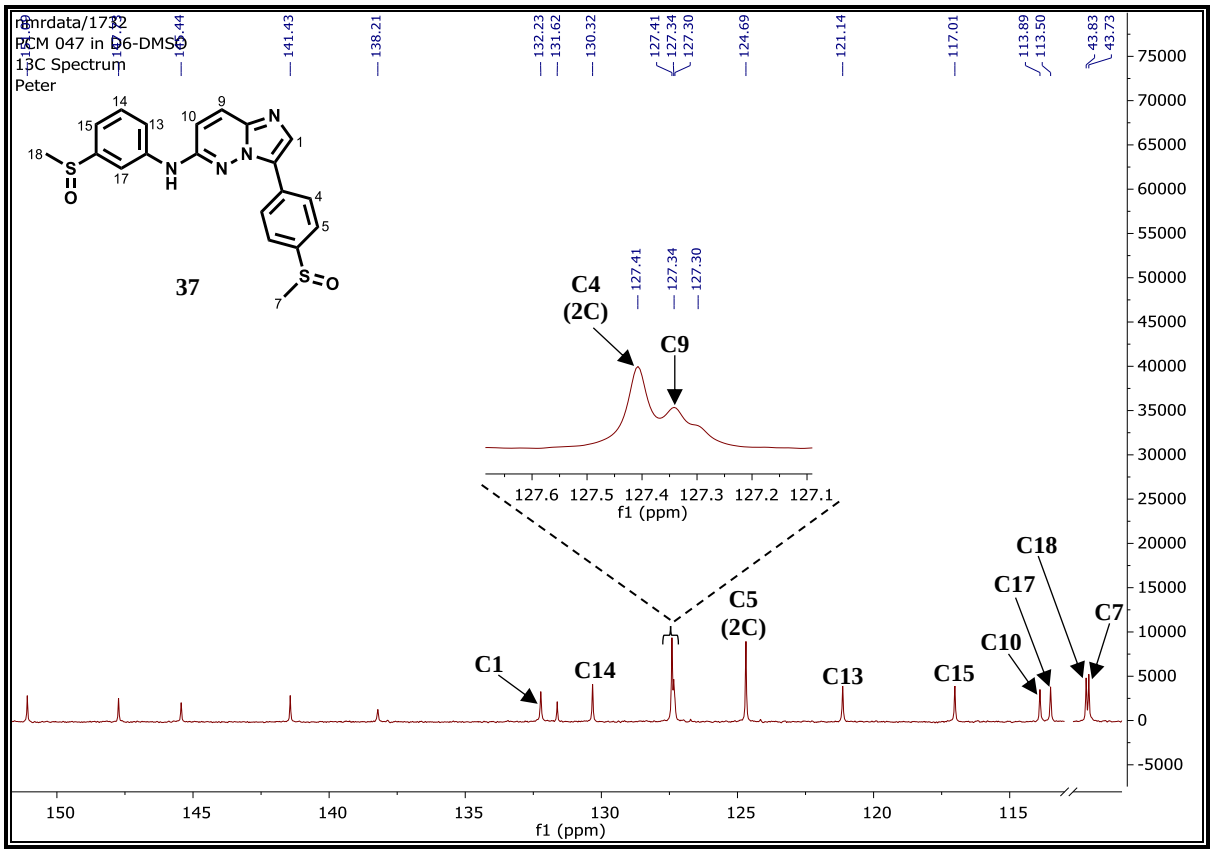

Figure 2.15: ^{13}C-NMR spectrum of **37** at 101 MHz in DMSO-d_6.

When subjected to HPLC-MS analysis, analogue **37** exhibited a quasi-molecular ion (*m/z* [M + H]$^+$ = 411.0, exact mass = 410.0871 at t_r = 2.636 min) under APCI$^+$ mode (Figure 2.16).

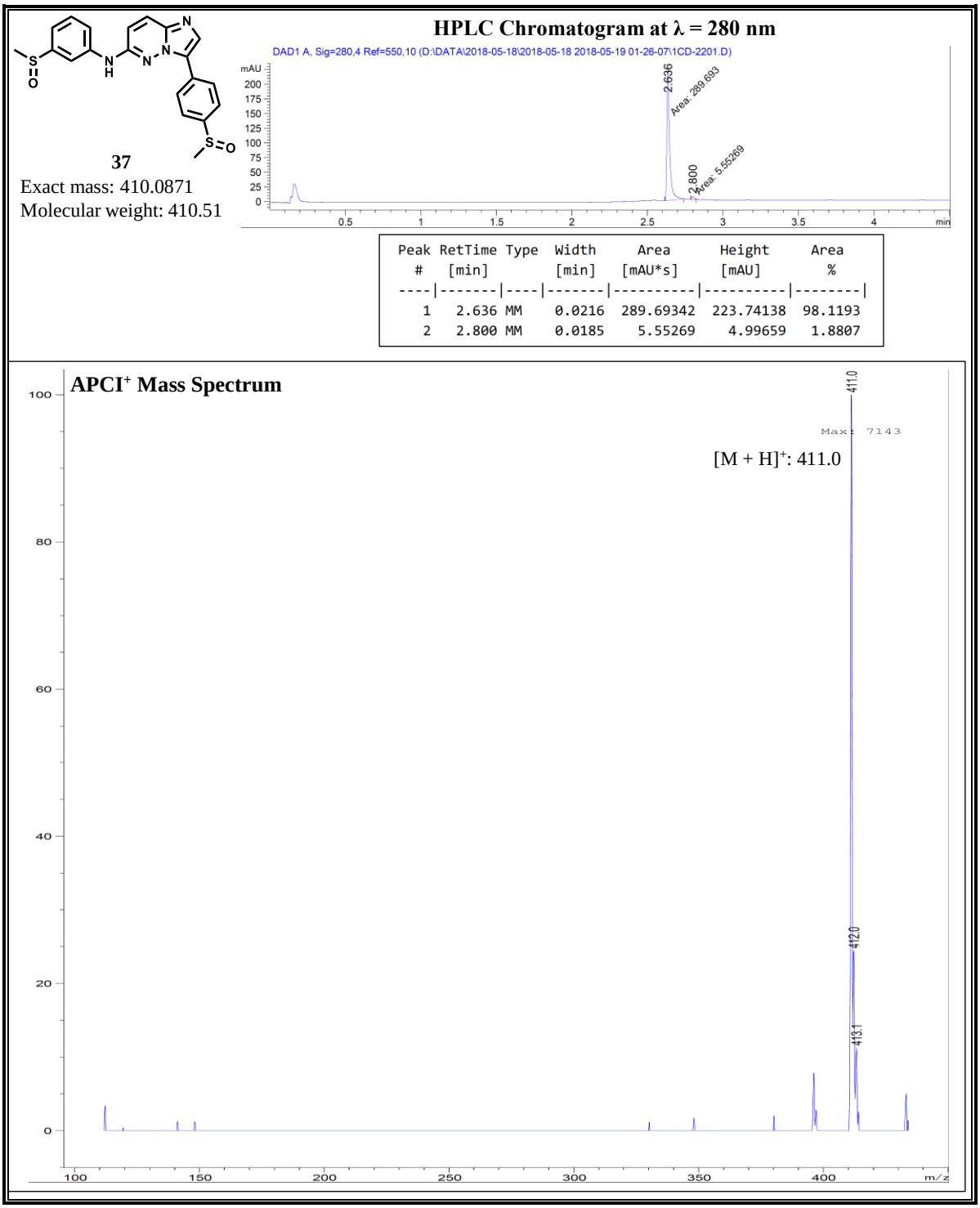

Figure 2.16: HPLC Chromatogram and APCI$^+$ mass spectrum of **37**.

The ^{1}H-NMR spectrum of **43** is shown in figure 2.17 to represent analogues possessing aliphatic amines. With the installation of the saturated cyclic amine substructure, there was a concomitant and expected decrease in the number of aromatic signals while aliphatic signals corresponding to the aliphatic protons of the piperidyl ring appeared. Notable diagnostic signals

include the N*H* proton (H7) which experiences coupling to proton H8 and, therefore, resonates as a doublet (J = 6.54 Hz, δ = 7.16 ppm). Since the piperidine ring predominantly assumes the chair conformation, the equatorial (e) and axial (a) protons resonated at different chemical shifts. Generally, the more deshielded pair of protons, H10e and H10a, appeared relatively downfield compared to the less deshielded H9e and H9a protons. COSY and HSQC experiments were also instrumental in facilitating accurate assignment of the two pairs of protons. Due to a multiplicity of coupling including geminal (J^2) and vicinal (J^3) coupling, which was also evident from COSY and HSQC experiments, the piperidyl protons resonated as multiplets. The H10e protons appeared slightly downfield at δ = 3.60 ppm as a multiplet while H10a resonated as a multiplet further upfield at δ = 3.01 ppm. Axial protons in chair conformations of piperidine are indeed known to be more shielded than their equatorial counterparts.[49] The same is true for protons H9e and H9a. Another multiplet signal integrating for one proton was observed at δ = 3.82 ppm, which was attributed to proton H8. As expected, an extra aliphatic singlet signal (δ = 2.94 ppm) integrating for three protons was unambiguously attributed to H11.

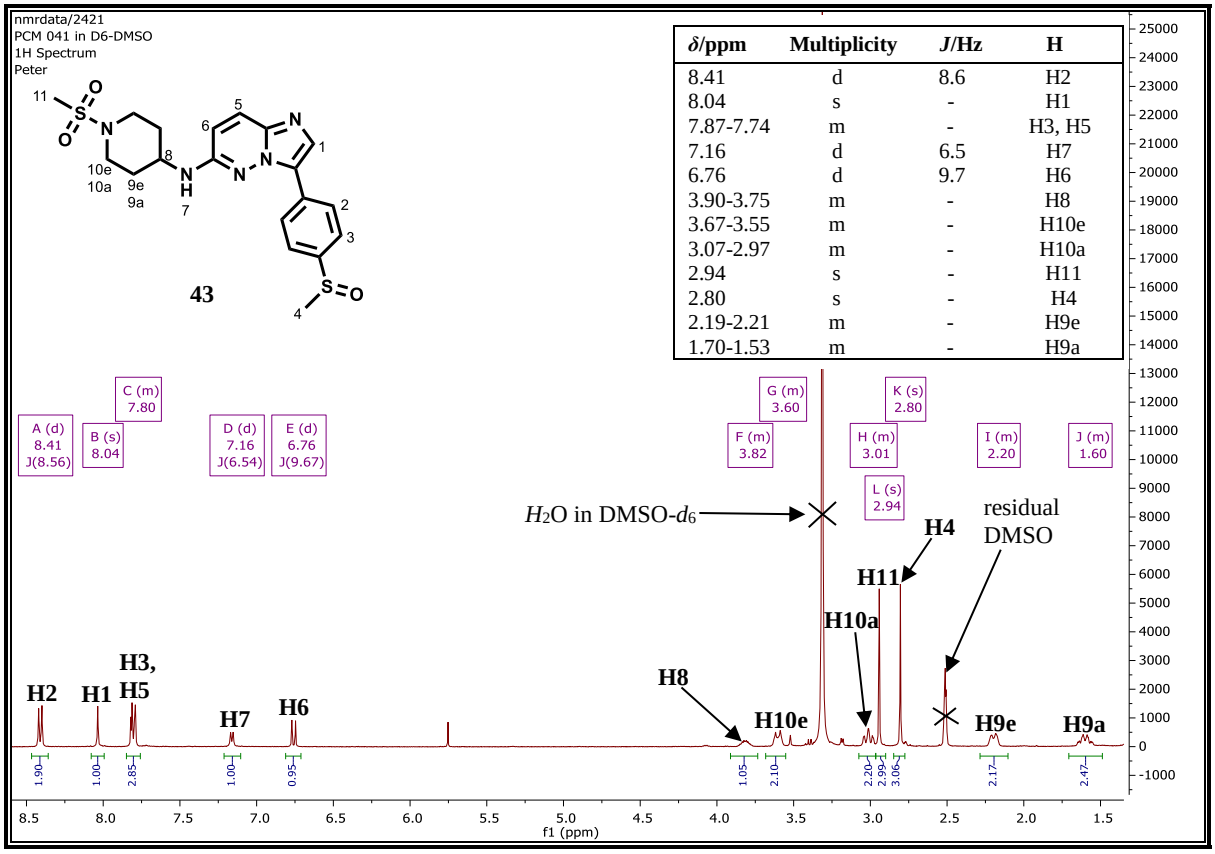

Figure 2.17: [1]H-NMR spectrum of **43** at 400 MHz in DMSO-d_6.

Correspondingly, the ^{13}C-NMR spectra for the analogues containing saturated heterocyclic rings (**41** – **43**) in place of the left-hand side phenyl ring had reduced signals in the aromatic region with a corresponding appearance of aliphatic signals. Figure 2.18 shows the ^{13}C-NMR spectrum for the representative analogue **43**. In addition to the aliphatic signal at δ = 43.62 ppm which corresponds to the methylsulfinyl carbon C7, another aliphatic-region signal was observed at δ = 35.15 ppm which was unambiguously assigned to the methylsulfonyl carbon C15. Furthermore, the five aliphatic carbons of the installed piperidine ring (C12, C13 and C14) resonated at δ = 48.00, 30.82 and 44.76 ppm respectively. The five relatively weaker unassigned signals were attributed to the five quaternary carbons.

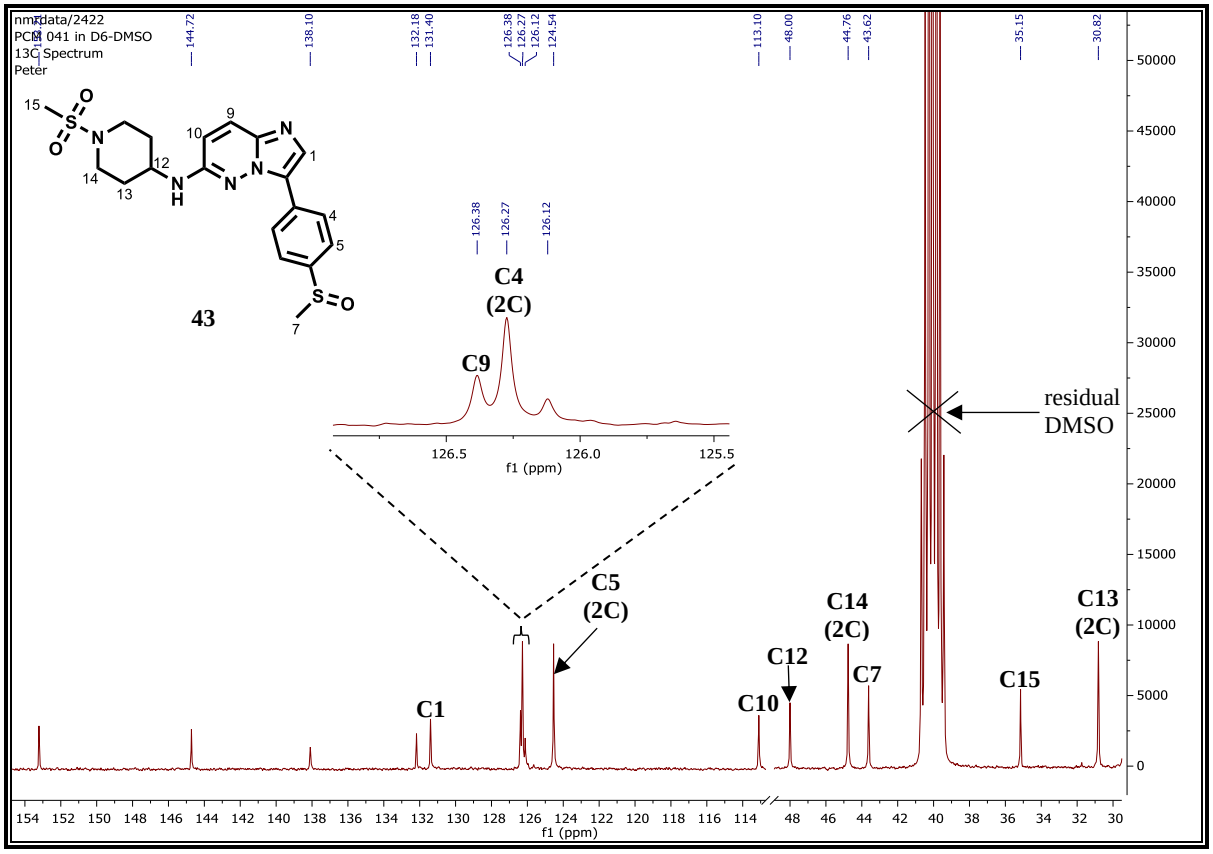

Figure 2.18: ^{13}C-NMR spectrum of **43** at 101 MHz in DMSO-d_6.

All the target compounds in this category were also characterized using HPLC-MS. A quasi-molecular ion, $[M + H]^+$, at *m/z* = 434.1 (calculated exact mass = 433.1242) was evident for analogue **43** (Figure 2.19).

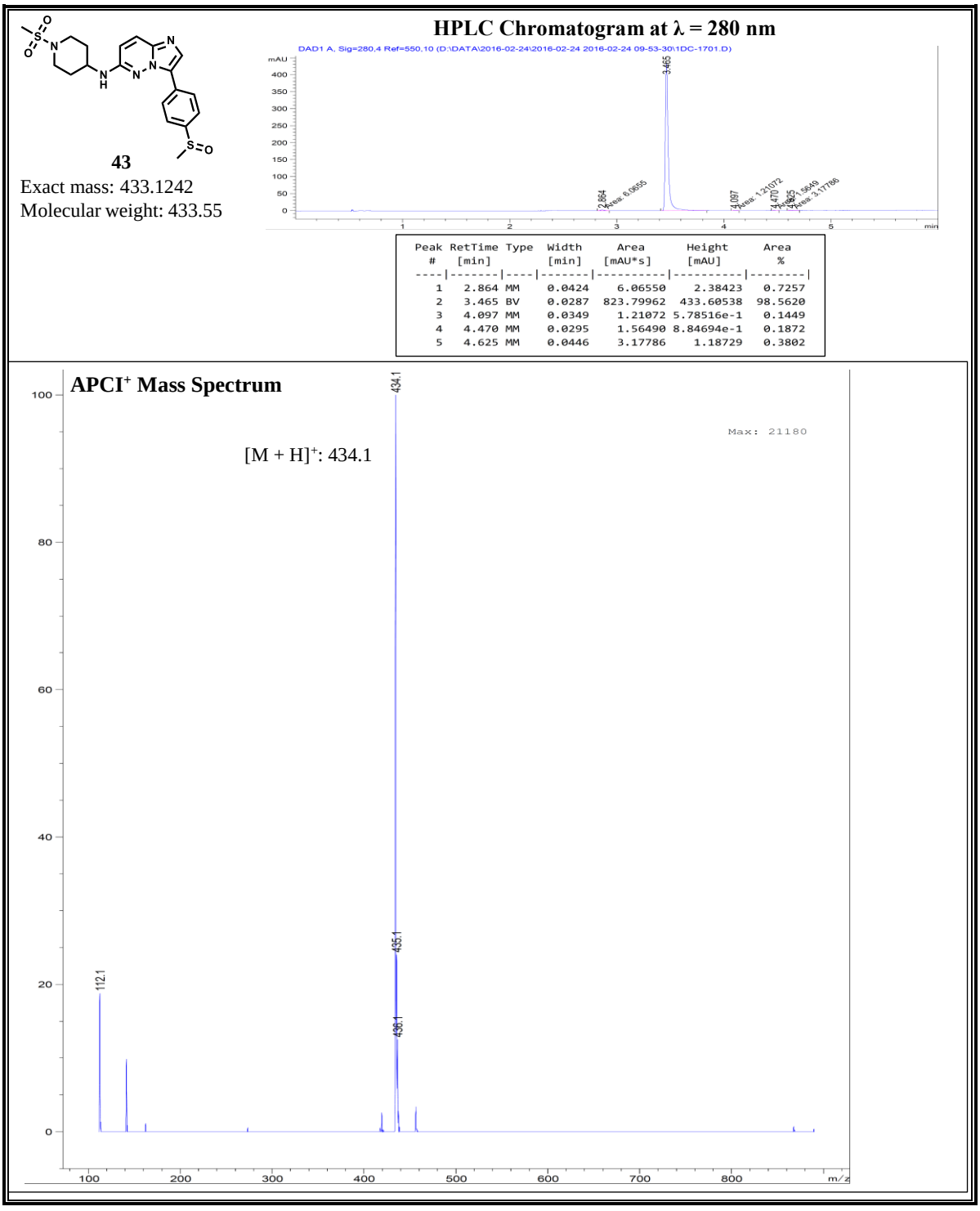

Figure 2.19: HPLC Chromatogram and APCI$^+$ mass spectrum of **43**.

2.3.2.6 *O*-Tosylation: Step (i), Scheme 2.2

Towards the synthesis of the amine precursor **5d** (Scheme 2.2), intermediate **5b** was synthesized.[50] However, this tosylated intermediate could not undergo ionization on HPLC-MS and, therefore, evidence for its successful formation was based on ^{1}H-NMR (Figure 2.20).

Two singlets in the aliphatic region at δ = 2.48 and 5.20 ppm, which integrated for three and two protons correspond to H3 and H4 respectively. Coupling with fluorine and proton H6 gave a triplet (J = 8.75 Hz) at δ = 7.22 ppm associated with proton H5. Protons H1 and H2 resonated as sharp doublets at δ = 7.38 (J = 7.97 Hz) and 7.84 ppm (J = 8.37 Hz) respectively. Further downfield, a multiplet integrating for two protons was observed corresponding to the aromatic protons H6 and H7.

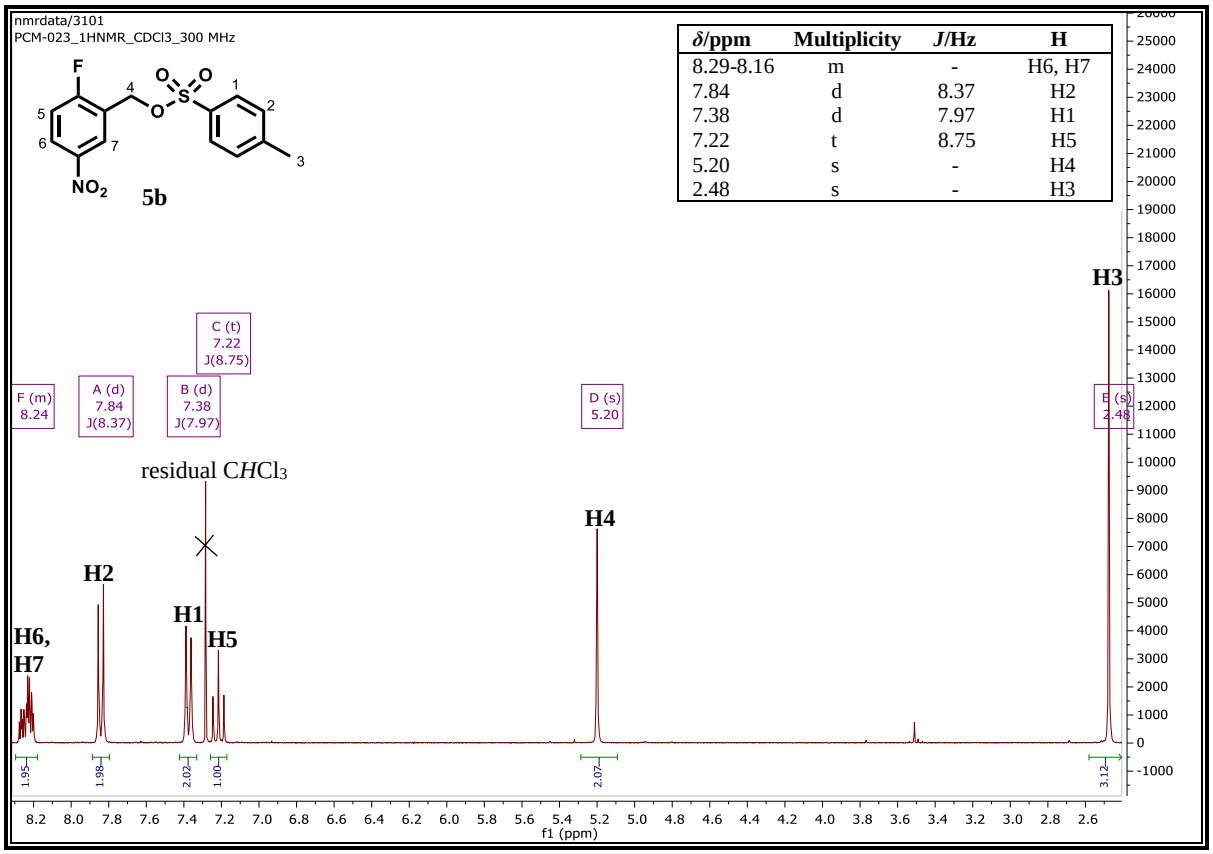

Figure 2.20: ^{1}H-NMR spectrum of **5b** at 300 MHz in $CDCl_3$.

2.3.2.7 Nucleophilic Substitution: Step (ii), Scheme 2.2

The tosylated intermediate **5b** was further subjected to nucleophilic substitution with diethylamine to afford the aminated intermediate **5c**. Successful substitution of the tosylate group with diethylamine was accompanied by appearance of a 6-proton triplet signal (δ = 1.10 ppm, J = 7.13 Hz); a 4-proton quartet signal (δ = 2.62 ppm, J = 7.12 Hz) and a 2-proton singlet signal (δ = 3.71 ppm) in the aliphatic region (Figure 2.21). This splitting pattern was similar to previous splitting patterns observed for analogues and intermediates containing the basic side chain. Additionally, a concomitant disappearance of the tosylate aromatic protons was also observed. At δ = 8.14 ppm, a doublet of doublet of doublets (J = 8.97, 4.40, and 2.97 Hz) was

observed and attributed to proton H5. Such a splitting pattern was rationalized on the basis of the existence of three unequal couplings. In this respect, proton H5 experiences coupling to H4, H6 and the fluorine atom. The doublet of doublets (J = 6.24 and 2.92 Hz) observed at δ = 8.48 ppm was associated with H4 which experiences two long range couplings to H5 and the fluorine atom. Consistent with the observation in the spectrum for **5b**, the proton adjacent to the fluorine atom, H6, resonated as a triplet (J = 8.93 Hz).

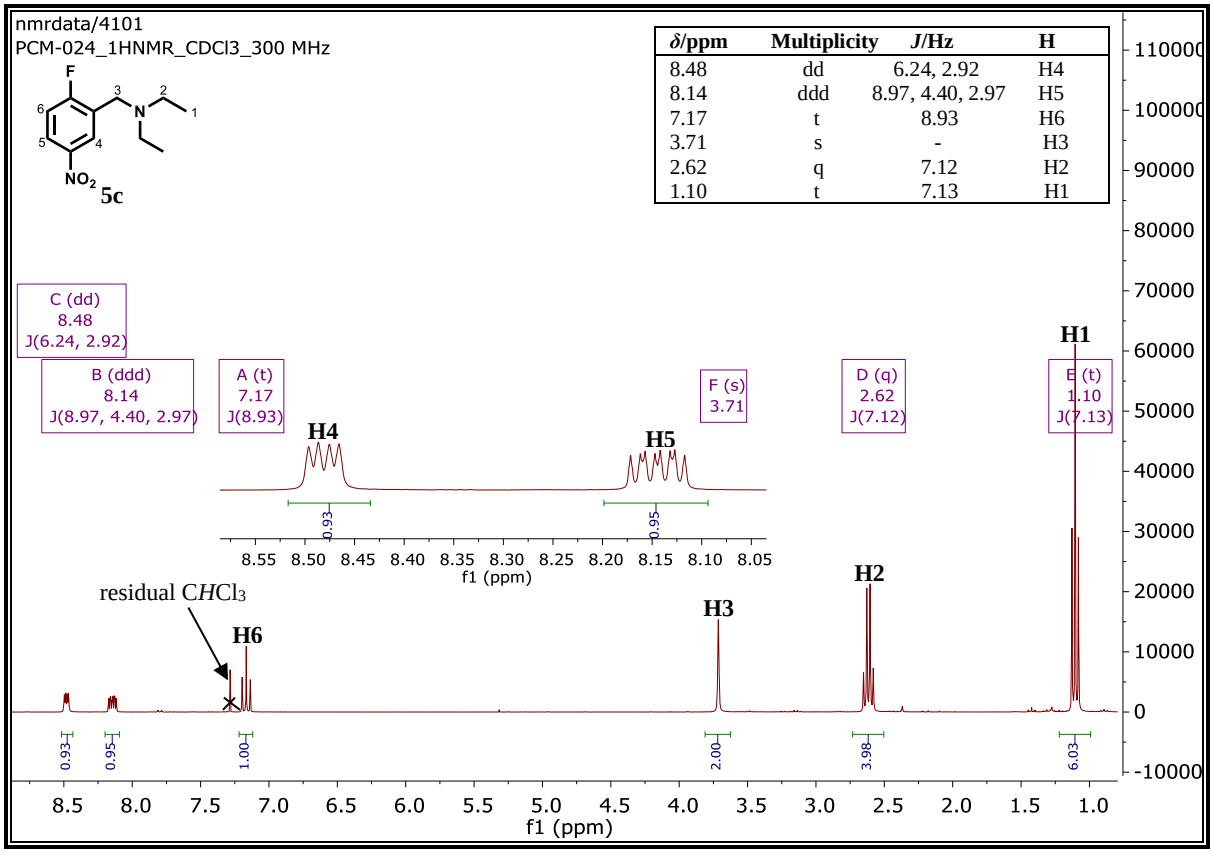

Figure 2.21: ^{1}H-NMR spectrum of **5c** at 300 MHz in $CDCl_3$.

2.3.2.8 Reduction of the Nitro Group: Step (iii), Scheme 2.2

The $SnCl_2$/HCl-mediated reduction of the nitro to the amino afforded the aniline starting material **5d**. With the reduction of the nitro group, a significant upfield shift of aromatic signals in the ^{1}H-NMR spectrum was observed (Figure 2.22) with protons H4 and H6 resonating at approximately the same chemical shift (δ = 6.86 – 6.78 ppm) as a multiplet. A doublet of doublet of doublets was still observed for proton H5 albeit at a lower chemical shift (δ = 6.53 ppm, J = 8.65, 4.10, and 3.00 Hz). The preceding subsection has already discussed the magnetic interactions resulting in such a splitting pattern. The aliphatic signals also retained a similar splitting pattern as observed and noted in the preceding subsection. More corroborating

evidence for successful nitro reduction was obtained from HPLC-MS measurements which showed a quasi-molecular ion $[M + H]^+$ for **5d** (*m/z* = 197.1, calculated exact mass = 196.1376).

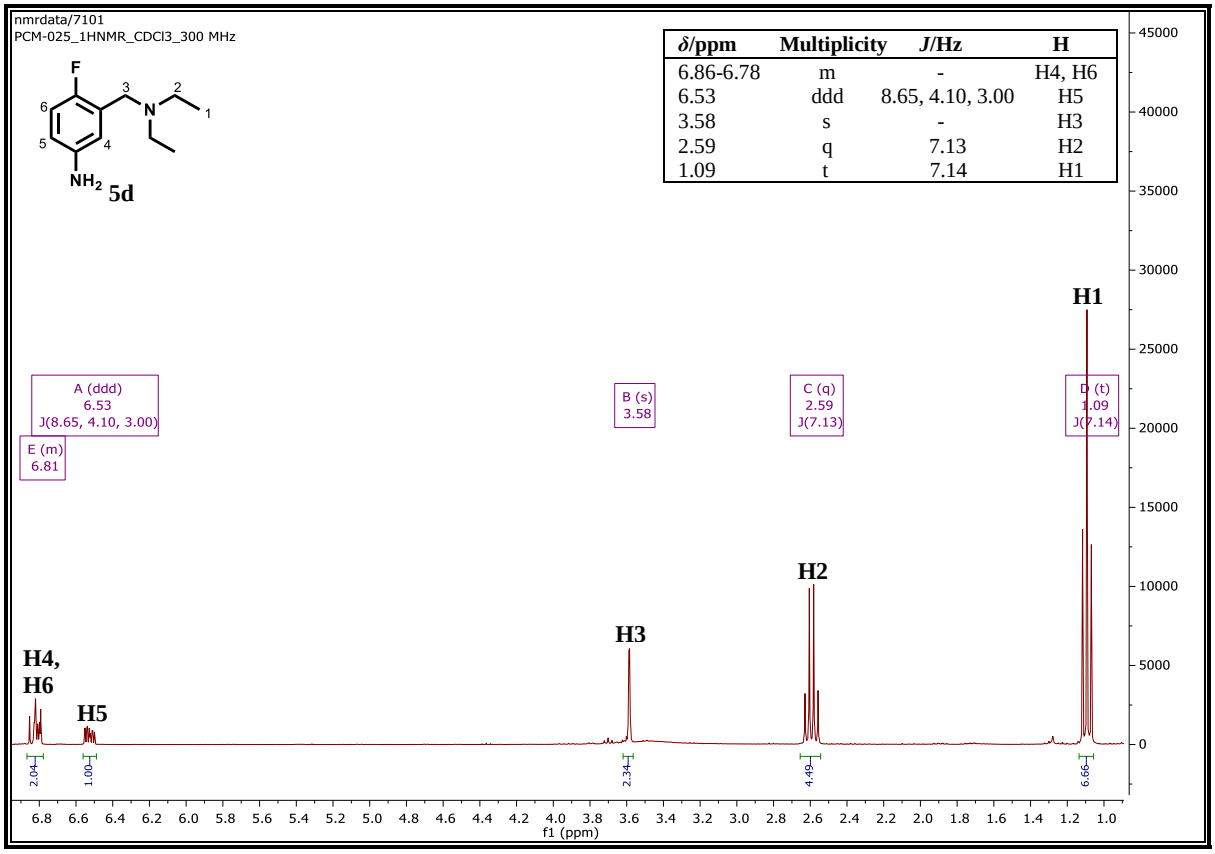

Figure 2.22: ^{1}H-NMR spectrum of **5d** at 300 MHz in $CDCl_3$.

2.3.2.9 *N*-Acetylation: Step (i), Scheme 2.3

As mentioned earlier, an acetylation step on 4-aminophenol was necessary to prevent formation of polysubstituted products[50] towards the synthesis of the phenolic starting material **5h**. Successful acetylation was accompanied by the appearance of an upfield ^{1}H-NMR singlet signal at δ = 2.10 ppm integrating for 3 protons (H1) of the acetyl methyl group (Figure 2.23). Protons H2 and H3 resonated as two doublets each integrating for 2 protons at δ = 7.31 and 6.74 ppm respectively. As expected, the two signals exhibited equal coupling constants (J = 9.05 Hz).

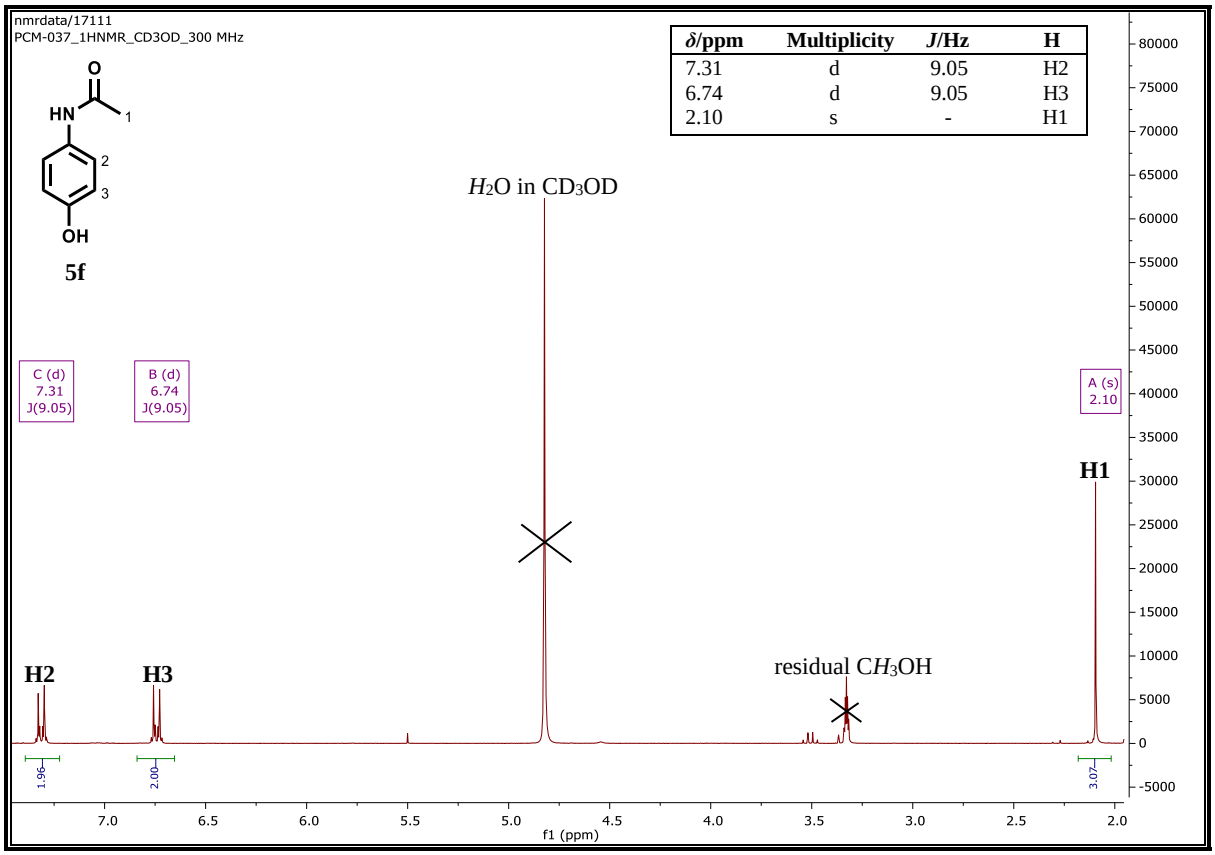

Figure 2.23: ^{1}H-NMR spectrum of **5f** at 300 MHz in CD_3OD.

Additionally, a characteristic $[M + H]^+$ *m/z* value was also observed on HPLC-MS for this acetylated intermediate (*m/z* = 152.1, calculated exact mass = 151.0633).

2.3.2.10 Mannich Reaction: Step (ii), Scheme 2.3

The deactivation of the amino group was then followed by aminomethylation via a Mannich reaction on the benzene ring to give intermediate **5g**. The characteristic ^{1}H-NMR signals corresponding to the newly-incorporated Mannich base-like side chain were observed. However, the spectrum also showed that this intermediate was still contaminated with diethylamine and was subsequently used in the next step without further purification. The spectrum is, therefore, not shown albeit the ^{1}H-NMR data is reported in the experimental section of this thesis. Moreover, a corresponding quasi-molecular ion $[M + H]^+$ was detected on HPLC-MS (*m/z* = 237.2, calculated exact mass = 236.1525) which further confirmed successful preparation of this intermediate.

2.3.2.11 Acid-catalysed Deacetylation: Step (iii), Scheme 2.3

Acid-catalysed hydrolysis of the amide bond in intermediate **5g** furnished the free aniline compound **5h**. Evidence for successful deacetylation was drawn from ^{1}H-NMR which showed the corresponding disappearance of the acetyl hydrogens (Figure 2.24). A well resolved pattern of multiplicity was observed for all the protons, both aromatic and aliphatic. A doublet (J = 8.43 Hz) at δ = 6.67 ppm and integrating for 1 proton was unambiguously associated with H3 which experiences short range coupling to H2. As expected, proton H2 also exhibits a reciprocal short-range coupling to H3 as evidenced from one of its coupling constant values (J = 8.44 Hz, δ = 6.56 ppm). Proton H2 further experiences a long-range coupling to H1 which was characterized by a second coupling constant relatively smaller in magnitude (J = 2.77 Hz). Additionally, proton H1, only experiencing long-range coupling to H2, appears as a doublet at δ = 6.41 ppm (J = 2.73 Hz). The aliphatic protons H4, H5 and H6 gave the same splitting pattern as that observed in previous analogues/intermediates possessing a basic side chain. When subjected to mass spectroscopy, **5h** also exhibited a quasi-molecular ion $[M + H]^{+}$ (m/z = 195.2, calculated exact mass = 194.1419).

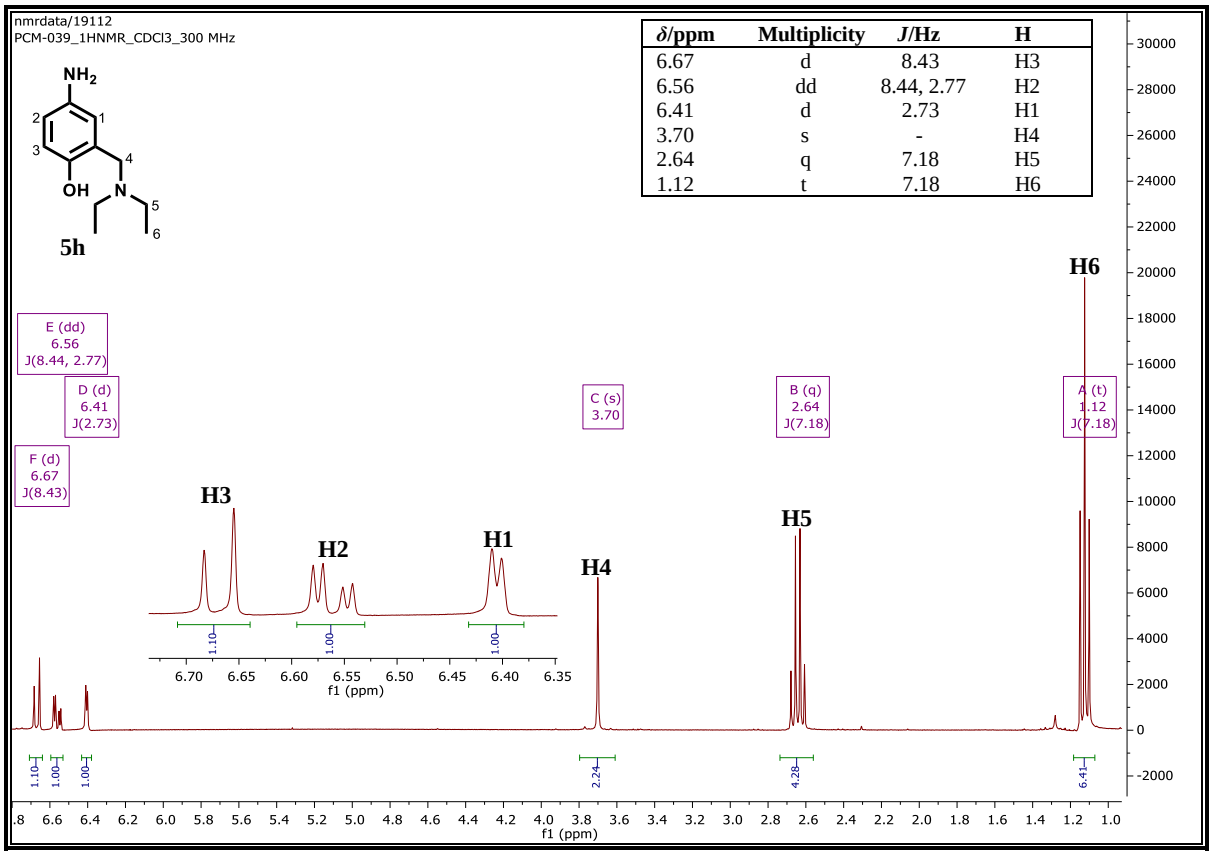

Figure 2.24: ^{1}H-NMR spectrum of **5h** at 300 MHz in $CDCl_3$.

2.3.2.12 Suzuki-Miyaura Cross-coupling: Step (i), Scheme 2.4A

A one pot Suzuki-Miyaura cross coupling reaction in scheme 2.4A led to formation of diarylated imidazopyridazines **25** and **50**. The characterization of these two analogues has been represented by compounds obtained in scheme 2.1 step (iv).

2.3.2.13 Suzuki-Miyaura Cross-coupling: Step (ii), Scheme 2.4B

A Suzuki-Miyaura cross coupling reaction on the pyridazine-chlorinated intermediate **2a** gave the mono-phenylated intermediate **6a** which was characterized by ^{1}H-NMR (Figure 2.25).

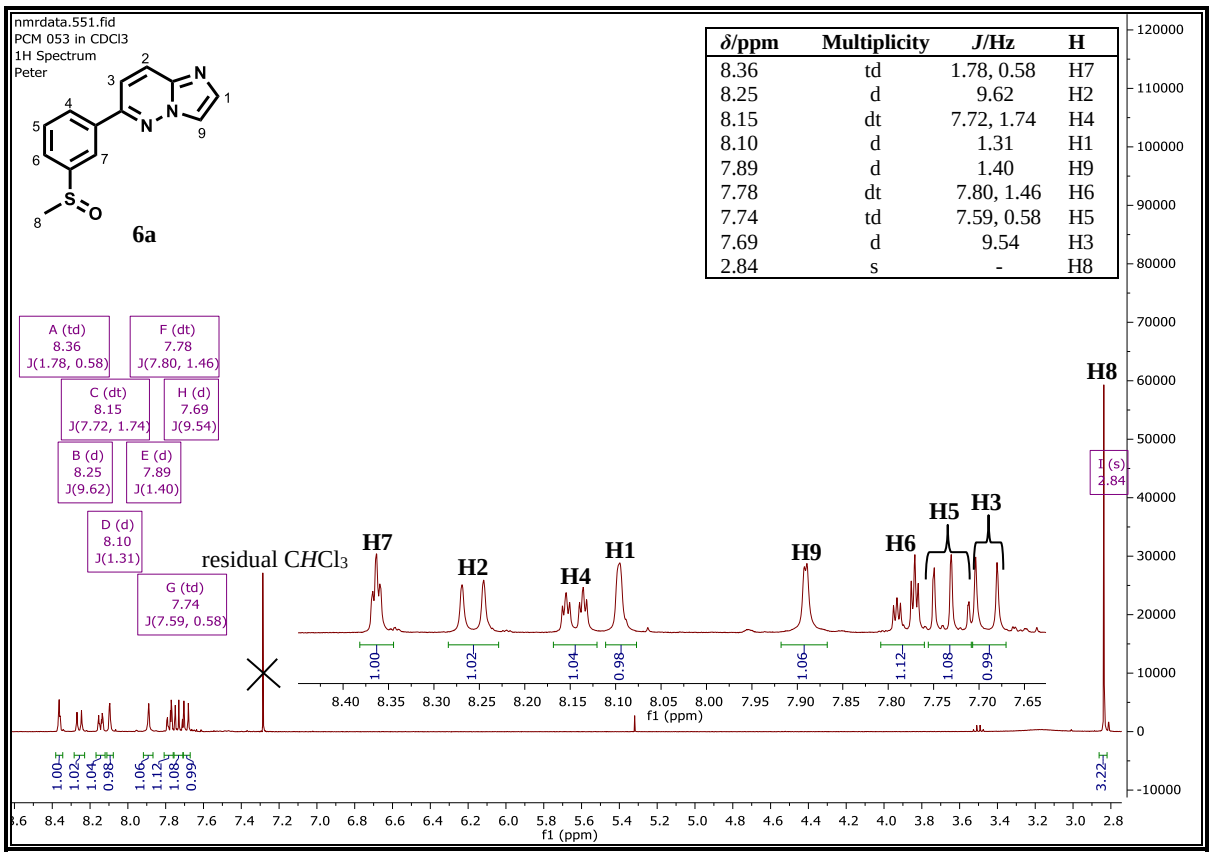

Figure 2.25: ^{1}H-NMR spectrum of **6a** at 400 MHz in $CDCl_3$.

The two imidazo protons H1 (δ = 8.10 ppm, doublet) and H9 (δ = 7.89 ppm, doublet) exhibited weak coupling, J = 1.31 and 1.40 Hz respectively. Such a magnitude of coupling constants for imidazo protons H1 and H9 was consistent with literature precedence.[51] Although quite unusual for this class of compounds, proton H7, resonating as a 1-proton triplet of doublets signal at δ = 8.36 ppm, experienced long-range coupling (J^5 = 0.58 Hz) with H5 in addition to its coupling (J^4 = 1.78 Hz) to protons H4 and H6. Proton H4, in like manner, resonated as a doublet of triplets with short-range coupling (J^3 = 7.72 Hz) to H5 as well as equal long-range coupling (J^4 = 1.74 Hz) to protons H6 and H7 accounting for this splitting pattern. Another well resolved

doublet of triplets signal integrating for one proton at δ = 7.78 ppm was observed which corresponds to proton H6. Once again, short range coupling (J^3 = 7.80 Hz) to H5 and equal long-range coupling (J^4 = 1.46 Hz) to H4 and H7 explains this multiplicity pattern. Proton H5 resonated as a triplet of doublets at δ = 7.74 ppm, which was accounted for by short range coupling to H4 and H6 (J^3 = 7.59 Hz) as well as a much weaker long-range coupling to H7 (J^5 = 0.58 Hz). For protons H3 and H2, a similar splitting pattern and corresponding coupling constants to those observed in previous intermediates and target compounds were observed. Mass spectroscopy further confirmed the successful formation of this intermediate with a quasi-molecular ion observed at *m/z* $[M + H]^+$ = 258.1 (calculated exact mass = 257.0623), under ESI^+ mode.

2.3.2.14 Electrophilic Aromatic Bromination: Step (iii), Scheme 2.4B

For the mechanism of this reaction, refer to subsection 2.3.2.2. Electrophilic aromatic bromination of the intermediate **6a** to give the brominated intermediate **6b** was accompanied by the disappearance of the ^{1}H-NMR signal corresponding to the substituted proton H9 (Figure 2.26). However, the ^{1}H-NMR signals for this key intermediate were not as resolved as those of its precursor **6a**. Successful hydrogen-bromine substitution was also evident from the mass spectrum which showed two *m/z* $[M + H]^+$ peaks (336.0 and 338.0, calculated exact mass = 334.9728) of virtually equal percentage abundance. Such a pattern of mass spectral peaks is typical of bromine-containing molecules owing to the fact that the isotopic abundances of the two stable isotopes of bromine (^{79}Br and ^{81}Br) is nearly 1 : 1.[52]

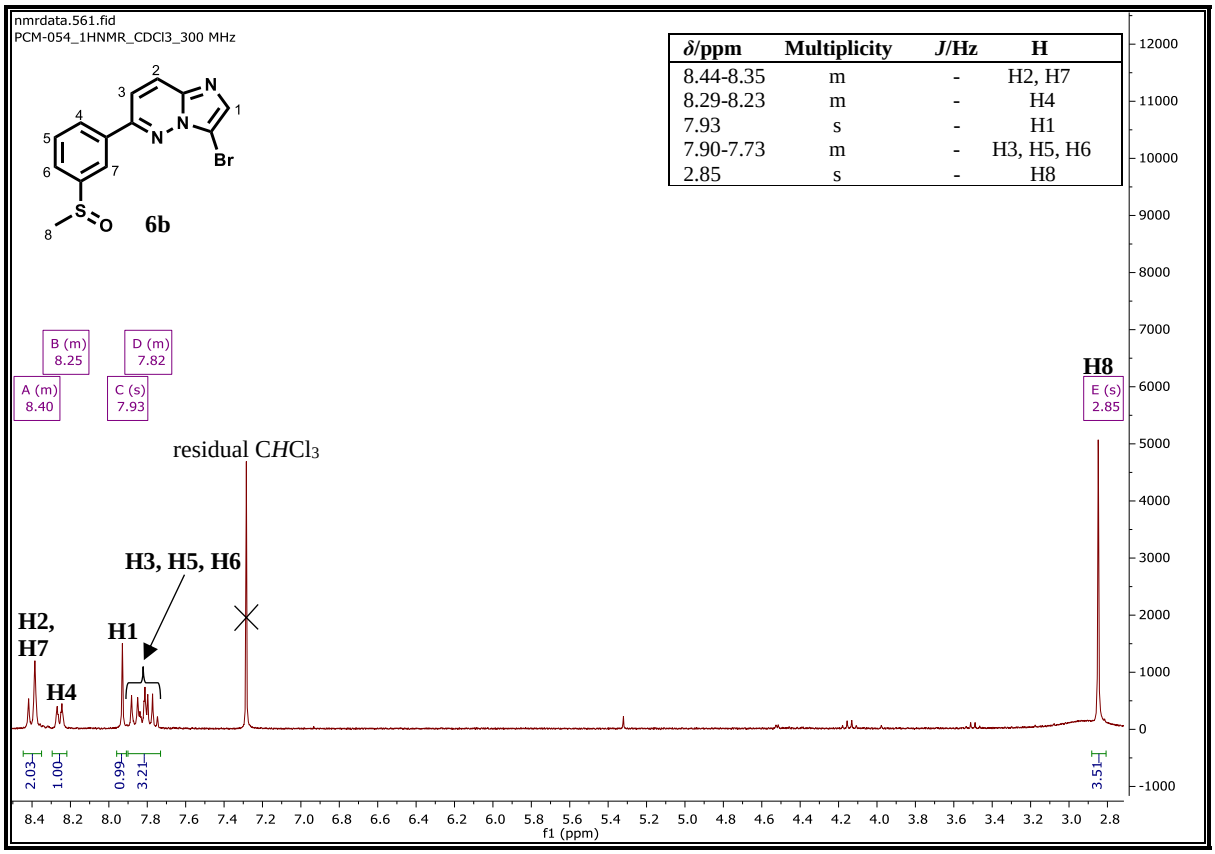

Figure 2.26: ^{1}H-NMR spectrum of **6b** at 300 MHz in $CDCl_3$.

2.3.2.15 Buchwald-Hartwig Amination: Step (v), Scheme 2.4B

The analogues **46 - 49** (Table 2.2) were realized through an amination reaction on the imidazo ring portion. For the reaction mechanism, refer to subsection 2.3.2.5. An important diagnostic feature in all the ^{1}H-NMR spectra of all the four analogues was the appearance of a signal relatively downfield at $\delta \sim 9.0$ ppm corresponding to the N*H* proton. To represent these imidazo-aminated analogues, the characterization of **49** is discussed. The ^{1}H-NMR spectrum of this derivative is shown in figure 2.27. In this target compound, the N*H* proton (H2) was observed as a sharp singlet at $\delta = 8.83$ ppm. Other notable signals associated with the incorporated aniline moiety include two doublets at $\delta = 7.53$ and 7.03 ppm corresponding to protons H3 and H4 respectively. The two signals, integrating for two protons each, exhibited approximately equal coupling constants, $J = 8.56$ and 8.44 Hz for H3 and H4 respectively. Also notable is the aliphatic singlet signal at $\delta = 2.69$ ppm integrating for three protons, which was attributed to H5 protons.

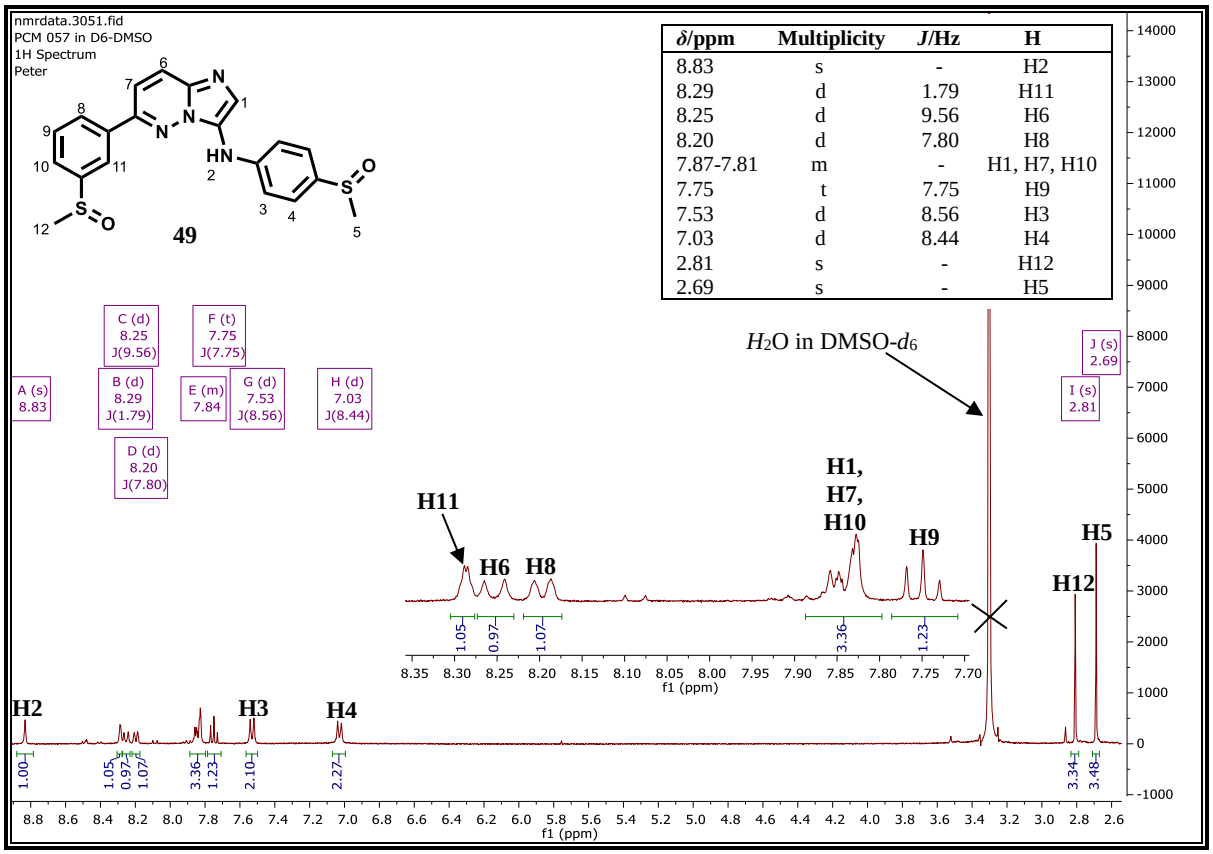

Figure 2.27: ^{1}H-NMR spectrum of **49** at 400 MHz in DMSO-d_6.

Introduction of the *para*-substituted aniline group was accompanied by the appearance of corresponding ^{13}C-NMR signals (Figure 2.28). An extra aliphatic signal corresponding to the sulfinylmethyl carbon C7 was observed at δ = 43.75 ppm. As expected, C7 resonated almost at the same chemical shift as the other sulfinylmethyl carbon C17 (δ = 43.63 ppm). Other diagnostic signals appeared at δ = 125.84 and 114.92 ppm with equal intensities corresponding to the aromatic carbons C4 and C5, respectively. Other carbon atoms connected to hydrogens such as C1, C9, C10, C13 – C15 and C18 were also unambiguously assigned while all the seven unassigned signals were attributed to the seven quaternary carbons. Additionally, analogue **49**, like other isomeric analogues such as **37** (Figure 2.16), **38** (Table 2.1) and **48** (Table 2.2) exhibited a protonated molecular ion $[M + H]^+$ at *m/z* = 411.1 (calculated exact mass = 410.0871).

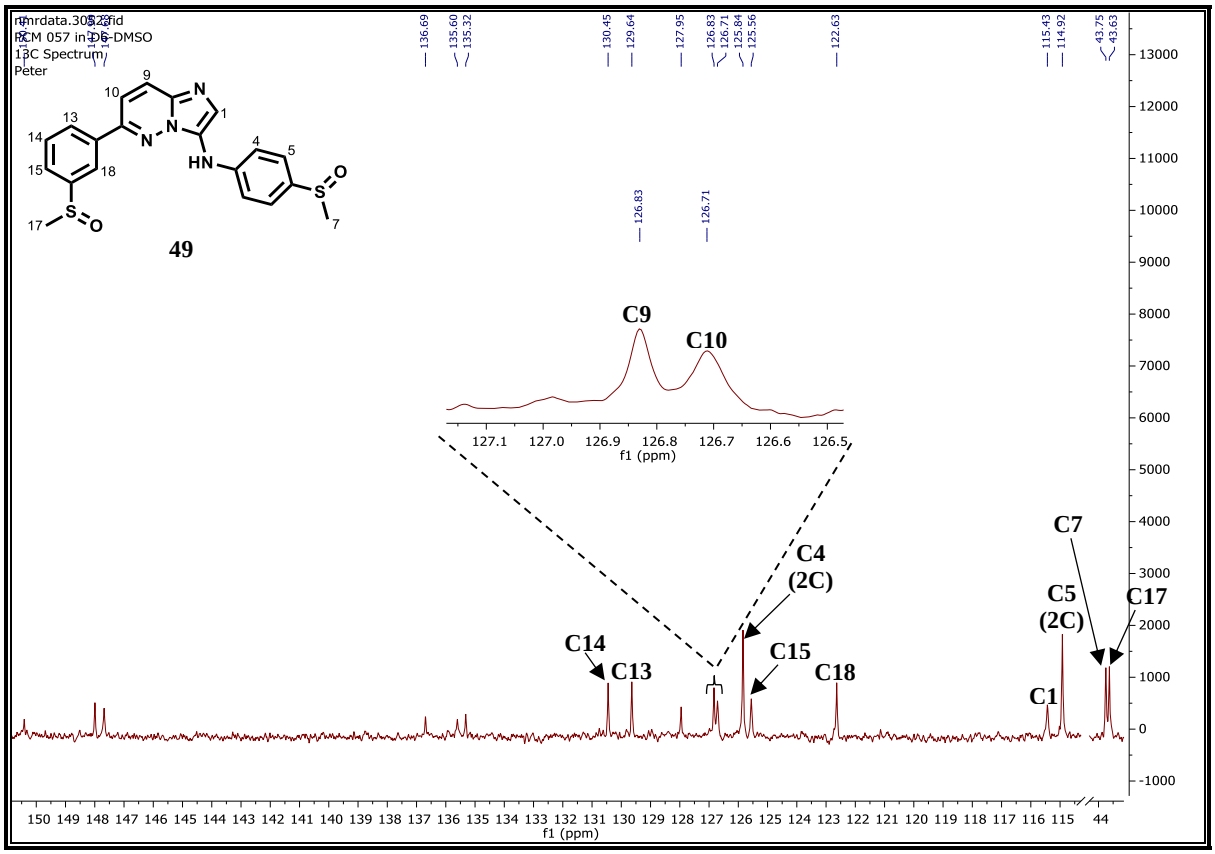

Figure 2.28: ^{13}C-NMR spectrum of **49** at 101 MHz in DMSO-d_6.

2.3.2.16 Suzuki-Miyaura Cross-coupling: Steps (i) and (ii), Scheme 2.5

The successful synthesis of intermediate **7a**, a precursor to the silicon-containing analogues, was confirmed by HPLC-MS analysis, which showed a corresponding quasi-molecular ion [M + H]$^+$ peak (*m/z* = 274.0, calculated exact mass = 273.0305). Further confirmation was provided by ^{1}H-NMR, which revealed a well resolved multiplicity of aromatic-region signals corresponding to the seven aromatic protons (Figure 2.29). As envisaged, the ^{1}H-NMR spectrum showed four doublet signals with the symmetrical phenyl protons (H3 and H2) accounting for two doublets integrating for two protons each (δ = 8.26 and 8.09 ppm, respectively) and exhibiting approximately equal coupling constants (J ~ 8.6 Hz). In a similar fashion, protons H4 and H5 resonated as 1-proton doublets at δ = 7.48 and 8.34 ppm, respectively, and showed coupling to each other (J = 9.48 Hz).

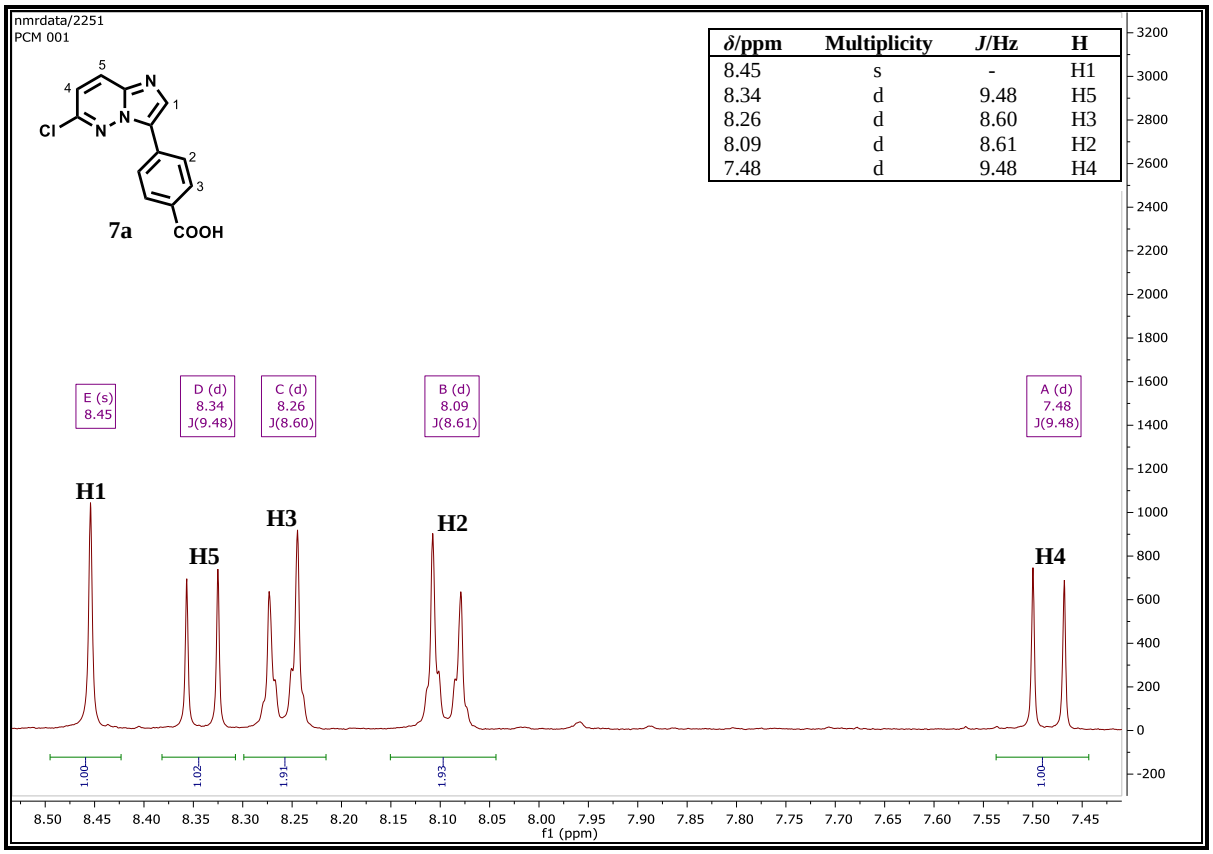

Figure 2.29: ^{1}H-NMR spectrum of **7a** at 300 MHz in DMSO-d_6.

The second Suzuki-Miyaura cross-coupling step in scheme 2.5 to give corresponding carboxylic acid intermediates was accompanied by appearance of extra aromatic protons. This confirmed successful incorporation of an aromatic functionality. For derivative **7d**, whose ^{1}H-NMR spectrum will be used as a representative (Figure 2.30), the relatively shielded methyl group of the methylsulfonyl substituent resonated upfield (δ = 3.35 ppm), albeit partially overlapping with the water signal. Although some aromatic protons resonated as clusters of multiplets, some well-resolved multiplicities are noteworthy. Proton H9 resonated downfield (δ = 8.67 ppm) as a 1-proton triplet, experiencing long-range coupling to protons H6 and H8, as evidenced by the small magnitude of the coupling constant observed (J = 1.66 Hz). On the contrary, the more close-range (J^3) coupling to protons H6 and H8 that proton H7 experiences gave rise to a triplet at δ = 7.91 ppm with a comparatively large coupling constant (J = 7.87 Hz).

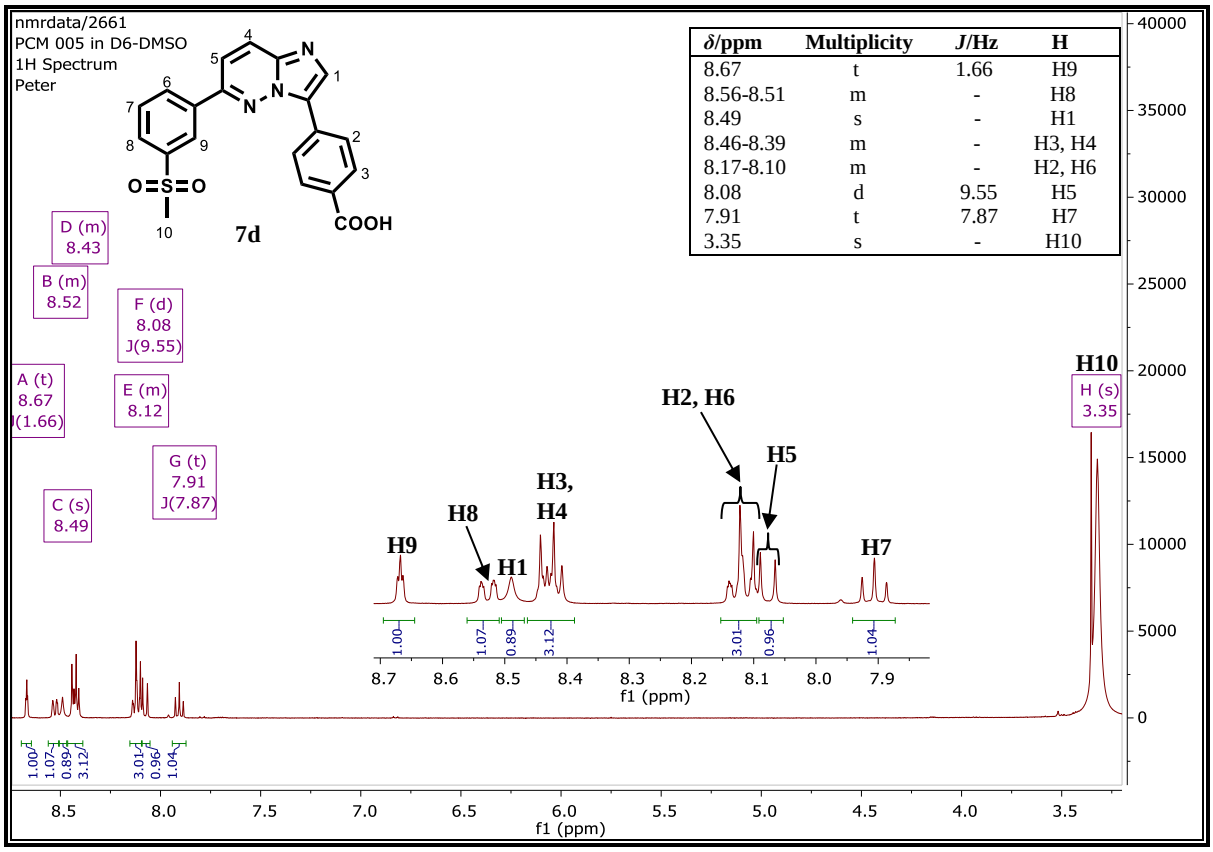

Figure 2.30: ^{1}H-NMR spectrum of **7d** at 400 MHz in DMSO-d_6.

These carboxylic acid precursors (**7b-d**; scheme 2.5) also exhibited characteristic *m/z* values corresponding to their protonated molecular ions $[M + H]^+$ on HPLC-MS (**7b**: *m/z* = 378.1, calculated exact mass = 377.0834; **7c**: *m/z* = 384.0, calculated exact mass = 383.0882 and **7d**: *m/z* = 394.1, calculated exact mass = 393.0783).

2.3.2.17 Amide Bond Formation: Step (iii), Scheme 2.5

The formation of the amide bond to give the silicon-containing compounds (**55 - 57**; scheme 2.5) proceeds via the known textbook mechanism detailed in scheme 2.10 below.[39,53–55] The deprotonated carboxylic acid attacks the carbodiimide carbon of EDCI to give the *O*-acylisourea mixed ester where the carbonyl carbon is rendered more electrophilic and, therefore, more prone to nucleophilic attack. The desired amide bond and a urea by-product are then formed by the reaction of the amine with the activated *O*-acylisourea mixed ester intermediate. The reaction is thought to be driven by the formation of a stable urea by-product.[39] However, a commonly encountered undesirable side reaction often occurs. The unstable *O*-acylisourea mixed ester could rearrange via an acetyl transfer to the stable *N*-acylurea, a reaction that significantly compromises the yield of an amide bond-formation

reaction.[39] The addition of DMAP substantially circumvents this side reaction by reacting with the *O*-acylisourea mixed ester at a relatively faster rate compared to the rearrangement. This faster reaction gives the DMAP intermediate still reactive enough to react with the amine.

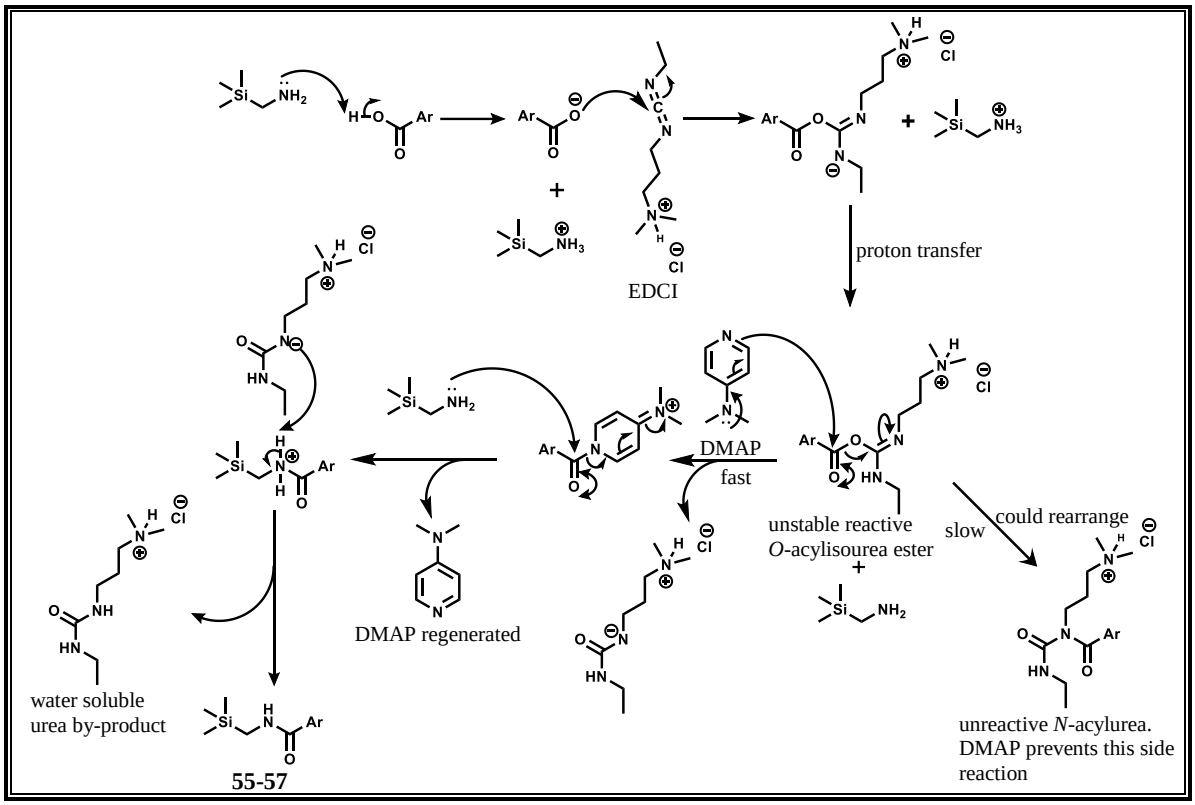

Scheme 2.10: Mechanism of amide bond formation.[39,53–55]

Compounds **55-57** all contain the highly shielded trimethylsilyl protons. The acquired ^{1}H-NMR spectra for these compounds were all consistent with this molecular feature. In this regard, the highly shielded nine trimethylsilyl protons resonated upfield at around δ = 0.18 ppm as a sharp singlet. Save for analogue **55**, the methylene protons common to all compounds gave rise to a 2-proton doublet signal at around δ = 3.00 ppm. A representative ^{1}H-NMR for analogue **57** is shown in figure 2.31 below. Interestingly, the N*H* proton H4 coupling to H5 was reasonably well resolved as a triplet (J = 5.53 Hz) at δ = 6.18 ppm.

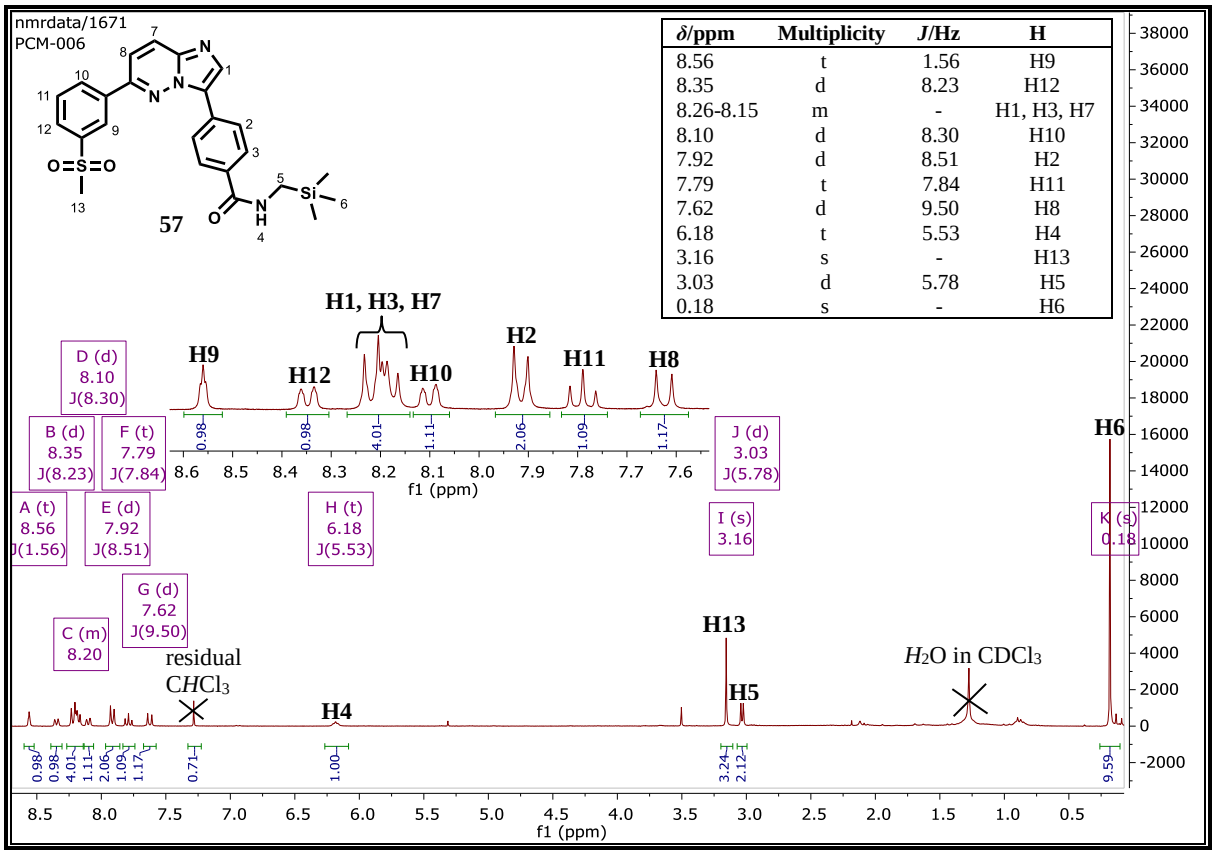

Figure 2.31: ^{1}H-NMR spectrum of **57** at 300 MHz in $CDCl_3$.

When subjected to molecular weight characterization by HPLC-MS, all the silicon containing analogues exhibited $[M + H]^+$ *m/z* values corresponding to their protonated molecules (**55**: *m/z* = 463.1, calculated exact mass = 462.1546; **56**: *m/z* = 469.2, calculated exact mass = 468.1593 and **57**: *m/z* = 479.1, calculated exact mass = 478.1495). As a representative example, the HPLC chromatogram and mass spectrum for compound **57** is shown in figure 2.32.

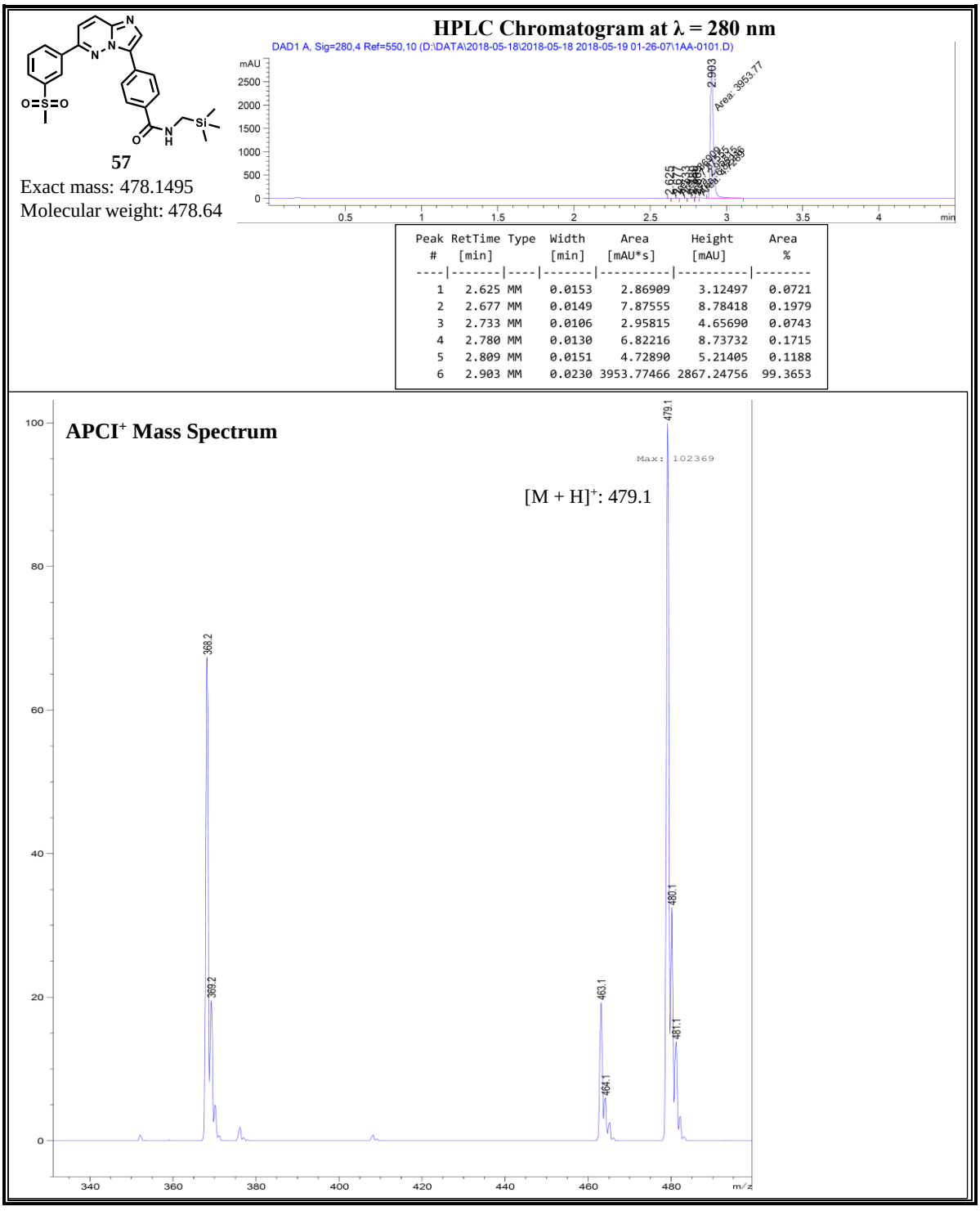

Figure 2.32: HPLC Chromatogram and APCI$^+$ mass spectrum of **57**.

2.4 Chemistry: Aminopyrazine Analogues

2.4.1 Synthesis of Aminopyrazine Analogues

2.4.1.1 Synthesis of Analogues 24 and 59 – 62

Compounds **24** and **59** – **62** were synthesized according to scheme 2.11. Two consecutive Suzuki-Miyaura cross coupling steps[56] with appropriate boronic acids delivered compounds **24**

and **59** in 61 and 21% yields respectively. Reduction of the alkene double bond in presence of ammonium formate (NH_4HCO_2), hydrogen gas and palladium catalyst[57] gave the piperidine-substituted compound **60** in good yield (68%). *N*-boc-deprotection mediated by HCl[58] followed by a mesylation[59] step afforded compound **62** in 66 % yield.

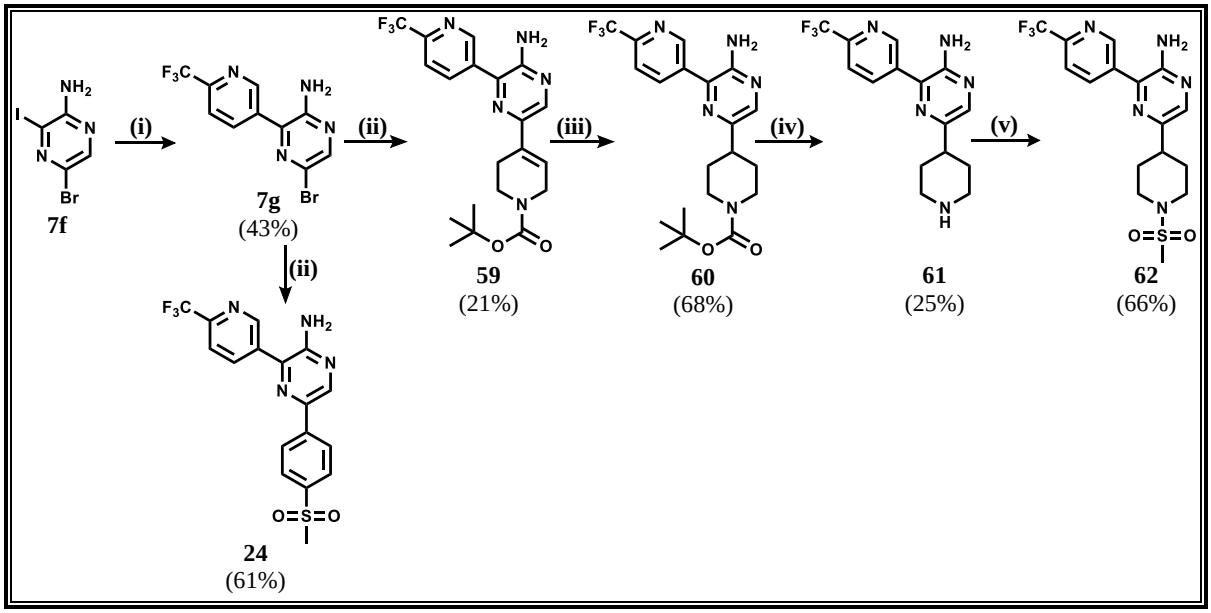

Scheme 2.11: Synthetic approach to aminopyrazine compounds **24** and **59** – **62**.

Reagents and reaction conditions: (i) 2-(trifluoromethyl)pyridine-5-boronic acid pinacol ester, $Pd(PPh_3)_2Cl_2$, 1 M aq K_2CO_3, 1,4-dioxane, 110 ºC, 20 h; (ii) appropriate boronic acid or boronic acid pinacol ester, $Pd(PPh_3)_2Cl_2$, 1 M aq K_2CO_3, 1,4-dioxane, 100 ºC (**24**), 110 ºC (**59**), 3 h (**24**), 13 h (**59**); (iii) NH_4HCO_2, Pd/C, H_2 (balloon), methanol, rt (24 ºC), 2.5 h; (iv) 4 M HCl in 1,4-dioxane, rt (24 ºC), 30 min; (v) methanesulfonyl chloride, triethylamine, dichloromethane, 0 ºC – rt (23 ºC), 1 h.

2.4.1.2 Synthesis of Analogues 63 – 66 and 69

The installation of a piperidyl group on position 3 of the aminopyrazine scaffold was achieved following a synthetic protocol shown in scheme 2.12 which was similar to that described in scheme 2.11. Using a 4-carboxyphenylboronic acid in step (i) delivered compound **69** in 79% yield.

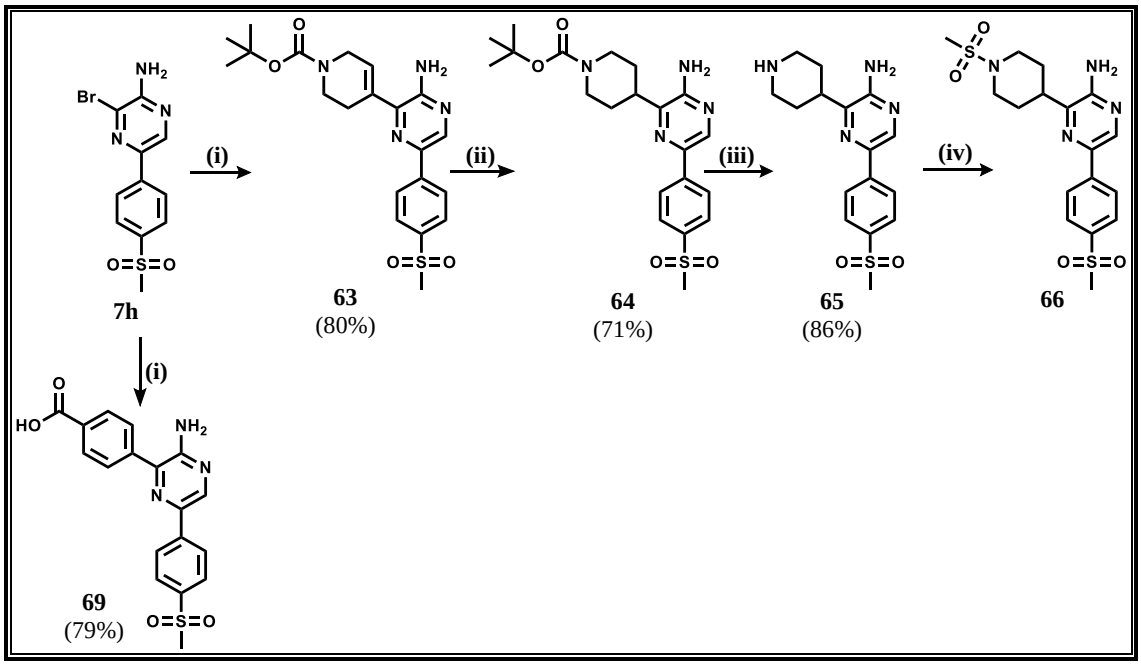

Scheme 2.12: Synthetic approach to aminopyrazine compounds **63** – **66** and **69**.

Reagents and reaction conditions: (i) appropriate boronic acid or boronic acid pinacol ester, $Pd(PPh_3)_2Cl_2$, 1 M aq K_2CO_3, 1,4-dioxane, 110 ºC, 2 h; (ii) NH_4HCO_2, Pd/C, H_2 (balloon), methanol, rt (24 ºC), 1 h; (iii) 4 M HCl in 1,4-dioxane, rt (24 ºC), 1 h; (iv) methanesulfonyl chloride, triethylamine, dichloromethane, 0 ºC – rt (24 ºC), 1 h.

2.4.1.3 Synthesis of Analogues 70 – 72

In this category of compounds, partial and full saturation at positions 3 and 5 of the aminopyrazine scaffold were simultaneously introduced using a synthetic approach in scheme 2.13. In the first step, a one-pot Suzuki-Miyaura cross-coupling reaction[56] at both reaction sites in the presence of 2.2 equivalents of the boronic acid pinacol ester afforded compound **70** with tetrahydropyridine motifs in 68 % yield. Analogue **71**, with fully saturated piperidine rings, was then realized via reduction of the double bond in presence of NH_4HCO_2, hydrogen gas and carbon-supported palladium catalyst.[57] An HCl-promoted boc-deprotection step[58] followed by *N*-methylsulfonylation[59] at both piperidine nitrogens afforded **72** in very low yield (23 %).

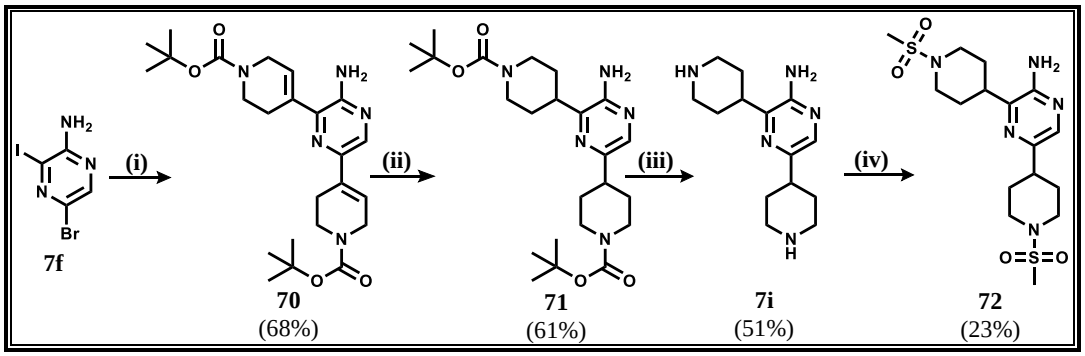

Scheme 2.13: Synthetic approach to aminopyrazine compounds **70** – **72**.

Reagents and reaction conditions: (i) *N*-boc-1,2,5,6-tetrahydropyridine-4-boronic acid pinacol ester (excess, 2.2 eq), $Pd(PPh_3)_2Cl_2$, 1 M aq K_2CO_3, 1,4-dioxane, 110 ºC, 4 h; (ii) NH_4HCO_2, Pd/C, H_2 (balloon), methanol, rt (20 ºC), 4 h; (iii) 4 M HCl in 1,4-dioxane, rt (23 ºC), 1.5 h; (iv) methanesulfonyl chloride, triethylamine, dichloromethane, 0 ºC – rt (21.5 ºC), 12 h.

2.4.1.4 Synthesis of Analogues 67 and 68

Analogues **67** and **68** were synthesized according to synthetic scheme 2.14. Although the nucleophilic aromatic substitution in the first step was intended to deliver the *N*-boc-protected piperazine intermediate (1-boc-piperazine was used in the reaction), *in situ* boc-deprotection occurred resulting in the formation of the free piperazine-substituted compound **67**. Since the reaction was carried out at 170 °C, such an *in situ* removal of the boc group is unsurprising and is in conformity with literature reports.[60,61] The obtained free amine was then mesylated[59] in the presence of methanesulfonyl chloride and triethylamine to deliver compound **68** in 74% yield.

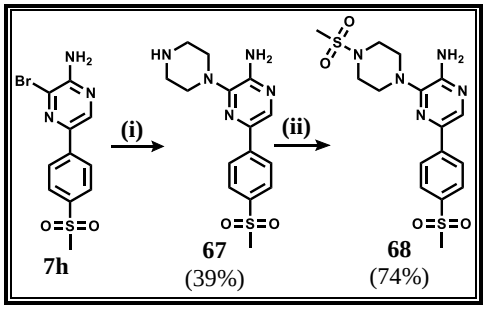

Scheme 2.14: Synthetic approach to aminopyrazine compounds **67** and **68**.

Reagents and reaction conditions: (i) 1-boc-piperazine, triethylamine, 170 ºC, sealed tube, 4 h; (ii) methanesulfonyl chloride, triethylamine, dichloromethane, 0 ºC – rt (20 ºC), 30 min.

2.4.2 Proposed Mechanistic Details and Characterization

2.4.2.1 Suzuki-Miyaura Cross-coupling: Step (i), Scheme 2.11

The bromo-intermediate **7g**, obtained in this step, was confirmed by both ^{1}H-NMR and HPLC-MS. The ^{1}H-NMR for **7g** was solved as shown in figure 2.33. The most deshielded proton H3 resonated as a singlet relatively downfield at δ = 9.16 ppm. As anticipated, J^{3} coupling between protons H4 (δ = 8.30 ppm) and H5 (δ = 7.85 ppm) resulted in two doublets with approximately equal coupling constants (J ~ 8 Hz). A singlet at δ = 8.20 ppm was attributed to H1 while a broad singlet integrating for two protons at δ = 4.84 ppm was assigned to the two amino hydrogens (H2).

Under negative ionization mode, the mass spectrum of intermediate **7g** exhibited two peaks at *m/z* = 317.0 ([M – H]$^{-}$, calculated exact mass = 317.9728) and 319.9 of virtually equal percentage abundance. As earlier mentioned in subsection 2.3.2.14, this observation is characteristic of bromo-containing compounds - bromine has two stable isotopes whose natural abundance is nearly equal.[52]

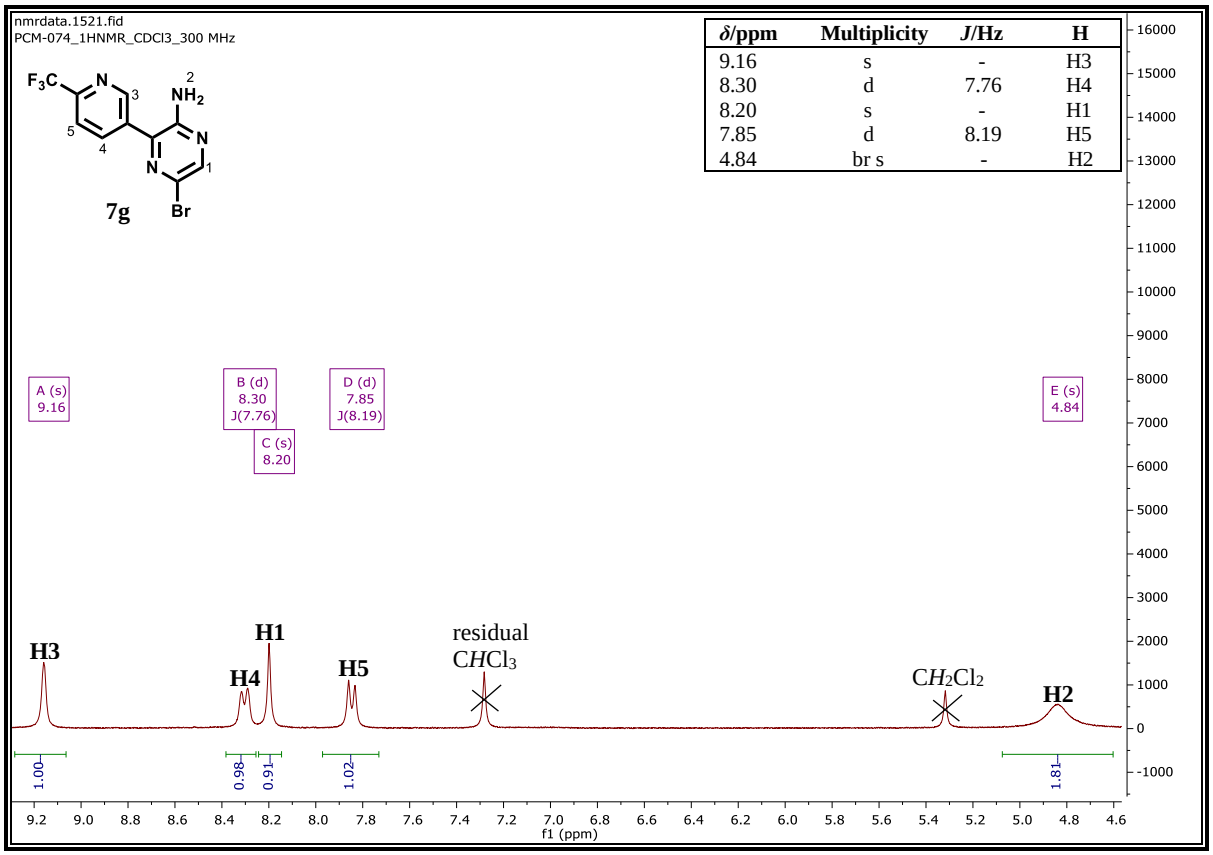

Figure 2.33: ^{1}H-NMR spectrum of **7g** at 300 MHz in $CDCl_3$.

2.4.2.2 Suzuki-Miyaura Cross-coupling: Step (ii), Scheme 2.11

Although step (ii) in scheme 2.11 resulted in compounds **24** and **59**, the NMR and mass spectral interpretation of **24** has been omitted because this has already been dealt with in literature.[56] The ^{1}H-NMR for compound **59** is captured in figure 2.34 below. For the aromatic region signals, the splitting pattern remained somewhat the same as that for the preceding intermediate **7g**. However, it is worth noting that unlike proton H5 in **7g**, which resonated as a clear doublet, proton H10 resonated as a doublet of doublets. The larger coupling constant (J = 8.14 Hz) was associated with the J^3 coupling to H9 while the smaller J value (0.79 Hz) resulted from long-range coupling to H8. On the other hand, despite having a typical doublet of doublets appearance, the multiplicity for the H9 signal was not well resolved and this was consequently recognized as a multiplet. The reaction was further accompanied by the appearance of extra signals corresponding to the introduced boc-protected tetrahydropyridyl moiety. In this regard, the vinylic proton H7 resonated as a broad singlet at δ = 6.57 ppm, which is within the range of chemical shifts (δ = 5.5–7.5 ppm) expected for conjugated vinylic systems.[62] However, the expected splitting pattern (triplet) of H7 was not observed. Nevertheless, the broad nature of the observed singlet could suggest that this, in fact, was a triplet, which was not just well resolved. This observation was also noted for H3, which resonated as a broad singlet with a triplet-like appearance when closely examined. On the other hand, protons H6 resonated as a doublet (δ = 4.15 ppm, J = 3.13 Hz) suggesting coupling to H7 while protons H4 resonated as a 2-proton triplet signal (δ = 3.67 ppm, J = 5.67 Hz) suggesting coupling to H3. The most shielded nine hydrogens of the boc group (H5) resonated as an intense singlet signal (δ = 1.51 ppm) integrating for 9 protons.

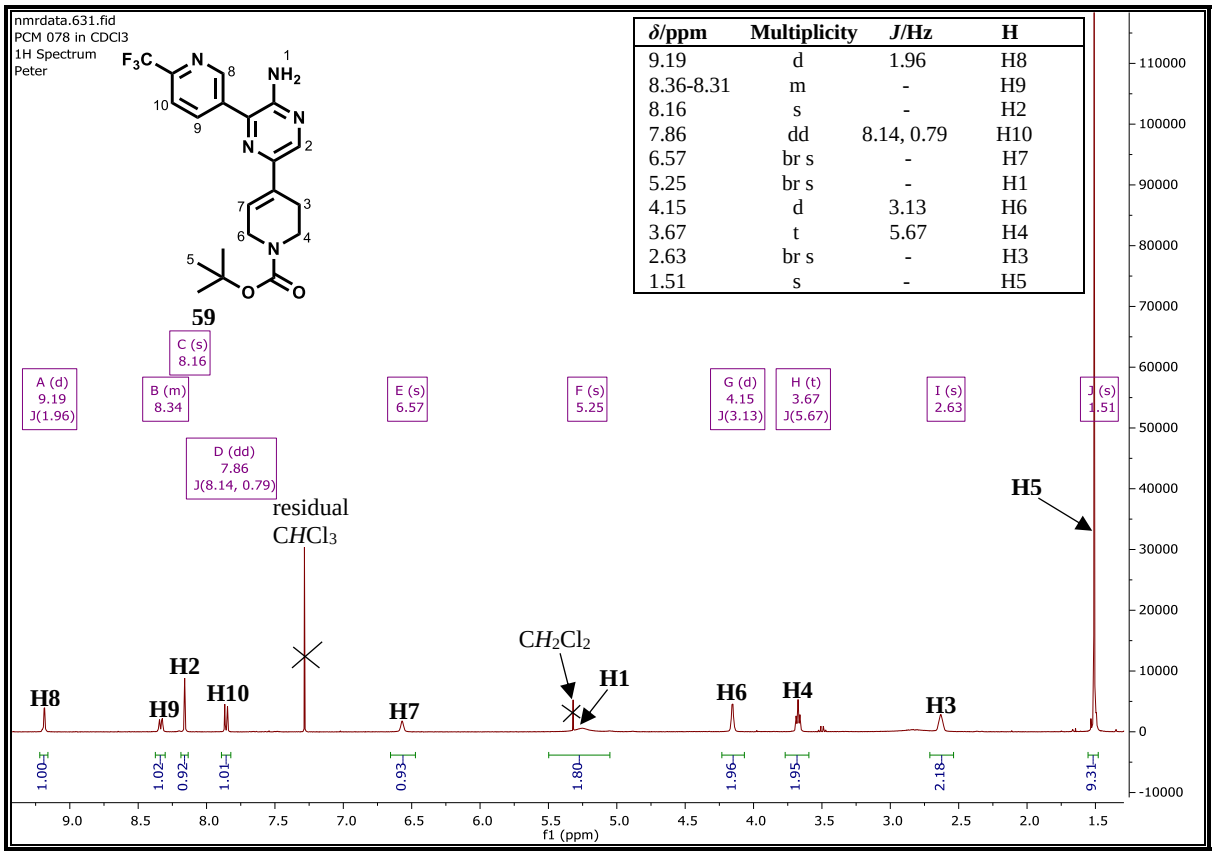

Figure 2.34: ^{1}H-NMR spectrum of **59** at 400 MHz in $CDCl_3$.

Under the $APCI^+/ESI^+$ mode, the molecular ion or its protonated/adduct version could not be observed on HPLC-MS for compound **59**. The mass spectrum for this compound was, therefore, acquired in $APCI^-$ mode. At a retention time t_r = 2.919 min, a quasi-molecular ion peak was observed at *m/z* = 420.1 (calculated exact mass = 421.1726) corresponding to the deprotonated (M – H) molecule of **59**.

2.4.2.3 Reduction of the Alkene Double Bond: Step (iii), Scheme 2.11

Hydrogen transfer reaction mechanisms are poorly understood. Particularly, the ammonium-formate-mediated reduction is believed to occur via a mechanism shown in scheme 2.15.[63–65] The formation of CO_2, a very stable molecule, is the driving force behind the ammonium formate-mediated transfer hydrogenation reduction.[64] In the first step, the chemisorption of the formate ion onto the palladium metal catalyst surface promotes its decomposition to CO_2 and a hydride ion. The hydride ion then attacks the double bond resulting in the abstraction of an ammonium ion proton by the π bond electrons. It is also likely that the hydride ion abstracts an ammonium ion proton directly resulting in the *in situ* generation of molecular hydrogen (H_2).

In this case, the addition of hydrogen across the double bond occurs via the well-known syn addition catalysed by the metal surface.[66]

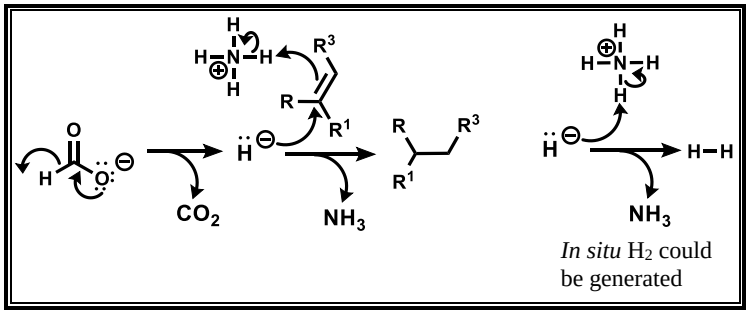

Scheme 2.15: Proposed reaction mechanism for formate-mediated alkene double bond reduction.[63–65]

Following this reduction step, analogue **60** was obtained and confirmed by ^{1}H-NMR (Figure 2.35). The most striking diagnostic feature confirming successful reduction was the disappearance of the vinylic proton (H7) signal which was observed in the ^{1}H-NMR spectrum of compound **59** (Figure 2.34). The reduction to a fully saturated piperidine ring was accompanied by the appearance of aliphatic signals associated with equatorial (e) and axial (a) protons of the piperidine chair conformation. Being relatively more deshielded, the equatorial protons H4e resonated as a multiplet at δ = 4.26 ppm while the more shielded axial protons H4a resonated at the same chemical shift as that of the tertiary hydrogen H6 (δ = 2.86 ppm).[49] Protons H3 signals were also resolved into H3e and H3a signals resonating as multiplets at δ = 1.93 and 1.76 ppm respectively, each integrating for two protons.

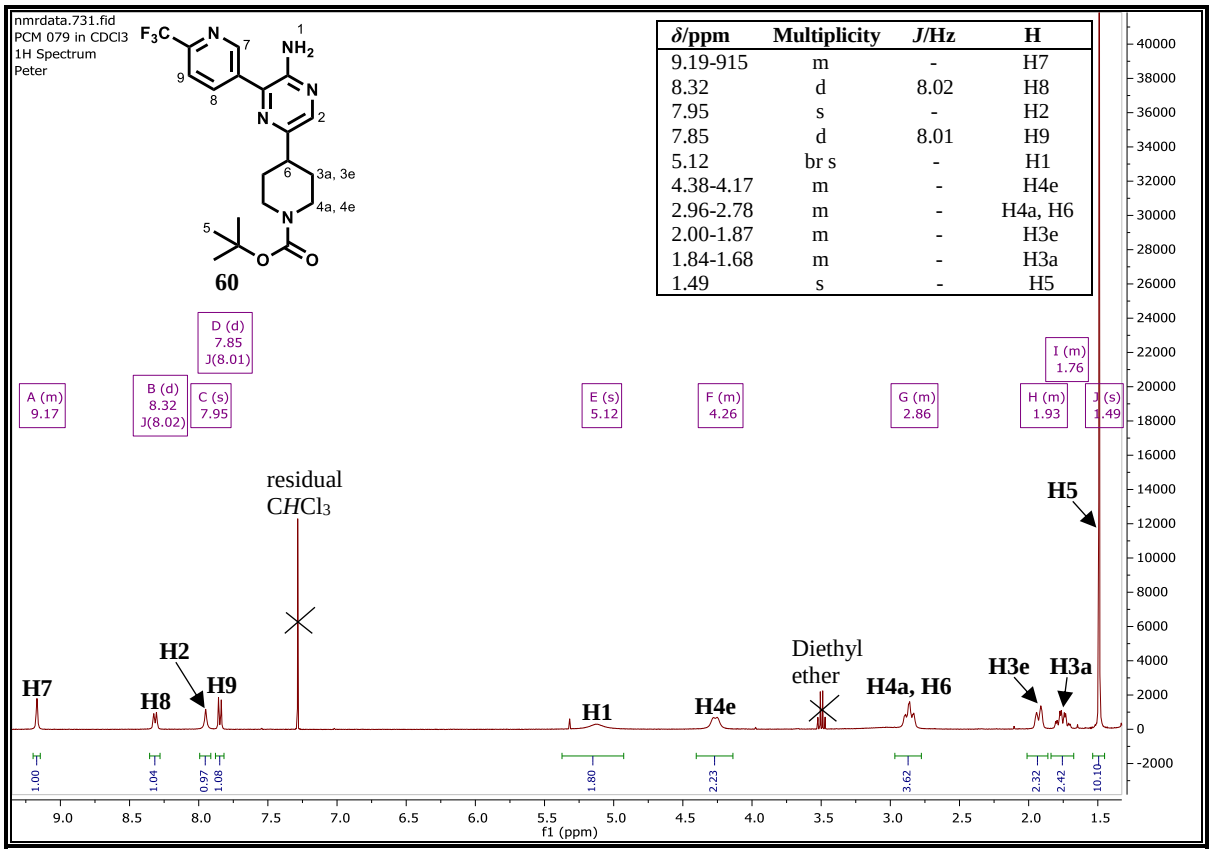

Figure 2.35: ^{1}H-NMR spectrum of **60** at 400 MHz in $CDCl_3$.

As expected, successful reduction was also confirmed by the corresponding appearance of a pseudo-molecular ion peak (*m/z* $[M - H]^-$ = 422.1, calculated exact mass = 423.1882) in negative ionization mode which differed from that of the alkene intermediate by two *m/z* units.

2.4.2.4 *N*-Boc-deprotection: Step (iv), Scheme 2.11

The boc-deprotection step leading to formation of compound **61** occurs according to the reaction mechanism shown in scheme 2.16.[67] The carbamate oxygen is first protonated by the acid, in this case, HCl. Carbamic acid is then generated following the loss of a *tert*-butyl carbocation. Loss of CO_2 through a decarboxylation step gives the free amine which undergoes protonation in excess acid to give the corresponding salt. Treatment of the salt with a base, in this case NaOH, liberates the free amine compound **61**. Following deprotonation, the generated carbocation forms isobutylene gas which, together with the generated CO_2 escape from the reaction mixture. It is also likely that the formed *tert*-butyl carbocation can either be quenched by a suitable trapping agent or may polymerize to form isobutylene oligomers.

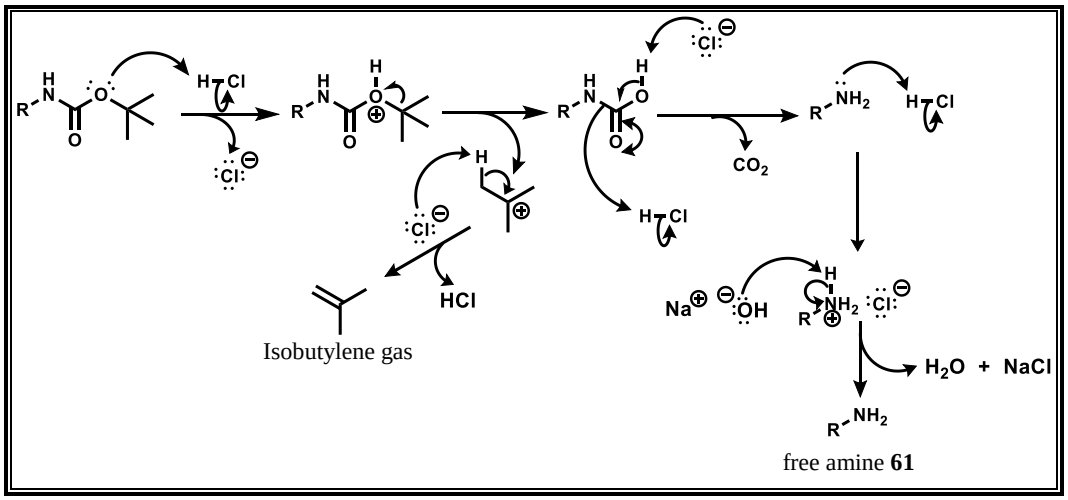

Scheme 2.16: General reaction mechanism for acid-mediated boc-deprotection reaction.[67]

The *N*-boc-deprotection step to afford analogue **61** was accompanied by the disappearance of the upfield signal of the *tert*-butyl group (Figure 2.36). As anticipated, since the spectrum was acquired in deuterated methanol, the exchangeable amino hydrogens (NH_2 and N*H*) were not observed. Strikingly, the multiplicity patterns for this analogue were also somewhat different from its precursors. Proton H6 resonated at δ = 9.10 ppm as a doublet (J = 2.10 Hz) arising from J^4 coupling to H7. A doublet of doublets of triplets (J = 8.20, 2.11 & 0.73 Hz) integrating for one proton was observed for proton H7. This was attributed to J^3 coupling to H8, a long-range (J^4) coupling to H6 and potentially a space coupling to two neighbouring protons, in this case amino protons (NH_2). Proton H1 resonated as a doublet with weak coupling (J^4 = 0.41 Hz, δ = 7.96 ppm) to H2. At δ = 7.93 ppm, a 1-proton doublet of doublets signal was observed which was unambiguously assigned to H8 experiencing both short-range coupling (J^3 = 8.20 Hz) to H7 and long-range coupling (J^5 = 0.86 Hz) to H6. For the aliphatic signals, the most deshielded protons H4 resonated relatively downfield compared to the more shielded H3 protons. Additionally, a clear resolution between equatorial and axial protons was evident. The most deshielded equatorial protons H4e resonated as a 2-proton multiplet signal at δ = 3.17 ppm while the more shielded axial protons H4a resonated as a triplet of doublets (J = 12.43, 2.85 Hz, δ = 2.77 ppm). Axial protons in cyclohexane and piperidine rings are known to experience almost equal coupling to an equatorial proton at the same carbon ($J^{a\text{-}e}$, geminal) and an axial proton at an adjacent carbon ($J^{a\text{-}a}$, vicinal).[68] The triplet pattern could be arising from these interactions. A weak coupling to the vicinal equatorial proton H3e, which also has literature precedence,[68] further splits the triplet into triplet of doublets. Furthermore, a multiplet signal integrating for two protons at δ = 1.91 ppm was attributed to H3e protons while protons

H3a accounted for a doublet of triplets of doublets at 1.80 ppm. This H3a splitting pattern arises from coupling to an axial proton H2 ($J^{a\text{-}a}$ = 13.32 Hz), equal coupling to H3e and H4a ($J^{a\text{-}e}$ = $J^{a\text{-}a}$ = 12.01 Hz) and a weak coupling to a vicinal equatorial proton H4e ($J^{a\text{-}e}$ = 4.02 Hz). The splitting pattern of H3a was also informative of the stereochemistry of proton H2 and the bulky pyrazinyl group about the tertiary piperidine carbon. Since vicinal axial-axial couplings are known to be stronger than vicinal axial-equatorial couplings,[68] a large coupling constant (J = 13.32 Hz) observed between H3a and H2 indicates the H2 proton is axial while the bulky pyrazinyl group is equatorial.

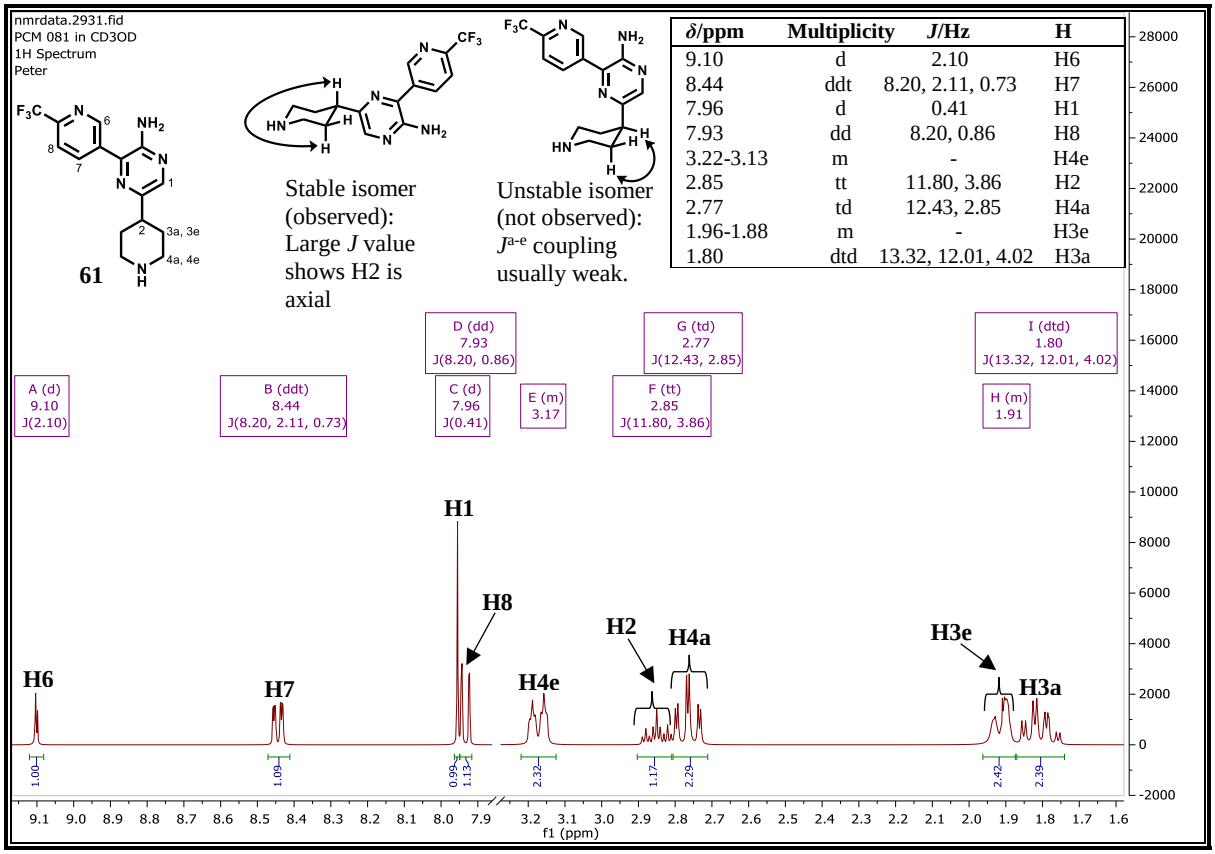

Figure 2.36: ^{1}H-NMR spectrum of **61** at 400 MHz in CD_3OD.

Upon *N*-boc-deprotection, a mass loss of 100 *m/z* units corresponding to the mass of the removed boc group was observed on the mass spectrum of compound **61**. Under negative ionization mode, this corresponded to a pseudo-molecular ion M – H (*m/z* = 321.8, calculated exact mass = 323.1358) which further confirmed successful deprotection.

2.4.2.5 *N*-Mesylation: Step (v), Scheme 2.11

Mechanistic studies[69] employing kinetic isotope effects on the hydrolysis of methanesulfonyl chloride (i.e., nucleophilic substitution of the Cl for OH in $MeSO_2Cl$) have revealed that, in basic media, the reaction occurs via the formation of a sulfene intermediate (scheme 2.17). Although the piperidine nitrogen is capable of directly attacking the electrophilic sulfur centre, the abstraction of the acidic alpha (α) proton proceeds much faster to form the sulfene intermediate. However, for the tosylation reaction (see scheme 2.2), which involves toluenesulfonyl chloride with no acidic α hydrogens, the nucleophile directly attacks the sulfur in an S_N2 fashion. In the second step, the piperidine nitrogen then adds to the sulfene sulfur, which is then followed by proton transfer steps to give the *N*-mesylated compound.

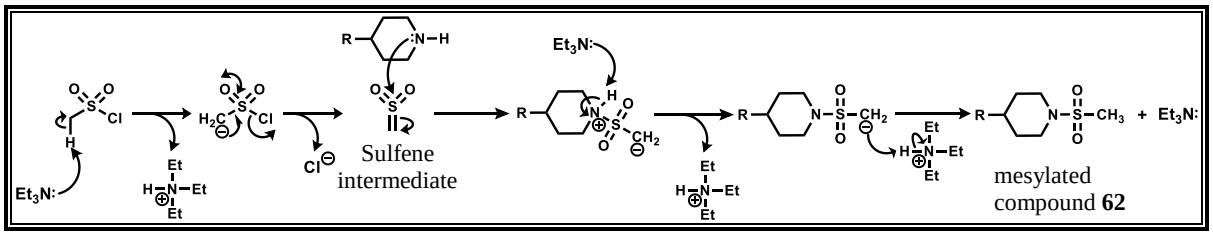

Scheme 2.17: General reaction mechanism for *N*-mesylation.[69]

Successful *N*-mesylation was confirmed by the appearance of a sharp ^{1}H-NMR methyl signal which co-resonated with protons H3 and H5a at δ = 2.84 ppm (Figure 2.37). Other aliphatic protons in the piperidine ring resonated as multiplets with the most shielded H4 protons resonating upfield. The aromatic region still retained a similar pattern of signals as that observed for the precursors of this final compound.

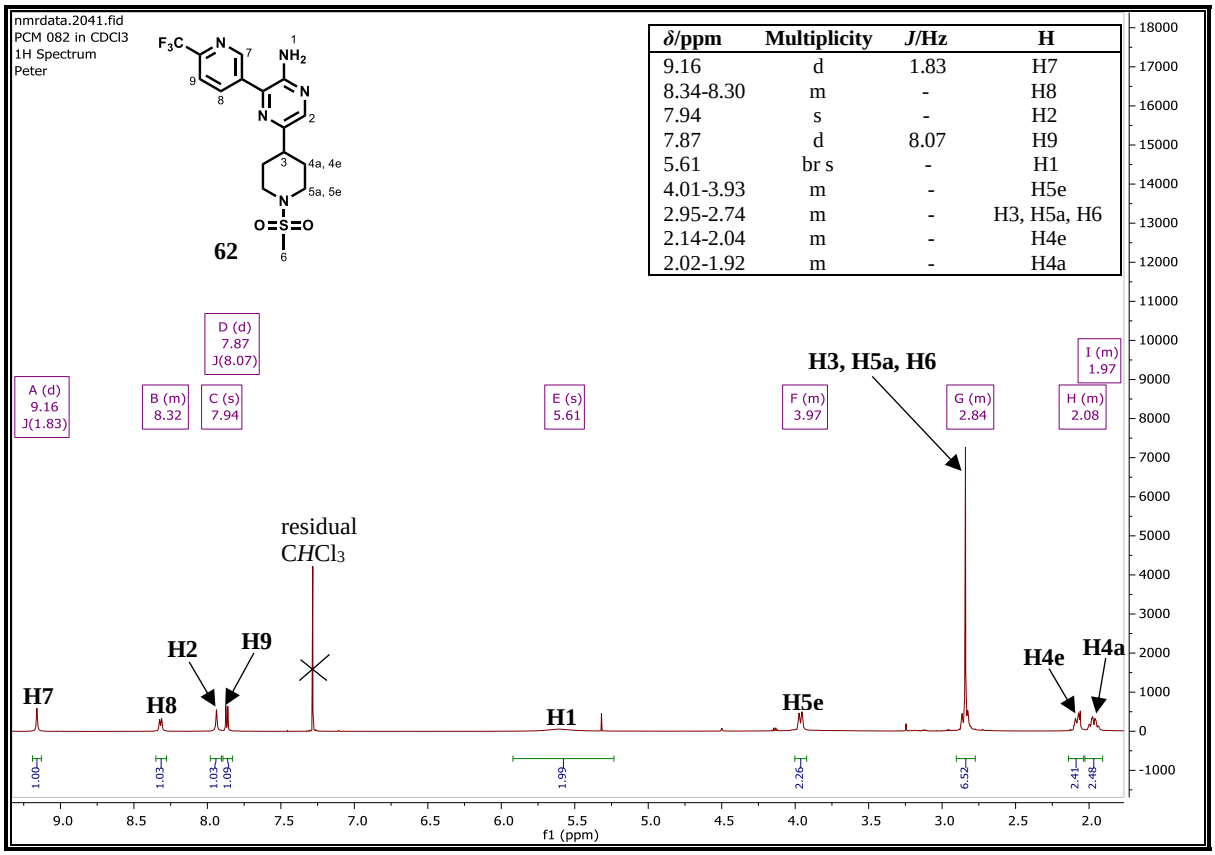

Figure 2.37: ^{1}H-NMR spectrum of **62** at 600 MHz in $CDCl_3$.

The target compound **62** was also further confirmed by ^{13}C-NMR (Figure 2.38) with well-resolved aliphatic carbon signals. The introduced methylsulfonyl carbon C6 resonated at δ = 35.21 ppm with nearly equal intensity to the C3 (δ = 40.10 ppm) signal. Similarly, the two piperidinyl carbons, C4 (δ = 30.93 ppm) and C5 (δ = 46.00 ppm) resonated as equal intensity peaks and were approximately twice as intense as C3 and C6 signals. The aromatic carbons also resonated as well-resolved signals and were unambiguously assigned. However, almost all quaternary carbons co-resonated around the same chemical shift further downfield.

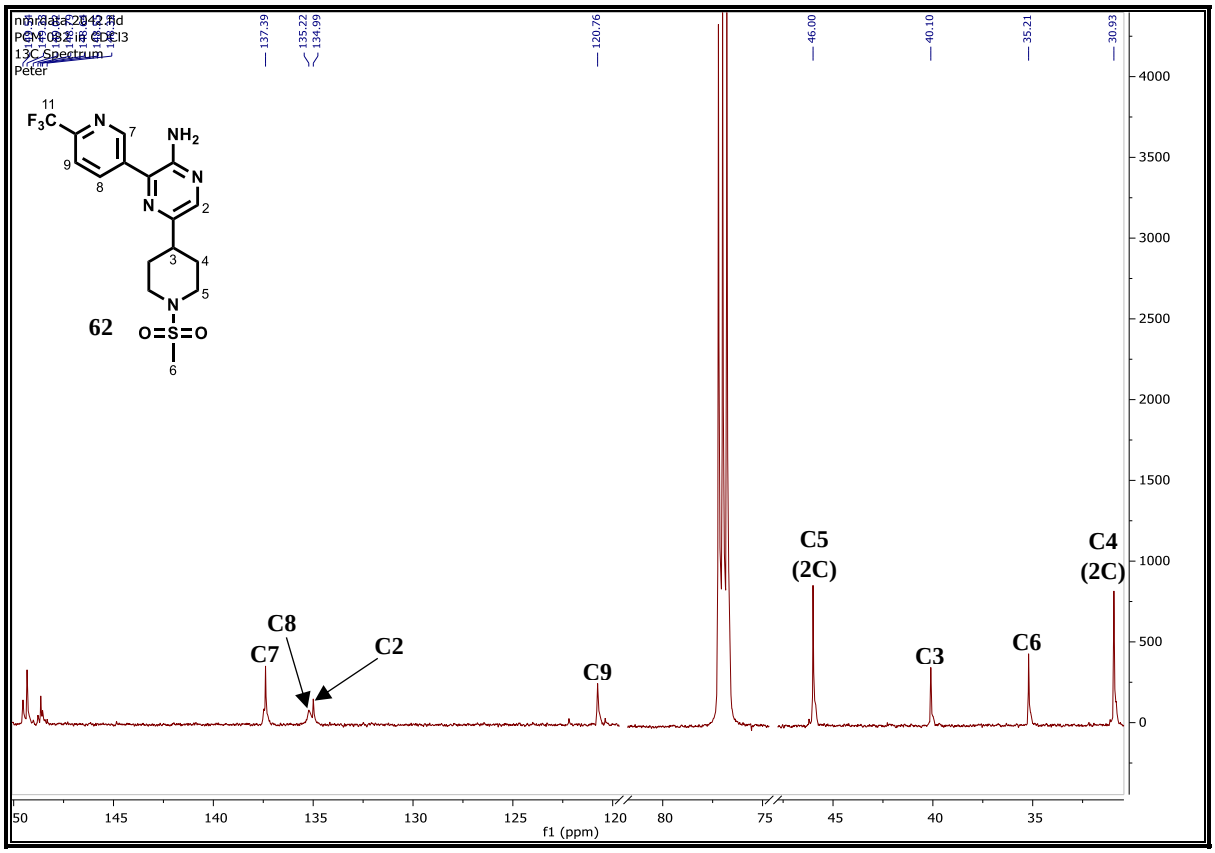

Figure 2.38: ^{13}C-NMR spectrum of **62** at 151 MHz in $CDCl_3$.

Compound **62** was further characterized by HPLC-MS and exhibited a retention time of 2.517 min with a pseudo-molecular ion (*m/z* $[M + H]^+$ = 402.1, calculated exact mass = 401.1133) being detected under $APCI^+$ mode (Figure 2.39).

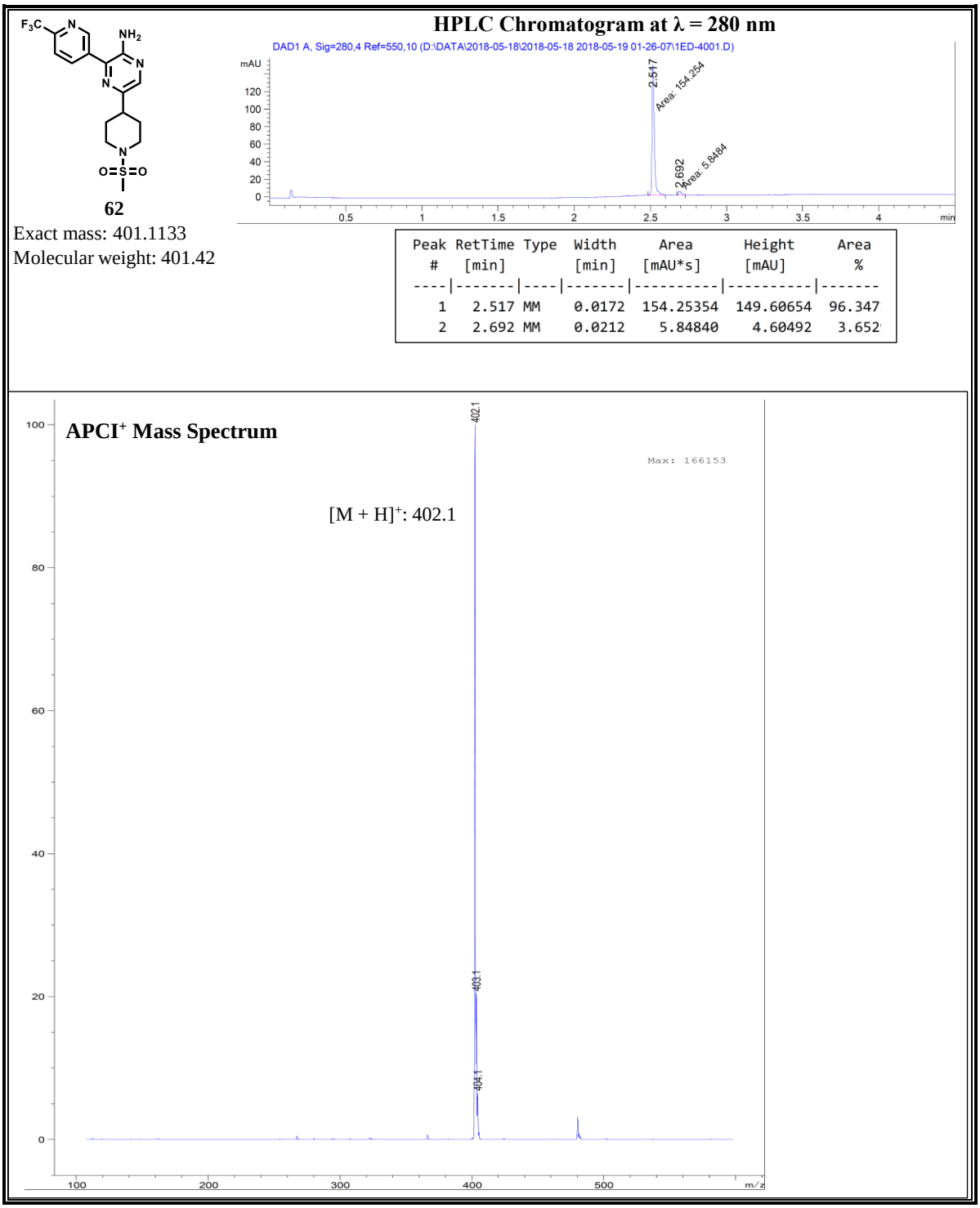

Figure 2.39: HPLC Chromatogram and APCI$^+$ mass spectrum of **62**.

2.4.2.6 Suzuki-Miyaura Cross-coupling: Step (i), Scheme 2.12

Successful Suzuki-Miyaura coupling to deliver compound **63** was confirmed by ^{1}H-NMR (Figure 2.40). A singlet integrating for one proton observed at the most downfield chemical shift (δ = 8.36 ppm) was attributed to H2. The well resolved doublets at δ = 8.10 and 8.01 ppm, both exhibiting equal coupling interactions (J = 8.50 and 8.49 Hz respectively) were

unambiguously assigned to H3 and H4 respectively. Although protons H6 (δ = 6.39 ppm) and H9 (δ = 2.73 ppm) were theoretically expected to resonate as triplets, this was not the case. Both resonated as broad singlets indicating they could, in fact, be triplets which are not just well resolved. Typical of amino protons, these (H1) resonated at δ = 5.63 ppm as a broad singlet. On the other hand, protons H7 (δ = 4.17 ppm, J = 3.34 Hz) and H8 (δ = 3.71 ppm, J = 5.65 Hz) resonated as a doublet and triplet respectively, which confirmed the count of their vicinal neighbours. Furthermore, sharp signals at δ = 3.08 and 1.51 ppm were attributed to the methyl protons H5 and H10 respectively.

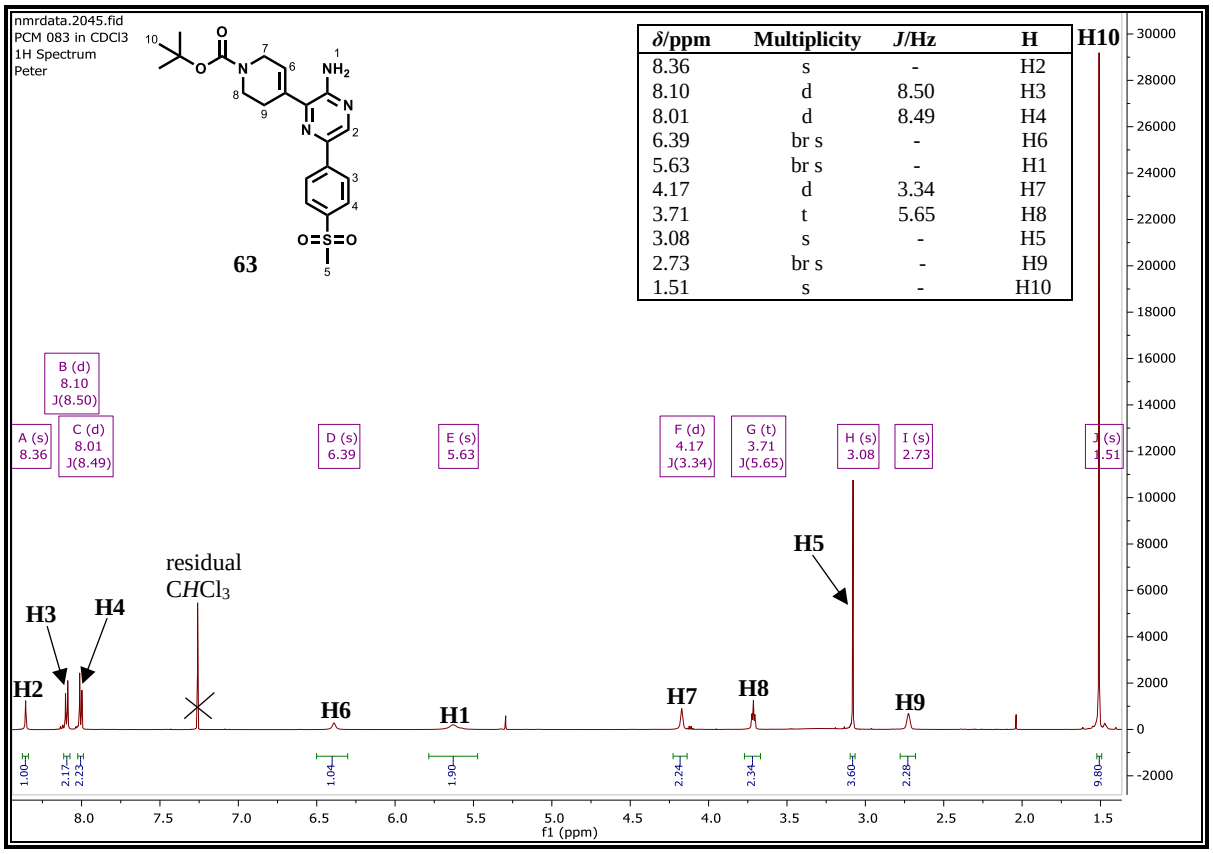

Figure 2.40: ^{1}H-NMR spectrum of **63** at 600 MHz in $CDCl_3$.

Compound **63** was further subjected to HPLC-MS characterization, which revealed a deprotonated molecular ion (*m/z* $[M - H]^-$ = 429.1, calculated exact mass = 430.1675) in the negative APCI mode and a retention time of 2.703 min.

The reduction of the alkene double bond in **63** delivered **64** which, as revealed by ^{1}H-NMR was still contaminated with trace amounts of the former. Compound **64** was used without further purification in the boc-deprotection step. The ^{1}H-NMR spectrum of **64** is, therefore, not shown, albeit the chemical shifts are reported in the experimental chapter of this thesis.

For compound **69**, the introduction of the 4-carboxyphenyl ring was confirmed by the corresponding appearance of two 2-proton doublet signals at δ = 8.26 ppm (J = 8.80 Hz) and δ = 7.98 ppm (J = 8.74 Hz) in the ^{1}H-NMR spectrum (Figure 2.41). Respectively, these signals were assigned to H6 and H7, which were differentiated from those of H3 and H4 based on differences in coupling constants.

On HPLC-MS, compound **69** eluted at t_r = 2.496 min and exhibited a pseudo-molecular ion (m/z $[M + H]^+$ = 370.1, calculated exact mass = 369.0783) under APCI$^+$ mode.

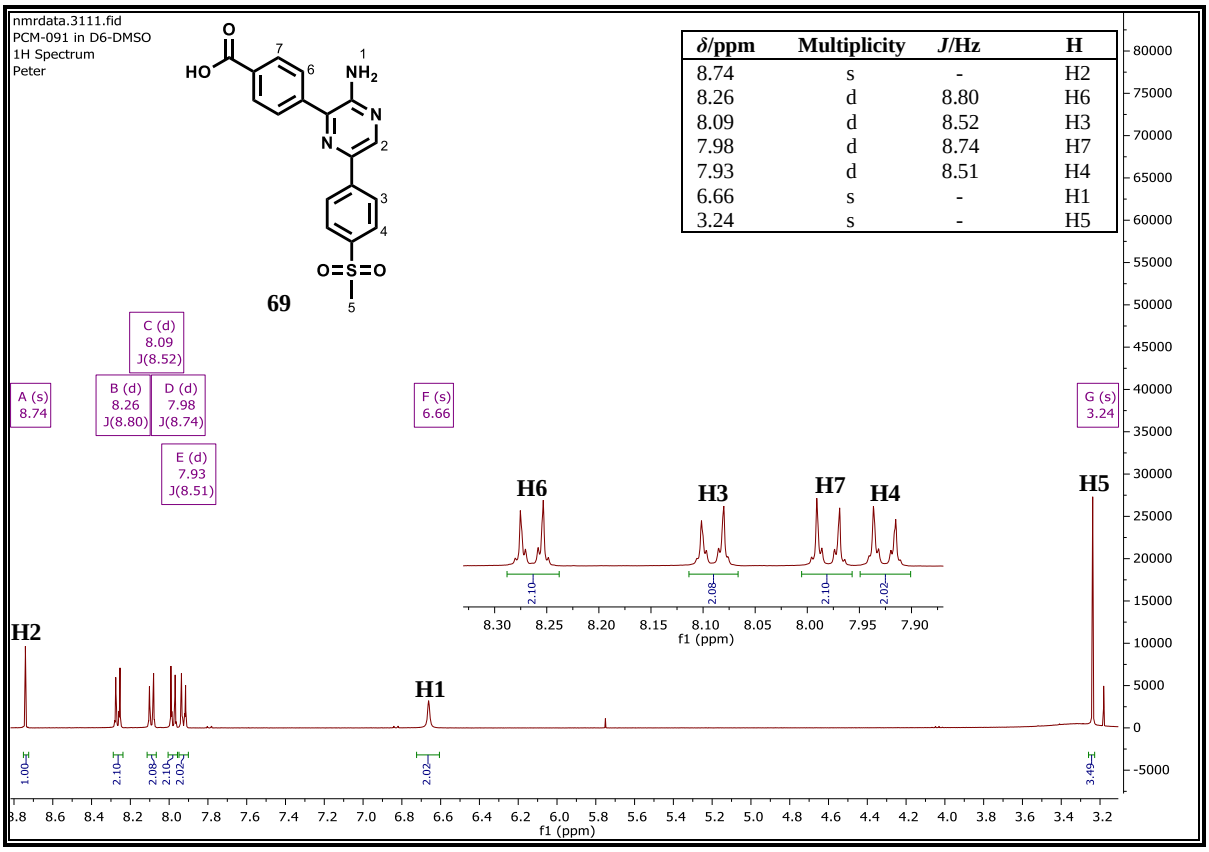

Figure 2.41: ^{1}H-NMR spectrum of **69** at 400 MHz in DMSO-d_6.

2.4.2.7 *N*-Boc-deprotection: Step (iii), Scheme 2.12

The *N*-boc-deprotection reaction, whose mechanism has already been described (see subsection 2.4.2.4), was accompanied by the disappearance of the signal corresponding to the boc *tert*-butyl group (Figure 2.42). Save for the equatorial protons H7e, which resonated as a doublet (J = 12.23 Hz) at δ = 3.09 ppm, all the other piperidine protons resonated as multiplets. In this case, the doublet signal corresponding to H7e arises from geminal coupling to H7a while vicinal coupling to H6a and H6e was not detected at this resolution.

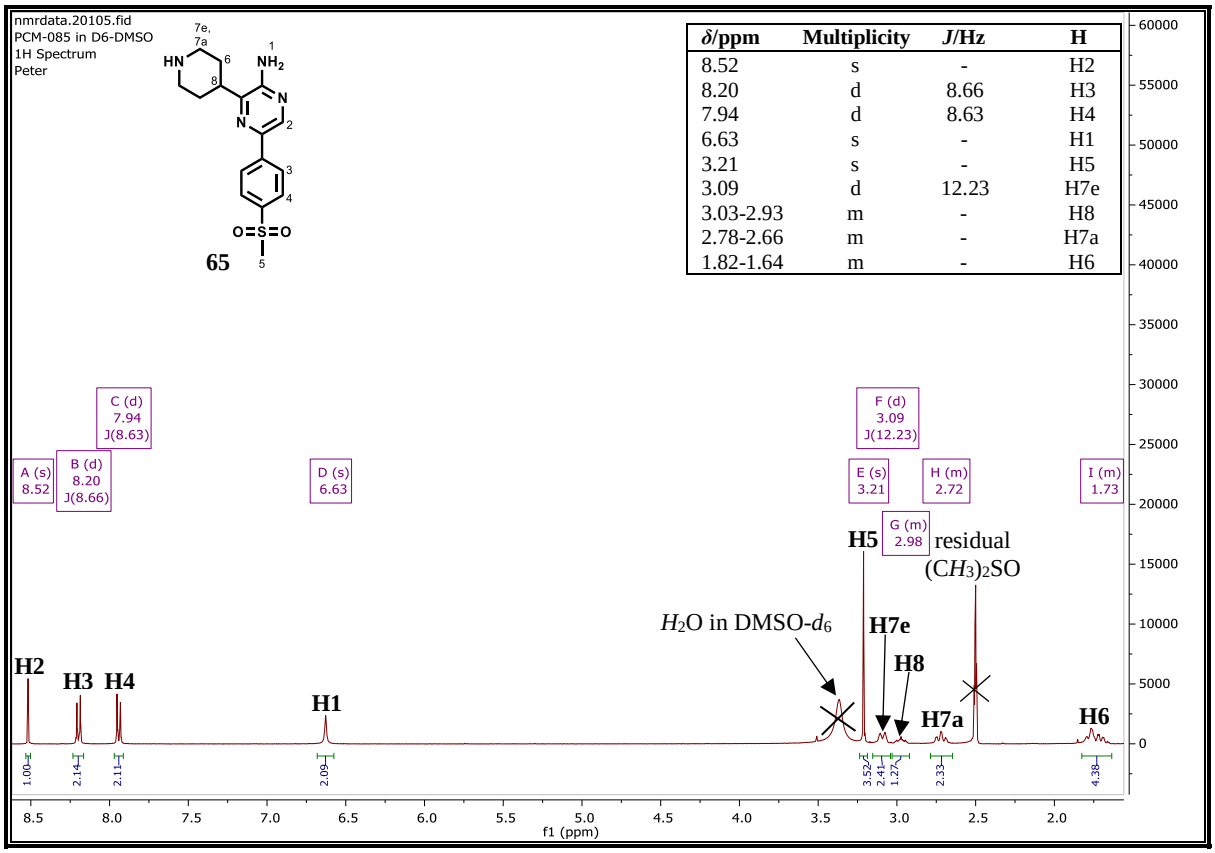

Figure 2.42: ^{1}H-NMR spectrum of **65** at 400 MHz in DMSO-d_6.

As anticipated, the polar compound **65** eluted relatively quicker on the reversed phase column conditions of the HPLC (t_r = 0.249 min). A corresponding pseudo-molecular ion (*m/z* $[M + H]^+$ = 332.8, calculated exact mass = 332.1307) was observed under APCI$^+$ mode.

2.4.2.8 *N*-Mesylation: Step (iv), Scheme 2.12

The *N*-mesylation step (see mechanism in subsection 2.4.2.5) was accompanied by the appearance of an additional methyl signal in ^{1}H-NMR spectrum (not shown) as observed in the synthetic target **62** described in subsection 2.4.2.5. The molecular mass of compound **66** was also confirmed by HPLC-MS which showed a pseudo-molecular ion peak of *m/z* $[M + H]^+$ = 410.7 (calculated exact mass = 410.1082) at t_r = 2.434 min.

2.4.2.9 Suzuki-Miyaura Cross-coupling: Step (i), Scheme 2.13

The one-pot Suzuki-Miyaura cross coupling reaction in step (i) of scheme 2.13 led to introduction of partially saturated substituents at both positions 3 and 5 of the 2-aminopyrazine core-scaffold. Consistent with this transformation, the ^{1}H-NMR spectrum of the resulting compound **70** (Figure 2.43) only exhibited one aromatic singlet signal at δ = 7.73 ppm

corresponding to H2. The spectrum revealed that protons at the same positions of the two tetrahydropyridyl rings were nearly magnetically equivalent as shown by small differences in their chemical shifts. While H12 resonated as a broad singlet at a distinct chemical shift (δ = 6.59 ppm), the corresponding proton H7 on the tetrahydropyridyl ring at position 5 co-resonated with H1 as a 3-proton multiplet signal at δ = 6.39 ppm. Protons H11 (δ = 4.19 ppm, J = 3.06 Hz) and H6 (δ = 4.15 ppm, J = 3.50 Hz) resonated as doublets with weak coupling to their neighbours H12 and H7 respectively. The two triplet signals at δ = 3.70 and 3.67 ppm (J = 5.55 Hz) were attributed to H9 and H4 respectively. On the other hand, protons H8 and H3 resonated as broad singlets as previously observed. Furthermore, the boc *tert*-butyl groups (H10 and H5) resonated upfield of all the other protons overlapping with a water peak in $CDCl_3$.

HPLC-MS showed a pseudo-molecular ion *m/z* $[M + H]^+$ = 458.2 (calculated exact mass = 457.2689) at t_r = 3.01 min further confirming that compound **70** was successfully synthesized.

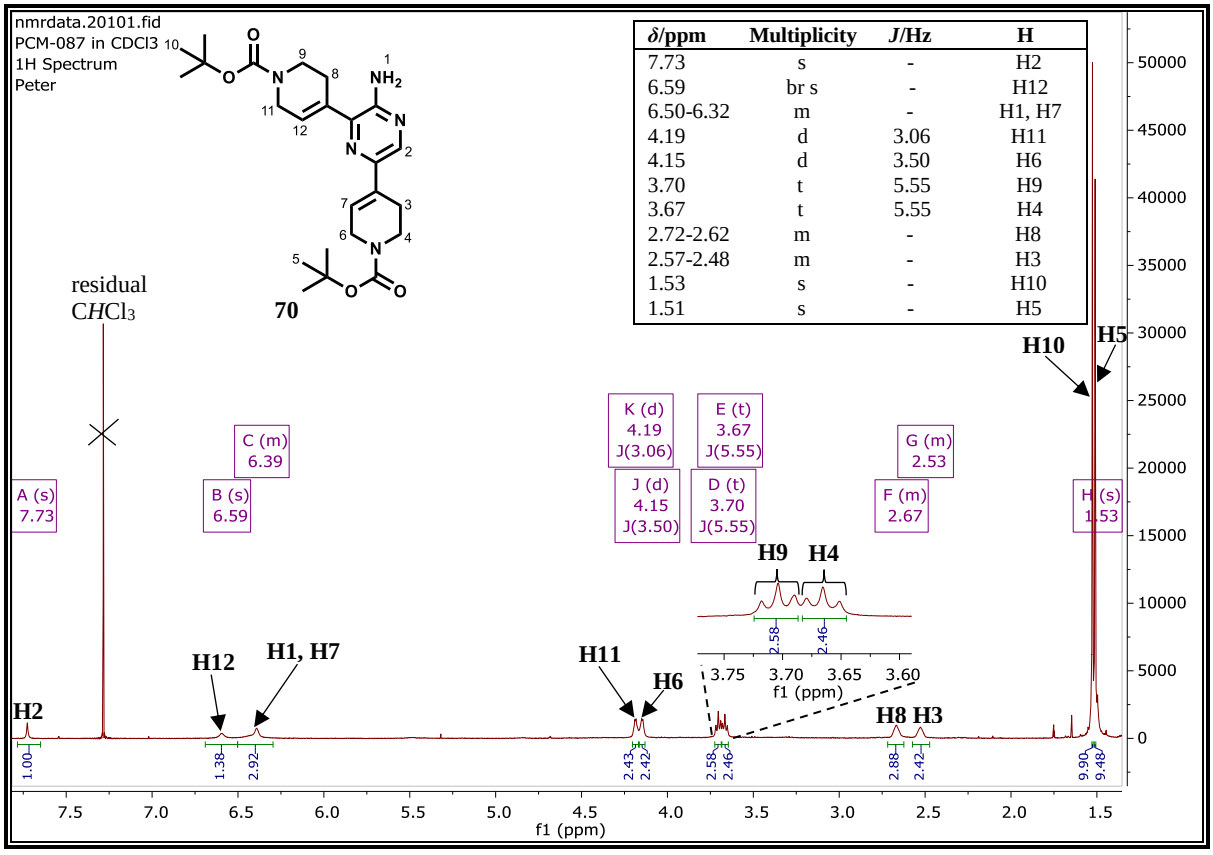

Figure 2.43: ^{1}H-NMR spectrum of **70** at 400 MHz in $CDCl_3$.

2.4.2.10 Reduction of the Alkene Double Bond: Step (ii), Scheme 2.13

The reduction of the alkene double bond (see mechanism in subsection 2.4.2.3) in compound **70** gave compound **71** (^{1}H-NMR spectrum shown in figure 2.44). This reduction step led to the corresponding disappearance of the vinylic proton signals and a concomitant appearance of more upfield multiplet signals between δ = 1.93 and 1.58 ppm indicating the double bond was successfully reduced.

Additionally, although the pseudo-molecular ion corresponding to a mass increase of four *m/z* units could not be observed, two fragment ions, one corresponding to loss of one boc group (*m/z* $[M - boc + H]^+$ = 362.2, calculated exact mass = 461.3002) and another corresponding to loss of both boc groups (*m/z* $[M - 2boc + H]^+$ = 262.2, calculated exact mass = 461.3002) were observed.

The boc-deprotection step afforded a very polar compound **7i** (Scheme 2.13) which presented challenges during purification. This compound was confirmed by ultra-pressure liquid chromatography mass spectrometry (UPLC-MS) (*m/z* $[M + H]^+$ = 262.1, calculated exact mass = 261.1953). It was subsequently mesylated without further purification.

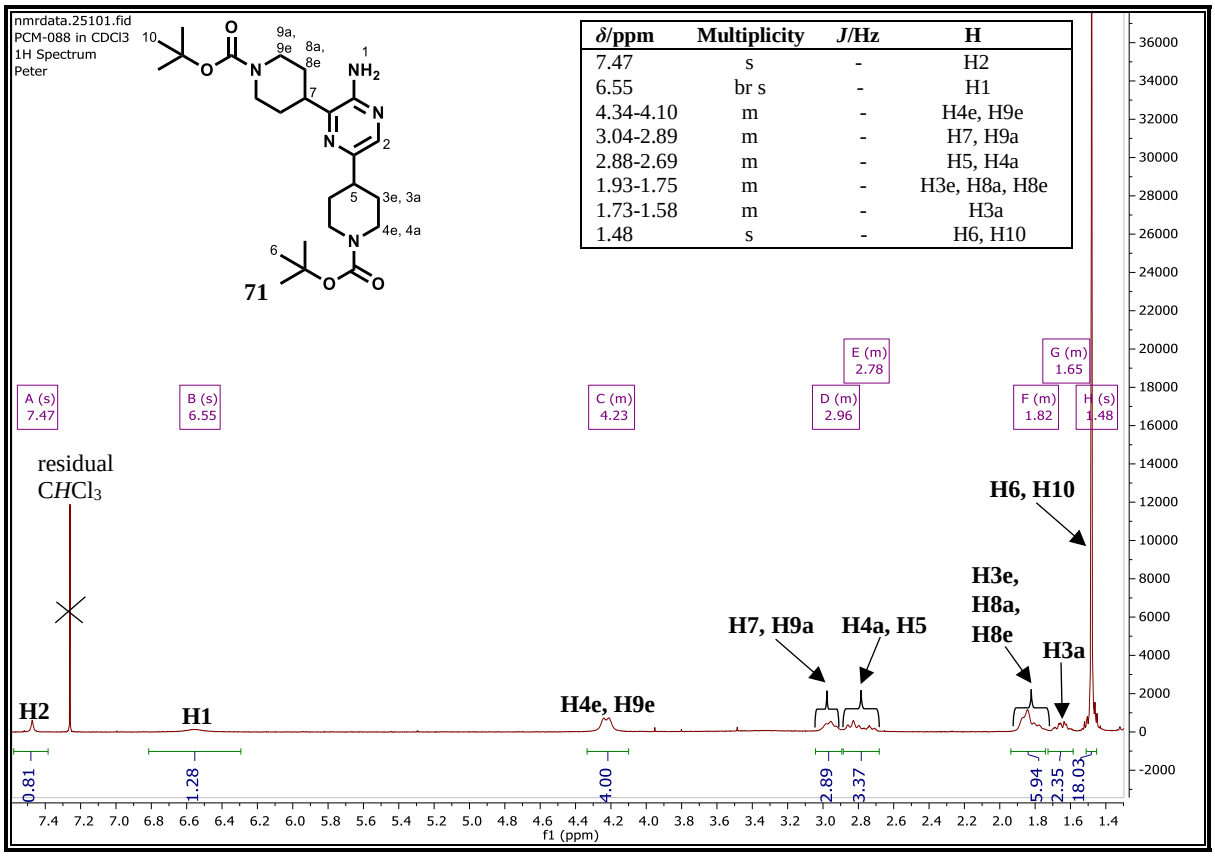

Figure 2.44: ^{1}H-NMR spectrum of **71** at 400 MHz in $CDCl_3$.

2.4.2.11 *N*-Mesylation: Step (iv), Scheme 2.13

The boc-deprotection step and subsequent *N*-mesylation (see mechanism in subsection 2.4.2.5) to give compound **72** was accompanied by a disappearance of the upfield *tert*-butyl hydrogen signals of the boc groups and a corresponding appearance of relatively deshielded sulfone-bonded methyl signals in the ^{1}H-NMR spectrum (Figure 2.45). However, these co-resonated with other piperidyl protons as a multiplet at δ = 2.88 ppm. On HPLC-MS, the pseudo-molecular ion corresponding to this compound was not observed.

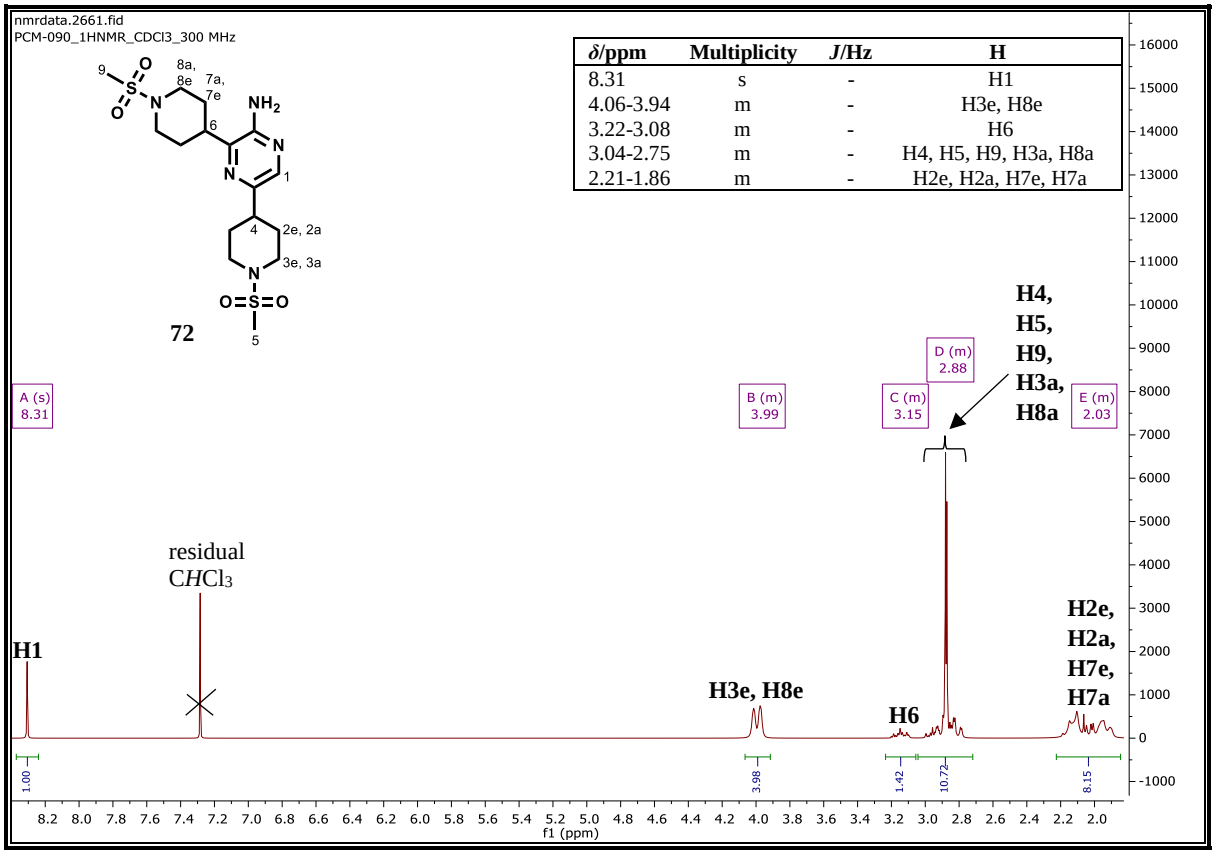

Figure 2.45: ^{1}H-NMR spectrum of **72** at 300 MHz in $CDCl_3$.

2.4.2.12 Nucleophilic Aromatic Substitution: Step (i), Scheme 2.14

The reaction mechanism for the nucleophilic aromatic substitution (S_NAr) proceeds most likely via an addition-elimination pathway (Scheme 2.18).[70] Nucleophilic attack of the nucleophile, in this case, 1-boc-piperazine on the brominated carbon generates an anion intermediate. Aromatization to eliminate the bromide anion followed by deprotonation gives the boc-protected compound. Under the influence of high temperature (170 °C), the boc-protecting group decomposes giving the free amine compound **67**, CO_2 and a *tert*-butyl carbocation. It is also likely that this thermolysis could also occur directly on the 1-boc-piperazine before it

attacks the bromo-containing starting material. The generated *tert*-butyl carbocation has the same fate as that described in scheme 2.16.

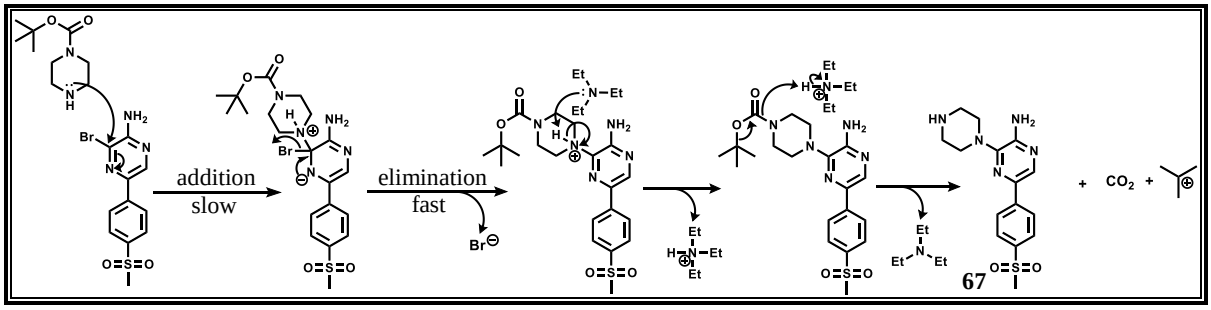

Scheme 2.18: Reaction mechanism for nucleophilic aromatic substitution (S_NAr).[70]

The introduction of the piperazine moiety was confirmed by the appearance of two multiplet 4-proton signals at δ = 3.09 and 2.90 ppm corresponding to H6 and H7 respectively (Figure 2.46). It is also noteworthy that the peak for protons H5 significantly overlapped with a water peak in DMSO-d_6.

Additionally, compound **67** eluted relatively earlier under the reversed phase conditions on HPLC-MS (t_r = 0.170 min) with its pseudo-molecular ion (*m/z* $[M + H]^+$ = 334.1, calculated exact mass = 333.1259) being observed in $APCI^+$ mode.

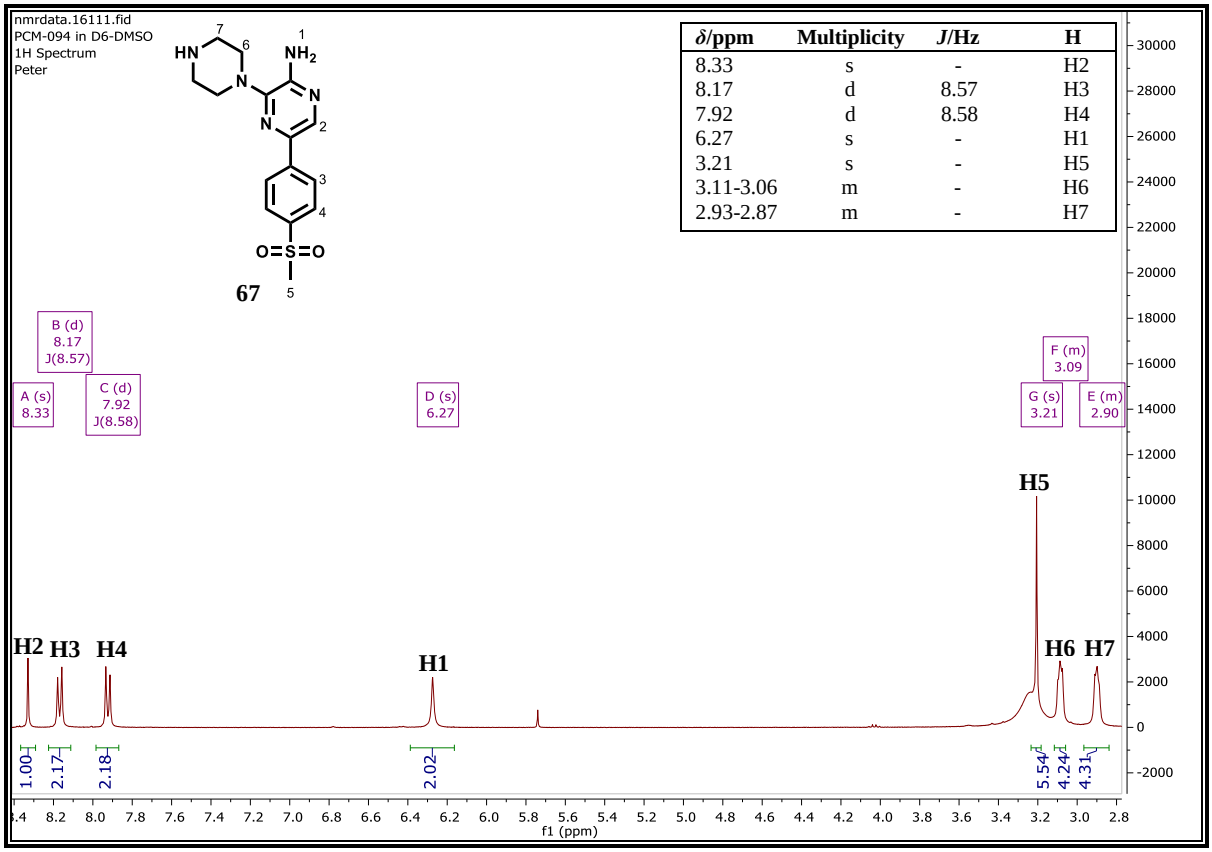

Figure 2.46: ^{1}H-NMR spectrum of **67** at 400 MHz in DMSO-d_6.

2.4.2.13 *N*-Mesylation: Step (ii), Scheme 2.14

The mesylation reaction occurs via a mechanism outlined in scheme 2.17. The ^{1}H-NMR spectrum for the obtained compound (**68**) is shown in figure 2.47. Correspondingly, an additional sharp 3-proton signal at δ = 2.94 ppm was observed confirming successful mesylation. The signal for protons H7 was obscured by a water peak at δ = 3.37 ppm.

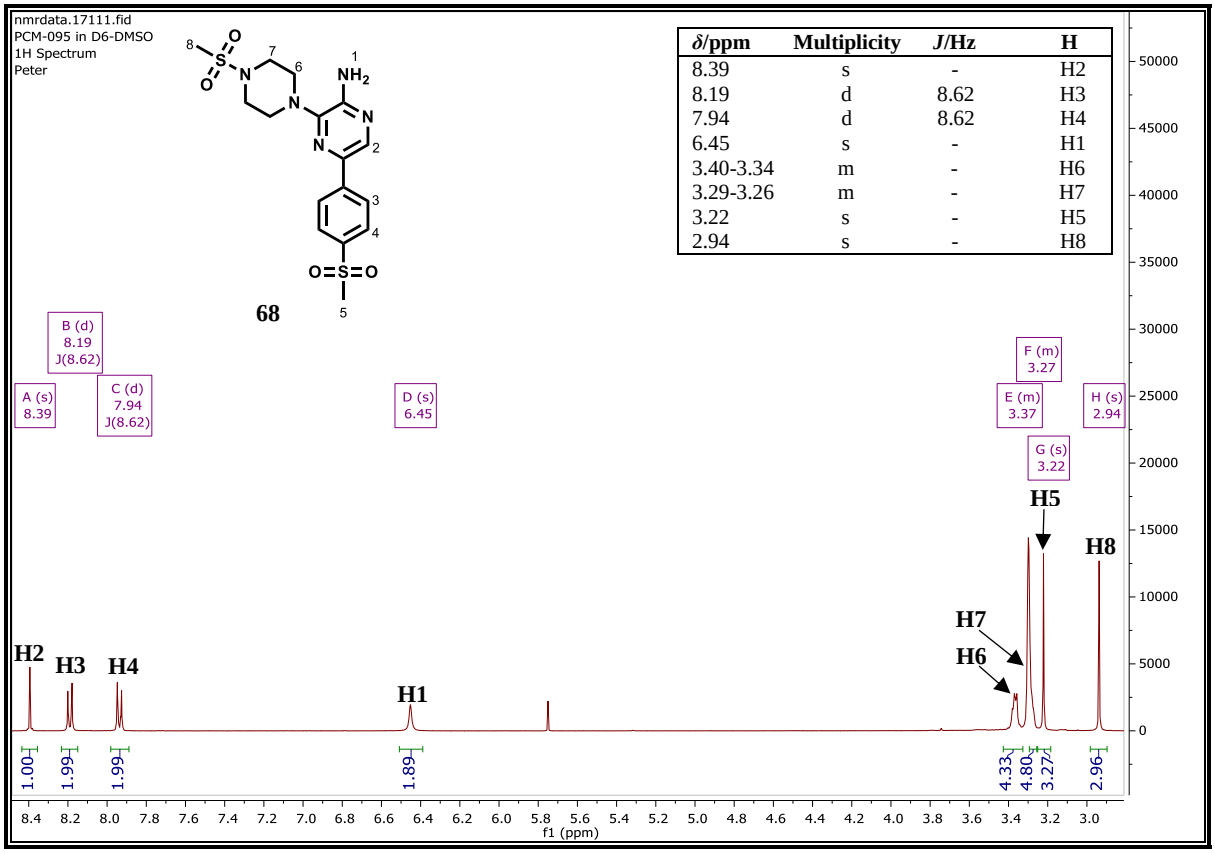

Figure 2.47: ^{1}H-NMR spectrum of **68** at 400 MHz in DMSO-d_6.

The ^{13}C-NMR spectrum accounted for all carbons in the expected structure of compound **68** (Figure 2.48). Expectedly, the five quaternary carbons resonated as five relatively weak signals downfield of all other carbons. The two sharp and intense signals in the aromatic region (δ = 127.84 and 125.67 ppm) were respectively attributed to C4 and C3 of the phenyl ring. Similarly, the two sharp and equally intense peaks in the aliphatic region at δ = 47.65 and 45.50 ppm were assigned to the two piperazinyl carbons C7 and C6 respectively. The introduced methylsulfonyl carbon C8 resonated at the most upfield chemical shift δ = 34.76 ppm followed by C5 at δ = 44.20 ppm. The aromatic carbon (C2) was the most deshielded of the aromatic

hydrogen-bearing carbons. This is also true for ^{1}H-NMR spectra of the precursors to compound **68** where proton H2 consistently resonates downfield of protons H3 and H4.

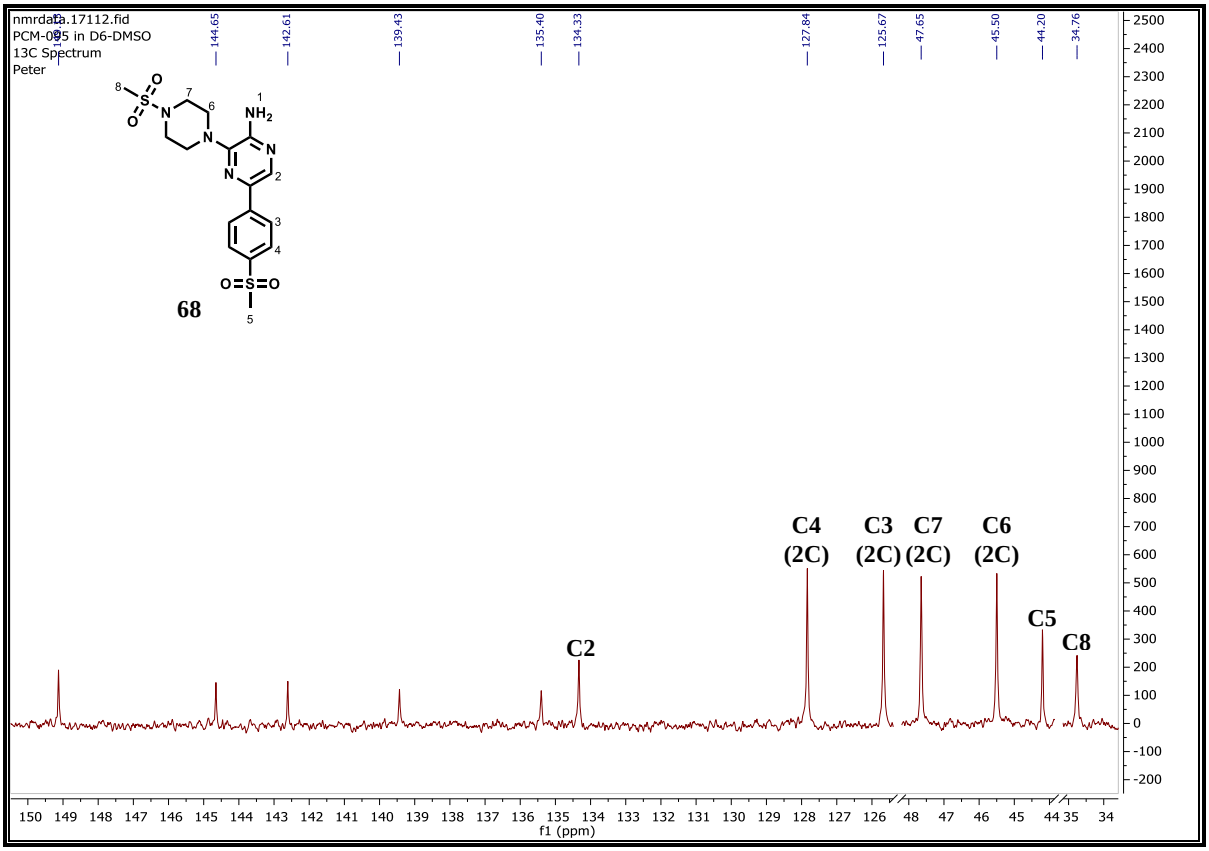

Figure 2.48: ^{13}C-NMR spectrum of **68** at 101 MHz in DMSO-d_6.

A pseudo-molecular ion (*m/z* $[M + H]^+$ = 412.1, calculated exact mass = 411.1035) at a retention time of 2.447 min was observed when **68** was subjected to HPLC-MS analysis under $APCI^+$ mode which further confirmed the authenticity of this compound (Figure 2.49).

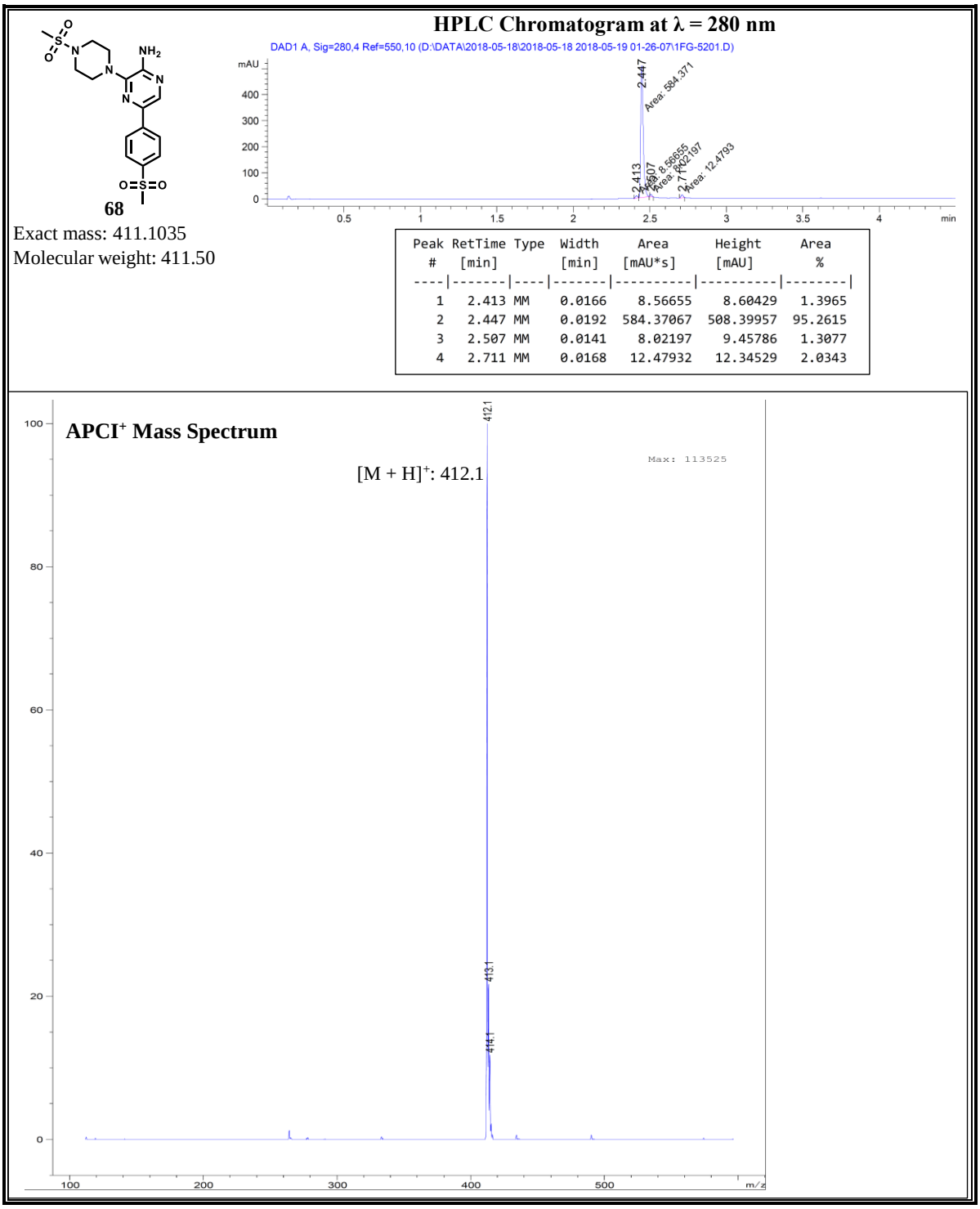

Figure 2.49: HPLC Chromatogram and APCI$^+$ mass spectrum of **68**.

2.5 Concluding Remarks

In this chapter, the rationale behind the design of the synthesized target compounds have been described. The imidazopyridazine and aminopyrazine target compounds were obtained in 8 – 80 % and 21 – 86% yields respectively. The target compounds were characterized by, among other techniques, NMR, HPLC-MS and UPLC-MS. HPLC-MS also ensured the target

compounds were of acceptable purity (≥ 95%) for solubility and biological evaluation which is the focus of the next chapter.

2.6 References

(1) Le Manach, C.; Gonzàlez Cabrera, D.; Douelle, F.; Nchinda, A. T.; Younis, Y.; Taylor, D.; Wiesner, L.; White, K. L.; Ryan, E.; March, C.; Duffy, S.; Avery, V. M.; Waterson, D.; Witty, M. J.; Wittlin, S.; Charman, S. A.; Street, L. J.; Chibale, K. Medicinal Chemistry Optimization of Antiplasmodial Imidazopyridazine Hits from High Throughput Screening of a SoftFocus Kinase Library: Part 1. *J. Med. Chem.* **2014**, *57*, 2789–2798.

(2) Le Manach, C.; Paquet, T.; Gonzàlez Cabrera, D.; Younis, Y.; Taylor, D.; Wiesner, L.; Lawrence, N.; Schwager, S.; Waterson, D.; Witty, M. J.; Wittlin, S.; Street, L. J.; Chibale, K. Medicinal Chemistry Optimization of Antiplasmodial Imidazopyridazine Hits from High Throughput Screening of a SoftFocus Kinase Library: Part 2. *J. Med. Chem.* **2014**, *57*, 8839–8848.

(3) Le Manach, C.; Paquet, T.; Brunschwig, C.; Njoroge, M.; Han, Z.; Gonzàlez Cabrera, D.; Bashyam, S.; Dhinakaran, R.; Taylor, D.; Reader, J.; Botha, M.; Churchyard, A.; Lauterbach, S.; Coetzer, T. L.; Birkholtz, L.-M.; Meister, S.; Winzeler, E. A.; Waterson, D.; Witty, M. J.; Wittlin, S.; Jiménez-Díaz, M.-B.; Santos Martínez, M.; Ferrer, S.; Angulo-Barturen, I.; Street, L. J.; Chibale, K. A Novel Pyrazolopyridine with in Vivo Activity in Plasmodium Berghei - and Plasmodium Falciparum - Infected Mouse Models from Structure–Activity Relationship Studies around the Core of Recently Identified Antimalarial Imidazopyridazines. *J. Med. Chem.* **2015**, *58*, 8713–8722.

(4) Bell, I. M.; Gallicchio, S. N.; Abrams, M.; Beshore, D. C.; Buser, C. A.; Culberson, J. C.; Davide, J.; Ellis-Hutchings, M.; Fernandes, C.; Gibbs, J. B.; Graham, S. L.; Hartman, G. D.; Heimbrook, D. C.; Homnick, C. F.; Huff, J. R.; Kassahun, K.; Koblan, K. S.; Kohl, N. E.; Lobell, R. B.; Lynch, J. J.; Miller, P. A.; Omer, C. A.; Rodrigues, A. D.; Walsh, E. S.; Williams, T. M. Design and Biological Activity of (*S*)-4-(5-{[1-(3-Chlorobenzyl)-2- Oxopyrrolidin-3-ylamino]Methyl}imidazol-1-ylmethyl)Benzonitrile, a 3-Aminopyrrolidinone Farnesyltransferase Inhibitor with Excellent Cell Potency. *J. Med. Chem.* **2001**, *44*, 2933–2949.

(5) Fish, L. R.; Gilligan, M. T.; Humphries, A. C.; Ivarsson, M.; Ladduwahetty, T.; Merchant, K. J.; O'Connor, D.; Patel, S.; Philipps, E.; Vargas, H. M.; Hutson, P. H.; MacLeod, A. M. 4-Fluorosulfonylpiperidines: Selective 5-HT2A Ligands for the Treatment of Insomnia. *Bioorg. Med. Chem. Lett.* **2005**, *15*, 3665–3669.

(6) Kasuga, J.; Ishikawa, M.; Yonehara, M.; Makishima, M.; Hashimoto, Y.; Miyachi, H. Improvement of Water-Solubility of Biarylcarboxylic Acid Peroxisome Proliferator-

Activated Receptor (PPAR) δ-Selective Partial Agonists by Disruption of Molecular Planarity/Symmetry. *Bioorg. Med. Chem.* **2010**, *18*, 7164–7173.

(7) Mitcheson, J. S.; Chen, J.; Lin, M.; Culberson, C.; Sanguinetti, M. C. A Structural Basis for Drug-Induced Long QT Syndrome. *Proc. Natl. Acad. Sci.* **2000**, *97*, 12329–12333.

(8) Fernandez, D.; Ghanta, A.; Kauffman, G. W.; Sanguinetti, M. C. Physicochemical Features of the hERG Channel Drug Binding Site. *J. Biol. Chem.* **2004**, *279*, 10120–10127.

(9) Vaz, R. J.; Gao, Z.; Pribish, J.; Chen, X.; Levell, J.; Davis, L.; Albert, E.; Brollo, M.; Ugolini, A.; Cramer, D. M.; Cairns, J.; Sides, K.; Liu, F.; Kwong, J.; Kang, J.; Rebello, S.; Elliot, M.; Lim, H.; Chellaraj, V.; Singleton, R. W.; Li, Y. Design of Bivalent Ligands Using Hydrogen Bond Linkers: Synthesis and Evaluation of Inhibitors for Human β-Tryptase. *Bioorg. Med. Chem. Lett.* **2004**, *14*, 6053–6056.

(10) Fraley, M. E.; Arrington, K. L.; Buser, C. A.; Ciecko, P. A.; Coll, K. E.; Fernandes, C.; Hartman, G. D.; Hoffman, W. F.; Lynch, J. J.; McFall, R. C.; Rickert, K.; Singh, R.; Smith, S.; Thomas, K. A.; Wong, B. K. Optimization of the Indolyl Quinolinone Class of KDR (VEGFR-2) Kinase Inhibitors. *Bioorg. Med. Chem. Lett.* **2004**, *14*, 351–355.

(11) Fletcher, S. R.; Burkamp, F.; Blurton, P.; Cheng, S. K. F.; Clarkson, R.; O'Connor, D.; Spinks, D.; Tudge, M.; van Niel, M. B.; Patel, S.; Chapman, K.; Marwood, R.; Shepheard, S.; Bentley, G.; Cook, G. P.; Bristow, L. J.; Castro, J. L.; Hutson, P. H.; MacLeod, A. M. 4-(Phenylsulfonyl)Piperidines: Novel, Selective, and Bioavailable 5-HT 2A Receptor Antagonists. *J. Med. Chem.* **2002**, *45*, 492–503.

(12) Cooper, L. C.; Carlson, E. J.; Castro, J. L.; Chicchi, G. G.; Dinnell, K.; Di Salvo, J.; Elliott, J. M.; Hollingworth, G. J.; Kurtz, M. M.; Ridgill, M. P.; Rycroft, W.; Tsao, K.-L.; Swain, C. J. 4,4-Disubstituted Cyclohexylamine NK1 Receptor Antagonists II. *Bioorg. Med. Chem. Lett.* **2002**, *12*, 1759–1762.

(13) Friesen, R. W.; Ducharme, Y.; Ball, R. G.; Blouin, M.; Boulet, L.; Côté, B.; Frenette, R.; Girard, M.; Guay, D.; Huang, Z.; Jones, T. R.; Laliberté, F.; Lynch, J. J.; Mancini, J.; Martins, E.; Masson, P.; Muise, E.; Pon, D. J.; Siegl, P. K. S.; Styhler, A.; Tsou, N. N.; Turner, M. J.; Young, R. N.; Girard, Y. Optimization of a Tertiary Alcohol Series of Phosphodiesterase-4 (PDE4) Inhibitors: Structure−Activity Relationship Related to PDE4 Inhibition and Human Ether-a-Go-Go Related Gene Potassium Channel Binding Affinity. *J. Med. Chem.* **2003**, *46*, 2413–2426.

(14) Bilodeau, M. T.; Balitza, A. E.; Koester, T. J.; Manley, P. J.; Rodman, L. D.; Buser-Doepner, C.; Coll, K. E.; Fernandes, C.; Gibbs, J. B.; Heimbrook, D. C.; Huckle, W. R.;

Kohl, N.; Lynch, J. J.; Mao, X.; McFall, R. C.; McLoughlin, D.; Miller-Stein, C. M.; Rickert, K. W.; Sepp-Lorenzino, L.; Shipman, J. M.; Subramanian, R.; Thomas, K. A.; Wong, B. K.; Yu, S.; Hartman, G. D. Potent N-(1,3-Thiazol-2-yl)Pyridin-2-Amine Vascular Endothelial Growth Factor Receptor Tyrosine Kinase Inhibitors with Excellent Pharmacokinetics and Low Affinity for the hERG Ion Channel. *J. Med. Chem.* **2004**, *47*, 6363–6372.

(15) White, N. J. The Treatment of Malaria. *N. Engl. J. Med.* **1996**, *335*, 800–806.

(16) Hatton, C. S.; Peto, T. E.; Bunch, C.; Pasvol, G.; Russell, S. J.; Singer, C. R.; Edwards, G.; Winstanley, P. Frequency of Severe Neutropenia Associated with Amodiaquine Prophylaxis against Malaria. *Lancet.* **1986**, *1*, 411–414.

(17) Winstanley, P.; Coleman, J.; Maggs, J.; Breckenridge, A.; Park, B. The Toxicity of Amodiaquine and Its Principal Metabolites towards Mononuclear Leucocytes and Granulocyte/Monocyte Colony Forming Units. *Br. J. Clin. Pharmacol.* **1990**, *29*, 479–485.

(18) Naisbitt, D. J.; Williams, D. P.; O'Neill, P. M.; Maggs, J. L.; Willock, D. J.; Pirmohamed, M.; Park, B. K. Metabolism-Dependent Neutrophil Cytotoxicity of Amodiaquine: A Comparison with Pyronaridine and Related Antimalarial Drugs. *Chem. Res. Toxicol.* **1998**, *11*, 1586–1595.

(19) Larrey, D.; Castot, A.; Pëssayre, D.; Merigot, P.; Machayekhy, J. P.; Feldmann, G.; Lenoir, A.; Rueff, B.; Benhamou, J. P. Amodiaquine-Induced Hepatitis. A Report of Seven Cases. *Ann. Intern. Med.* **1986**, *104*, 801–803.

(20) AlKadi, H. O. Antimalarial Drug Toxicity: A Review. *Chemotherapy.* **2007**, *53*, 385–391.

(21) World Health Organization (1993) 19th Expert Committee on Malaria Report, World Health Organization, Geneva, Switzerland.

(22) Jewell, H.; Maggs, J. L.; Harrison, A. C.; O'Neill, P. M.; Ruscoe, J. E.; Park, B. K. Role of Hepatic Metabolism in the Bioactivation and Detoxication of Amodiaquine. *Xenobiotica.* **1995**, *25*, 199–217.

(23) Heidari, R.; Babaei, H.; Eghbal, M. A. Amodiaquine-Induced Toxicity in Isolated Rat Hepatocytes and the Cytoprotective Effects of Taurine and/or N-Acetyl Cysteine. *Res. Pharm. Sci.* **2014**, *9*, 97–105.

(24) Tingle, M. D.; Jewell, H.; Maggs, J. L.; O'Neill, P. M.; Park, B. K. The Bioactivation of Amodiaquine by Human Polymorphonuclear Leucocytes in Vitro: Chemical Mechanisms and the Effects of Fluorine Substitution. *Biochem. Pharmacol.* **1995**, *50*,

1113–1119.

(25) O'Neill, P. M.; Mukhtar, A.; Stocks, P. A.; Randle, L. E.; Hindley, S.; Ward, S. A.; Storr, R. C.; Bickley, J. F.; O'Neil, I. A.; Maggs, J. L.; Hughes, R. H.; Winstanley, P. A.; Bray, P. G.; Park, B. K. Isoquine and Related Amodiaquine Analogues: A New Generation of Improved 4-Aminoquinoline Antimalarials. *J. Med. Chem.* **2003**, *46*, 4933–4945.

(26) Pearlstein, R. A.; Vaz, R. J.; Kang, J.; Chen, X.-L.; Preobrazhenskaya, M.; Shchekotikhin, A. E.; Korolev, A. M.; Lysenkova, L. N.; Miroshnikova, O. V; Hendrix, J.; Rampe, D. Characterization of hERG Potassium Channel Inhibition Using CoMSiA 3D QSAR and Homology Modeling Approaches. *Bioorg. Med. Chem. Lett.* **2003**, *13*, 1829–1835.

(27) Aronov, A. M. Common Pharmacophores for Uncharged Human Ether-a-Go-Go-Related Gene (hERG) Blockers. *J. Med. Chem.* **2006**, *49*, 6917–6921.

(28) Gately, S.; West, R. Novel Therapeutics with Enhanced Biological Activity Generated by the Strategic Introduction of Silicon Isosteres into Known Drug Scaffolds. *Drug Dev. Res.* **2007**, *68*, 156–163.

(29) Le Manach, C.; Nchinda, A. T.; Paquet, T.; Gonzàlez Cabrera, D.; Younis, Y.; Han, Z.; Bashyam, S.; Zabiulla, M.; Taylor, D.; Lawrence, N.; White, K. L.; Charman, S. A.; Waterson, D.; Witty, M. J.; Wittlin, S.; Botha, M. E.; Nondaba, S. H.; Reader, J.; Birkholtz, L.-M.; Jiménez-Díaz, M. B.; Martínez, M. S.; Ferrer, S.; Angulo-Barturen, I.; Meister, S.; Antonova-Koch, Y.; Winzeler, E. A.; Street, L. J.; Chibale, K. Identification of a Potential Antimalarial Drug Candidate from a Series of 2-Aminopyrazines by Optimization of Aqueous Solubility and Potency across the Parasite Life Cycle. *J. Med. Chem.* **2016**, *59*, 9890–9905.

(30) Goodfellow, V. S.; Nguyen, T. X.; Ravula, S. B.; Gelbard, .A. Preparation of Imidazopyridine Compounds as Mixed Lineage Kinase Inhibitors. US 20140256733, 2014.

(31) Olah, G. A.; Wang, Q.; Sandford, G.; Surya Prakash, G. K. Synthetic Methods and Reactions. 181. Iodination of Deactivated Aromatics with N-Iodosuccinimide in Trifluoromethanesulfonic Acid (NIS-CF_3SO_3H) via in Situ Generated Superelectrophilic Iodine(I) Trifluoromethanesulfonate. *J. Org. Chem.* **1993**, *58*, 3194–3195.

(32) Miyaura, N.; Suzuki, A. Palladium-Catalyzed Cross-Coupling Reactions of Organoboron Compounds. *Chem. Rev.* **1995**, *95*, 2457–2483.

(33) Thompson, A. E.; Hughes, G.; Batsanov, A. S.; Bryce, M. R.; Parry, P. R.; Tarbit, B. Palladium-Catalyzed Cross-Coupling Reactions of Pyridylboronic Acids with Heteroaryl Halides Bearing a Primary Amine Group: Synthesis of Highly Substituted Bipyridines and Pyrazinopyridines. *J. Org. Chem.* **2005**, *70*, 388–390.

(34) Wolfe, J. P.; Wagaw, S.; Buchwald, S. L. An Improved Catalyst System for Aromatic Carbon−Nitrogen Bond Formation: The Possible Involvement of Bis(Phosphine) Palladium Complexes as Key Intermediates. *J. Am. Chem. Soc.* **1996**, *118*, 7215–7216.

(35) Driver, M. S.; Hartwig, J. F. A Second-Generation Catalyst for Aryl Halide Amination: Mixed Secondary Amines from Aryl Halides and Primary Amines Catalyzed by (DPPF)$PdCl_2$. *J. Am. Chem. Soc.* **1996**, *118*, 7217–7218.

(36) Delacourte, A.; Melnyk, P.; Burlet, S.; Lefur, N. Preparation of 7-Chloro-Quinolin-4-Amine Compounds and Uses Thereof for the Prevention or Treatment of Diseases Involving Formation of Amyloid Plaques And/or Where a Dysfunction of the App Metabolism Occur. WO2011073322 A1, 2011.

(37) Solomons, T. W. G.; Fryhle, C. B. *Organic Chemistry*, 10th ed.; John Wiley & Sons: Hoboken, 2011.

(38) Lücking, U. Sulfoximines: A Neglected Opportunity in Medicinal Chemistry. *Angew. Chemie Int. Ed.* **2013**, *52*, 9399–9408.

(39) Montalbetti, C. A. G. N.; Falque, V. Amide Bond Formation and Peptide Coupling. *Tetrahedron.* **2005**, *61*, 10827–10852.

(40) Green, T. W.; Wuts, P. G. M. *Protective Groups in Organic Synthesis*; Wiley-Interscience: New York, 1999.

(41) On Acetals and Hemiacetals. https://www.masterorganicchemistry.com/2010/05/28/on-acetals-and-hemiacetals/. Accessed: 2018-05-17. (Archived by WebCite® at http://www.webcitation.org/6zTzK2rI9).

(42) Carreño, M. C.; García Ruano, J.; Sanz, G.; Toledo, M. A.; Urbano, A. Mild and Regiospecific Nuclear Iodination of Methoxybenzenes and Naphthalenes with N-Iodosuccinimide in Acetonitrile. *Tetrahedron Lett.* **1996**, *37*, 4081–4084.

(43) March, J. *Advanced Organic Chemistry: Reactions, Mechanisms, and Structure*, 4th ed.; John Wiley & Sons: New York, 1992.

(44) Miyaura, N.; Yamada, K.; Suzuki, A. A New Stereospecific Cross-Coupling by the Palladium-Catalyzed Reaction of 1-Alkenylboranes with 1-Alkenyl or 1-Alkynyl Halides. *Tetrahedron Lett.* **1979**, *20*, 3437–3440.

(45) Lichter, R. L.; Wasylishen, R. E. Fluoropyridines. Carbon-13 Chemical Shifts and

Carbon-Fluorine Coupling Constants. *J. Am. Chem. Soc.* **1975**, *97*, 1808–1813.

(46) Buchwald-Hartwig amination. http://www.name-reaction.com/buchwald-hartwig-amination. Accessed: 2018-05-22. (Archived by WebCite® at http://www.webcitation.org/6zbJuPPZn).

(47) Guram, A. S.; Buchwald, S. L. Palladium-Catalyzed Aromatic Aminations with in Situ Generated Aminostannanes. *J. Am. Chem. Soc.* **1994**, *116*, 7901–7902.

(48) Paul, F.; Patt, J.; Hartwig, J. F. Palladium-Catalyzed Formation of Carbon-Nitrogen Bonds. Reaction Intermediates and Catalyst Improvements in the Hetero Cross-Coupling of Aryl Halides and Tin Amides. *J. Am. Chem. Soc.* **1994**, *116*, 5969–5970.

(49) Reich, H. J. Chemical Shift. http://www.chem.wisc.edu/areas/reich/nmr/05-hmr-02-delta.htm. Accessed: 2018-09-13. (Archived by WebCite® at http://www.webcitation.org/72P4nIADp).

(50) Solomons, T. W. G.; Fryhle, C. B. *Organic Chemistry*, 10th ed.; John Wiley & Sons: Hoboken, 2011.

(51) Mas, T.; Claramunt, R. M.; María, D. S.; Sanz, D.; Alarcón, S. H.; Pérez-Torralba, M.; Elguero, J. Structure and Spectroscopy of Imidazo[1,2-*a*]Imidazoles and Imidazo[1,2-*a*]Benzimidazoles. *Arkivoc.* **2002**, *2002*, 48.

(52) Isotopes of the Element Bromine. https://education.jlab.org/itselemental/iso035.html. Accessed: 2018-09-13. (Archived by WebCite® at http://www.webcitation.org/72P5O9zkB).

(53) Rebek, J.; Feitler, D. Improved Method for the Study of Reaction Intermediates. Mechanism of Peptide Synthesis Mediated by Carbodiimides. *J. Am. Chem. Soc.* **1973**, *95*, 4052–4053.

(54) Rebek, J.; Feitler, D. Mechanism of the Carbodiimide Reaction. II. Peptide Synthesis on the Solid Phase. *J. Am. Chem. Soc.* **1974**, *96*, 1606–1607.

(55) Cheuka, P. M. Synthesis of Aminomethylthiazole Analogues for Evaluation as Antiplasmodial Agents, University of Cape Town, 2014.

(56) Younis, Y.; Douelle, F.; González Cabrera, D.; Le Manach, C.; Nchinda, A. T.; Paquet, T.; Street, L. J.; White, K. L.; Zabiulla, K. M.; Joseph, J. T.; Bashyam, S.; Waterson, D.; Witty, M. J.; Wittlin, S.; Charman, S. A.; Chibale, K. Structure–Activity-Relationship Studies around the 2-Amino Group and Pyridine Core of Antimalarial 3,5-Diarylaminopyridines Lead to a Novel Series of Pyrazine Analogues with Oral in Vivo Activity. *J. Med. Chem.* **2013**, *56*, 8860–8871.

(57) Barsanti, P. A.; Aversa, R. J.; Jin, X.; Pan, Y.; Lu, Y.; Elling, R.; Jain, R.; Knapp, M.;

Lan, J.; Lin, X.; Rudewicz, P.; Sim, J.; Taricani, L.; Thomas, G.; Xiao, L.; Yue, Q. Structure-Based Drug Design of Novel Potent and Selective Tetrahydropyrazolo[1,5-*a*]Pyrazines as ATR Inhibitors. *ACS Med. Chem. Lett.* **2015**, *6*, 37–41.

(58) Wuts, P. G. M.; Greene, T. W. *Greene's Protective Groups in Organic Synthesis*, 4th ed.; John Wiley & Sons: New York, 2007.

(59) Lakrout, S.; K'tir, H.; Amira, A.; Berredjem, M.; Aouf, N.-E. A Simple and Eco-Sustainable Method for the Sulfonylation of Amines under Microwave-Assisted Solvent-Free Conditions. *RSC Adv.* **2014**, *4*, 16027–16032.

(60) Krakowiak, K. E.; Bradshaw, J. S. Thermal Removal of Boc-Protecting Groups During Preparation of Open-Chain Polyamines. *Synth. Commun.* **1996**, *26*, 3999–4004.

(61) Bogdan, A. R.; Charaschanya, M.; Dombrowski, A. W.; Wang, Y.; Djuric, S. W. High-Temperature Boc Deprotection in Flow and Its Application in Multistep Reaction Sequences. *Org. Lett.* **2016**, *18*, 1732–1735.

(62) Table of characteristic proton NMR chemical shifts. https://orgchemboulder.com/Spectroscopy/Reference.pdf. Accessed: 2018-06-04. (Archived by WebCite® at http://www.webcitation.org/6zvgNlc3X).

(63) Andrade, C.; Silva, W. One-Step Reduction of Chalcones to Saturated Alcohols by Ammonium Formate/Palladium on Carbon: A Versatile Method. *Lett. Org. Chem.* **2006**, *3*, 39–41.

(64) Introduction to Catalytic Transfer Hydrogenation http://shodhganga.inflibnet.ac.in/bitstream/10603/35906/5/chapter 2.pdf. Accessed: 2018-06-05. (Archived by WebCite® at http://www.webcitation.org/6zwoGtOpN).

(65) Phillips, B. Catalytic Transfer Hydrogenation of Nitroalkenes to Primary Amines. https://digitalcommons.ursinus.edu/cgi/viewcontent.cgi?article=1002&context=chem_hon. Accessed: 2018-06-05. (Archived by WebCite® at http://www.webcitation.org/6zwovtKTX).

(66) Hydrogenation of Alkenes. http://www.chem.ucalgary.ca/courses/351/Carey5th/Ch06/ch6-3.html. Accessed: 2018-06-05. (Archived by WebCite® at http://www.webcitation.org/6zwskbrem).

(67) Boc Deprotection. http://www.commonorganicchemistry.com/Rxn_Pages/Boc_Protection/Boc_Protection_TFA_Mech.htm. Accessed: 2018-06-06. (Archived by WebCite® at http://www.webcitation.org/6zy4KXshm).

(68) Reich, H. J. 5-HMR-5 Vicinal Proton-Proton Coupling 3JHH.

https://www.chem.wisc.edu/areas/reich/nmr/05-hmr-05-3j.htm. Accessed: 2018-06-22. (Archived by WebCite® at http://www.webcitation.org/70MV9pEFA).

(69) King, J. F.; Lam, J. Y. L.; Skonieczny, S. Organic Sulfur Mechanisms. 35. Mechanisms of Hydrolysis and Related Nucleophilic Displacement Reactions of Alkanesulfonyl Chlorides: pH Dependence and the Mechanism of Hydration of Sulfenes. *J. Am. Chem. Soc.* **1992**, *114*, 1743–1749.

(70) Hunt, I. Addition-Elimination Mechanism. http://www.chem.ucalgary.ca/courses/350/Carey5th/Ch23/ch23-3-3.html. Accessed: 2018-06-25. (Archived by WebCite® at http://www.webcitation.org/70R5mniAH).

CHAPTER 3
RESULTS AND DISCUSSION: BIOLOGICAL AND SOLUBILITY DATA

3.1 Chapter Overview

In this chapter, the biological and solubility results of the synthesized target compounds are discussed. The chapter commences with a discussion of the *in vitro* asexual blood stage antiplasmodial activity and solubility of all synthesized imidazopyridazine analogues. The *in vitro* gametocytocidal and liver stage antiplasmodial activity of selected imidazopyridazine compounds is then discussed followed by a discussion of cytotoxicity and hERG inhibition results. Metabolic stability studies on selected imidazopyridazine compounds are then covered before a discussion of the *in vitro* asexual blood stage antiplasmodial activity and solubility evaluation of the aminopyrazines. The chapter closes with a subsection dedicated to target-based rationalization of *in vitro* antiplasmodial SAR using a homology model of *Plasmodium falciparum* phosphatidylinositol 4-kinase, *Pf*PI4K.

3.2 Imidazopyridazines

3.2.1 *In Vitro* Asexual Blood Stage Antiplasmodial Activity and Solubility Evaluation

The synthesized target compounds were subjected to HPLC-MS purity check experiments to ensure acceptable purity (≥ 95%) before *in vitro* asexual blood stage antiplasmodial and solubility evaluation. Primarily, all the target compounds were evaluated against the drug-sensitive strain of *P. falciparum* (NF54). After this primary screen, compounds possessing significant potency (IC_{50} < 1 μM) were further tested against the chloroquine- and pyrimethamine-resistant strain of *P. falciparum* (K1). A modified [^{3}H]-hypoxanthine uptake assay[1] was used to evaluate parasite viability in presence of test compounds, which was calculated as percentage of recorded radioactivity relative to the untreated parasites. The experimental chapter of this thesis describes this method in detail. The IC_{50} values on the NF54 strain are used in the descriptions of all SAR explorations.

Solubility evaluation of all synthesized analogues was performed in parallel. A miniaturized shake flask method[2] was used to measure the solubility of all imidazopyridazine compounds. Briefly, this involved preparation of calibration standards (10 – 220 μM in DMSO) for each compound whose absorbance values were measured using an HPLC-DAD (diode array detector) to plot the calibration curves as absorbance versus concentration. The absorbance values of duplicate aqueous samples were used to read off solubility from the calibration curve.

This method is given in detail in the experimental chapter of this thesis. A summary of *in vitro* antiplasmodial (IC_{50}) and solubility values for all the synthesized target compounds is shown in tables 3.1 – 3.3.

3.2.1.1 SAR and Solubility of Pyridazine-Substituted Analogues

In the initial phase of SAR exploration, saturated ring systems, subtle modifications and water-solubilizing groups at position 6 were introduced while keeping a 4-methylsulfinylphenyl group at position 3 of the imidazopyridazine core-scaffold constant (Table 3.1). Relative to the previously reported[3] lead compound **19** (IC_{50} = 0.0034 μM), all analogues in this series exhibited lower antiplasmodial potency (IC_{50} = 0.14 – 2.7 μM). The antiplasmodial activity results for analogues tested on both the NF54 and K1 parasites show that they are equipotent across these two parasite strains suggesting the absence of cross resistance and potentially a novel mechanism of action for this class of analogues. This pan-activity was also observed for all the other imidazopyridazine analogues explored in this project and those previously reported in literature.[4]

Table 3.1: *In vitro* antiplasmodial activity against *P. falciparum* (NF54 and K1) and solubility of pyridazine-substituted analogues

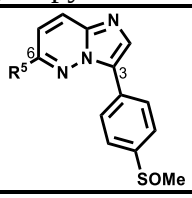

Code	R^5	*P. f* IC_{50}, μM[b,c]		Solubility, μM, pH 6.5[d]
		NF54	K1	
25	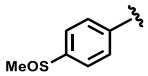	0.67	0.50	200
27	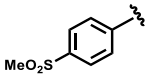	0.97	0.82	5
28	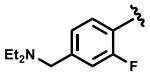	1.9	[e]ND	180
29	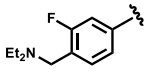	1.7	[e]ND	195
30	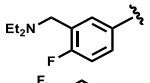	0.14	0.11	200
44	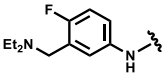	1.6	[e]ND	200
45	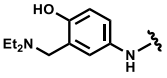	0.92	0.77	195
36	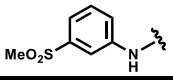	0.27	0.24	20

Table 3.1: *In vitro* antiplasmodial activity against *P. falciparum* (NF54 and K1) and solubility of pyridazine-substituted analogues

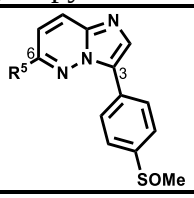

Code	R^5	*P. f* IC_{50}, μM[b,c]		Solubility, μM, pH 6.5[d]
		NF54	K1	
37	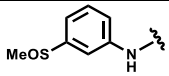	0.82	0.85	190
38	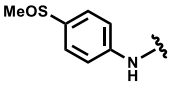	0.55	0.49	195
39	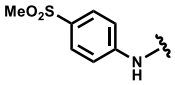	0.42	0.24	< 5
40	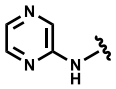	0.47	0.44	25
41	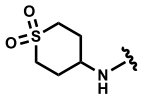	0.52	0.49	10
42	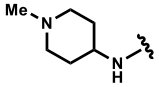	2.7	[e]ND	200
43	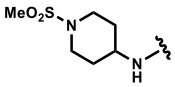	0.50	0.44	70

[b]Mean from n values of ≥ 2 independent experiments with multidrug resistant (K1) and sensitive (NF54) strains of *P. falciparum*. The majority of the individual values differed less than 2-fold (maximum 2-fold).
[c]Artesunate [IC_{50} = 2.2 ng/mL (NF54), 0.93 ng/mL (K1)] and chloroquine [IC_{50} = 4.3 ng/mL (NF54), 83 ng/mL (K1)] were used as reference drugs.
[d]Determined using a miniaturized shake flask method.[2]
[e]ND, not determined.

As demonstrated by analogues **25** (IC_{50} = 0.67 μM) and **27** (IC_{50} = 0.97 μM), *para* substitution with either a sulfone or sulfoxide group at the phenyl ring on position 6 of the imidazopyridazine core was detrimental to potency. As expected, compared to the sulfone-substituted analogue **27** which exhibited poor aqueous solubility (5 μM), the sulfoxide derivative **25** was highly soluble (200 μM). This can be explained when one considers the energetics of interactions between these two groups (sulfone and sulfoxide) and water. Examination of interactions of the sulfoxide with water shows that these are energetically favoured compared to those of the sulfone. For this reason, despite having more hydrogen bonding sites and a larger dipole moment, sulfones have limited solubility in water compared to their sulfoxide counterparts. It is known that hydrogen bonding also involves the partial interaction of non-bonding electrons with the antibonding sigma orbitals (σ*) of the H_2O molecules.[5] In this regard, sulfoxides have higher energy orbitals than sulfones, which results

in the greatest stabilization and net drop in energy upon interaction with water than is the case with sulfones.

Compound **30** exhibited the highest potency (IC_{50} = 0.14 μM) amongst analogues substituted with a fluoro group and a bulky basic side chain (**28**, **29** and **30**, Table 3.1) highlighting the importance to potency of the *para*-fluoro and *meta*-diethylaminomethyl substitution pattern. Also notable is the fact that, of all the analogues in this series, compound **30** was the most potent. On the other hand, the solubility of such basic amine-substituted analogues was significantly improved (180 – 200 μM).

In the case of aminated imidazopyridazines, antiplasmodial potency was generally compromised albeit most of them still retained sub-micromolar potency. A particular example in this class is compound **36** (IC_{50} = 0.27 μM) which was more active than its reduced version **37** (IC_{50} = 0.82 μM) by a 3-fold margin. On the contrary, compounds **38** (IC_{50} = 0.55 μM) and **39** (IC_{50} = 0.42 μM) which are the *para*-substituted forms were equipotent. Additionally, in the quest to improve solubility, analogues **41** – **43** (Table 3.1) with saturated heterocyclic rings at position 6, which were envisaged to discourage the solubility-suppressing effect of π – π stacking, were designed.[6] As reflected in compounds **43** (IC_{50} = 0.50 μM) and **42** (IC_{50} = 2.7 μM), the sulfone group in **43** was found to be crucial to the retention of sub-micromolar potency – compound **42** devoid of this group was 5-fold less potent. When evaluated for solubility, the NH-linked compounds generally had improved solubility with sulfoxide analogues, as expected, exhibiting superior solubility compared to the sulfones.

3.2.1.2 SAR and Solubility of Imidazo-Substituted Analogues

In the next phase of SAR studies, various substitutions at position 3 of the core-scaffold were explored while keeping a *meta*-substituted group, the 3-methylsulfinylphenyl, at position 6 of the core-scaffold fixed. The choice of a *meta*-substituted group at position 6 was motivated by previous studies[3] which found this substitution pattern optimal for potency. Table 3.2 summarizes all antiplasmodial and solubility results for this series of analogues. While one analogue (**35**) with promising potency against both the NF54 (IC_{50} = 0.15 μM) and K1 (IC_{50} = 0.087 μM) strains was identified, analogues in this series displayed the lowest antiplasmodial activity (IC_{50} = 0.99 – 7.6 μM) compared to other SAR explorations. Consequently, this portion of SAR was not explored further. However, these analogues exhibited moderate to high solubility (35 – 200 μM) which resulted from the introduced water-solubilizing groups. The observed difference in solubility between the *ortho*-fluorinated analogue **32** (200 μM) and the

meta-fluorinated regioisomer **33** (35 μM) could be attributed to the increase in dihedral angle which accompanies *ortho* substitution of biaryl systems. Such an increase in dihedral angle disrupts π – π stacking which increases solubility.[6] As noted previously, compared to the sulfone-substituted aminated analogues **47** (40 μM) and **46** (60 μM) which were only moderately soluble, sulfoxide-substituted aminated compounds **48** (150 μM) and **49** (165 μM) were highly soluble.

Table 3.2: *In vitro* antiplasmodial activity against *P. falciparum* (NF54 and K1) and solubility of imidazo-substituted analogues

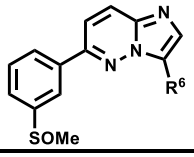

Code	R^6	*P. f* IC_{50}, μM[b,c]		Solubility, μM, pH 6.5[d]
		NF54	K1	
32	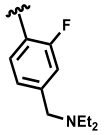	3.2	[e]ND	200
33	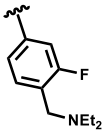	1.1	[e]ND	35
34	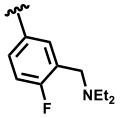	0.99	0.56	200
35	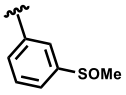	0.15	0.087	200
46	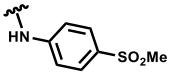	3.6	[e]ND	60
47	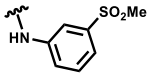	7.6	[e]ND	40
48	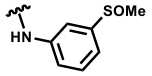	4.7	[e]ND	150
49	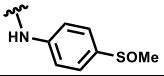	3.8	[e]ND	165

[b]Mean from n values of ≥ 2 independent experiments with multidrug resistant (K1) and sensitive (NF54) strains of *P. falciparum*. The majority of the individual values differed less than 2-fold (maximum 2-fold).
[c]Artesunate [IC_{50} = 2.2 ng/mL (NF54), 0.93 ng/mL (K1)] and chloroquine [IC_{50} = 4.3 ng/mL (NF54), 83 ng/mL (K1)] were used as reference drugs.
[d]Determined using a miniaturized shake flask method.[2]
[e]ND, not determined.

3.2.1.3 SAR and Solubility of Discreetly-Modified Analogues

Different drug discovery programmes have successfully detuned hERG activity by making subtle changes to drug molecules,[7] a strategy which was also exploited in this thesis work as

shown in analogues **26**, **50** – **54** (Table 3.3), **25**, **27** (Table 3.1) and **35** (Table 3.2). Under this category of molecules, sulfones were swapped with sulfoxide groups in addition to the peripheral positional changes of these two groups on the two phenyl rings. Such changes were also inspired by the need to preserve antiplasmodial potency since more drastic modifications made in other portions of SAR drastically compromised potency. Also included in this series, for comparison purposes, was compound **31** (Table 3.3) a sulfone version of analogue **29** (Table 3.1). Interestingly, a highly potent compound **50** (IC_{50} = 0.031 μM) which is a positional isomer of the previously reported[3] lead compound **19** was identified suggesting a *para*-to-*meta* positional change of the right-hand side sulfone is tolerated although solubility (< 5 μM) remained unresolved. However, this positional change is accompanied by a 9-fold decrease in potency compared to the lead compound **19** (IC_{50} = 0.0034 μM). As shown in analogues **51** (IC_{50} = 0.40 μM) and **52** (IC_{50} = 0.26 μM), *para* substitution on the left-hand side phenyl ring, regardless of the nature of the substituent, while keeping a sulfone at the *meta* position on the right-hand side phenyl ring was detrimental to potency. Similarly, antiplasmodial potency was also compromised when the sulfoxide was fixed at the *meta* position on the right-hand side phenyl ring while a sulfone or sulfoxide group was installed at the *para* position of the left-hand side phenyl ring (see analogues **53**, IC_{50} = 1.7 μM and **54**, IC_{50} = 0.87 μM). It is also noteworthy that the sulfone-substituted analogue **53** was 2-fold less potent compared to the sulfoxide version **54**. When compared to its previously reported[4] regioisomer, compound **26** was 7-fold less potent, which further confirms how unfavourable *para* substitution on the left-hand side phenyl ring is. Furthermore, all analogues bearing at least one sulfone group had sub-optimal solubility (< 5 – 10 μM) except **31** whose impressive solubility (200 μM) could be ascribed to its water-solubilizing basic side chain. On the other hand, and as anticipated, analogue **54** possessing sulfoxide groups on both phenyl rings was highly soluble (200 μM).

Table 3.3: *In vitro* antiplasmodial activity against *P. falciparum* (NF54 and K1) and solubility for discreetly-modified analogues

Code	Structure	*P. f* IC_{50}, μM[b,c]		Solubility, μM, pH 6.5[d]
		NF54	K1	
26	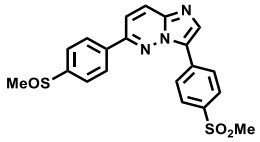	0.28	0.21	10
31	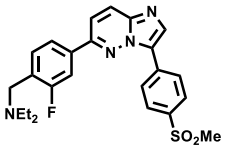	0.82	[e]ND	200

Table 3.3: *In vitro* antiplasmodial activity against *P. falciparum* (NF54 and K1) and solubility for discreetly-modified analogues

Code	Structure	*P. f* IC_{50}, µM[b,c]		Solubility, µM, pH 6.5[d]
		NF54	K1	
19	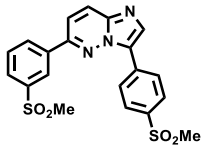	0.0034	0.0023	10
50	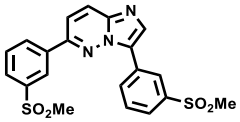	0.031	0.025	< 5
51	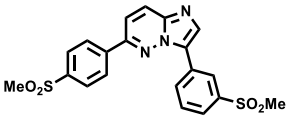	0.40	0.31	< 5
52	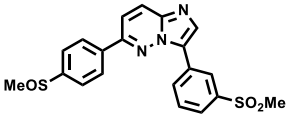	0.26	0.19	< 5
53	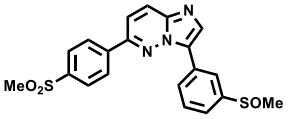	1.7	[e]ND	< 5
54	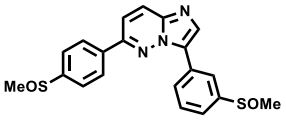	0.87	0.87	200
56	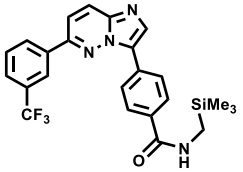	0.95	1.4	< 5
55	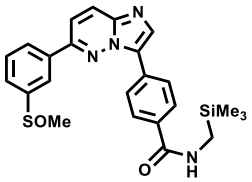	0.16	0.38	< 5
57	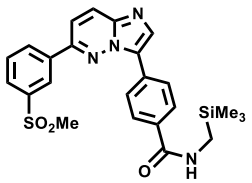	0.14	0.11	< 5

[b]Mean from n values of ≥ 2 independent experiments with multidrug resistant (K1) and sensitive (NF54) strains of *P. falciparum*. The majority of the individual values differed less than 2-fold (maximum 2-fold).
[c]Artesunate [IC_{50} = 2.2 ng/mL (NF54), 0.93 ng/mL (K1)] and chloroquine [IC_{50} = 4.3 ng/mL (NF54), 83 ng/mL (K1)] were used as reference drugs.
[d]Determined using a miniaturized shake flask method.[2]
[e]ND, not determined.

Finally, three other silicon-containing compounds (**55 – 57**, Table 3.3) were also designed and synthesized purely on the principle of introducing novelty. Two of these silylamide derivatives were found to possess marked potency – **55** (IC_{50} = 0.16 µM) and **57** (IC_{50} = 0.14 µM). The

two analogues were equipotent, suggesting that variation between the sulfone (**57**) and sulfoxide (**55**) at the *meta* position of the left-hand side phenyl ring does not affect potency. Replacement with a trifluoromethyl group at the same position, however, resulted in a marked decrease in potency (**56**, IC_{50} = 0.95 μM). Furthermore, the three analogues exhibited poor solubility (< 5 μM), presumably due to the introduced lipophilic trimethylsilyl group.

3.2.2 *In Vitro* Gametocytocidal and Liver Stage Activity

As outlined in subsection 1.7.1.1 of chapter 1, to achieve the goals of the malaria eradication agenda, new TPPs for new antimalarial medicines have been spelled out by the malaria community. Amongst these is the need to deliver antimalarial drugs which target multiple stages of parasite development.[8,9] In line with this requirement, the transmission blocking potential of a selected number of analogues was assessed by evaluating their *in vitro* gametocytocidal activity employing both early and late stage gametocyte assays. Two transgenic luciferase reporter cell lines of the NF54 strain of *P. falciparum*, NF54-PfS16-GFP-Luc and NF54-Mal8p1.16-GFP-Luc were used to assess the early and late stage gametocytocidal activity respectively. Briefly, this assay involved the exposure of parasites to test compounds for 48 hours. Luciferase activity was then determined by adding luciferin substrate to the parasite lysate and measuring the resulting bioluminescence.[10] Furthermore, an ATP assay was used to independently evaluate late stage gametocytocidal activity.[10] For this assay, the parasites were exposed to test samples for 24 hours after which ATP was added to measure its uptake. The full details of the methodology for both the luciferase and ATP assays are given in the experimental chapter of this thesis.

Initially, 13 selected compounds (**19**, **26**, **35**, **38 - 41**, **45**, **50**, **51**, **54**, **56** and **57** (see structures in tables 3.1 – 3.3) were screened for their percentage inhibition against both the early stage (> 90% stage II/III) and late stage (> 90% stage IV/V) gametocytes at two concentrations (1 and 5 μM) (Figure 3.1A). Compounds which displayed good activity (> 70% inhibition at 5 μM and > 50% inhibition at 1 μM) in this primary dual point screen were prioritized for full dose-response IC_{50} determination (n = 3 independent experiments). On the other hand, those with moderate activity (> 70% inhibition at 5 μM and < 50% inhibition at 1 μM; < 70% inhibition at 5 μM and > 50% inhibition at 1 μM; 50 - 70% inhibition at 5 μM and < 50% inhibition at 1 μM) underwent a single IC_{50} determination (n = 1 experiment). An exception was compound **26** whose ATP-based full dose-response IC_{50} was determined despite not meeting this selection criteria.

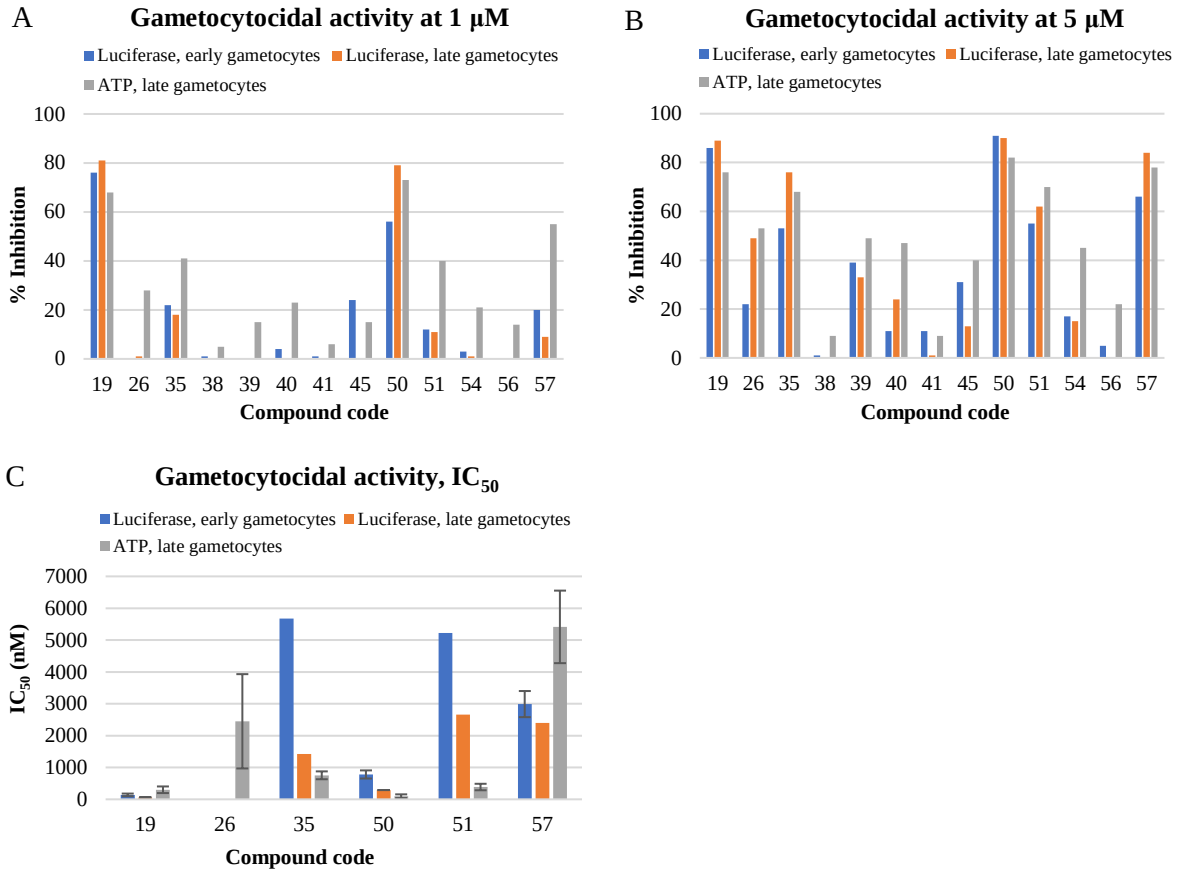

Figure 3.1: Gametocytocidal activity of selected compounds:
(A) % Inhibition of gametocytes at 1 µM; (B) % Inhibition of gametocytes at 5 µM; (C) Gametocytocidal activity measured as IC_{50} values (values with error bars represent measurements from three independent biological replicates while those without error bars represent a single experiment); Methylene blue [IC_{50} = 200 nM (luciferase, early gametocytes), 140 nM (luciferase, late gametocytes), 900 nM (ATP, late gametocytes)] and dihydroartemisinin [IC_{50} = 43 nM (luciferase, early gametocytes), 11 nM (luciferase, late gametocytes), 15.0 µM (ATP, late gametocytes)] were used as reference drugs.

The lead compound **19** (68 – 81% and 76 – 89% inhibition at 1 and 5 µM respectively) and its regioisomer **50** (56 – 79% and 82 – 91% inhibition at 1 and 5 µM respectively) exhibited good activity in the primary dual point screen assays across both the luciferase and ATP assays (Figures 3.1A and B). Also notable is compound **57** which exhibited good activity (55% inhibition at 1 µM) albeit only on the ATP platform. When evaluated under dose-response mode (Figure 3.1C), compounds **19** (IC_{50} = 0.062 – 0.30 µM) and **50** (IC_{50} = 0.098 – 0.78 µM) exhibited submicromolar potency across the two assay platforms. It is also worth noting that, when compared based on the luciferase platform, compounds **19**, **35**, **50** and **51** exhibited stage-

specific activity for the late stage gametocytes as shown by the ≥ 2-fold difference between early and late stage gametocytocidal IC_{50} values.

Parasitic development in the liver precedes the blood stage parasite life cycle.[11] Blocking the establishment of the asymptomatic liver stage infection has potential to offer prophylaxis against both the liver stage and symptomatic blood stage infection. New antimalarials need to have such liver stage activity which is another important TPP expected to accelerate malaria eradication.[8,9] In this regard, seven compounds (**19**, **26**, **39**, **41**, **50**, **54** and **56**) were evaluated against the liver stage sporozoites of *P. berghei* parasites using the Huh7 human liver cell line. The tested compounds were chosen in such a way as to represent each SAR explored. In each SAR, only compounds exhibiting submicromolar (IC_{50} < 1 μM) *in vitro* asexual blood stage antiplasmodial potency and selectivity indices (SI) > 100 over the Chinese Hamster Ovarian (CHO) mammalian cell line (see SI values in table 3.4) were tested. The choice of compounds for this assay was also influenced by availability of material at the time. Luminescence intensity in Huh7 cells infected with a firefly luciferase-expressing *P. berghei* parasite strain, *Pb*GFP-Luc_{con}, was used as a measure of inhibition of liver stage infection.[12] Briefly, this assay involved the treatment of the Huh7 cells with appropriate concentrations of each compound followed by infection with sporozoites freshly harvested from the salivary glands of infected female *Anopheles stephensi* mosquitoes. Luminescence measurement using a luciferase assay system kit was used to determine parasite load 48 hours post-infection. This was achieved by lysing the Huh7 cells followed by addition of luciferase substrate to the resulting lysate to detect luciferase activity. The full details of this procedure are given in the experimental chapter of this thesis.

In a similar approach to that employed for gametocytocidal activity, compounds were subjected to a primary luciferase four-point assay at concentrations of 0.01, 0.1, 1.0 and 10 μM. Compounds for full IC_{50} determination were selected based on activity in this primary screen and the absence of toxicity on the hepatocytes. Consequently, compounds **19**, **50** and **54** which met these criteria were progressed for full IC_{50} determination. The lead compound **19** was highly potent displaying single digit nanomolar activity (IC_{50} = 0.0020 μM). Its new regioisomer, compound **50**, was also highly potent with double digit nanomolar range potency (IC_{50} = 0.045 μM). On the other hand, an IC_{50} value for **54** could not be determined because this compound did not display dose-dependent activity.

3.2.3 *In Vitro* Mammalian Cytotoxicity and hERG Inhibition

In vitro cytotoxicity against the mammalian CHO cell line was determined for compounds exhibiting submicromolar (IC_{50} < 1 μM) *in vitro* asexual blood stage antiplasmodial potency. The corresponding cytotoxic IC_{50} value was divided by the antiplasmodial (*P. f* NF54) IC_{50} value to get selectivity index values. The MTT [3-(4,5-dimethylthiazol-2-yl)-2,5-diphenyltetrazolium bromide] assay[13] which measures cellular growth and survival calorimetrically was used to assess the cytotoxicity of the compounds. Tetrazolium salt formation was used to measure growth and chemosensitivity with emetine being used as a reference drug. Triplicate serial dilutions of 6 concentrations were used to generate dose-response curves, which enabled the determination of IC_{50} values. A detailed description of the method has been given in the experimental chapter.

Similarly, analogues with submicromolar *in vitro* asexual blood stage antiplasmodial activity were generally progressed to hERG inhibition studies. On the other hand, only representative compounds were tested for hERG inhibition for compounds representing discreet peripheral changes (e.g., **25** - **27**, **35**, **50** – **52** and **54**) despite possessing submicromolar antiplasmodial activity. The hERG inhibition assay was performed by Metrion Biosciences Ltd of the United Kingdom (UK) using the CHO cell line stably expressing the hERG channel on a QPatch gigaseal automated patch clamp platform. Samples were screened in triplicate in dose-response mode at four concentrations to enable IC_{50} determination. For compounds which could not exhibit > 40% hERG inhibition at the highest tested concentration (10 μM), extrapolated IC_{50} values are reported. Thus, all IC_{50} values above 10 μM are extrapolated and are not to be considered accurate but approximate indicators of hERG activity. Verapamil was used as a reference positive control. Details of the procedure including cell preparation, recording solutions and voltage pulses used to elicit currents are given in the experimental chapter of this thesis.

Encouragingly, most analogues demonstrated a clean cytotoxicity profile with selectivity indices in the range 72 - > 874 (Table 3.4). However, the basic side chain-containing analogues (**30**, **31**, **34** and **45**) possessed marked cytotoxicity with lower selectivity (SI = 10 – 30).

Table 3.4 also summarizes the hERG evaluation results for selected analogues. Compound **19** exhibited hERG potency (IC_{50} = 3.6 μM) which is in conformity with previous findings.[3] Compounds **50** (IC_{50} = 2.4 μM) and **51** (IC_{50} = 4.0 μM) which are regioisomers of **19** also still retained hERG potency. However, hERG activity was detuned by almost 4-fold when sulfones

in compound **50** were replaced with sulfoxides as shown in compound **35** (IC_{50} = 8.5 μM). Moreover, hERG activity was further significantly lowered following a *meta*-to-*para* positional change of the left-hand side sulfoxide in **35** (see **54**, IC_{50} = 21 μM). As shown in analogue **26** (IC_{50} = 18 μM), hERG activity was reduced by 5-fold compared to the lead compound **19** upon *para* sulfoxide substitution on the left hand-side phenyl ring. Strikingly, compounds **30** (IC_{50} = 0.59 μM), **31** (IC_{50} = 5.2 μM) and **45** (IC_{50} = 7.8 μM) possessing basic side chains were relatively potent on the hERG channel. Indeed, a basic nitrogen is a known pharmacophore for hERG binding since it can potentially get protonated at physiological pH consequently promoting cation – π interactions between the protonated nitrogen and the π electron cloud of suitably positioned aromatic amino acid residues in the channel.[7] The observed hERG activity for these basic analogues is, therefore, unsurprising. For the aniline-substituted compounds **36** – **39**, hERG activity seems enhanced with *meta* sulfonylation (see **36**, IC_{50} = 2.4 μM). Interestingly, as demonstrated in analogue **37** (IC_{50} = 18 μM), replacing a sulfone in **36** with a sulfoxide detunes hERG activity by 8-fold. A further decrease in hERG potency was noted in compound **38** (IC_{50} = 32 μM) a *para*-substituted regioisomer of **37**. Additionally, an 11-fold reduction in hERG activity was observed following a *meta*-to-*para* positional change (**36** to **39**). Furthermore, analogues **41** and **43**, with saturated rings replacing aromatic groups, were designed with the hypothesis that such a saturation strategy would minimize hERG binding by discouraging π – π interactions between phenyl rings in molecules and those embedded in the cavity of the hERG channel.[7] Consistent with this reasoning, significantly weaker hERG inhibition was observed for the two compounds (**41**, IC_{50} = 29 μM and **43**, IC_{50} = 26 μM).

Table 3.4: *In vitro* mammalian cytotoxicity and hERG inhibition profiling for selected analogues

Code	Structure	Cytotoxicity[f] CHO cells		hERG IC_{50}, μM (SD)[g]
		IC_{50}, μM (SD)	SI[h]	
19	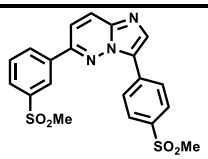	> 234	> 69,000	3.6 (0.62)
50	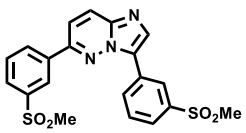	12 (0.89)	377	2.4 (0.46)

Table 3.4: *In vitro* mammalian cytotoxicity and hERG inhibition profiling for selected analogues

Code	Structure	Cytotoxicity[f] CHO cells		hERG IC_{50}, µM (SD)[g]
		IC_{50}, µM (SD)	SI[h]	
35	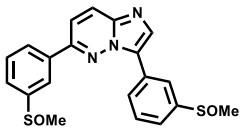	31 (0.2)	206	8.5 (0.8)
51	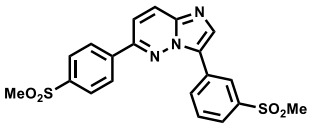	180 (5.2)	457	4 (0.83)
52	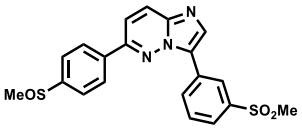	19 (1.5)	72	[e]ND
54	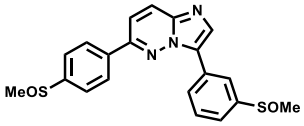	110 (21)	122	21 (2.8)
25	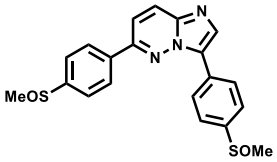	> 253	> 376	[e]ND
27	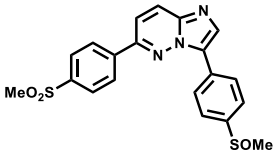	> 243	> 249	[e]ND
26	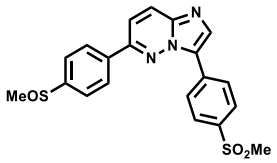	> 243	> 874	18 (5.6)
30	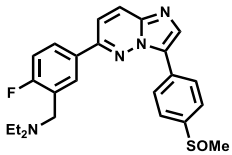	4.1 (0.96)	30	0.59 (0.02)
45	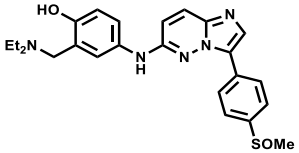	9.4 (3.0)	10	7.8 (1.2)
36	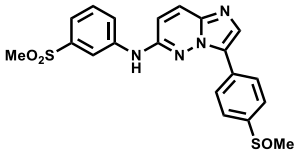	120 (0.4)	449	2.4 (0.21)
37	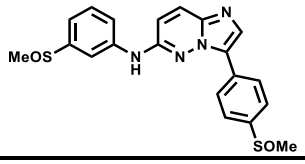	[e]ND	[e]ND	18 (8.5)

Table 3.4: *In vitro* mammalian cytotoxicity and hERG inhibition profiling for selected analogues

Code	Structure	Cytotoxicity[f] CHO cells		hERG IC_{50}, µM (SD)[g]
		IC_{50}, µM (SD)	SI[h]	
38	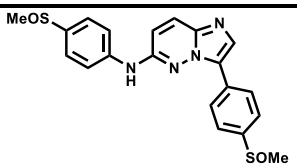	> 244	> 442	32 (1.5)
39	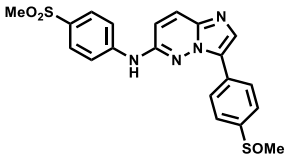	> 234	> 553	26 (6.3)
40	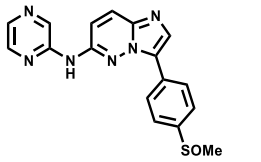	280 (18)	592	7.8 (0.76)
43	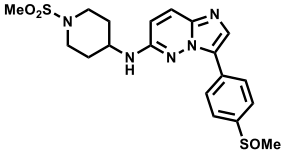	> 231	> 464	26 (1.8)
41	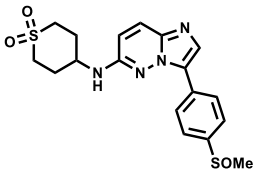	> 247	> 471	29 (3.6)
31	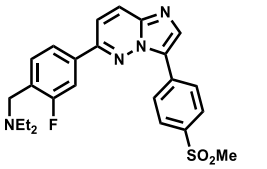	9.4 (2.1)	11	5.2 (0.44)
34	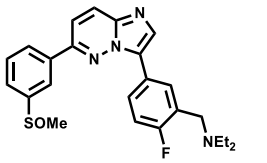	12 (2.7)	12	[e]ND

[e]ND, not determined.
[f]Mean from n = 3 independent experiments; SD, standard deviation; Emetine was used as a reference drug (IC_{50} = 0.033 ± 0.006 µM).
[g]Mean from n = 3 independent experiments; Verapamil was used as a positive control (IC_{50} = 0.56 ± 0.096 µM).
[h]SI = selectivity index = IC_{50} (CHO)/IC_{50} (*P. f* NF54).

3.2.4 Metabolic Stability of Selected Analogues

The design of molecules that will, not only exert the desired therapeutic effect, but also exhibit sustained action is one of the primary concerns of medicinal chemists. Metabolic stability, a subset of ADME (absorption, distribution, metabolism and excretion) studies, can influence pharmacokinetic parameters such as bioavailability and half-life which in turn influence the drug's duration of action.[14] Although various tissues such as the intestinal wall, lung, kidneys,

skin and blood are potential sites for the metabolism of drugs and xenobiotics, the liver is considered the main site of drug metabolism.[15] Therefore, a fast and cost-effective way to determine the metabolic stability of drug candidates is to expose them to hepatocytes or liver microsomes. In this regard, selected compounds (**35**, **38** and **41**) exhibiting submicromolar *in vitro* asexual blood stage antiplasmodial potency (IC_{50} < 1 μM), reasonable solubility (> 50 μM) and selectivity over hERG (IC_{50} > 8 μM) and the CHO cell line (SI > 100) were evaluated for metabolic stability in human (H), rat (R) and mouse (M) liver microsomal preparations (Table 3.5).[16] As an exception, compound **41** was nominated for metabolic testing to represent analogues with saturated heterocyclic ring systems despite possessing suboptimal solubility (10 μM). Compounds not tested despite meeting these criteria were not available at the time of testing. Compounds were incubated in the presence of human, rat and mouse liver microsomes and the percentage (%) of compound remaining after 30 minutes was determined.

Compound **35** was metabolically unstable in liver microsomes of all the three species with a high hepatic extraction ratio (E_H) of about 0.7. This rapid *in vitro* metabolism is most likely mainly an oxidation of the sulfoxide groups to sulfones. In an earlier report, Le Manach *et al*.,[4] observed a rapid *in vivo* biotransformation of sulfoxide-substituted imidazopyridazine analogues into corresponding sulfones. Consistent with these initial findings, compound **35** was designed to act as a solubility-enhancing prodrug of the very potent sulfone (**50**, Table 3.4). This rapid metabolism was, therefore, anticipated. On the other hand, the aniline derivative **38** retained excellent metabolic stability (97.6 – 100% remaining) across the three species with a projected half-life ($t_{1/2}$) of > 150 min and E_H values of < 0.42. Additionally, compound **41** was highly stable in human (100% remaining) and mouse (94.7% remaining) liver microsomes while exhibiting slightly less metabolic stability in rat microsomes (89.5% remaining). Overall, metabolic stability was consistent across the three species for compounds **38** and **41** while **35** was more metabolically stable in human liver microsomes than in the rat and mouse ones potentially suggesting a species difference in its metabolism.

Table 3.5: Human, rat and mouse liver microsomal metabolic stability of analogues **35**, **38** and **41**

Code	Structure	Metabolic stability (% remaining after 30 min)	Projected $t_{1/2}$ (min)	Hepatic extraction ratio (E_H)
		$H^i/R^j/M^k$	$H^i/R^j/M^k$	$H^i/R^j/M^k$
35	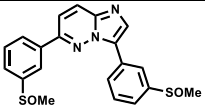	54/37/37.1	33.7/22.3/21	0.74/0.72/0.73

Table 3.5: Human, rat and mouse liver microsomal metabolic stability of analogues **35**, **38** and **41**

Code	Structure	Metabolic stability (% remaining after 30 min)	Projected $t_{1/2}$ (min)	Hepatic extraction ratio (E_H)
		$H^i/R^j/M^k$	$H^i/R^j/M^k$	$H^i/R^j/M^k$
38	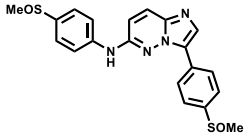	99.9/100/97.6	>150/>150/>150	<0.42/<0.30/<0.33
41	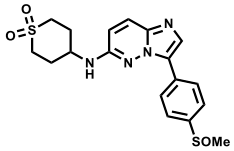	100/89.5/94.7	>150/120.1/>150	<0.42/0.32/<0.33

^{i}H, human; ^{j}R, rat; ^{k}M, mouse.

3.3 Aminopyrazines: *In Vitro* Asexual Blood Stage Antiplasmodial Activity and Solubility

The aminopyrazine compounds were tested for *in vitro* asexual blood stage antiplasmodial activity against both the NF54 and K1 strains of *P. falciparum* using the same assay as the one used for the imidazopyridazines (see brief description in subsection 3.2.1). The SAR for this class of analogues is also discussed with respect to IC_{50} values on the NF54 strain.

Unlike imidazopyridazines whose solubility was determined using a miniaturized shake flask method[2] employing an HPLC-DAD to measure absorbance, the solubility of aminopyrazine analogues was determined using a turbidimetric (kinetic) solubility assay.[17] This involved preparing solutions of test compounds in a solvent in which they are freely soluble, in this case DMSO. Aliquots of these solutions were then added to a buffered (pH = 7.4) aqueous media to give nominal serial dilutions. The concentration value above which the test compound causes turbidity by precipitating from solution is taken to be its approximate solubility. A UV-Visible spectrometer was used to detect turbidity by measuring the absorbance of the suspension at a wavelength the test compound is not expected to absorb electromagnetic radiation (620 nm in this case). This method is simple, cost-effective, fast, requires small amounts of sample and is suitable for high throughput screening of a large number of compounds although it has limited accuracy compared to the alternative HPLC-based method. The antiplasmodial and solubility results are summarized in table 3.6.

Compared to the previously reported lead compound **24** (IC_{50} = 0.0081 μM), all the new analogues generally exhibited drastically reduced potency (IC_{50} = 1.2 - > 10 μM). An exception was **62** which still retained submicromolar potency (IC_{50} = 0.51 μM). Additionally, there are still interesting structure activity relationships worth discussing. The benzoic acid derivative

(**69**) was inactive (IC_{50} = 3.8 μM), suggesting the trifluoromethylpyridyl group is critical to potency. Reduction of the alkene double bond in **59** (IC_{50} = 1.2 μM) results in nearly 7-fold reduction in potency (see **60**, IC_{50} = 8.4 μM). Strikingly, the *N*-mesylated analogue **62** was over 20-fold more potent (IC_{50} = 0.51 μM) than its free amine version **61** (IC_{50} > 10 μM). On the other hand, in analogues were the trifluoromethylpyridyl group was replaced, double bond reduction (**63** to **64**) results in over 2-fold increase in antiplasmodial activity while *N*-boc-deprotection (**64** to **65**) was detrimental to potency.

Table 3.6: *In vitro* antiplasmodial activity against *P. falciparum* (NF54 and K1) and solubility for aminopyrazine analogues

Code	Structure	*P. f* IC_{50}, μM[b,c]		Solubility, μM, pH 7.4[l]
		NF54	K1	
24	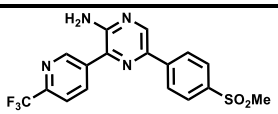	0.0081	0.006	10
69	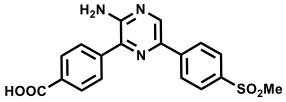	3.8	3.7	> 200
59	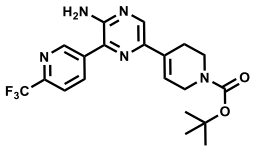	1.2	0.85	80
60	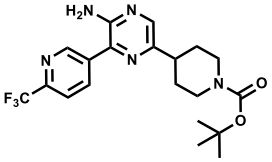	8.4	7.4	40
61	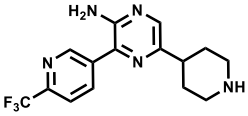	> 10	8.7	160
62	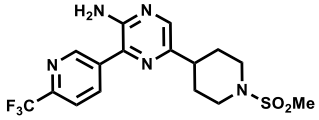	0.51	0.47	160
63	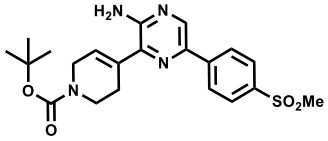	9.8	8.4	80
64	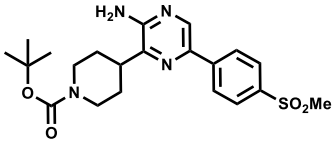	4.5	4.0	160
65	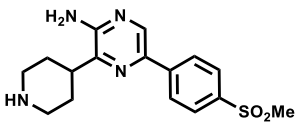	> 10	> 10	> 200

Table 3.6: *In vitro* antiplasmodial activity against *P. falciparum* (NF54 and K1) and solubility for aminopyrazine analogues

Code	Structure	*P. f* IC_{50}, μM[b,c]		Solubility, μM, pH 7.4[l]
		NF54	K1	
66	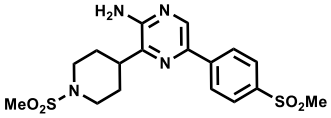	> 6.0	[e]ND	40
70	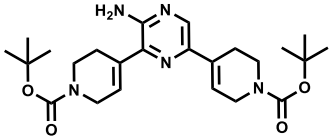	3.1	1.6	160
71	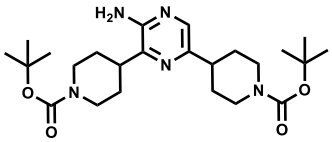	5.5	2.0	80
72	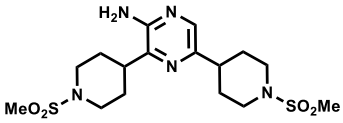	> 6.0	[e]ND	> 200
67	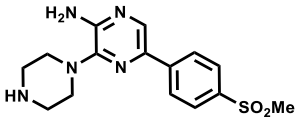	> 6.0	[e]ND	> 200
68	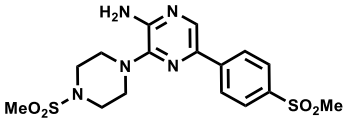	> 6.0	[e]ND	160

[b]Mean from n values of ≥ 2 independent experiments with multidrug resistant (K1) and sensitive (NF54) strains of *P. falciparum*. The majority of the individual values differed less than 2-fold (maximum 2-fold).
[c]Artesunate [IC_{50} = 2.2 ng/mL (NF54), 0.93 ng/mL (K1)] and chloroquine [IC_{50} = 4.3 ng/mL (NF54), 83 ng/mL (K1)] were used as reference drugs.
[e]ND, not determined.
[l]Determined using kinetic (turbidimetric) solubility assay.[17]

Although the modifications made compromised antiplasmodial activity, such changes substantially improved solubility compared to the lead **24** (10 μM). As anticipated, the benzoic acid derivative **69** was highly soluble (> 200 μM) most likely due to its water-solubilizing carboxylic acid group. As initially hypothesized, the replacement of the aromatic rings with partially and fully saturated heterocyclic rings substantially improved solubility (40 - > 200 μM). Expectedly, the free amines **61** (160 μM) and **65** (> 200 μM) were more soluble than their corresponding boc-protected intermediates **60** (40 μM) and **64** (160 μM) respectively. Furthermore, mesylated analogues were generally more soluble than the boc-protected forms (cf. **60** vs **62** and **71** vs **72**).

3.4 Retrospective Target-based Rationalization of *In Vitro* Antiplasmodial Results

3.4.1 Aminopyrazines

Employing genomic and chemoproteomic approaches, the *Pf*PI4K has been identified as the antiplasmodial target of the aminopyridine clinical candidate **MMV390048** (Figure 1.10, chapter 1).[18,19] More recently, PI4K has also been confirmed as a target of the structurally analogous second generation aminopyrazine preclinical candidate **UCT943** (Figure 1.10, chapter 1) with improved solubility and antiplasmodial potency.[20] Therefore, in an attempt to explain the drastic reduction in antiplasmodial activity observed for new aminopyrazine analogues described in this thesis, their binding to a homology model of *Pf*PI4K built against a crystal structure of a human PI4KIIIβ (PDB ID: 4D0L) as a template, was retrospectively assessed.[21] This homology model has been used to model interactions of *Pf*PI4K inhibitors in the absence of a crystal structure.[22]

Briefly, the compound SMILES (Simplified Molecular Input Line Entry Specification) were imported into Maestro 11.6 of the Schrodinger 2018-2 (Schrodinger LLC, New York) suite of molecular modelling software. Protonation states and tautomers around the sulfoxide moieties were generated using the Schrodinger LigPrep protocol. Compounds were then docked against a *Pf*PI4K homology model prepared by Dr Joe Eyermann of the University of Cape Town Drug Discovery and Development Centre, H3D.[22] The docking grid was generated centred on the ATP binding site using the default grid size with no van der Waal scaling. Hydrogen bonding constraints to the backbone amide and carbonyl of Val 1357 (V1357) were added to the grid. The compounds were then docked against this grid using the XP precision with both hydrogen bonding constraints for the aminopyrazines and just the V1357 amide donor constraint for the imidazopyridazines. Docked poses were all visually inspected before a minimization and MM-GBSA calculation of the binding energy using Prime. All residues within an 8 Å radius from the ligand were minimized using the VSGB implicit solvent model and the OPLSe forcefield followed before approximating the binding energy using the MM-GBSA protocol.

Docking studies showed that the lead compound **24** (Table 3.6) sits deep in the ATP binding pocket occupying the catalytic site, hinge region and the ribose binding pocket (Figure 3.2A). Two putative hydrogen bond interactions were noted – one between the pyrazinyl nitrogen at position 1 and the back-bone NH of the hinge residue V1357 and another between the 2-amino group and the carbonyl group of the same hinge residue. This is consistent with previous parasite-based SAR findings which have shown the 2-amino group and the nitrogen at position 1 essential for activity.[23] The two oxygens of the sulfone group, which extend into the catalytic

site, are also known to interact with the catalytic residue Lys 1308 (K1308) by making a hydrogen bond contact. However, the exact pose of the residue K1308 may be a bit inaccurate due to rigid docking. Fluorine atoms are known to be part-time hydrogen bond acceptors.[24,25] In this regard, it is also shown that the fluorine atoms of the trifluoromethyl group, which extend into the ribose pocket, can interact with the residues K1369 and Ser 1365 (S1365) by accepting hydrogen bonds from these two residues. Indeed, these residues and the trifluoromethyl group are within hydrogen bonding distance of 3.0 Å. This is also in agreement with prior parasite-based SAR findings, which have demonstrated the importance of the trifluoromethyl group to activity.[26] The phenyl ring of the phenyl alanine residue Phe 827 (F827) could also potentially interact with the pyridyl and phenyl rings of compound **24** through $\pi - \pi$ stacking. A two-dimensional model illustrating these possible interactions is shown in figure 3.2B.

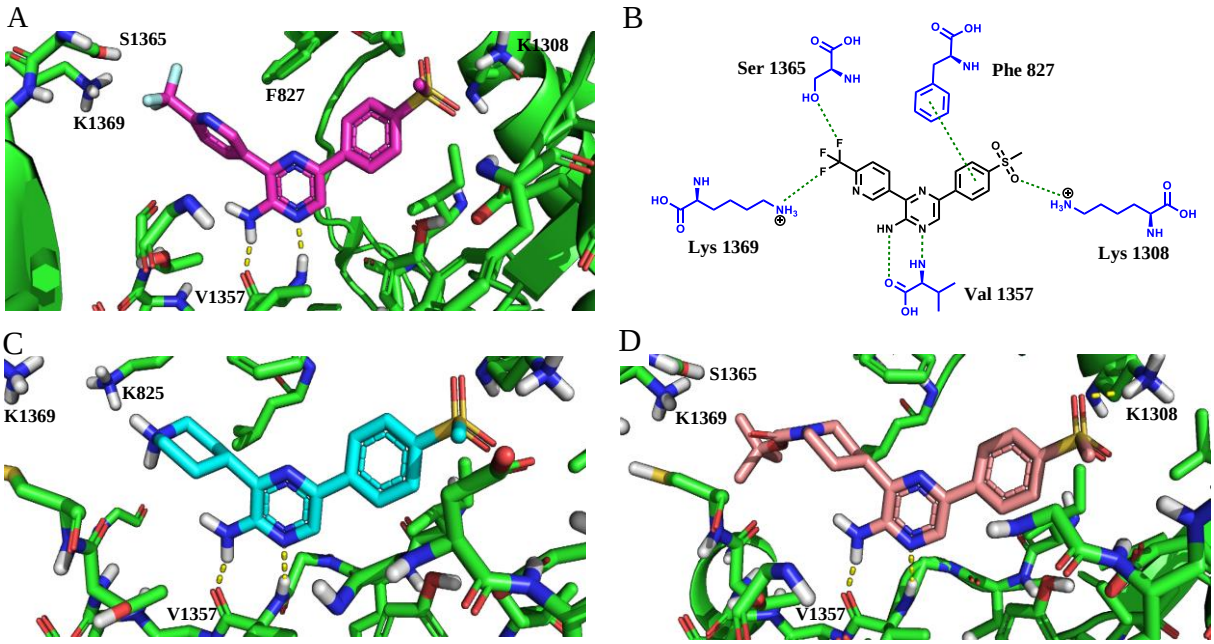

Figure 3.2: Homology model of *Pf*PI4K with **24** (A) [(B) a two-dimensional model illustrating possible interactions of **24**] and representative new analogues **65** (C) and **64** (D) in the ATP binding pocket.

The substitution of some of these molecular features could explain the drastic fall in potency observed in the new analogues. For analogues **65** and **67** (Table 3.6), with a basic secondary amino group on the left-hand side of the aminopyrazine core, the piperidine and piperazine motifs extend into the ribose binding site (**65**, Figure 3.2C). In this pose, the protonated forms of these two analogues are unlikely to interact favourably with the positively charged proximal lysine residues (K1369 and K825). The removal of the trifluoromethyl group also removes a potential hydrogen bond acceptor.

The presence of the boc-protecting group on the left-hand side of the aminopyrazine core (analogues **63**, **64**, **70** and **71**, Table 3.6) extends this lipophilic group into the solvent wall, which may create an entropic penalty (**64**, Figure 3.2D). The introduced boc-protecting group may also not interact favourably with the polar hydrogen bond donor residues K1369 and S1365. The replacement of the 4-methylsulfonylphenyl group at position 5 with partially or fully saturated boc-protected heterocyclic groups, most likely, has the same effect – disrupting hydrogen bonding interactions with the catalytic lysine residue K1308.

Additionally, compound **61** (Table 3.6), like **65** and **67**, is most likely protonated and will, therefore, not interact favourably with the positively charged lysine residue K1308. Interestingly, when compound **61** (IC_{50} > 10 μM) was mesylated to give analogue **62** (IC_{50} = 0.51 μM, Table 3.6), an over 20-fold increase in parasite potency was observed. The sharp increase in potency could be attributed to potential hydrogen bonding interactions between the sulfone oxygens and the lysine residue K1308 much like those observed in the case of the lead compound **24** (Figure 3.2A and B). It is also possible that the presence of a partially or fully saturated heterocyclic ring system at least on the left-hand side of the core in the new analogues disrupts π – π stacking interactions with the nearby phenyl alanine residue F827. Furthermore, it is important to note that the *in vitro* antiplasmodial activity for the new aminopyrazine analogues could be affected by other factors such as sub-optimal physicochemical profiles which may limit their access to the site of action in the parasite.

3.4.2 Imidazopyridazines

As with the aminopyrazine series, *Pf*PI4K has also been shown to be the target of imidazopyridazines.[27,28] Using a *Pf*PI4K homology model, the imidazopyridazines were also shown to bind to the ATP binding pocket. Docking experiments were also performed on the imidazopyridazine series to generate a structure-based hypothesis to help explain the *in vitro* antiplasmodial SAR.

Docking experiments show the imidazopyridazine series to sit deep in the ATP binding pocket. For the lead compound **19** (Table 3.4), three putative interactions were noted (Figure 3.3A). The sulfone oxygens on the pyridazine-attached phenyl ring form an interaction by accepting a hydrogen bond from an OH of the ribose pocket residue S1362. In the hinge region, the imidazole nitrogen at position 1 accepts a hydrogen bond from an NH proton of a valine residue V1357. This interaction is typical of most kinase inhibitors and was observed for both the aminopyrazine and imidazopyridazine analogues. The sulfone oxygens at the *para* position of

the imidazo-attached phenyl ring facilitate a third hydrogen bonding interaction to the catalytic lysine residue K1308. The possible interactions are also further clarified in a two-dimensional model in figure 3.3B.

When the sulfone on the imidazo-attached phenyl ring is moved to a *meta* position resulting in analogue **50** (Table 3.4), this hydrogen bonding interaction is lost (Figure 3.3C). This result is in agreement with the *in vitro* antiplasmodial SAR which has revealed a 9-fold reduction in potency of **50** (IC_{50} = 0.031 μM) compared to **19** (IC_{50} = 0.0034 μM). However, like **19**, compound **50** still interacts with a hinge residue V1357 via the imidazole nitrogen at position 1. Additionally, this analogue also shows a hydrogen bonding interaction between a sulfone oxygen on the pyridazine-attached phenyl ring and the OH group of the residue S1365 in the ribose pocket. A much weaker interaction between the other sulfone oxygen and an NH hydrogen of the ribose pocket residue S1362 was also observed.

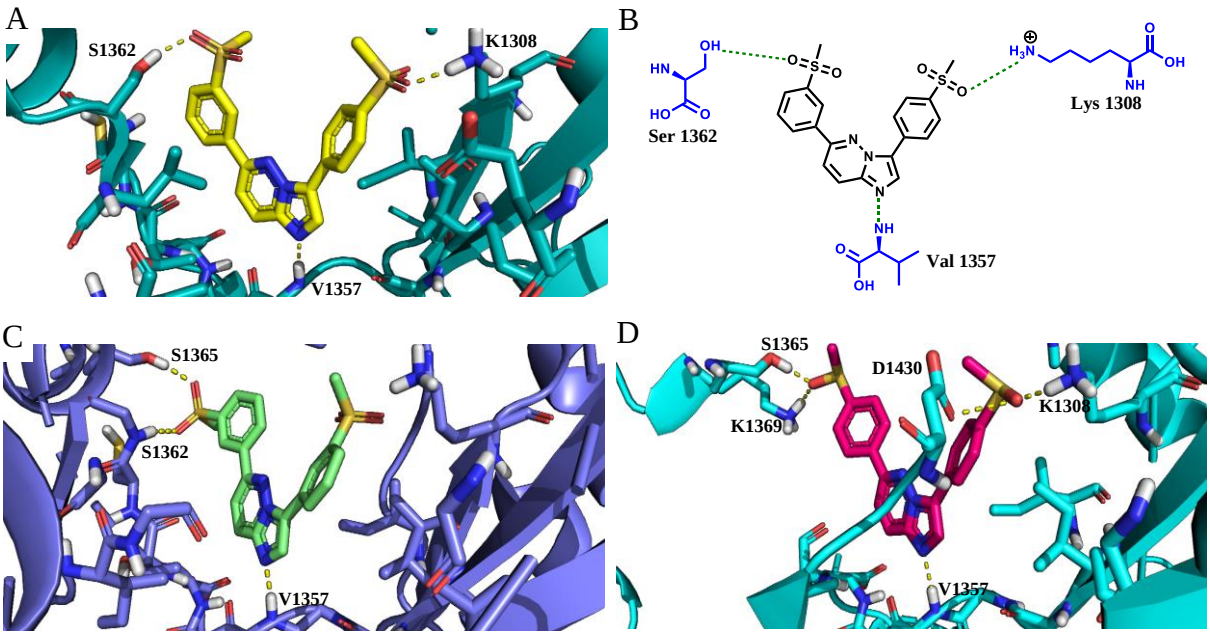

Figure 3.3: Homology model of *Pf*PI4K with **19** (A) [(B) a two-dimensional model illustrating possible interactions of **19**] and representative new analogues **50** (C) and **25** (D) in the ATP binding pocket.

Like the lead compound **19**, analogue **25** (Table 3.4), also *para* substituted on the imidazole-attached phenyl ring has a key hydrogen bonding interaction with a catalytic residue K1308 (Figure 3.3D). *Para* substitution at this phenyl ring, therefore, appears important for binding to the catalytic site (cf. **50**). In addition to hinge region binding, two additional hydrogen bonding interactions between the two sulfoxide groups and the residues K1369 and D1430 (Asp 1430) in the ribose and catalytic pockets respectively were also observed.

Also, quiet striking was the result obtained from the docking experiments of compound **47** (Table 3.2, figure not shown). The binding of this analogue was disrupted, and Glide was unable to find a plausible pose for this analogue. Of all the analogues synthesised in the imidazopyridazine series, this compound had the poorest *in vitro* antiplasmodial potency (IC_{50} = 7.6 μM). Consistent with this observation, compound **47** could not sit in the binding site in a pose the imidazopyridazine analogues are known to assume (see figures 3.3A – D). Compound **47** is, therefore, a poor binder consistent with the *in vitro* antiplasmodial data.

3.5 Conclusion

In conclusion, the antiplasmodial SAR of imidazopyridazine and aminopyrazine analogues was expanded. Various imidazopyridazine analogues with good antiplasmodial activity against the asexual (IC_{50} = 0.031 – 0.99 μM) and sexual (IC_{50} = 0.062 – 0.78 μM) blood stages as well as liver stage (IC_{50} = 0.045 μM) parasites were identified. Moreover, analogues with improved solubility (60 - 200 μM), good selectivity over the mammalian CHO cell line (SI = 72 - > 874) and a substantially improved hERG inhibition profile (IC_{50} = 7.8 – 32 μM) were also identified. Additionally, two out of the three imidazopyridazine compounds evaluated for metabolic stability in this series were stable across human, rat and mouse liver microsomes (% remaining after 30 minutes = 89.5 – 100). For the aminopyrazines, although the chemical modifications made drastically compromised antiplasmodial potency, a drastic improvement in solubility (40 - > 200 μM) was observed. One analogue in this series still retained submicromolar antiplasmodial activity (IC_{50} = 0.51 μM). Furthermore, some aspects of the SAR findings for both series were rationalized using a homology model of *Pf*PI4K. In the next chapter, factors that affect solubility of both the imidazopyridazine and aminopyrazine series are explored.

3.6 References

(1) Desjardins, R. E.; Canfield, C. J.; Haynes, J. D.; Chulay, J. D. Quantitative Assessment of Antimalarial Activity in Vitro by a Semiautomated Microdilution Technique. *Antimicrob. Agents Chemother.* **1979**, *16*, 710–718.

(2) Hill, A. P.; Young, R. J. Getting Physical in Drug Discovery: A Contemporary Perspective on Solubility and Hydrophobicity. *Drug Discov. Today.* **2010**, *15*, 648–655.

(3) Le Manach, C.; Gonzàlez Cabrera, D.; Douelle, F.; Nchinda, A. T.; Younis, Y.; Taylor, D.; Wiesner, L.; White, K. L.; Ryan, E.; March, C.; Duffy, S.; Avery, V. M.; Waterson, D.; Witty, M. J.; Wittlin, S.; Charman, S. A.; Street, L. J.; Chibale, K. Medicinal Chemistry Optimization of Antiplasmodial Imidazopyridazine Hits from High Throughput Screening of a SoftFocus Kinase Library: Part 1. *J. Med. Chem.* **2014**, *57*, 2789–2798.

(4) Le Manach, C.; Paquet, T.; Gonzàlez Cabrera, D.; Younis, Y.; Taylor, D.; Wiesner, L.; Lawrence, N.; Schwager, S.; Waterson, D.; Witty, M. J.; Wittlin, S.; Street, L. J.; Chibale, K. Medicinal Chemistry Optimization of Antiplasmodial Imidazopyridazine Hits from High Throughput Screening of a SoftFocus Kinase Library: Part 2. *J. Med. Chem.* **2014**, *57*, 8839–8848.

(5) Kingsbury, C. A. Why are the Nitro and Sulfone Groups Poor Hydrogen Bonders? https://digitalcommons.unl.edu/cgi/viewcontent.cgi?referer=https://www.google.co.za/&httpsredir=1&article=1080&context=chemfacpub. Accessed: 2018-07-18. (Archived by WebCite® at http://www.webcitation.org/7107YWmgd).

(6) Ishikawa, M.; Hashimoto, Y. Improvement in Aqueous Solubility in Small Molecule Drug Discovery Programs by Disruption of Molecular Planarity and Symmetry. *J. Med. Chem.* **2011**, *54*, 1539–1554.

(7) Jamieson, C.; Moir, E. M.; Rankovic, Z.; Wishart, G. Medicinal Chemistry of hERG Optimizations: Highlights and Hang-Ups. *J. Med. Chem.* **2006**, *49*, 5029–5046.

(8) Burrows, J. N.; Hooft van Huijsduijnen, R.; Möhrle, J. J.; Oeuvray, C.; Wells, T. N. Designing the next Generation of Medicines for Malaria Control and Eradication. *Malar. J.* **2013**, *12*, 187.

(9) Wells, T. N. C.; van Huijsduijnen, R. H.; Van Voorhis, W. C. Malaria Medicines: A Glass Half Full? *Nat. Rev. Drug Discov.* **2015**, *14*, 424–442.

(10) Reader, J.; Botha, M.; Theron, A.; Lauterbach, S. B.; Rossouw, C.; Engelbrecht, D.; Wepener, M.; Smit, A.; Leroy, D.; Mancama, D.; Coetzer, T. L.; Birkholtz, L.-M. Nowhere to Hide: Interrogating Different Metabolic Parameters of Plasmodium

Falciparum Gametocytes in a Transmission Blocking Drug Discovery Pipeline towards Malaria Elimination. *Malar. J.* **2015**, *14*, 213.

(11) About Malaria: Biology. https://www.cdc.gov/malaria/about/biology/index.html. Accessed: 2018-03-28. (Archived by WebCite® at http://www.webcitation.org/6yFgts13H).

(12) Ploemen, I. H. J.; Prudêncio, M.; Douradinha, B. G.; Ramesar, J.; Fonager, J.; van Gemert, G.-J.; Luty, A. J. F.; Hermsen, C. C.; Sauerwein, R. W.; Baptista, F. G.; Mota, M. M.; Waters, A. P.; Que, I.; Lowik, C. W. G. M.; Khan, S. M.; Janse, C. J.; Franke-Fayard, B. M. D. Visualisation and Quantitative Analysis of the Rodent Malaria Liver Stage by Real Time Imaging. *PLoS ONE.* **2009**, *4*, e7881.

(13) Mosmann, T. Rapid Colorimetric Assay for Cellular Growth and Survival: Application to Proliferation and Cytotoxicity Assays. *J. Immunol. Methods.* **1983**, *65*, 55–63.

(14) Thompson, T. N. Early ADME in Support of Drug Discovery: The Role of Metabolic Stability Studies. *Curr. Drug Metab.* **2000**, *1*, 215–241.

(15) Schonborn, J. L.; Gwinnutt, C. The Role of the Liver in Drug Metabolism: Anaesthesia Tutorial of the Week 179. https://www.aagbi.org/sites/default/files/179-The-role-of-the-liver-in-drug-metabolism.pdf. Accessed: 2018-08-08. (Archived by WebCite® at http://www.webcitation.org/71WEKBHJj).

(16) Obach, R. S. Prediction of Human Clearance of Twenty-Nine Drugs from Hepatic Microsomal Intrinsic Clearance Data: An Examination of in Vitro Half-Life Approach and Nonspecific Binding to Microsomes. *Drug Metab. Dispos.* **1999**, *27*, 1350–1359.

(17) Bevan, C. D.; Lloyd, R. S. A High-Throughput Screening Method for the Determination of Aqueous Drug Solubility Using Laser Nephelometry in Microtiter Plates. *Anal. Chem.* **2000**, *72*, 1781–1787.

(18) Ghidelli-Disse, S.; Lafuente-Monasterio, M.; Waterson, D.; Witty, M.; Younis, Y.; Paquet, T.; Street, L. J.; Chibale, K.; Gamo-Benito, F.; Bantscheff, M.; Drewes, G. Identification of Plasmodium PI4 Kinase as Target of MMV390048 by Chemoproteomics. *Malar. J.* **2014**, *13*, 38.

(19) Paquet, T.; Le Manach, C.; Cabrera, D. G.; Younis, Y.; Henrich, P. P.; Abraham, T. S.; Lee, M. C. S.; Basak, R.; Ghidelli-Disse, S.; Lafuente-Monasterio, M. J.; Bantscheff, M.; Ruecker, A.; Blagborough, A. M.; Zakutansky, S. E.; Zeeman, A.-M.; White, K. L.; Shackleford, D. M.; Mannila, J.; Morizzi, J.; Scheurer, C.; Angulo-Barturen, I.; Martínez, M. S.; Ferrer, S.; Sanz, L. M.; Gamo, F. J.; Reader, J.; Botha, M.; Dechering, K. J.; Sauerwein, R. W.; Tungtaeng, A.; Vanachayangkul, P.; Lim, C. S.; Burrows, J.;

Witty, M. J.; Marsh, K. C.; Bodenreider, C.; Rochford, R.; Solapure, S. M.; Jiménez-Díaz, M. B.; Wittlin, S.; Charman, S. A.; Donini, C.; Campo, B.; Birkholtz, L.-M.; Hanson, K. K.; Drewes, G.; Kocken, C. H. M.; Delves, M. J.; Leroy, D.; Fidock, D. A.; Waterson, D.; Street, L. J.; Chibale, K. Antimalarial Efficacy of MMV390048, an Inhibitor of Plasmodium Phosphatidylinositol 4-Kinase. *Sci. Transl. Med.* **2017**, *9*, eaad9735.

(20) Brunschwig, C.; Lawrence, N.; Taylor, D.; Abay, E.; Njoroge, M.; Basarab, G. S.; Le Manach, C.; Paquet, T.; Cabrera, D. G.; Nchinda, A. T.; de Kock, C.; Wiesner, L.; Denti, P.; Waterson, D.; Blasco, B.; Leroy, D.; Witty, M. J.; Donini, C.; Duffy, J.; Wittlin, S.; White, K. L.; Charman, S. A.; Jiménez-Díaz, M. B.; Angulo-Barturen, I.; Herreros, E.; Gamo, F. J.; Rochford, R.; Mancama, D.; Coetzer, T. L.; van der Watt, M. E.; Reader, J.; Birkholtz, L.-M.; Marsh, K. C.; Solapure, S. M.; Burke, J. E.; McPhail, J. A.; Vanaerschot, M.; Fidock, D. A.; Fish, P. V.; Siegl, P.; Smith, D. A.; Wirjanata, G.; Noviyanti, R.; Price, R. N.; Marfurt, J.; Silue, K. D.; Street, L. J.; Chibale, K. UCT943, a Next-Generation Plasmodium Falciparum PI4K Inhibitor Preclinical Candidate for the Treatment of Malaria. *Antimicrob. Agents Chemother.* **2018**, *62*, e00012-18.

(21) Burke, J. E.; Inglis, A. J.; Perisic, O.; Masson, G. R.; McLaughlin, S. H.; Rutaganira, F.; Shokat, K. M.; Williams, R. L. Structures of PI4KIII Complexes Show Simultaneous Recruitment of Rab11 and Its Effectors. *Science.* **2014**, *344*, 1035–1038.

(22) Kandepedu, N.; Gonzàlez Cabrera, D.; Eedubilli, S.; Taylor, D.; Brunschwig, C.; Gibhard, L.; Njoroge, M.; Lawrence, N.; Paquet, T.; Eyermann, C. J.; Spangenberg, T.; Basarab, G. S.; Street, L. J.; Chibale, K. Identification, Characterization, and Optimization of 2,8-Disubstituted-1,5-Naphthyridines as Novel Plasmodium Falciparum Phosphatidylinositol-4-Kinase Inhibitors with in Vivo Efficacy in a Humanized Mouse Model of Malaria. *J. Med. Chem.* **2018**, *61*, 5692–5703.

(23) Younis, Y.; Douelle, F.; González Cabrera, D.; Le Manach, C.; Nchinda, A. T.; Paquet, T.; Street, L. J.; White, K. L.; Zabiulla, K. M.; Joseph, J. T.; Bashyam, S.; Waterson, D.; Witty, M. J.; Wittlin, S.; Charman, S. A.; Chibale, K. Structure–Activity-Relationship Studies around the 2-Amino Group and Pyridine Core of Antimalarial 3,5-Diarylaminopyridines Lead to a Novel Series of Pyrazine Analogues with Oral in Vivo Activity. *J. Med. Chem.* **2013**, *56*, 8860–8871.

(24) Howard, J. A. K.; Hoy, V. J.; O'Hagan, D.; Smith, G. T. How Good Is Fluorine as a Hydrogen Bond Acceptor? *Tetrahedron.* **1996**, *52*, 12613–12622.

(25) Dalvit, C.; Invernizzi, C.; Vulpetti, A. Fluorine as a Hydrogen-Bond Acceptor:

Experimental Evidence and Computational Calculations. *Chem. - A Eur. J.* **2014**, *20*, 11058–11068.

(26) Younis, Y.; Douelle, F.; Feng, T.-S.; Cabrera, D. G.; Le Manach, C.; Nchinda, A. T.; Duffy, S.; White, K. L.; Shackleford, D. M.; Morizzi, J.; Mannila, J.; Katneni, K.; Bhamidipati, R.; Zabiulla, K. M.; Joseph, J. T.; Bashyam, S.; Waterson, D.; Witty, M. J.; Hardick, D.; Wittlin, S.; Avery, V.; Charman, S. A.; Chibale, K. 3,5-Diaryl-2-Aminopyridines as a Novel Class of Orally Active Antimalarials Demonstrating Single Dose Cure in Mice and Clinical Candidate Potential. *J. Med. Chem.* **2012**, *55*, 3479–3487.

(27) McNamara, C. W.; Lee, M. C. S.; Lim, C. S.; Lim, S. H.; Roland, J.; Nagle, A.; Simon, O.; Yeung, B. K. S.; Chatterjee, A. K.; McCormack, S. L.; Manary, M. J.; Zeeman, A.-M.; Dechering, K. J.; Kumar, T. R. S.; Henrich, P. P.; Gagaring, K.; Ibanez, M.; Kato, N.; Kuhen, K. L.; Fischli, C.; Rottmann, M.; Plouffe, D. M.; Bursulaya, B.; Meister, S.; Rameh, L.; Trappe, J.; Haasen, D.; Timmerman, M.; Sauerwein, R. W.; Suwanarusk, R.; Russell, B.; Renia, L.; Nosten, F.; Tully, D. C.; Kocken, C. H. M.; Glynne, R. J.; Bodenreider, C.; Fidock, D. A.; Diagana, T. T.; Winzeler, E. A. Targeting Plasmodium PI(4)K to Eliminate Malaria. *Nature.* **2013**, *504*, 248–253.

(28) Zou, B.; Nagle, A.; Chatterjee, A. K.; Leong, S. Y.; Tan, L. J.; Sim, W. L. S.; Mishra, P.; Guntapalli, P.; Tully, D. C.; Lakshminarayana, S. B.; Lim, C. S.; Tan, Y. C.; Abas, S. N.; Bodenreider, C.; Kuhen, K. L.; Gagaring, K.; Borboa, R.; Chang, J.; Li, C.; Hollenbeck, T.; Tuntland, T.; Zeeman, A.-M.; Kocken, C. H. M.; McNamara, C.; Kato, N.; Winzeler, E. A.; Yeung, B. K. S.; Diagana, T. T.; Smith, P. W.; Roland, J. Lead Optimization of Imidazopyrazines: A New Class of Antimalarial with Activity on Plasmodium Liver Stages. *ACS Med. Chem. Lett.* **2014**, *5*, 947–950.

CHAPTER 4
PHYSICOCHEMICAL EVALUATION AND STRUCTURE-PROPERTY RELATIONSHIPS

4.1 Chapter Overview

In this chapter, physicochemical evaluation and the investigation of factors influencing solubility of new analogues described in this thesis are reported. The chapter first highlights the importance of physicochemical parameters on drug-likeness followed by physicochemical characterization with brief descriptions of the *in silico* and *in vitro* methods employed. This is then followed by an assessment of the drug-likeness compliance of the compounds with emphasis on Lipinski's Rule of Five (Ro5). The chapter concludes with a section on the investigation of factors influencing solubility for both series of analogues.

4.2 Impact of Physicochemical Properties on Drug-likeness

Pharmacokinetic, pharmacodynamic and drug safety profiles can be influenced by physicochemical and molecular properties. Between the years 2000 and 2010, drug discovery suffered a nosedive with increasingly less drug candidates making it to the clinic despite huge financial investments.[1] Poor oral bioavailability was identified as a potential cause of attrition and it soon became clear that this issue could be circumvented by identifying molecular features in drug molecules that are responsible for poor absorption. In order to assist the medicinal chemist to triage potential drug candidates, different sets of simple rules which define boundaries of fundamental properties considered acceptable for a compound to become a successful drug (drug-likeness) have been devised.[2] Chris Lipinski is arguably the most influential pioneer in this field. By examining structural features of compounds that entered phase II clinical studies, Lipinski and co-workers were able to correlate computed physicochemical properties of these molecules to their aqueous solubility, permeability and oral bioavailability.[3,4] Consequently, Lipinski and co-workers[3,4] were able to put forward some guidelines on properties of molecules that are likely to exhibit poor permeability and absorption. These guidelines, famously known as Lipinski's Ro5, state that a compound is likely to exhibit poor passive permeability or absorption if it has the following features: 1) > 5 hydrogen bond donors (HBD); 2) > 10 hydrogen bond acceptors (HBA); 3) molecular weight (MW) > 500 g/mol and 4) cLog P > 5.

Since Lipinski proposed the Ro5, variants of these guidelines have been put forward. In this regard, Veber *et al*.,[5] correlated molecular flexibility to permeability and established that for good permeability, the number of rotatable bonds in a drug candidate should not exceed 10. Veber *et al*.,[5] also established that the topological polar surface area (TPSA) values above 140 $Å^2$ are detrimental to permeability. Other extensions of the Ro5 relevant to fragment-based drug discovery such as the Rule of Three (Ro3) have been proposed.[6] In this thesis, some of these structural properties were characterized for the synthesized compounds towards assessing their Ro5 compliance. How parameters such as cLog P, TPSA, melting point and HPLC retention time affect the solubility of the compounds was further assessed.

4.3 Physicochemical Characterization

4.3.1 Brief Description of Methods

Some physicochemical parameters (MW, cLog P, TPSA, HBDs and HBAs) were calculated while others (HPLC retention time, melting point and solubility) were experimentally determined. The MW, TPSA, HBD and HBA values were calculated using StarDrop™ 64 while the cLog P values were calculated using ChemDraw Professional 16.0. The full details of methodologies for experimentally determined parameters are given in chapter 6 of this thesis. Calculated parameters such as MW, cLog P and TPSA were plotted on frequency distribution histograms to assess their compliance to Lipinski's Ro5. On the other hand, assessment of Ro5 compliance with respect to number of HBDs and HBAs was done by simple inspection of the values directly from the tables summarising all physicochemical parameters since there was not much variability in these parameters for both series of analogues.

Factors influencing solubility were then investigated by plotting solubility as a function of different physicochemical parameters, which included HPLC retention time, cLog P, TPSA, and melting point. For analogues whose solubility values were uncertain, such as < 5 and > 200 μM, definite values of 0 and 200 μM respectively were used in the plots. Microsoft excel version 2016 was used in plotting both the frequency distributions and correlations.

4.3.2 Results and Discussion

The calculated and experimentally determined physicochemical parameters are summarized in tables 4.1 – 4.4

Table 4.1: Physicochemical properties of pyridazine-substituted imidazopyridazine analogues

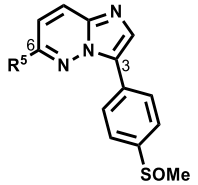

Code	R^5	Calculated physicochemical properties					Experimental physicochemical properties		
		MW,[m] g/mol	cLog P[n]	TPSA,[m] Å^2	HBD[m]	HBA[m]	t_r,[o] min	m.p.,[p] °C	Solubility,[q] µM
25	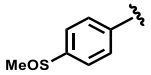	395.50	1.59	64.33	0	5	2.563	181.4	200
27	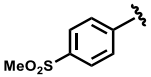	411.49	1.54	81.40	0	6	2.609	261.3	5
28	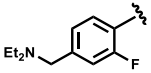	436.55	4.21	50.50	0	5	2.467	110.7	180
29	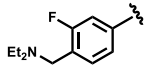	436.55	4.21	50.50	0	5	2.428	163.5	195
30	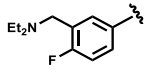	436.55	4.21	50.50	0	5	2.462	122.4	200
44	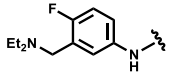	451.56	4.22	62.53	1	6	2.549	119.0	200
45	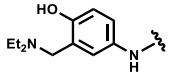	449.57	3.36	82.76	2	7	2.401	[e]ND	195
36	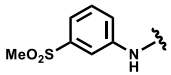	426.51	1.71	93.43	1	7	2.635	[e]ND	20
37	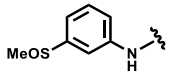	410.51	1.72	76.36	1	6	2.636	[e]ND	190
38	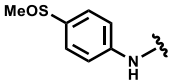	410.51	1.73	76.36	1	6	2.579	[e]ND	195

Table 4.1: Physicochemical properties of pyridazine-substituted imidazopyridazine analogues

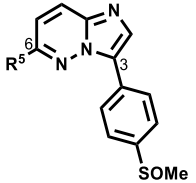

Code	R5	Calculated physicochemical properties					Experimental physicochemical properties		
		MW,[m] g/mol	cLog P[n]	TPSA,[m] Å^2	HBD[m]	HBA[m]	t_r,[o] min	m.p.,[p] °C	Solubility,[q] µM
39	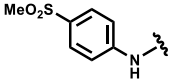	426.51	1.71	93.43	1	7	2.650	298.0	< 5
40	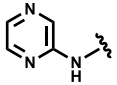	350.40	1.25	85.07	1	7	2.617	[e]ND	25
41	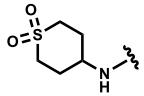	404.50	0.69	93.43	1	7	2.434	273.8	10
42	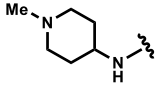	369.49	1.41	62.53	1	6	0.230	[e]ND	200
43	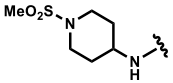	433.55	0.61	96.67	1	8	2.488	[e]ND	70

[e]ND, not determined.
[m]MW, molecular weight; TPSA, topological polar surface area; HBD, hydrogen bond donors; HBA, hydrogen bond acceptors: Calculated using StarDrop™ 64.
[n]cLog P, calculated log P: Calculated using ChemDraw Professional 16.0.
[o]t_r, retention time: Measured using HPLC-MS (method described in chapter 6).
[p]m.p., melting point (values are averages between the upper and lower limit values of the melting range): Measured using a Stuart automatic melting point machine SMP40.
[q]Determined using a miniaturized shake flask method at pH 6.5 (method described in chapter 6).

Table 4.2: Physicochemical properties of imidazo-substituted imidazopyridazine analogues

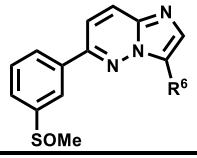

Code	R^6	Calculated physicochemical properties					Experimental physicochemical properties		
		MW,[m] g/mol	cLog P[n]	TPSA,[m] Å^2	HBD[m]	HBA[m]	t_r,[o] min	m.p.,[p] °C	Solubility,[q] µM
32	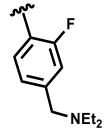	436.55	4.12	50.50	0	5	2.505	162.6	200
33	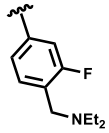	436.55	4.12	50.50	0	5	2.416	[e]ND	35
34	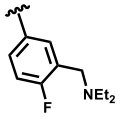	436.55	4.12	50.50	0	5	2.492	[e]ND	200
35	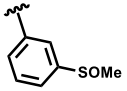	395.50	1.59	64.33	0	5	2.525	[e]ND	200
46	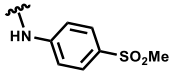	426.51	1.84	93.43	1	7	2.534	106.1	60
47	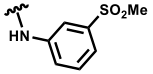	426.51	1.84	93.43	1	7	2.555	151.2	40
48	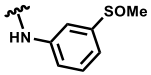	410.51	1.88	76.36	1	6	2.476	111.8	150
49	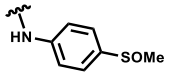	410.51	1.88	76.36	1	6	2.450	162.6	165

[e]ND, not determined.
[m]MW, molecular weight; TPSA, topological polar surface area; HBD, hydrogen bond donors; HBA, hydrogen bond acceptors: Calculated using StarDrop™ 64.
[n]cLog P, calculated log P: Calculated using ChemDraw Professional 16.0.
[o]t_r, retention time: Measured using HPLC-MS (method described in chapter 6).

[p]m.p., melting point (values are averages between the upper and lower limit values of the melting range): Measured using a Stuart automatic melting point machine SMP40.
[q]Determined using a miniaturized shake flask method at pH 6.5 (method described in chapter 6).

Table 4.3: Physicochemical properties of discreetly-modified imidazopyridazine analogues

Code	Structure	Calculated physicochemical properties					Experimental physicochemical properties		
		MW,[m] g/mol	cLog P[n]	TPSA,[m] Å^2	HBD[m]	HBA[m]	t_r,[o] min	m.p.,[p] °C	Solubility,[q] µM
26	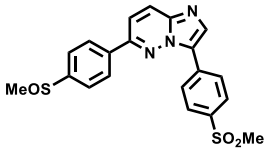	411.49	1.53	81.40	0	6	2.518	237.8	10
31	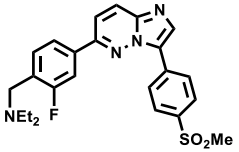	452.55	4.16	67.57	0	6	2.555	183.0	200
19	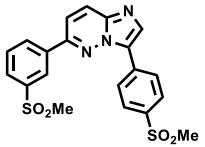	427.49	1.48	98.47	0	7	2.526	245.6	10
50	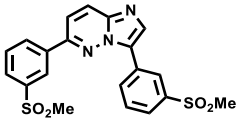	427.49	1.48	98.47	0	7	2.586	229.8	< 5
51	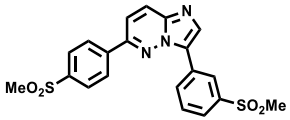	427.49	1.48	98.47	0	7	2.588	265.0	< 5
52	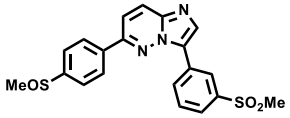	411.49	1.53	81.40	0	6	2.619	219.8	< 5
53	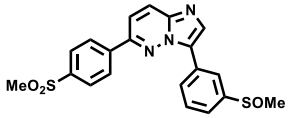	411.49	1.54	81.40	0	6	2.578	219.8	< 5

Table 4.3: Physicochemical properties of discreetly-modified imidazopyridazine analogues

Code	Structure	Calculated physicochemical properties					Experimental physicochemical properties		
		MW,[m] g/mol	cLog P[n]	TPSA,[m] Å^2	HBD[m]	HBA[m]	t_r,[o] min	m.p.,[p] °C	Solubility,[q] µM
54	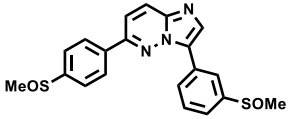	395.50	1.59	64.33	0	5	2.602	175.1	200
56	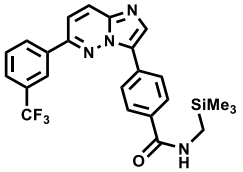	468.56	6.83	59.29	1	5	3.190	174.2	< 5
55	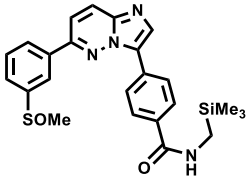	462.64	4.36	76.36	1	6	2.820	131.4	< 5
57	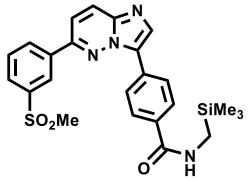	478.64	4.31	93.43	1	7	2.903	210.4	< 5

[m]MW, molecular weight; TPSA, topological polar surface area; HBD, hydrogen bond donors; HBA, hydrogen bond acceptors: Calculated using StarDrop™ 64.
[n]cLog P, calculated log P: Calculated using ChemDraw Professional 16.0.
[o]t_r, retention time: Measured using HPLC-MS (method described in chapter 6).
[p]m.p., melting point (values are averages between the upper and lower limit values of the melting range): Measured using a Stuart automatic melting point machine SMP40.
[q]Determined using a miniaturized shake flask method at pH 6.5 (method described in chapter 6).

Table 4.4: Physicochemical properties of aminopyrazine analogues

Code	Structure	Calculated physicochemical properties					Experimental physicochemical properties		
		MW,[m] g/mol	cLog P[n]	TPSA,[m] Å^2	HBD[m]	HBA[m]	t_r,[o] min	m.p.,[p] °C	Solubility,[r] µM
24	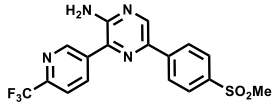	394.37	1.97	98.83	1	6	2.631	213.5	10
69	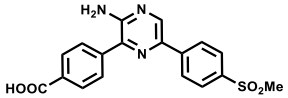	369.40	2.19	123.2	2	7	2.496	272.5	> 200
59	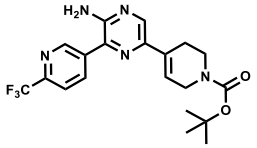	421.42	3.42	94.23	1	7	2.919	194.0	80
60	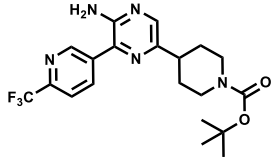	423.44	3.53	94.23	1	7	2.824	152.5	40
61	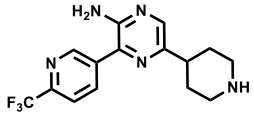	323.32	1.60	76.72	2	5	0.566	128.0	160
62	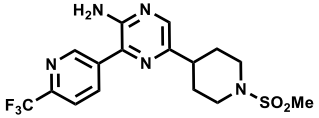	401.41	1.24	102.1	1	7	2.517	194.5	160
63	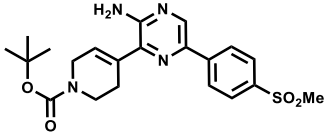	430.52	2.30	115.5	1	8	2.703	176.0	80
64	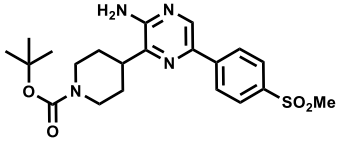	432.54	2.10	115.5	1	8	2.806	181.5	160

Table 4.4: Physicochemical properties of aminopyrazine analogues

Code	Structure	Calculated physicochemical properties					Experimental physicochemical properties		
		MW,[m] g/mol	cLog P[n]	TPSA,[m] Å^2	HBD[m]	HBA[m]	t_r,[o] min	m.p.,[p] °C	Solubility,[r] µM
65	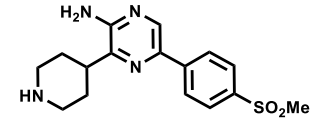	332.42	0.17	97.97	2	6	0.249	126.5	> 200
66	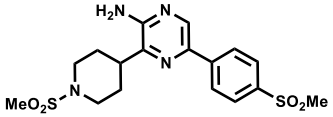	410.51	- 0.19	123.3	1	8	2.434	[e]ND	40
70	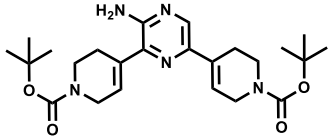	457.58	3.74	110.9	1	9	3.007	91.0	160
71	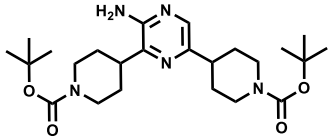	461.61	3.64	110.9	1	9	2.940	70.5	80
72	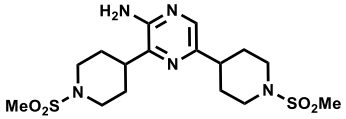	417.54	- 0.93	126.6	1	9	2.417	96.5	> 200
67	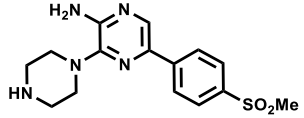	333.41	0.45	101.2	2	7	0.170	159.5	> 200
68	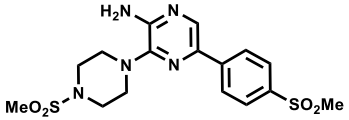	411.50	0.46	126.6	1	9	2.447	240.5	160

[e]ND, not determined.
[m]MW, molecular weight; TPSA, topological polar surface area; HBD, hydrogen bond donors; HBA, hydrogen bond acceptors: Calculated using StarDrop™ 64.
[n]cLog P, calculated log P: Calculated using ChemDraw Professional 16.0.
[o]t_r, retention time: Measured using HPLC-MS (method described in chapter 6).
[p]m.p., melting point (values are averages between the upper and lower limit values of the melting range): Measured using a Reichert-Jung Thermovar hot stage microscope.

[r]Determined using kinetic (turbidimetric) solubility assay at pH 7.4 (method described in chapter 6).

Table 4.5: Comparison of calculated physicochemical properties to drug-like guidelines

Compound class	MW, g/mol	cLog P	TPSA, Å^2	HBD	HBA
Imidazopyridazines	350.40 – 478.64	0.61 – 6.83	50.50 – 98.47	0 - 2	5 - 8
Aminopyrazines	323.32 – 461.61	- 0.93 – 3.74	76.72 – 126.6	1 - 2	5 - 9
Targeted criteria^s	< 500	< 5	< 140	< 5	< 10

^{s}Targeted criteria defined according to Lipinski's Ro5 (MW, cLog P, HBD and HBA)[3,4] and Veber's rule on TPSA.[5]

4.3.2.1 Assessment of Lipinski's Ro5 Compliance for Imidazopyridazines

For imidazopyridazines, four out of the five calculated molecular features were Ro5 compliant. These included MW (350.40 – 478.64 g/mol), TPSA (50.50 – 98.47 Å^2), HBDs (0 – 2) and HBAs (5 – 8) (Table 4.5). Except for one analogue (**56**, cLog P = 6.83, table 4.3), all the others possessed cLog P values below 5 which was in conformity to the Ro5. The frequency distribution for molecular weight (Figure 4.1A) shows most analogues in this class have molecular weights in the range 411 – 440 g/mol. On the other hand, the majority analogues have cLog P in the range 1.1 – 2 (Figure 4.1B) while the TPSA values are distributed over a wider range (Figure 4.1C).

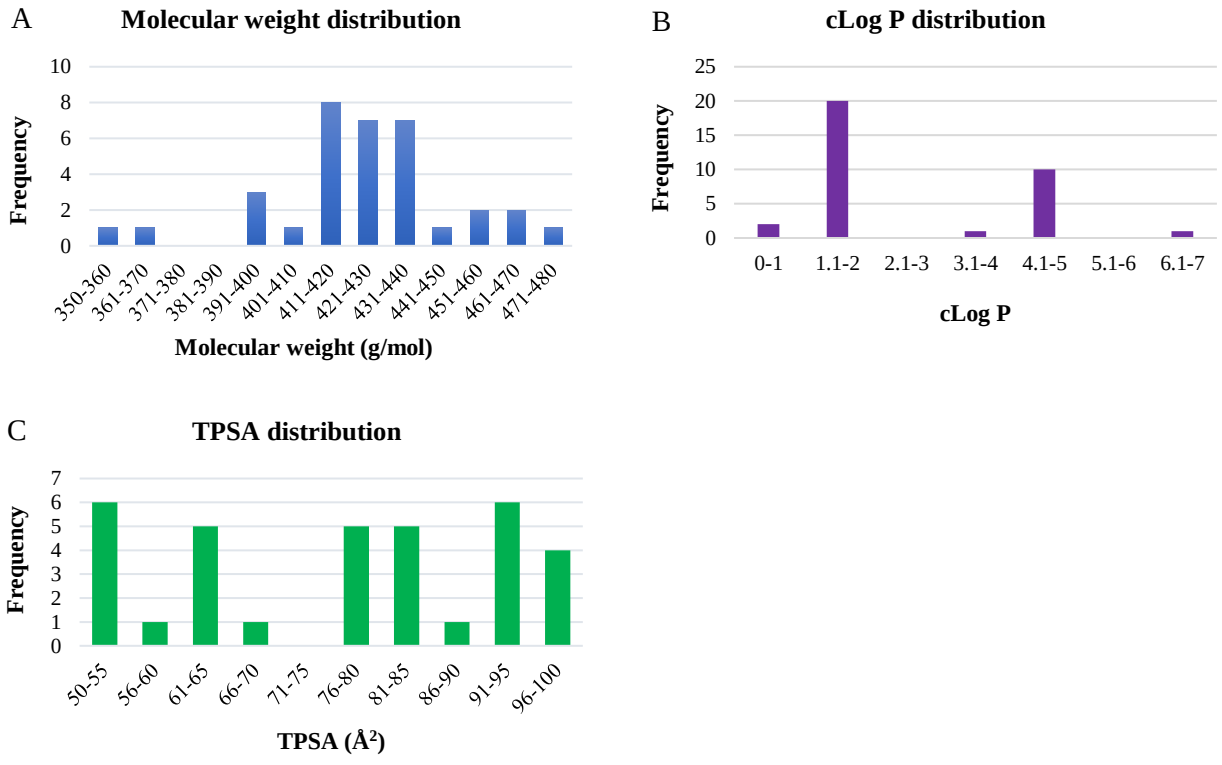

Figure 4.1: Frequency distribution of physicochemical parameters for imidazopyridazine analogues:

(A) Molecular weight; (B) Calculated Log P and (C) Topological polar surface area.

4.3.2.2 Assessment of Lipinski's Ro5 Compliance for Aminopyrazines

All the aminopyrazine analogues were Ro5 compliant across all the five physicochemical parameters: MW = 323.32 – 461.61 g/mol; cLog P = - 0.93 – 3.74; TPSA = 76.72 – 126.6 Å^2; HBDs = 1 – 2 and HBAs = 5 – 9 (Table 4.5). The frequency distribution plot showed majority of analogues have molecular weights in the range 391 – 465 g/mol (Figure 4.2A). Furthermore, except for one analogue with a TPSA value in the range 70 – 80 Å^2, all the other analogues have TPSA values in the range 91 – 130 Å^2 (Figure 4.2B). Unlike the imidazopyridazines, the cLog P values of aminopyrazines varied over a narrow range and, therefore, just like HBD and HBA values, were not plotted on a frequency distribution graph.

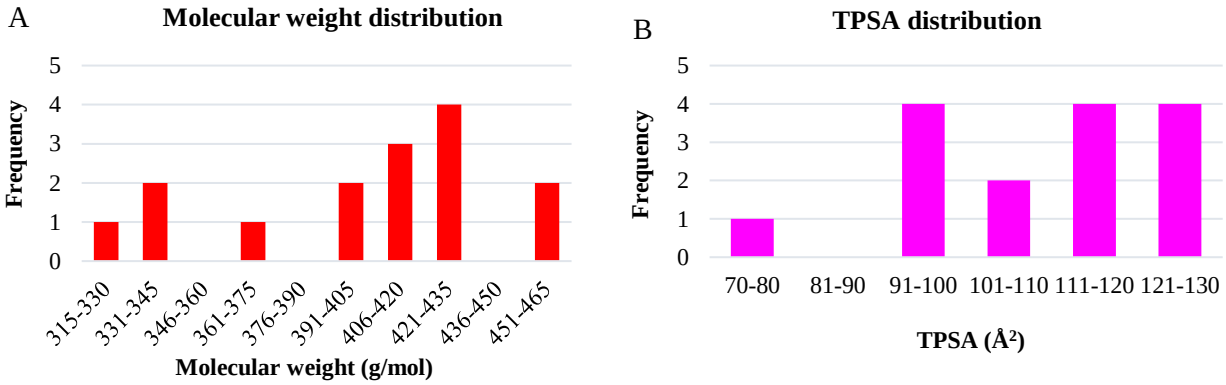

Figure 4.2: Frequency distribution of physicochemical parameters for aminopyrazine analogues: (A) Molecular weight; (B) Topological polar surface area.

4.3.2.3 Investigation of Factors Influencing Solubility of Imidazopyridazines

Figures 4.3 captures the correlation plots between solubility and different factors envisaged to potentially influence solubility. For this class of analogues, melting point seems to influence solubility the most (Figure 4.3A). Although the correlation is weak (R^2 = 0.3905), the observed negative trendline is consistent with the hypothesis and literature precedence.[7,8] In this regard, a high melting point is an indicator of efficient crystal packing and hence high crystal packing energy. This, in turn, discourages the dissolution of a solute in an aqueous medium. However, the weak correlation observed could suggest that there are other factors influencing solubility. Additionally, the strength of the correlation could also be affected by a number of data points whose solubility values were uncertain. For instance, analogues whose solubility values were

reported as < 5 µM were arbitrarily assigned a definite value of 0 µM, an estimation which could have affected the correlation.

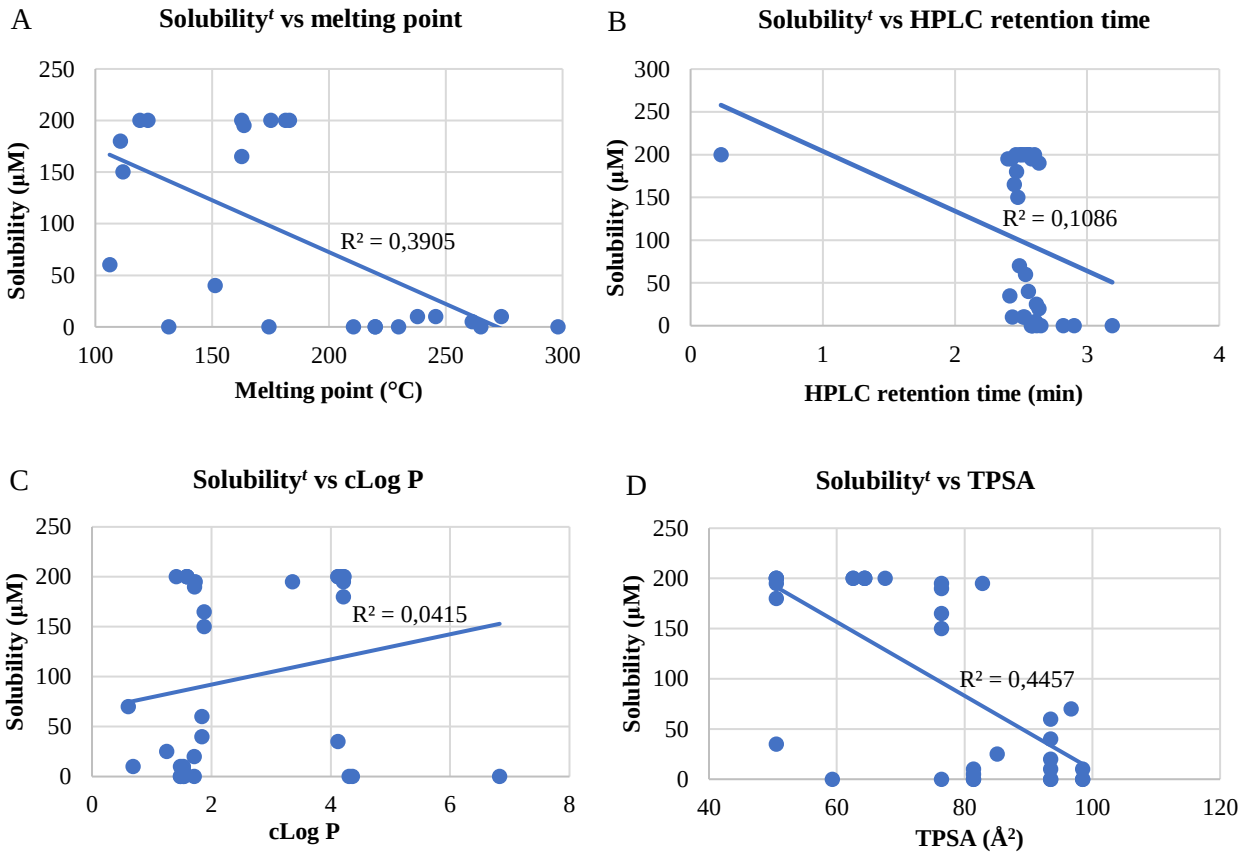

Figure 4.3: Correlations between solubility and different physicochemical parameters for imidazopyridazine analogues:

(A) Solubility versus melting point; (B) Solubility versus HPLC retention time; (C) Solubility versus calculated log P and (D) Solubility versus topological polar surface area.

[t]For the purpose of plotting the correlations, all compounds with uncertain solubility values, i.e., < 5 µM, as shown in tables 4.1 – 4.3, were arbitrarily assigned a definite solubility value of 0 µM.

A negative correlation between solubility and HPLC retention time (Figure 4.3B) was observed. Although this correlation was also weak (R^2 = 0.1086), the decrease in solubility with increase in retention time was anticipated. In this case, the HPLC retention time is used as a surrogate measure of the compound's ability to interact with the aqueous media of the reversed phase HPLC column. Therefore, this is also a more realistic measure of a compound's polarity. In reversed phase HPLC, the mobile phase is more polar than the stationary phase of the column[9] with each gradient run starting with a high percentage of the aqueous media which allows more water-soluble and hence more polar molecules to elute faster than lipophilic ones.

Also noted was limited diversity of retention times for the analysed analogues with most analogues possessing values between 2.4 and 2.9 min. Within this region, some analogues possess high solubility while others are poorly soluble. Additionally, as already mentioned, factors such as uncertain solubility values which needed arbitrary assignment of definite values to be plotted could have affected the strength of the correlation.

An unexpected weak (R^2 = 0.0415) positive correlation was observed between solubility and cLog P (Figure 4.3C). One major factor that significantly influenced this correlation was the data corresponding to a subset of analogues containing sulfoxides, sulfones and basic side chains. As stated earlier in subsection 3.2.1.1 of chapter 3, despite having a higher cLog P and lower hydrogen bonding sites than sulfones, sulfoxides are more water-soluble due to their energetically favourable hydrogen bonding interactions with water molecules.[10] Additionally, save for compound **33**, all the other analogues containing a basic side chain were expectedly highly soluble (see tables 4.1 – 4.3) although the cLog P values were relatively high due to the presence of the lipophilic ethyl groups. Therefore, the highly soluble sulfoxide- and amino-substituted derivatives with high cLog P values significantly skewed the trendline to a positive correlation. Indeed, a more realistic indicator of a molecule's capacity to interact with polar media such as water, the reversed phase HPLC retention time, shows a negative correlation with solubility (Figure 4.3B).

When solubility was plotted as a function of TPSA, an even much stronger (R^2 = 0.4457) unexpected negative correlation was observed (Figure 4.3D). Once again, the highly soluble analogues containing sulfoxides and basic side chains yet possessing lower calculated TPSA compared to sulfones significantly influenced the trendline.

4.3.2.4 Investigation of Factors Influencing Solubility of Aminopyrazines

For the aminopyrazine analogues, captured in table 4.4, retention time was found to be a major factor influencing solubility compared to cLog P, TPSA and melting point. In this regard, the correlation between solubility and retention time (Figure 4.4A) was found to be much stronger (R^2 = 0.2449) than the corresponding solubility-cLog, -TPSA and -melting point correlations (R^2 = 0.0016 – 0.1645, Figures 4.4B – D). However, in absolute terms, the solubility-retention time correlation is weak suggesting there are other factors driving the solubility of this class of analogues. For this series, solubility was determined by a turbidimetric assay as briefly described in subsection 3.3 of the preceding chapter. In this method, serial dilutions of the test

compound such as 0, 5.0, 10.0, 20.0, 40.0, 80.0, 160.0 and 200 µM in buffered aqueous media were incubated for 2 hours at 37 °C to mimic body temperature. The absorbance values of the test concentrations were then recorded using a UV-Visible spectrometer at a wavelength the test compound is not expected to absorb (620 nm in this case). Any absorbance values recorded were thus attributed to the turbidity caused by precipitation of the test compound at a certain concentration above which the compound crushes out from solution. Thus, the solubility values obtained from this method are limited to the aforementioned serial dilution concentrations. This makes it difficult to certainly determine solubility values for compounds which crush out of solution at concentrations other than those used in the assay set-up. Indeed, as can be noted from the correlation plots in figure 4.4, solubility values for all compounds are limited to these definite concentrations used in the assay. Therefore, due to the uncertainty of the solubility values determined from such an assay, the strength of the correlations obtained may have been affected. Moreover, for analogues possessing solubility values > 200 µM, a definite value of 200 µM was arbitrarily assigned for the purpose of plotting the graphs which could have further affected the correlations.

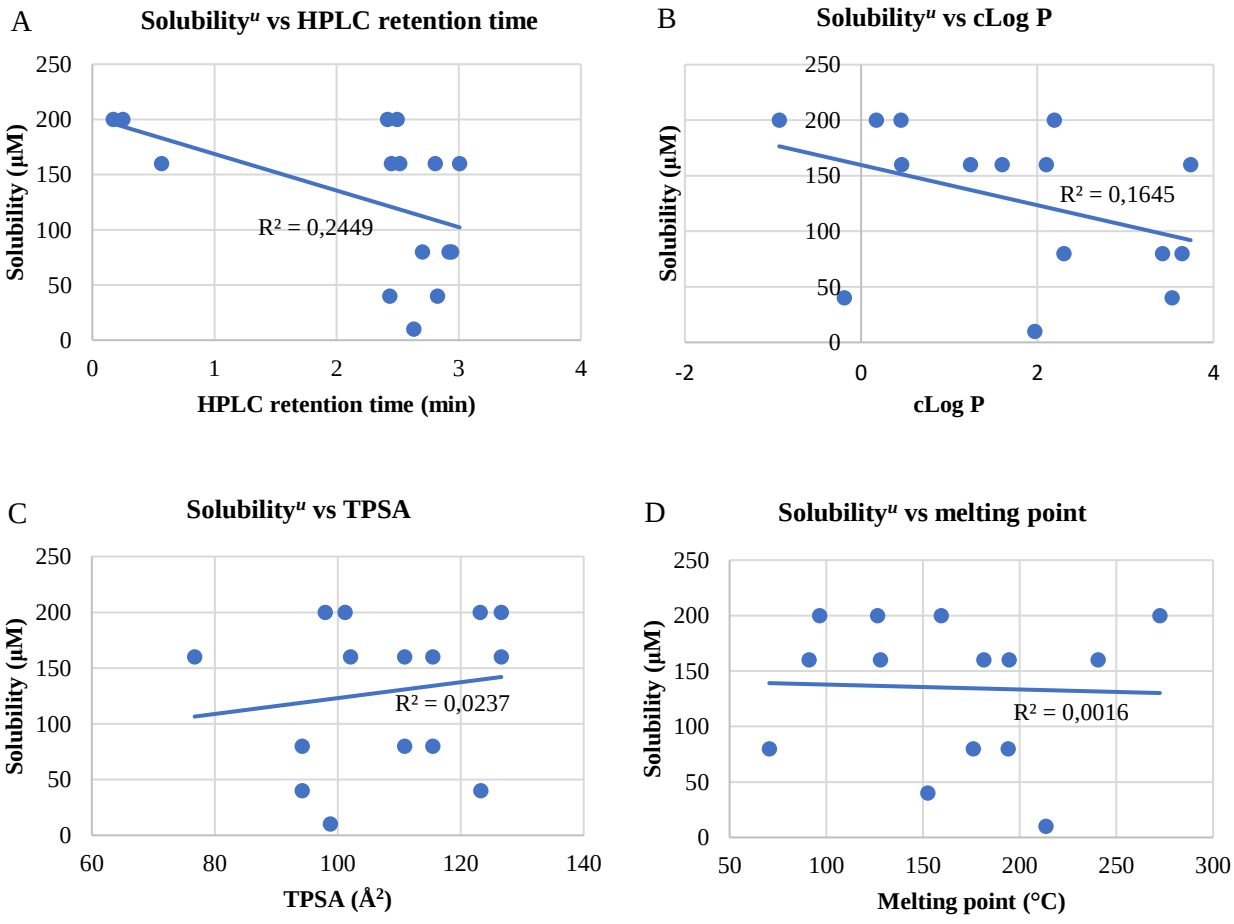

Figure 4.4: Correlations between solubility and different physicochemical parameters for aminopyrazine analogues:
(A) Solubility versus HPLC retention time; (B) Solubility versus calculated log P; (C) Solubility versus topological polar surface area and (D) Solubility versus melting point.
[u]For the purpose of plotting the correlations, all compounds with uncertain solubility values, i.e., > 200 μM, as shown in table 4.4, were taken to possess a definite solubility value of 200 μM.

Unlike the imidazopyridazine derivatives which exhibited a positive solubility – cLog P correlation, the aminopyrazines showed the expected negative correlation between these two parameters (Figure 4.4B). This is consistent with the fact that in this series, there was no combination of sulfoxide-, sulfone- and diethylaminomethyl-substituted analogues which could have influenced the trendline in the same manner as observed in the imidazopyridazine class. Furthermore, although the correlation was very weak (R^2 = 0.0237, Figure 4.4C), the expected positive trendline was obtained between solubility and TPSA for the aminopyrazine compounds while the opposite is true for the imidazopyridazines. On the other hand, there was no observed meaningful correlation (R^2 = 0.0016) between solubility and melting point (Figure 4.4D).

4.4 Conclusions

In conclusion, physicochemical profiling revealed that all imidazopyridazine and aminopyrazine analogues were Ro5 compliant except for compound **33** which has a cLog P > 5. Evaluation of factors influencing solubility for imidazopyridazine analogues showed that melting point influenced solubility to a greater extent than HPLC retention time, cLog P and TPSA. For the aminopyrazine series, the HPLC retention time was found to be the most influential parameter of solubility compared to cLog P, TPSA and melting point.

4.5 References

(1) Pollastri, M. P. Overview on the Rule of Five. *Curr. Protoc. Pharmacol.* **2010**, *49*, 9–12.

(2) Vallianatou, T.; Giaginis, C.; Tsantili-Kakoulidou, A. The Impact of Physicochemical and Molecular Properties in Drug Design: Navigation in the "Drug-Like" Chemical Space. In *GeNeDis 2014*; Vlamos, P., Alexiou, A., Eds.; Springer: Cham, 2015; pp 187–194.

(3) Lipinski, C. A. Drug-like Properties and the Causes of Poor Solubility and Poor Permeability. *J. Pharmacol. Toxicol. Methods.* **2000**, *44*, 235–249.

(4) Lipinski, C. A.; Lombardo, F.; Dominy, B. W.; Feeney, P. J. Experimental and Computational Approaches to Estimate Solubility and Permeability in Drug Discovery and Development Settings. *Adv. Drug Deliv. Rev.* **1997**, *23*, 3–25.

(5) Veber, D. F.; Johnson, S. R.; Cheng, H.-Y.; Smith, B. R.; Ward, K. W.; Kopple, K. D. Molecular Properties That Influence the Oral Bioavailability of Drug Candidates. *J. Med. Chem.* **2002**, *45*, 2615–2623.

(6) Congreve, M.; Carr, R.; Murray, C.; Jhoti, H. A. 'Rule of Three' for Fragment-Based Lead Discovery? *Drug Discov. Today.* **2003**, *8*, 876–877.

(7) Banerjee, S.; Yalkowsky, S. H.; Valvani, C. Water Solubility and Octanol/Water Partition Coefficients of Organics. Limitations of the Solubility-Partition Coefficient Correlation. *Environ. Sci. Technol.* **1980**, *14*, 1227–1229.

(8) Jain, N.; Yalkowsky, S. H. Estimation of the Aqueous Solubility I: Application to Organic Nonelectrolytes. *J. Pharm. Sci.* **2001**, *90*, 234–252.

(9) Aguilar, M. I. Reversed-Phase High-Performance Liquid Chromatography. In *HPLC of Peptides and Proteins. Methods in Molecular Biology*; Aguilar, M. I., Ed.; Springer: Totowa, NJ, 2004; pp 9–22.

(10) Kingsbury, C. A. Why are the Nitro and Sulfone Groups Poor Hydrogen Bonders? https://digitalcommons.unl.edu/cgi/viewcontent.cgi?referer=https://www.google.co.za/&httpsredir=1&article=1080&context=chemfacpub. Accessed: 2018-07-18. (Archived by WebCite® at http://www.webcitation.org/7107YWmgd).

CHAPTER 5

SUMMARY, CONCLUSIONS AND RECOMMENDATIONS FOR FUTURE WORK

5.1 Summary and Conclusions

5.1.1 Imidazopyridazines

The target compounds were synthesized by diverse protocols centred around metal-mediated coupling reactions and were obtained in poor to very good yields (8 – 80%). The compounds were then characterized by TLC, HPLC-MS, ^{1}H-NMR, ^{13}C-NMR and melting point.

Initial SAR studies[1–3] on this class of compounds identified lead compounds such as **19**, among others which, despite exhibiting good *in vitro* antiplasmodial activity (NF54 IC_{50} = 0.0034 μM; K1 IC_{50} = 0.0023 μM) and *in vivo* antimalarial efficacy (98% at 4 × 50 mg/kg, po), was plagued by poor solubility (10 μM at pH 6.5) and a hERG inhibition liability (IC_{50} = 3.6 μM). In an effort to address these liabilities, further expansion of the SAR for this class of analogues is reported. In this regard, the SAR was pursued in such a way as to introduce molecular features to improve solubility and counter hERG inhibition while preserving antiplasmodial potency. The newly synthesized analogues represented drastic as well as more subtle and discreet modifications around the imidazopyridazine core-scaffold.

Although all the newly synthesized analogues were not as potent as the lead **19**, the reported SAR further provides a guide for future SAR studies. Moreover, the introduced modifications resulted in the identification of analogues with drastically improved solubility and reduced hERG inhibition. The SAR and SSR (structure solubility relationship) summary is shown in figure 5.1 with only representative analogues shown for each class of modifications. The *P.f* NF54 IC_{50} values shown in this figure refer to activity at the asexual blood stage of parasite development. Derivatization at the pyridazine-attached phenyl ring (SAR1 and 3) identified analogue **30** with potent antiplasmodial activity (IC_{50} = 0.14 μM) and high solubility (200 μM) but was still beset by a serious hERG inhibition liability (IC_{50} = 0.59 μM). Other analogues containing the basic side chain were also found to be generally highly soluble (180 – 200 μM) but two analogues tested on hERG were found to be relatively potent on this channel. However, hERG activity was successfully detuned to a large extent by introducing saturation at this position as exemplified by compounds **41** (IC_{50} = 29 μM) and **43** (IC_{50} = 26 μM) in figure 5.1. Other subtle changes, which included switching sulfones with sulfoxides as well as positional changes of these groups, also diminished hERG activity (see analogues **36** - **39** in table 3.4, chapter 3). Additionally, the solubilities of sulfoxide-substituted analogues were significantly

higher than those of the corresponding sulfones (cf. **25** vs **27** and **38** vs **39**, figure 5.1). This observation was also true for all the other sulfone and sulfoxide derivatives from other portions of SAR.

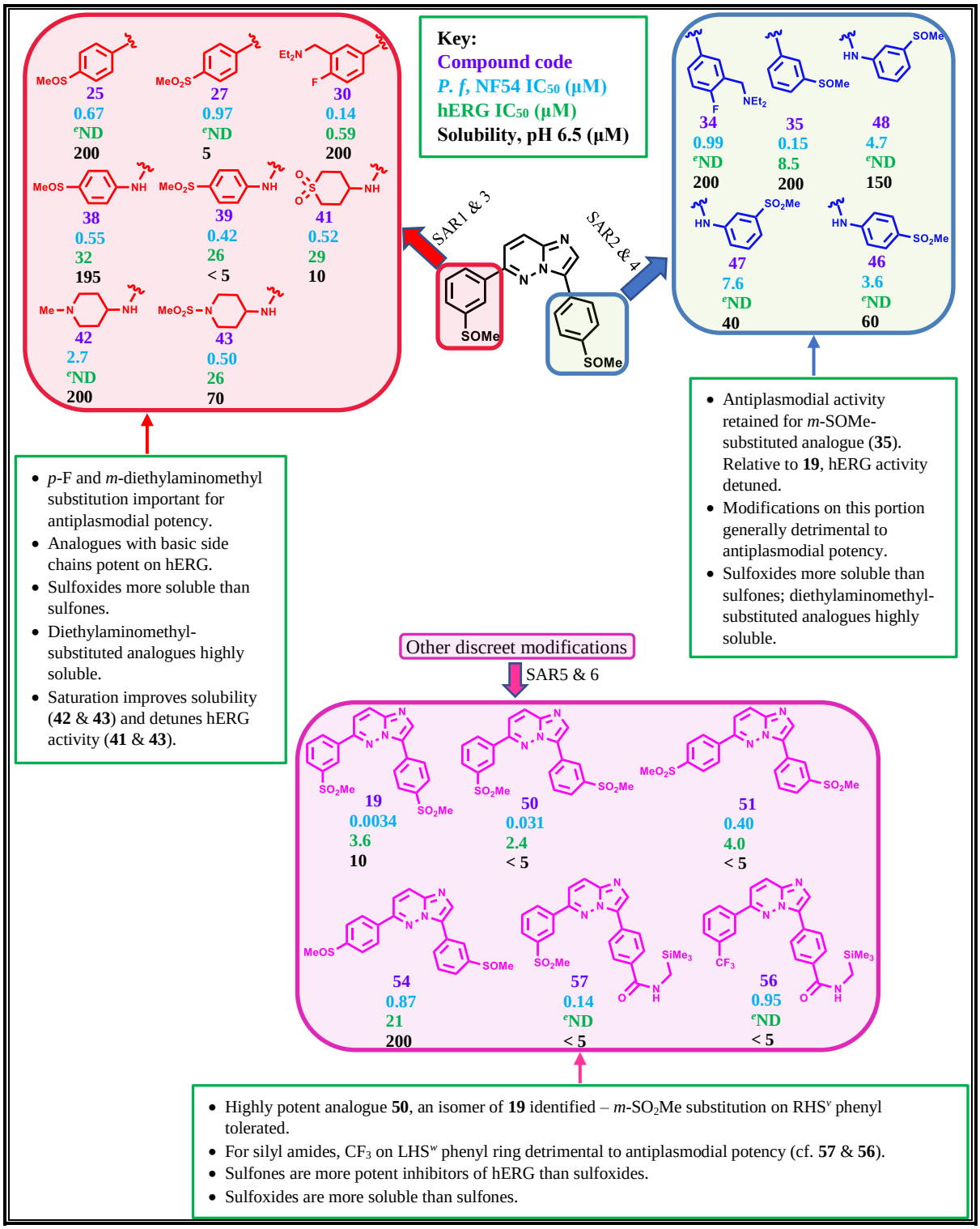

Figure 5.1: SAR and SSR summary of imidazopyridazine analogues.

[e]ND, not determined; [v]RHS, right hand side; [w]LHS, left hand side.

CHAPTER 5: SUMMARY, CONCLUSIONS AND RECOMMENDATIONS FOR FUTURE WORK

Generally, exploration of SAR2 and 4 (Figure 5.1) led to analogues with the lowest antiplasmodial potency (IC_{50} = 0.99 – 7.6 μM). However, compound **35** which still retained strong submicromolar potency (IC_{50} = 0.15 μM) was identified. This compound is also a potential prodrug of a highly potent sulfone analogue **50** (IC_{50} = 0.031 μM) (SAR5 and 6) which has poor solubility (< 5 μM). Compared to **50**, analogue **35** has a nearly 4-fold reduced hERG potency. Nevertheless, hERG inhibition upon the anticipated biotransformation *in vivo* is still a concern. Consistent with this observation, the sulfoxide **54** was also found to have weak hERG activity (IC_{50} = 21 μM) while its sulfone version **51** was more active on hERG (IC_{50} = 4.0 μM). Furthermore, a silicon-containing analogue **57** with relatively potent antiplasmodial activity (IC_{50} = 0.14 μM) was also identified. This analogue and its sulfoxide counterpart **55** (IC_{50} = 0.16 μM, table 3.3, chapter 3) had equipotent antiplasmodial activity while a trifluoromethylated version **56** was nearly 7-fold less potent highlighting the importance of a polar electron withdrawing substituent on the phenyl ring. However, all silyl amides retained poor solubility (< 5 μM).

Selected analogues with good to excellent gametocytocidal (IC_{50} = 0.031 – 0.99 μM) and liver stage (IC_{50} = 0.045 μM) activities on plasmodium parasites were identified (see subsection 3.2.2 of chapter 3). These data suggest the analogues have potential for transmission blocking and chemoprotection, a very important TPP for the malaria eradication agenda. Furthermore, docking studies on a *Pf*PI4K homology model correlated well with parasite-based SAR.

Additionally, most analogues evaluated for cytotoxicity had a wide safety margin with selectivity indices over the CHO mammalian cell line in the range 72 - > 874 (Table 3.4, chapter 3). However, all analogues possessing a basic side chain were relatively more cytotoxic (SI = 10 – 30).

Two out of the three analogues evaluated for metabolic stability were stable across liver microsomal preparations from three species – human, rat and mouse (Table 3.5, chapter 3). The poor metabolic stability for the sulfoxide analogue **35** was anticipated – this compound, in the presence of microsomes, could be undergoing rapid oxidation to the corresponding sulfone derivative **50**. Nevertheless, metabolite identification studies are needed to confirm this hypothesis.

Physicochemical profiling showed the new imidazopyridazine analogues were Ro5 compliant with only one violating this guideline with respect to cLog P (Table 4.5, chapter 4).

Additionally, melting point was found to be the most influential factor of solubility for this class of analogues (Figure 4.3A).

5.1.2 Aminopyrazines

The aminopyrazine analogues were realized in low to very good yields (21 – 86%) via metal-mediated coupling, reduction, deprotection, nucleophilic aromatic substitution and mesylation reactions. The target compounds were characterized by the same techniques as those used for the imidazopyridazines.

In an effort to identify aminopyrazine analogues with better physicochemical properties, further SAR explorations not covered in previous reports[4,5] have been presented and discussed. The obtained data suggest that the introduction of partial or full saturation at positions 3 and 5 of the aminopyrazine core-scaffold is highly detrimental to antiplasmodial potency – most analogues were poorly active (IC_{50} = 1.2 - > 10 μM) compared to the lead **24** (IC_{50} = 0.0081 μM) (Table 3.6, chapter 3). An exception in this series was compound **62** (possessing an *N*-methylsulfonylpiperidinyl group) which retained submicromolar potency (IC_{50} = 0.51 μM). The methylsulfonyl group in this molecule was critical to antiplasmodial potency – the removal of this group, as shown in analogue **61** (IC_{50} > 10 μM), eliminates potency. Furthermore, using a homology model of *Pf*PI4K, parasite-based SAR were rationalized. Such docking studies showed the introduced molecular features disrupted key binding interactions of the lead molecule **24**. The most active analogue **62** was shown to resemble the lead **24** regarding the interactions experienced by the methylsulfonyl group in the binding site.

Although antiplasmodial potency was drastically affected by the introduced chemical modifications, the solubility of all analogues was improved by a 4 - > 20-fold margin compared to the lead compound **24** (Table 3.6, chapter 3). These data confirmed the hypothesis that introducing partial or full saturation should disrupt planarity and discourage π – π stacking, consequently resulting in improved solubility. Installation of a water-solubilizing carboxylic acid in compound **69** also drastically improved solubility. All the analogues in this class were Ro5 compliant (Table 4.5, chapter 4), and the solubility values showed the strongest correlation with HPLC retention time (Figure 4.4, chapter 4).

To conclude, this PhD thesis has reported the synthesis, biological evaluation and physicochemical profiling of new imidazopyridazine and aminopyrazine analogues. The efforts to detune off-target activities and improve physicochemical properties for these two

chemotypes is of paramount importance in drug discovery. Indeed, optimization of activity for a desired target during lead optimization is important. Nevertheless, translatability of such activity to the *in vivo* and clinical situations may not be achieved if the optimization of physicochemical parameters is neglected.

5.2 Recommendations for Future Work

Based on the results obtained in this study, a summary of proposed SAR (pSAR) for future studies is shown in figure 5.2. For imidazopyridazines, the introduction of an NH linker between the core-scaffold and aromatic as well as saturated heterocyclic ring systems was detrimental to antiplasmodial potency. In pSAR1 and 2, to potentially address the hERG inhibition and solubility issue, future SAR studies should focus on introducing saturated and aromatic groups with hydrogen bond acceptors and donors (sulfones, sulfoximines and tetrazolones) while avoiding NH linking. It is also recommended that the *meta* and *para* substitution patterns in pSAR1 and 2 respectively be preserved to avoid compromising activity as revealed by both parasite-based SAR and docking studies on the *Pf*PI4K homology model. The same recommendation applies for pSAR3 explorations where both phenyl rings would be simultaneously replaced by two saturated piperidine rings. Generation of analogues with *ortho*-fluoro or -methyl substitution in both pSAR1 and 2 will ensure molecular planarity is disrupted to possibly improve solubility while avoiding the disruption of key interactions in the binding site. The replacement of the imidazopyridazine core-scaffold with other fused ring heterocyclics which can potentially preserve binding to the hinge region of *Pf*PI4K while possibly addressing the hERG and solubility issues is further recommended (pSAR4). Moreover, testing the analogues in a *Pf*PI4K biochemical assay to guide the computational modelling and synthesis is another important aspect future studies should consider.

For the aminopyrazines, it is recommended that the replacement of position 3 and 5 aromatic rings with saturated ring systems is avoided since such modifications led to a drastic reduction in antiplasmodial potency. Efforts to improve the solubility of this class should instead focus on more discreet modifications such as introduction of planarity-disrupting *ortho* substituents as well as water-solubilizing tetrazolone groups (pSAR5 and 6) (Figure 5.2).

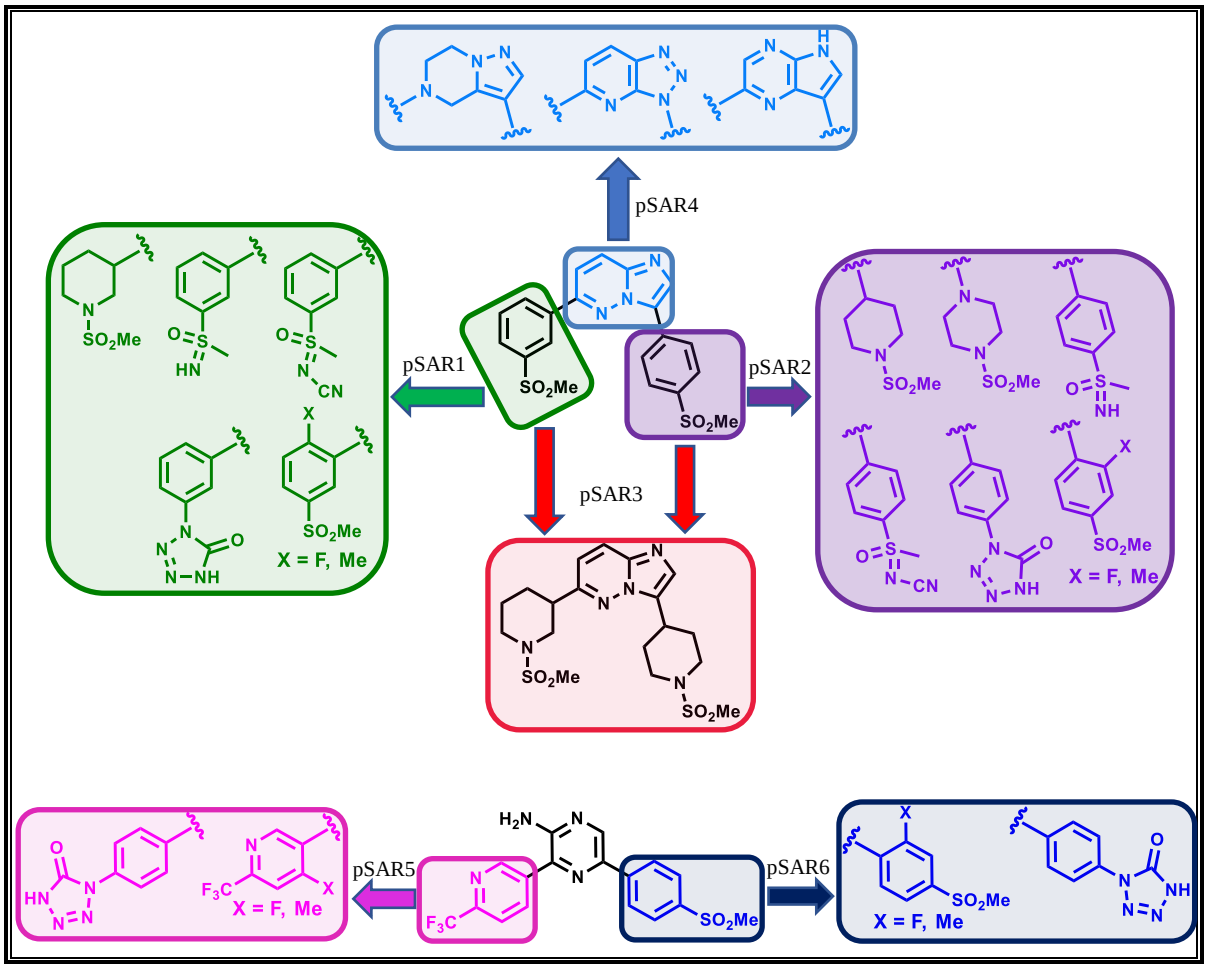

Figure 5.2: Recommendations for future SAR studies.

5.3 References

(1) Le Manach, C.; Gonzàlez Cabrera, D.; Douelle, F.; Nchinda, A. T.; Younis, Y.; Taylor, D.; Wiesner, L.; White, K. L.; Ryan, E.; March, C.; Duffy, S.; Avery, V. M.; Waterson, D.; Witty, M. J.; Wittlin, S.; Charman, S. A.; Street, L. J.; Chibale, K. Medicinal Chemistry Optimization of Antiplasmodial Imidazopyridazine Hits from High Throughput Screening of a SoftFocus Kinase Library: Part 1. *J. Med. Chem.* **2014**, *57*, 2789–2798.

(2) Le Manach, C.; Paquet, T.; Gonzàlez Cabrera, D.; Younis, Y.; Taylor, D.; Wiesner, L.; Lawrence, N.; Schwager, S.; Waterson, D.; Witty, M. J.; Wittlin, S.; Street, L. J.; Chibale, K. Medicinal Chemistry Optimization of Antiplasmodial Imidazopyridazine Hits from High Throughput Screening of a SoftFocus Kinase Library: Part 2. *J. Med. Chem.* **2014**, *57*, 8839–8848.

(3) Le Manach, C.; Paquet, T.; Brunschwig, C.; Njoroge, M.; Han, Z.; Gonzàlez Cabrera, D.; Bashyam, S.; Dhinakaran, R.; Taylor, D.; Reader, J.; Botha, M.; Churchyard, A.; Lauterbach, S.; Coetzer, T. L.; Birkholtz, L.-M.; Meister, S.; Winzeler, E. A.; Waterson, D.; Witty, M. J.; Wittlin, S.; Jiménez-Díaz, M.-B.; Santos Martínez, M.; Ferrer, S.; Angulo-Barturen, I.; Street, L. J.; Chibale, K. A Novel Pyrazolopyridine with in Vivo Activity in Plasmodium Berghei - and Plasmodium Falciparum - Infected Mouse Models from Structure–Activity Relationship Studies around the Core of Recently Identified Antimalarial Imidazopyridazines. *J. Med. Chem.* **2015**, *58*, 8713–8722.

(4) Younis, Y.; Douelle, F.; González Cabrera, D.; Le Manach, C.; Nchinda, A. T.; Paquet, T.; Street, L. J.; White, K. L.; Zabiulla, K. M.; Joseph, J. T.; Bashyam, S.; Waterson, D.; Witty, M. J.; Wittlin, S.; Charman, S. A.; Chibale, K. Structure–Activity-Relationship Studies around the 2-Amino Group and Pyridine Core of Antimalarial 3,5-Diarylaminopyridines Lead to a Novel Series of Pyrazine Analogues with Oral in Vivo Activity. *J. Med. Chem.* **2013**, *56*, 8860–8871.

(5) Le Manach, C.; Nchinda, A. T.; Paquet, T.; Gonzàlez Cabrera, D.; Younis, Y.; Han, Z.; Bashyam, S.; Zabiulla, M.; Taylor, D.; Lawrence, N.; White, K. L.; Charman, S. A.; Waterson, D.; Witty, M. J.; Wittlin, S.; Botha, M. E.; Nondaba, S. H.; Reader, J.; Birkholtz, L.-M.; Jiménez-Díaz, M. B.; Martínez, M. S.; Ferrer, S.; Angulo-Barturen, I.; Meister, S.; Antonova-Koch, Y.; Winzeler, E. A.; Street, L. J.; Chibale, K. Identification of a Potential Antimalarial Drug Candidate from a Series of 2-Aminopyrazines by Optimization of Aqueous Solubility and Potency across the Parasite Life Cycle. *J. Med. Chem.* **2016**, *59*, 9890–9905.

CHAPTER 6
EXPERIMENTAL

6.1 Chemistry

6.1.1 General Comments on Experimental Data

All reagents and chemicals used in all reactions were purchased from various commercial sources and used without further purification. All the solvents used in the reactions were anhydrous save for ethanol which was absolute (99.9%). Reactions were monitored by a combination of analytical TLC, HPLC-MS and UPLC-MS. The TLC plates were sourced from Merck (TLC Silica gel 60 F_{254} aluminium-backed) and were developed in a 100 mL beaker covered with either a watch glass or aluminium foil. The plates were visualized under ultraviolet light (UV 254 and 366 nm). An Agilent HPLC-MS instrument with the following components was used for compound purity checks and reaction monitoring: Agilent 1260® Infinity Binary Pump, Agilent 1260® Infinity Diode Array Detector, Agilent 1290® Infinity Column Compartment, Agilent 1260® Infinity Autosampler, Agilent 6120® Quadrupole LC-MS, and Peak Scientific® Genius 1050 Nitrogen Generator. An X-bridge® (C18, 2.5 µm, 3.0 mm (ID) x 50 mm length) column maintained at 35 °C or 40 °C was used. The HPLC mobile phase compositions and run times for reaction monitoring for final compounds and intermediates varied during the entire period in which this PhD study was undertaken. Therefore, the retention times for all intermediates were not determined under the same conditions. However, the retention times used in the solubility – retention time correlation plots for all final compounds, as shown in chapter 4, were measured using the same conditions. These included a Kinetex Core (C18, 2.6 µm, 2.1 mm (ID) x 30 mm length) column maintained at 40 °C, a flow rate of 0.7 mL/min and an injection volume of 2 µL. The chromatographic mobile phase was composed of 10 mM aqueous ammonium acetate (NH_4OAc) spiked with 0.4% acetic acid while the organic phase was composed of 10 mM NH_4Ac in 90% methanol in water spiked with 0.4% acetic acid. The gradient conditions are summarised in table 6.1 below.

Table 6.1: HPLC gradient conditions used to measure retention times for final compounds

Time (min)	%A[x]	%B[y]
0.00	85	15
0.30	85	15
1.20	0.0	100
4.50	0.0	100

[x]A: 10 mM aqueous ammonium acetate (NH_4OAc) spiked with 0.4% acetic acid.
[y]B: 10 mM NH_4Ac in 90% methanol in water spiked with 0.4% acetic acid.

The mass spectra were acquired using electrospray ionisation (ESI) and atmospheric pressure chemical ionization (APCI) either in the positive or negative ionisation mode.

Biotage grade silica gel was employed for column chromatographic purifications on the Biotage Isolera One Flash Chromatography system. Additionally, Analtech Uniplate preparative TLC (prep-TLC) plates (silica gel GF, 20 × 20 cm, 2000 microns) were used for prep-TLC purifications. The mobile phase solvents were AR grade and were used without further distillation.

^{1}H-NMR and ^{13}C-NMR spectra were acquired on either of the following instruments: Bruker AV 400 (^{1}H 400.0, ^{13}C 101 MHz), Varian Mercury 300 (^{1}H 300.1 MHz) or Bruker Ascend™ 600 (^{1}H 600.0, ^{13}C 151 MHz) spectrometers. The ^{13}C-NMR spectra for compounds **30**, **44**, **57**, **66** and **72** were not acquired due to insufficient material to undertake such analyses.

All final compounds were subjected to purity check experiments using HPLC-MS to ensure acceptable purity (≥ 95%). Melting points were measured using the Automatic Stuart Melting Point Apparatus SMP40 (imidazopyridazines) and a Reichert-Jung Thermovar hot stage microscope (aminopyrazines) and are uncorrected.

6.1.2 Synthetic Methods for Imidazopyridazines

6.1.2.1 Procedure for Synthesis of 6-chloroimidazo[1,2-*b*]pyridazine (2a)[1]

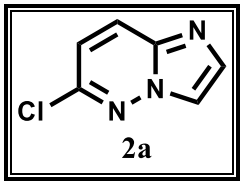

2a

Bromoacetaldehyde diethylacetal (12.0 mL, 78 mmol) was added to a suspension of 3-amino-6-chloropyridazine (5.00 g, 39 mmol) in absolute ethanol (99.9%) (78 mL) and deionized water (50 mL). A 48% aqueous solution of HBr (4.4 mL, 39 mmol) was added after which the suspension cleared. The reaction mixture was refluxed at 103 °C for 22 hours. The resulting brown solution was extracted with ethyl acetate (EtOAc) (100 mL × 3). The combined organic layers were concentrated *in vacuo* to obtain **2a** as a brown solid which was used in the next step without further purification (HPLC-MS, ESI^{+}/APCI^{+}: *m/z* $[M + H]^{+}$ = 154.0, calculated exact mass = 153.0094, t_r = 1.5 min).

6.1.2.2 Procedure for Synthesis of 6-chloro-3-iodoimidazo[1,2-*b*]pyridazine (3a)[1]

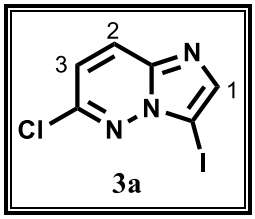

3a

A reddish solution of 6-chloroimidazo[1,2-*b*]pyridazine (**2a**) (4.60 g, 30 mmol) in 30 mL of *N*,*N*-dimethylformamide (DMF) was purged with nitrogen for 30 minutes. *N*-Iodosuccinimide (NIS) (7.41 g, 33 mmol) was then added followed by the addition of another 45 mL of DMF. The reaction mixture was then left to stir at room temperature (~ 21 °C) for 5 days (initially a suspension, the reaction mixture cleared after 2 days of magnetic stirring). DMF was then removed under reduced pressure. The resulting brown residue was taken up in 200 mL dichloromethane (DCM) and washed with deionized water (100 mL × 3), a saturated aqueous solution of a mixture of sodium metabisulfite ($Na_2S_2O_5$) and sodium bisulfite ($NaHSO_3$) (100 mL × 2). The organic layer was concentrated *in vacuo* to afford **3a** as a brown solid (6.82 g, 81%); ^{1}H-NMR δ_H (300 MHz; $CDCl_3$) 7.92 (1H, d, J = 9.4 Hz, H_2), 7.88 (1H, s, H_1), 7.14 (1H, d, J = 9.4 Hz, H_3); HPLC-MS, ESI^+/$APCI^+$: m/z $[M + H]^+$ = 279.8, calculated exact mass = 278.9060, t_r = 3.0 min.

6.1.2.3 General Procedure for Synthesis of Chloro-substituted Intermediates (4a – g)

A suspension of 6-chloro-3-iodoimidazo[1,2-*b*]pyridazine (**3a**) (1.0 eq), an appropriate boronic acid or boronic acid pinacol ester (1.1 eq) and $Pd(PPh_3)_2Cl_2$ (0.05 eq) in DMF (3 mL/mmol of **3a**) was purged with nitrogen for 20 minutes. A 1 M aqueous solution of K_2CO_3 (1.05 eq) was then added after which the reaction mixture was heated to 80 °C and left to magnetically stir at that temperature for 3.5 – 46 hours. The reaction mixture was diluted with DCM, washed with deionized water (8 ×), saturated aqueous solutions of $NaHCO_3$ (3 ×), NH_4Cl (3 ×) and NaCl (1 ×). For analogues **4e** – **g**, containing the basic side chain, washing with aq NH_4Cl was avoided. After drying the organic layer ($MgSO_4$), the solvent was removed *in vacuo* and the resulting residue subjected to automated column chromatography on silica to give the chloro-substituted derivatives in 26 – 77% yield.

6-Chloro-3-(4-(methylsulfinyl)phenyl)imidazo[1,2-*b*]pyridazine (4a)

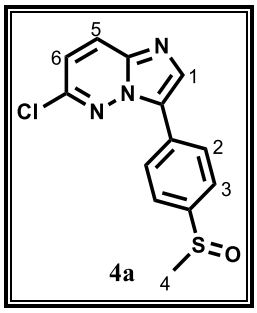

Purified by flash chromatography (0 – 3% CH_3OH/DCM). Yellow solid (0.587 g, 77%); ^{1}H-NMR δ_H (300 MHz; $CDCl_3$) 8.24 (2H, d, *J* = 8.2 Hz, H_2), 8.18 (1H, s, H_1), 8.11 (1H, d, *J* = 9.4 Hz, H_5), 7.82 (2H, d, *J* = 8.0 Hz, H_3), 7.22 (1H, d, *J* = 8.8 Hz, H_6), 2.81 (3H, s, H_4); HPLC-MS, ESI^+/$APCI^+$: *m/z* $[M + H]^+$ = 292.0, calculated exact mass = 291.0233, t_r = 3.0 min.

6-Chloro-3-(4-(methylsulfonyl)phenyl)imidazo[1,2-*b*]pyridazine (4b)

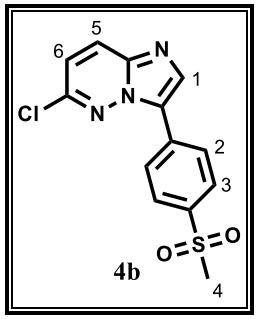

Purified by flash chromatography (0 – 2% CH_3OH/DCM). Yellow solid (0.577 g, 65%); ^{1}H-NMR δ_H (300 MHz; $CDCl_3$) 8.30 (2H, d, *J* = 8.8 Hz, H_3), 8.23 (1H, s, H_1), 8.18 - 8.07 (4H, m, H_2, H_5, H_6), 3.13 (3H, s, H_4); HPLC-MS, ESI^+/$APCI^+$: *m/z* $[M + H]^+$ = 308.0, calculated exact mass = 307.0182, t_r = 3.1 min.

6-Chloro-3-(3-(methylsulfinyl)phenyl)imidazo[1,2-*b*]pyridazine (4c)

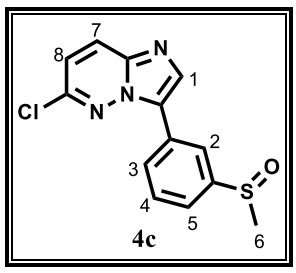

Purified by flash chromatography (0 – 3% CH_3OH/DCM). Yellow solid (0.1713 g, 66%); ^{1}H-NMR δ_H (300 MHz; $CDCl_3$) 8.32 (1H, s, H_2), 8.28 – 8.20 (1H, m, H_4), 8.19 (1H, s, H_1), 8.05 (1H, d, *J* = 9.4 Hz, H_7), 7.74 – 7.69 (2H, m, H_3, H_5), 7.18 (1H, d, *J* = 9.4 Hz, H_8), 2.84 (3H, s, H_6).

6-Chloro-3-(3-(methylsulfonyl)phenyl)imidazo[1,2-*b*]pyridazine (4d)

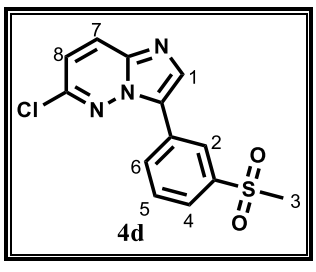

Purified by flash chromatography (0 – 4% CH_3OH/DCM). Yellow solid (0.1797 g, 66%); ^{1}H-NMR δ_H (300 MHz; $CDCl_3$) 8.63 (1H, s, H_2), 8.41 (1H, d, *J* = 8.1 Hz, H_6), 8.20 (1H, s, H_1), 8.04 (1H, d, *J* = 9.5 Hz, H_7), 7.99 (1H, d, *J* = 8.9 Hz, H_4), 7.76 (1H, t, *J* = 8.0 Hz, H_5), 7.19 (1H, d, *J* = 9.4 Hz, H_8), 3.16 (3H, s, H_3); HPLC-MS, $APCI^+$: *m/z* $[M + H]^+$ = 308.0, calculated exact mass = 307.0182, t_r = 3.4 min.

***N*-(4-(6-Chloroimidazo[1,2-*b*]pyridazin-3-yl)-3-fluorobenzyl)-*N*-ethylethanamine (4e)**

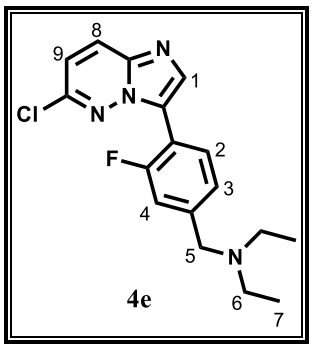

Purified by flash chromatography (0 – 5% CH_3OH/DCM), then prep-TLC (developed in 6% CH_3OH/DCM). Yellow oil (0.097 g, 26%); ^{1}H-NMR δ_H (300 MHz; $CDCl_3$) 8.23 – 8.10 (2H, m, H_1, H_2), 8.00 (1H, d, J = 9.4 Hz, H_8), 7.40 – 7.30 (2H, m, H_3, H_4), 7.12 (1H, d, J = 9.4 Hz, H_9), 3.70 (2H, s, H_5), 2.65 (4H, q, J = 7.1 Hz, H_6), 1.13 (6H, t, J = 7.1 Hz, H_7); HPLC-MS, ESI$^+$/APCI$^+$: *m/z* $[M + H]^+$ = 333.1, calculated exact mass = 332.1204, t_r = 2.5 min.

***N*-(4-(6-Chloroimidazo[1,2-*b*]pyridazin-3-yl)-2-fluorobenzyl)-*N*-ethylethanamine (4f)**

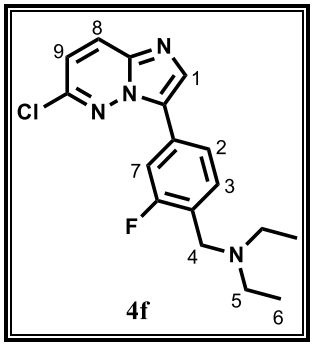

Purified by flash chromatography (0 – 3% CH_3OH/DCM). Yellow crystalline solid (0.135 g, 37%); ^{1}H-NMR δ_H (300 MHz; $CDCl_3$) 8.10 (1H, s, H_1), 7.98 (1H, d, J = 9.4 Hz, H_8), 7.89 – 7.77 (2H, m, H_2, H_7), 7.66 (1H, t, J = 7.9 Hz, H_3), 7.12 (1H, d, J = 9.4 Hz, H_9), 3.76 (2H, s, H_4), 2.65 (4H, q, J = 7.1 Hz, H_5), 1.14 (6H, t, J = 7.1 Hz, H_6).

***N*-(5-(6-Chloroimidazo[1,2-*b*]pyridazin-3-yl)-2-fluorobenzyl)-*N*-ethylethanamine (4g)**

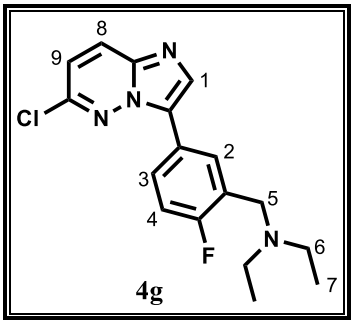

Purified by flash chromatography (0 – 4% CH_3OH/DCM). Yellow oil (0.182 g, 50%); ^{1}H-NMR δ_H (300 MHz; $CDCl_3$) 8.24 (1H, s, H_1), 8.09 (1H, s, H_2), 7.98 (1H, d, J = 9.4 Hz, H_8), 7.95 - 7.91 (1H, m, H_3), 7.26 – 7.16 (1H, m, H_4), 7.10 (1H, d, J = 9.4 Hz, H_9), 3.86 (2H, s, H_5), 2.73 (4H, d, J = 6.5 Hz, H_6), 1.21 (6H, t, J = 6.5 Hz, H_7); HPLC-MS, ESI$^+$/APCI$^+$: *m/z* $[M + H]^+$ = 333.1, calculated exact mass = 332.1204, t_r = 2.8 min.

6.1.2.4 General Procedure for Synthesis of Diarylated Imidazopyridazines (19, 26 – 34, 51 – 54 and 58)

A suspension of the relevant chloro-substituted intermediate (**4a – g**) (1.0 eq), appropriate boronic acid or boronic acid pinacol ester (1.1 eq) and $Pd(PPh_3)_2Cl_2$ (0.05 eq) in DMF (3 mL/mmol of **4a** – **g**) was purged with nitrogen for 20 minutes. A 1 M aqueous solution of K_2CO_3 (1.05 eq) was then added after which the reaction mixture was heated to 100 °C and magnetically stirred at that temperature for 4 – 21 hours. The reaction mixture was then diluted

with DCM, washed with deionized water (8 ×), saturated aqueous solutions of $NaHCO_3$ (3 ×), NH_4Cl (3 ×) and NaCl (1 ×). For analogues **28** – **34**, with basic side chains, washing with NH_4Cl (aq) was avoided. The organic layer was dried ($MgSO_4$ for **19** and **28 - 34**; Na_2SO_4 for **26**, **27** and **51** – **54**) after which the solvent was removed *in vacuo* and the resulting crude mixture subjected to further purification procedures.

6-(4-(Methylsulfinyl)phenyl)-3-(4-(methylsulfonyl)phenyl)imidazo[1,2-*b*]pyridazine (26)

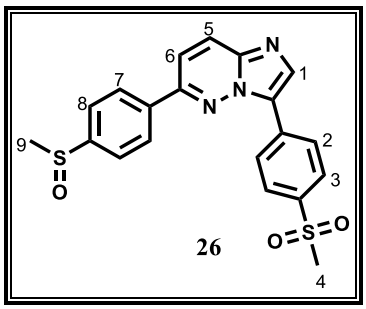

Purified by prep-TLC (developed in 4% CH_3OH/DCM) and trituration in ethyl acetate. Yellow solid (0.0683 g, 57%), m.p. 236.6 – 239.0 °C; R_f (CH_3OH : CH_2Cl_2 4 : 96) 0.18; ^{1}H-NMR δ_H (400 MHz; $CDCl_3$) 8.41 (2H, d, J = 8.8 Hz, H_2), 8.27 (1H, s, H_1), 8.24 (1H, d, J = 9.5 Hz, H_5), 8.19 (2H, d, J = 8.7 Hz, H_7), 8.13 (2H, d, J = 8.8 Hz, H_3), 7.88 (2H, d, J = 8.7 Hz, H_8), 7.70 (1H, d, J = 9.5 Hz, H_6), 3.15 (3H, s, H_4), 2.84 (3H, s, H_9); ^{13}C-NMR δ_C (101 MHz; $CDCl_3$) 151.23, 148.38, 140.09, 139.43, 137.92, 134.52, 133.74, 128.08 (3C), 127.97 (2C), 127.05 (2C), 126.65, 124.49 (2C), 116.66, 44.58, 44.00; HPLC-MS, APCI$^+$: *m/z* $[M + H]^+$ = 412.0, calculated exact mass = 411.0711, purity: 98.8%, t_r = 2.518 min.

3-(4-(Methylsulfinyl)phenyl)-6-(4-(methylsulfonyl)phenyl)imidazo[1,2-*b*]pyridazine (27)

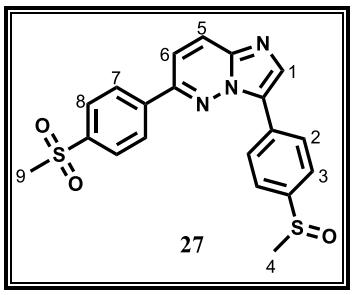

Purified by prep-TLC (developed in 4% CH_3OH/DCM). Yellow solid (0.067 g, 60%), m.p. 260.0 – 262.5 °C; R_f (CH_3OH : CH_2Cl_2 4 : 96) 0.33; ^{1}H-NMR δ_H (400 MHz; $CDCl_3$) 8.34 (3H, m, H_5, H_7), 8.23 (3H, m, H_3, H_6), 8.16 (2H, d, J = 8.0 Hz, H_2), 7.85 (2H, d, J = 7.7 Hz, H_8), 7.65 (1H, s, H_1), 3.15 (3H, s, H_9), 2.84 (3H, s, H_4); ^{13}C-NMR δ_C (101 MHz; $CDCl_3$) 150.25, 145.50, 142.06, 140.63, 131.18, 128.31 (4C), 128.09 (3C), 127.49 (2C), 126.74, 124.15 (2C), 115.95, 44.50, 44.04; HPLC-MS, APCI$^+$: *m/z* $[M + H]^+$ = 412.0, calculated exact mass = 411.0711, purity: 97.5%, t_r = 2.609 min.

_N_-Ethyl-_N_-(3-fluoro-4-(3-(4-(methylsulfinyl)phenyl)imidazo[1,2-_b_]pyridazin-6-yl)benzyl)ethanamine (28)

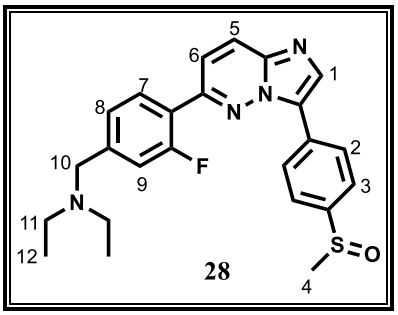

Purified by flash chromatography (0 – 4% CH_3OH/DCM) and trituration in diethyl ether. Yellow solid (0.128 g, 59%), m.p. 110.7 – 113.0 °C; R_f (CH_3OH : CH_2Cl_2 6 : 94) 0.32; ^{1}H-NMR δ_H (300 MHz; $CDCl_3$) 8.35 (2H, d, J = 8.3 Hz, H_2), 8.20 (1H, s, H_1), 8.11 (1H, d, J = 9.0 Hz, H_5), 7.94 – 7.75 (3H, m, H_3, H_7), 7.62 (1H, d, J = 9.2 Hz, H_6), 7.46 – 7.34 (2H, m, H_8, H_9), 3.76 (2H, s, H_{10}), 2.81 (3H, s, H_4), 2.70 (4H, br s, H_{11}), 1.17 (6H, t, J = 6.8 Hz, H_{12}); ^{13}C-NMR δ_C (100.6 MHz; $CDCl_3$) 162.1, 159.4, 148.8, 144.8, 134.1, 131.6, 130.5, 127.3 (4C), 125.8 (2C), 124.0 (3C), 119.0, 117.4, 56.6, 46.9 (2C), 44.0, 11.2 (2C); HPLC-MS, ESI$^+$/APCI$^+$: _m/z_ $[M + H]^+$ = 437.1, calculated exact mass = 436.1733, purity: 99.6%, t_r = 2.467 min.

_N_-Ethyl-_N_-(2-fluoro-4-(3-(4-(methylsulfinyl)phenyl)imidazo[1,2-_b_]pyridazin-6-yl)benzyl)ethanamine (29)

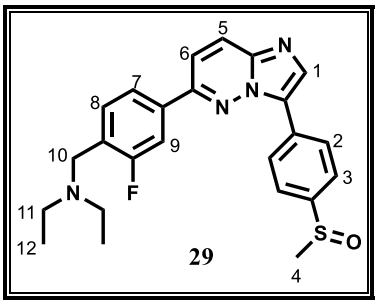

Purified by flash chromatography (0 – 4% CH_3OH/DCM), trituration in diethyl ether. Yellow solid (0.112 g, 57%), m.p. 162.0 – 165.0 °C; R_f (CH_3OH : CH_2Cl_2 6 : 94) 0.23; ^{1}H-NMR δ_H (300 MHz; $CDCl_3$) 8.35 (2H, d, J = 8.4 Hz, H_2), 8.20 (1H, s, H_1), 8.14 (1H, d, J = 9.4 Hz, H_5), 7.98 – 7.78 (4H, m, H_3, H_7, H_8), 7.74 (1H, d, J = 11.4 Hz, H_9), 7.58 (1H, d, J = 9.4 Hz, H_6), 3.89 (2H, s, H_{10}), 3.50 (4H, q, J = 7.0 Hz, H_{11}), 2.83 (3H, s, H_4), 1.23 (6H, t, J = 7.0 Hz, H_{12}); ^{13}C-NMR δ_C (101 MHz; $CDCl_3$) 162.9, 160.5, 145.0, 140.0, 134.4 (2C), 132.9, 131.4, 127.9, 127.4 (2C), 126.5, 124.1 (2C), 122.9, 115.7 (2C), 114.0 (d, J = 24.4 Hz), 65.8 (2C), 46.8, 44.0, 15.2 (2C); HPLC-MS, ESI$^+$/APCI$^+$: _m/z_ $[M + H]^+$ = 437.2, calculated exact mass = 436.1733, purity: 99.6%, t_r = 2.428 min.

_N_-Ethyl-_N_-(2-fluoro-5-(3-(4-(methylsulfinyl)phenyl)imidazo[1,2-_b_]pyridazin-6-yl)benzyl)ethanamine (30)

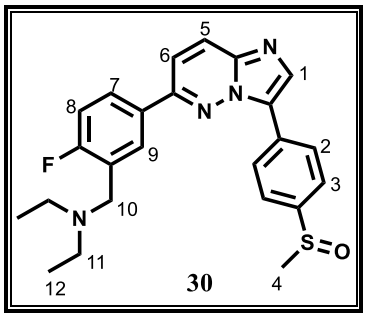

Purified by flash chromatography (0 – 4% CH_3OH/DCM), trituration in diethyl ether. Yellow solid (0.243 g, 80%), m.p. 122.4 – 124.5 °C; R_f (CH_3OH : CH_2Cl_2 6 : 94) 0.33; ^{1}H-NMR δ_H (300 MHz; $CDCl_3$) 8.37 (2H, d, J = 8.6 Hz, H_2), 8.23 (1H, d, J = 6.6 Hz, H_9), 8.17 (1H, s, H_1), 8.11 (1H, d, J = 9.5 Hz, H_5), 7.98 – 7.87 (1H, m, H_7), 7.80 (2H, d, J = 8.6 Hz, H_3), 7.63 (1H, d, J = 9.4 Hz, H_6), 7.25 – 7.15 (1H, m, H_8), 3.78 (2H, s, H_{10}), 2.81 (3H, s, H_4), 2.67 (4H, q, J = 7.1 Hz, H_{11}), 1.14 (6H, t, J = 7.1 Hz, H_{12}); HPLC-MS, ESI$^+$/APCI$^+$: _m/z_ $[M + H]^+$ = 437.1, calculated exact mass = 436.1733, purity: 99.9%, t_r = 2.462 min.

_N_-Ethyl-_N_-(2-fluoro-4-(3-(4-(methylsulfonyl)phenyl)imidazo[1,2-_b_]pyridazin-6-yl)benzyl)ethanamine (31)

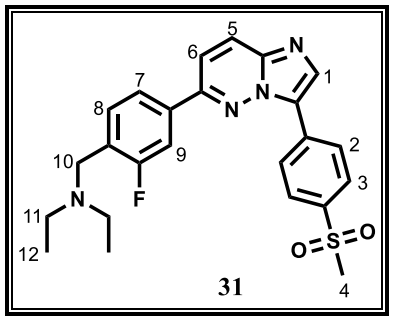

Purified by flash chromatography (0 – 1% CH_3OH/DCM), trituration in methanol. Yellow solid (0.0627 g, 13%), m.p. 183.0 – 186.0 °C; R_f (CH_3OH : CH_2Cl_2 6 : 94) 0.28; ^{1}H-NMR δ_H (400 MHz; $CDCl_3$) 8.41 (2H, d, J = 8.8 Hz, H_3), 8.23 (1H, s, H_1), 8.15 (1H, d, J = 9.5 Hz, H_5), 8.12 (2H, d, J = 8.7 Hz, H_2), 7.79 (2H, m, H_7, H_8), 7.71 (1H, d, J = 10.9 Hz, H_9), 7.61 (1H, d, J = 9.5 Hz, H_6), 3.82 (2H, s, H_{10}), 3.15 (3H, s, H_4), 2.70 (4H, br d, J = 6.6 Hz, H_{11}), 1.17 (6H, t, J = 7.1 Hz, H_{12}); ^{13}C-NMR δ_C (100.6 MHz; $CDCl_3$) 162.9, 160.4, 150.9, 140.4, 139.2, 134.9, 134.0, 132.4, 127.9 (4C), 126.9 (2C), 126.6, 122.7, 116.3, 113.8 (d, J = 24.7 Hz), 49.6, 47.0 (2C), 44.6, 11.4 (2C); HPLC-MS, ESI$^+$/APCI$^+$: _m/z_ $[M + H]^+$ = 453.1, calculated exact mass = 452.1682, purity: 99.2%, t_r = 2.555 min.

_N_-Ethyl-_N_-(3-fluoro-4-(6-(3-(methylsulfinyl)phenyl)imidazo[1,2-_b_]pyridazin-3-yl)benzyl)ethanamine (32)

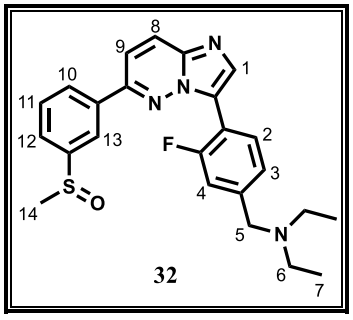

Purified by prep-TLC (developed in 6% CH_3OH/DCM). Yellow oil (0.0483 g, 38%); R_f (CH_3OH : CH_2Cl_2 6 : 94) 0.26; ^{1}H-NMR δ_H (300 MHz; $CDCl_3$) 8.51 (1H, t, J = 7.7 Hz, H_{11}), 8.30 (1H, s, H_{13}), 8.26 (1H, s, H_1), 8.21 – 8.13 (2H, m, H_2, H_8), 7.82 – 7.71 (3H, m, H_3, H_{10}, H_{12}), 7.67 (1H, d, J = 9.5 Hz, H_9), 7.61 (1H, d, J = 12.2 Hz, H_4), 4.15 (2H, s, H_5), 3.08 (4H, br s, H_6), 2.83 (3H, s,

H_{14}), 1.44 (6H, t, *J* = 6.6 Hz, H_7); ^{13}C-NMR δ_C (100.6; $CDCl_3$) 160.8, 158.3, 150.6, 147.2, 139.5, 137.1, 136.8, 130.2, 129.8, 129.6 (2C), 126.5 (3C), 125.0, 122.1, 118.2, 116.0, 55.5, 46.2 (2C), 44.2, 9.0 (2C); HPLC-MS, $ESI^+/APCI^+$: *m/z* $[M + H]^+$ = 437.2, calculated exact mass = 436.1733, purity: 98.5%, t_r = 2.505 min.

_N_-Ethyl-_N_-(2-fluoro-4-(6-(3-(methylsulfinyl)phenyl)imidazo[1,2-_b_]pyridazin-3-yl)benzyl)ethanamine (33)

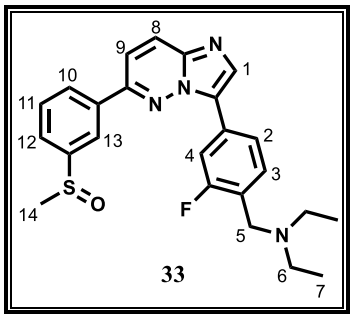

Purified by flash chromatography (0 – 4% CH_3OH/DCM), prep-TLC (silica, developed in 10% CH_3OH/DCM). Yellow oil (0.0484 g, 27%); R_f (CH_3OH : CH_2Cl_2 6 : 94) 0.15; ^{1}H-NMR δ_H (300 MHz; $CDCl_3$) 8.30 (1H, s, H_{13}), 8.25 – 8.09 (3H, m, H_1, H_8, H_{10}), 8.01 (1H, d, *J* = 11.6 Hz, H_4), 7.90 (1H, d, *J* = 8.0 Hz, H_3), 7.85 – 7.60 (4H, m, H_2, H_9, H_{11}, H_{12}), 3.81 (2H, s, H_5), 2.84 (3H, s, H_{14}), 2.70 (4H, br d, *J* = 7.1 Hz, H_6), 1.17 (6H, t, *J* = 7.0 Hz, H_7); ^{13}C-NMR δ_C (100.6 MHz; $CDCl_3$) 162.7, 160.2, 150.6, 147.3, 139.9, 137.1, 134.3, 132.6, 130.3, 129.6, 127.3, 126.6, 125.0 (2C), 122.5, 122.1, 115.6, 113.1 (d, *J* = 25.4 Hz), 49.3, 46.6 (2C), 44.1, 15.2 (2C); HPLC-MS, $ESI^+/APCI^+$: *m/z* $[M + H]^+$ = 437.2, calculated exact mass = 436.1733, purity: 99.9%, t_r = 2.416 min.

_N_-Ethyl-_N_-(2-fluoro-5-(6-(3-(methylsulfinyl)phenyl)imidazo[1,2-_b_]pyridazin-3-yl)benzyl)ethanamine (34)

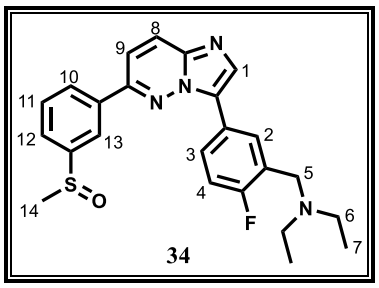

Purified by prep-TLC (developed in 6% CH_3OH/DCM). Yellow oil (0.101 g, 42%); R_f (CH_3OH : CH_2Cl_2 6 : 94) 0.21; ^{1}H-NMR δ_H (300 MHz; $CDCl_3$) 8.39 – 8.29 (2H, m, H_2, H_{10}), 8.25 (1H, dt, *J* = 7.4, 1.6 Hz, H_{12}), 8.16 – 8.07 (2H, m, H_1, H_8), 8.00 (1H, ddd, *J* = 8.4, 4.9, 2.4 Hz, H_3), 7.80 – 7.66 (2H, m, H_{11}, H_{13}), 7.61 (1H, d, *J* = 9.5 Hz, H_9), 7.25 – 7.15 (1H, m, H_4), 3.80 (2H, s, H_5), 2.82 (3H, s, H_{14}), 2.68 (4H, q, *J* = 7.1 Hz, H_6), 1.12 (6H, t, *J* = 7.1 Hz, H_7); ^{13}C-NMR δ_C (100.6 MHz; $CDCl_3$) 162.2, 159.8, 150.3, 147.1, 139.3, 137.3, 133.6, 130.1 (2C), 129.6, 128.3, 127.2, 126.4, 124.8, 124.6, 122.1, 115.6 (d, *J* = 22.9 Hz), 115.0, 49.9, 47.0 (2C), 44.1, 11.6 (2C); HPLC-MS, $ESI^+/APCI^+$: *m/z* $[M + H]^+$ = 437.2, calculated exact mass = 436.1733, purity: 98.2%, t_r = 2.492 min.

3-(3-(Methylsulfonyl)phenyl)-6-(4-(methylsulfonyl)phenyl)imidazo[1,2-*b*]pyridazine (51)

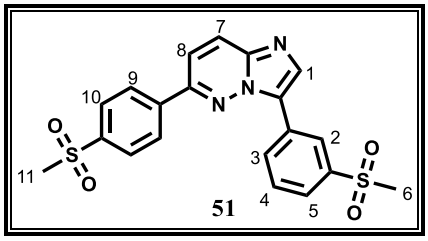

Purified by prep-TLC (developed in 4% CH_3OH/DCM). Yellow solid (0.0223 g, 20%), m.p. 264.0 – 267.5 °C; R_f (CH_3OH : CH_2Cl_2 4 : 96) 0.38; ^{1}H-NMR δ_H (400 MHz; DMSO-d_6) 9.12 – 9.08 (1H, m, H_2), 8.56 (1H, s, H_1), 8.53 (1H, d, J = 8.0 Hz, H_3), 8.50 (2H, d, J = 8.4 Hz, H_9), 8.45 (1H, d, J = 9.6 Hz, H_7), 8.13 (2H, d, J = 8.5 Hz, H_{10}), 8.09 (1H, d, J = 9.6 Hz, H_8), 8.00 – 7.96 (1H, m, H_5), 7.86 (1H, t, J = 7.9 Hz, H_4), 3.33 (6H, s, H_6, H_{11}); ^{13}C-NMR δ_C (101 MHz; DMSO-d_6) 150.20, 142.63, 142.04, 140.26, 140.07, 135.36, 131.32, 130.51, 129.90, 128.49 (2C), 128.17 (2C), 127.33, 126.10, 126.38, 124.60, 116.99, 44.08, 43.90; HPLC-MS, APCI$^+$: *m/z* [M + H]$^+$ = 428.0, calculated exact mass = 427.0660, purity: 95.8%, t_r = 2.588 min.

6-(4-(Methylsulfinyl)phenyl)-3-(3-(methylsulfonyl)phenyl)imidazo[1,2-*b*]pyridazine (52)

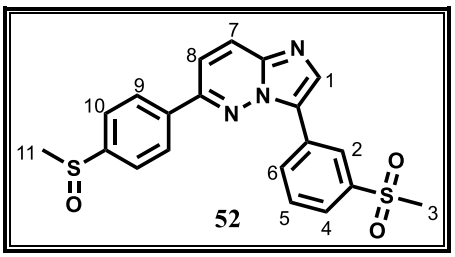

Purified by prep-TLC (developed in 4% CH_3OH/DCM). Crystallized in diethyl ether. Yellow solid (0.0441 g, 45%), m.p. 218.6 – 221.0 °C; R_f (CH_3OH : CH_2Cl_2 4 : 96) 0.32; ^{1}H-NMR δ_H (400 MHz; $CDCl_3$) 9.09 (1H, d, J = 1.9 Hz, H_2), 8.35 (1H, d, J = 7.9 Hz, H_6), 8.33 – 8.19 (4H, m, H_1, H_7, H_9), 8.03 – 7.97 (1H, m, H_4), 7.88 (2H, d, J = 8.1 Hz, H_{10}), 7.81 – 7.68 (2H, m, H_5, H_8), 3.16 (3H, s, H_3), 2.83 (3H, s, H_{11}); ^{13}C-NMR δ_C (101 MHz; $CDCl_3$) 150.81, 148.32, 141.42, 137.76, 131.20, 130.03, 129.88, 128.01 (4C), 126.63, 126.37, 125.34, 124.48 (3C), 116.07, 44.58, 43.94; HPLC-MS, APCI$^+$: *m/z* [M + H]$^+$ = 412.0, calculated exact mass = 411.0711, purity: 97.9%, t_r = 2.619 min.

3-(3-(Methylsulfinyl)phenyl)-6-(4-(methylsulfonyl)phenyl)imidazo[1,2-*b*]pyridazine (53)

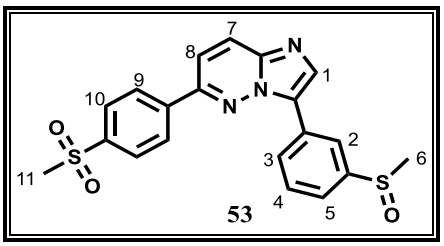

Purified by prep-TLC (developed in 4% CH_3OH/DCM). Crystallized in diethyl ether. Yellow solid (0.0436 g, 37%), m.p. 218.0 – 221.5 °C; R_f (CH_3OH : CH_2Cl_2 4 : 96) 0.29; ^{1}H-NMR δ_H (400 MHz; $CDCl_3$) 8.72 (1H, d, J = 1.7 Hz, H_2), 8.34 – 8.25 (4H, m, H_1, H_7, H_9), 8.23 (1H, d, J = 7.9 Hz, H_3), 8.17 (2H, d, J = 8.4 Hz, H_{10}), 7.75 – 7.66 (2H, m, H_4, H_8), 7.63 (1H, dt, J = 8.0, 1.2 Hz, H_5), 3.15 (3H, s, H_{11}), 2.84 (3H, s, H_6); ^{13}C-NMR δ_C (101 MHz; $CDCl_3$) 150.22, 149.15, 146.89, 142.09, 140.40, 135.72, 129.69 (2C), 128.91, 128.33 (3C), 128.09 (2C), 126.64,

123.00, 121.56, 115.90, 44.48, 44.18; HPLC-MS, APCI$^+$: *m/z* $[M + H]^+$ = 412.0, calculated exact mass = 411.0711, purity: 99.6%, t_r = 2.578 min.

3-(3-(Methylsulfinyl)phenyl)-6-(4-(methylsulfinyl)phenyl)imidazo[1,2-*b*]pyridazine (54)

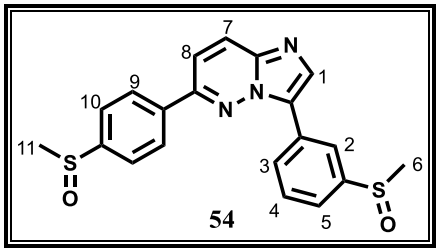

Purified by prep-TLC (developed in 4% CH_3OH/DCM). Crystallized in diethyl ether. Yellow solid (0.0666 g, 58%), m.p. 174.0 – 176.2 °C; R_f (CH_3OH : CH_2Cl_2 4 : 96) 0.14; ^{1}H-NMR δ_H (400 MHz; $CDCl_3$) 8.74 – 8.68 (1H, m, H_3), 8.30 – 8.18 (5H, m, H_1, H_2, H_7, H_{10}), 7.87 (2H, d, *J* = 8.8 Hz, H_9), 7.74 – 7.66 (2H, m, H_4, H_8), 7.66 – 7.62 (1H, m, H_5), 2.84 (3H, s, H_6), 2.83 (3H, s, H_{11}); ^{13}C-NMR δ_C (101 MHz; $CDCl_3$) 150.82, 148.20, 146.80, 137.97, 133.59, 129.90, 129.68 (2C), 128.91, 128.06 (3C), 126.47, 124.43 (2C), 122.86, 121.53, 115.96, 44.15, 43.95; HPLC-MS, APCI$^+$: *m/z* $[M + H]^+$ = 396.0, calculated exact mass = 395.0762, purity: 99.9%, t_r = 2.602 min.

6-(3-(Methylsulfinyl)phenyl)-3-(4-(methylsulfinyl)phenyl)imidazo[1,2-*b*]pyridazine (58)

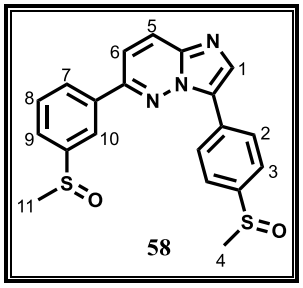

Purified by flash chromatography (0 – 5% CH_3OH/DCM). Crystallized in diethylether. Yellow solid (0.5453g, 51%); ^{1}H-NMR δ_H (300 MHz; $CDCl_3$) 8.37 – 8.32 (3H, m, H_2, H_{10}), 8.28 (1H, d, *J* = 9.5 Hz, H_5), 8.24 – 8.18 (2H, m, H_1, H_7), 7.85 (2H, d, *J* = 8.7 Hz, H_3), 7.79 – 7.72 (3H, m, H_6, H_8, H_9), 2.84 (6H, m, H_4, H_{11}); HPLC-MS, APCI$^+$: *m/z* $[M + H]^+$ = 396.0, calculated exact mass = 395.0762, purity: 99.9%, t_r = 2.601 min.

6.1.2.5 Procedure for Synthesis of 2-fluoro-5-nitrobenzyl 4-methylbenzenesulfonate (5b)[2]

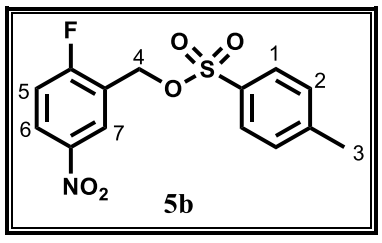

To a solution of NaOH (0.534 g, 13 mmol) in 3.8 mL deionized water cooled to ~ 0 °C was added a solution of 2-fluoro-5-nitrobenzyl alcohol (**5a**) (1.00 g, 5.8 mmol) in tetrahydrofuran (THF) (17 mL). *p*-Toluenesulfonyl chloride (1.89 g, 9.9 mmol) dissolved in THF (5.0 mL) was then added dropwise. The reaction mixture was left to stir at 0 – 11 °C for 2 hours. After completion of reaction as signalled by TLC (ionisation not observed on HPLC-MS), the reaction mixture was diluted with deionized water (50 mL) and extracted with DCM (100 mL × 3). The organic layer was dried ($MgSO_4$) and solvent removed *in vacuo* to give an oily residue which was further

crystallized and purified by trituration in methanol to afford **5b** as a cream white solid (1.25 g, 66%); ^{1}H-NMR δ_H (300 MHz; $CDCl_3$) 8.29 – 8.16 (2H, m, H_6, H_7), 7.84 (2H, d, J = 8.4 Hz, H_2), 7.38 (2H, d, J = 8.0 Hz, H_1), 7.22 (1H, t, J = 8.7 Hz, H_5), 5.20 (2H, s, H_4), 2.48 (3H, s, H_3).

6.1.2.6 Procedure for Synthesis of *N*-ethyl-*N*-(2-fluoro-5-nitrobenzyl)ethanamine (5c)[2]

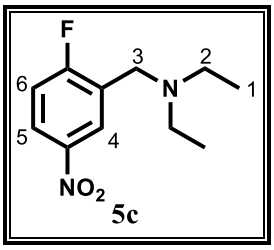

5c

Diethylamine (0.600 mL, 5.9 mmol) and triethylamine (0.800 mL, 5.9 mmol) were added to a solution of 2-fluoro-5-nitrobenzyl 4-methylbenzenesulfonate (**5b**) (1.28 g, 3.9 mmol) in anhydrous 1,4-dioxane (7.8 mL). The reaction mixture was heated to 55 °C and stirred for 5 hours. The solvent was removed *in vacuo* and the resulting yellowish residue taken up in DCM (150 mL) before washing with deionized water (60 mL × 1), and saturated aqueous solution of NaCl (50 mL × 1). The organic layer was dried ($MgSO_4$) before removing the solvent *in vacuo* to give **5c** as a yellow oil (0.771 g, 87%); ^{1}H-NMR δ_H (300 MHz; $CDCl_3$) 8.48 (1H, dd, J = 6.2, 2.9 Hz, H_4), 8.14 (1H, ddd, J = 9.0, 4.4, 3.0 Hz, H_5), 7.17 (1H, t, J = 8.9 Hz, H_6), 3.71 (2H, s, H_3), 2.62 (4H, q, J = 7.1 Hz, H_2), 1.10 (6H, t, J = 7.1 Hz, H_1).

6.1.2.7 Procedure for Synthesis of 3-((diethylamino)methyl)-4-fluoroaniline (5d)[2]

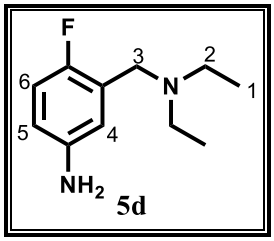

5d

A solution of stannous chloride ($SnCl_2$) (2.58 g, 13.6 mmol) in 1 M aqueous HCl (10.2 mL, 10.2 mmol) was added to a suspension of *N*-ethyl-*N*-(2-fluoro-5-nitrobenzyl)ethanamine (**5c**) (0.771 g, 3.4 mmol) in 15 mL THF. The reaction mixture was refluxed at 66 °C for 29 hours. THF was removed *in vacuo* where after the pH of the remaining aqueous mixture was adjusted to ~ 8 by gradual addition of saturated aqueous $NaHCO_3$. The resulting turbidy emulsion was extracted with DCM (150 mL × 6). The combined organic layers were dried ($MgSO_4$) after which the solvent was removed *in vacuo* to obtain the aniline compound **5d** as a yellow oil (0.661 g, quantitative); ^{1}H-NMR δ_H (300 MHz; $CDCl_3$) 6.86 – 6.78 (2H, m, H_4, H_6), 6.53 (1H, ddd, J = 8.6, 4.1, 3.0 Hz, H_5), 3.58 (2H, s, H_3), 2.59 (4H, q, J = 7.1 Hz, H_2), 1.09 (6H, t, J = 7.1 Hz, H_1); HPLC-MS, ESI^+/$APCI^+$: *m/z* $[M + H]^+$ = 197.1, calculated exact mass = 196.1376, t_r = 0.3 min.

6.1.2.8 Procedure for Synthesis of *N*-(4-hydroxyphenyl)acetamide (5f)

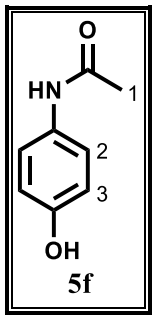

5f

A solution of 4-aminophenol **5e** (1.50 g, 13.7 mmol) and acetic anhydride (1.30 mL, 13.7 mmol) in THF (20 mL) was refluxed at 60 °C for 1.75 hours. The solvent was then removed *in vacuo* and the resulting brown residue purified by trituration in diethyl ether for 30 minutes to give the acetylated compound, **5f**, as a cream white solid (1.81 g, 87%); ^{1}H-NMR δ_H (300 MHz; CD_3OD) 7.31 (2H, d, J = 9.0 Hz, H_2), 6.74 (2H, d, J = 9.1 Hz, H_3), 2.10 (3H, s, H_1); HPLC-MS, $ESI^+/APCI^+$: *m/z* $[M + H]^+$ = 152.1, calculated exact mass = 151.0633, t_r = 1.0 min.

6.1.2.9 Procedure for Synthesis of *N*-(3-((diethylamino)methyl)-4-hydroxyphenyl)acetamide (5g)

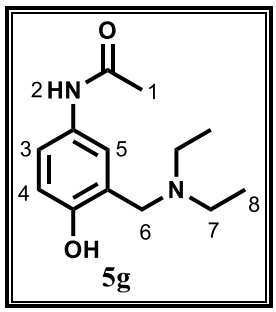

5g

Diethylamine (0.800 mL, 7.94 mmol) and 37% aqueous formaldehyde (0.600 mL, 7.94 mmol) were added to a solution of *N*-(4-hydroxyphenyl)acetamide (**5f**) (0.600 g, 3.97 mmol) in 5.0 mL absolute ethanol. The reaction mixture was heated to 80 °C under microwave irradiation for 1.5 hours after which the solvent was removed *in vacuo*. The brown residue was taken up in 40 mL DCM and extracted with 1 M HCl (35 mL × 1). The pH of the acidic aqueous layer was then adjusted to ~ 12 by gradual addition of a saturated aqueous solution of NaOH. The resultant basic mixture was then extracted with DCM (50 mL × 3). The combined organic layers were dried ($MgSO_4$) before removing the solvent *in vacuo* to afford **5g** as a brown oil, which subsequently crystallized upon standing (0.987 g, quantitative); ^{1}H-NMR δ_H (300 MHz; $CDCl_3$) 7.35 (1H, d, J = 2.4 Hz, H_5), 7.15 (1H, br s, H_2), 7.07 (1H, dd, J = 8.5, 2.6 Hz, H_3), 6.76 (1H, d, J = 8.6 Hz, H_4), 3.77 (2H, s, H_6), 2.64 (4H, q, J = 7.2 Hz, H_7), 2.15 (3H, s, H_1), 1.12 (6H, t, J = 7.2 Hz, H_8); HPLC-MS, $ESI^+/APCI^+$: *m/z* $[M + H]^+$ = 237.2, calculated exact mass = 236.1525, t_r = 0.58 min.

6.1.2.10 Procedure for Synthesis of 4-amino-2-((diethylamino)methyl)phenol (5h)

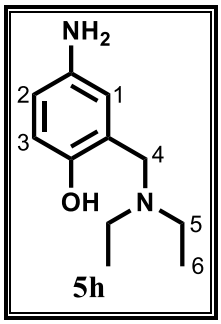

5h

N-(3-((Diethylamino)methyl)-4-hydroxyphenyl)acetamide (**5g**) (0.987 g, 4.18 mmol) was refluxed at 80 °C in 6 M aqueous HCl (4.20 mL , 25.1 mmol) for 2 hours. The reaction mixture was left to cool to room temperature before adjusting the pH to ~ 8 by gradual addition of a saturated aqueous solution of $NaHCO_3$. The black solution obtained was extracted with DCM (100 mL × 5). The combined organic layers were dried ($MgSO_4$), where after the solvent was removed *in vacuo*. The obtained black residue was subjected to

chromatography on silica (4% CH_3OH/DCM) to give the phenolic compound **5h** as a brown oil (0.352 g, 43%); ^{1}H-NMR δ_H (300 MHz; $CDCl_3$) 6.67 (1H, d, *J* = 8.4 Hz, H_3), 6.56 (1H, dd, *J* = 8.4, 2.8 Hz, H_2), 6.41 (1H, d, *J* = 2.7 Hz, H_1), 3.70 (2H, s, H_4), 2.64 (4H, q, *J* = 7.2 Hz, H_5), 1.12 (6H, t, *J* = 7.2 Hz, H_6); HPLC-MS, ESI$^+$/APCI$^+$: *m/z* $[M + H]^+$ = 195.2, calculated exact mass = 194.1419, t_r = 0.57 min.

6.1.2.11 Procedure for Synthesis of 3-(4-(methylsulfinyl)phenyl)-*N*-(3-(methylsulfonyl)phenyl)imidazo[1,2-*b*]pyridazin-6-amine (36)[3–6]

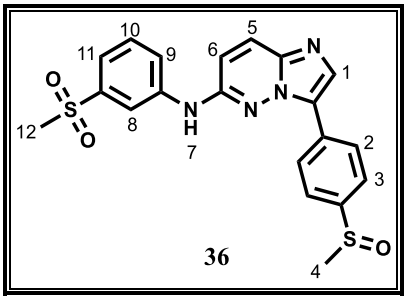

36

A mixture of 6-chloro-3-(4-(methylsulfinyl)phenyl)imidazo[1,2-*b*]pyridazine (**4a**) (0.100 g, 0.34 mmol), 3-(methylsulfonyl)aniline (0.0640 g, 0.37 mmol), $Pd_2(dba)_3$ (0.0249 g, 0.027 mmol), BrettPhos (0.0219 g, 0.041 mmol) and Cs_2CO_3 (0.222 g, 0.68 mmol) in 1.5 mL anhydrous 1,4-dioxane in a sealed tube was flashed with nitrogen for 25 minutes. The reaction mixture was then heated to 120 °C and stirred at this temperature for 24 hours. The solvent was removed *in vacuo* and the resulting black residue taken up in DCM (50 mL), washed with deionized water (30 mL × 1), saturated aqueous solutions of $NaHCO_3$ (30 mL × 2) and NaCl (30 mL × 1). The organic layer was dried ($MgSO_4$), after which the solvent was removed *in vacuo*. The yellowish residue was then subjected to prep-TLC (developed in 5% CH_3OH/DCM) to afford **36** as a brown solid (0.0228 g, 16%); R_f (CH_3OH : CH_2Cl_2 6 : 94) 0.24; ^{1}H-NMR δ_H (400 MHz; DMSO-d_6) 9.89 (1H, s, H_7), 8.32 – 8.24 (3H, m, H_2, H_8), 8.10 – 8.02 (2H, m, H_1, H_5), 7.99 (1H, dd, *J* = 8.2, 1.2 Hz, H_9), 7.85 (2H, d, *J* = 8.5 Hz, H_3), 7.66 (1H, t, *J* = 7.9 Hz, H_{10}), 7.57 (1H, d, *J* = 7.8 Hz, H_{11}), 7.03 (1H, d, *J* = 9.7 Hz, H_6), 3.19 (3H, s, H_{12}), 2.81 (3H, s, H_4); ^{13}C-NMR δ_C (101 MHz; DMSO-d_6) 151.01, 145.41, 142.07, 141.40, 138.32, 132.42, 131.55, 130.59, 127.51, 127.36, 127.25 (2C), 124.77 (2C), 123.68, 120.34, 116.42, 113.82, 44.10, 43.72; HPLC-MS, APCI$^+$: *m/z* $[M + H]^+$ = 427.0, calculated exact mass = 426.0820, purity: 99.9%, t_r = 2.635 min.

6.1.2.12 General Procedure for Synthesis of Aminated Analogues (37, 38, 40 and 43)[3–6]

A suspension of 6-chloro-3-(4-(methylsulfinyl)phenyl)imidazo[1,2-*b*]pyridazine (**4a**) (1.0 eq), an appropriate amine (1.1 eq), $Pd_2(dba)_3$ (0.08 eq), XPhos (0.12 eq) and sodium *tert*-butoxide (2.0 eq) in anhydrous 1,4-dioxane (6.0 mL/mmol of **4a**) in a sealed tube was flashed with nitrogen for 20 minutes. The reaction mixture was then heated to 120 °C and stirred for 6 - 20 hours. The solvent was removed *in vacuo* after which the resulting residue was taken up in

DCM, washed with saturated aqueous solutions of $NaHCO_3$ (2 ×) and NaCl (2 ×). The organic layer was dried ($MgSO_4$) (Na_2SO_4 for **38**), where after the solvent was removed *in vacuo* and obtained residue further purified.

_N_-(3-(Methylsulfinyl)phenyl)-3-(4-(methylsulfinyl)phenyl)imidazo[1,2-*b*]pyridazin-6-amine (37)

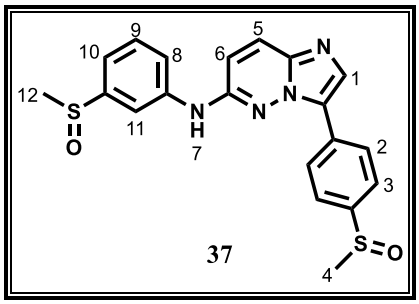

Purified by prep-TLC (developed twice in 6% CH_3OH/DCM). Brown solid (0.0175 g, 18%); R_f (CH_3OH : CH_2Cl_2 6 : 94) 0.19; ^{1}H-NMR δ_H (400 MHz; DMSO-d_6) 9.81 (1H, s, H_7), 8.28 (2H, d, J = 8.5 Hz, H_2), 8.11 (1H, s, H_{11}), 8.05 (1H, s, H_1), 8.03 (1H, d, J = 9.7 Hz, H_5), 7.85 (2H, d, J = 8.5 Hz, H_3), 7.77 (1H, dd, J = 8.1, 1.3 Hz, H_8), 7.57 (1H, t, J = 7.9 Hz, H_9), 7.31 (1H, d, J = 7.7 Hz, H_{10}), 7.02 (1H, d, J = 9.7 Hz, H_6), 2.82 (3H, s, H_4), 2.73 (3H, s, H_{12}); ^{13}C-NMR δ_C (101 MHz; DMSO-d_6) 151.09, 147.73, 145.44, 141.43, 138.21, 132.23, 131.62, 130.32, 127.41 (2C), 127.34 (2C), 124.69 (2C), 121.14, 117.01, 113.89, 113.50, 43.83, 43.73; HPLC-MS, APCI$^+$: *m/z* $[M + H]^+$ = 411.0, calculated exact mass = 410.0871, purity: 98.9%, t_r = 2.636 min.

_N_,3-Bis(4-(methylsulfinyl)phenyl)imidazo[1,2-*b*]pyridazin-6-amine (38)

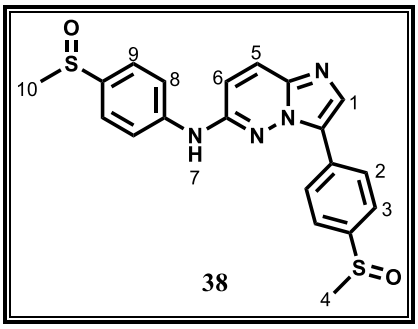

Purified by prep-TLC (developed once in 6% CH_3OH/DCM, then once in 7% CH_3OH/DCM), trituration in ethyl acetate for 20 h. Grey solid (0.0111 g, 8%); R_f (CH_3OH : CH_2Cl_2 4 : 96) 0.045; ^{1}H-NMR δ_H (400 MHz; DMSO-d_6) 9.84 (1H, s, H_7), 8.31 (2H, d, J = 8.5 Hz, H_2), 8.07 (1H, s, H_1), 8.03 (1H, d, J = 9.7 Hz, H_5), 7.91 (2H, d, J = 8.7 Hz, H_9), 7.86 (2H, d, J = 8.5 Hz, H_3), 7.70 (2H, d, J = 8.7 Hz, H_8), 7.04 (1H, d, J = 9.7 Hz, H_6), 2.83 (3H, s, H_4), 2.75 (3H, s, H_{10}); ^{13}C-NMR δ_C (101 MHz; DMSO-d_6) 150.98, 145.52, 142.95, 138.55, 138.18, 132.22, 131.59, 127.29 (2C), 127.18, 126.80, 125.30 (2C), 124.53 (2C), 119.27 (2C), 113.89, 43.70 (2C); HPLC-MS, APCI$^+$: *m/z* $[M + H]^+$ = 411.1, calculated exact mass = 410.0871, purity: 96.8%, t_r = 2.579 min.

3-(4-(Methylsulfinyl)phenyl)-*N*-(pyrazin-2-yl)imidazo[1,2-*b*]pyridazin-6-amine (40)

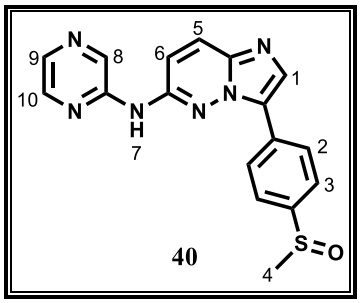

Purified by prep-TLC (developed in 5% CH_3OH/DCM). Light yellow solid (0.0242 g, 29%); R_f (CH_3OH : CH_2Cl_2 6 : 94) 0.3; ^{1}H-NMR δ_H (400 MHz; DMSO-d_6) 10.43 (1H, s, H_7), 9.23 (1H, d, J = 1.3 Hz, H_8), 8.38 (1H, dd, J = 2.6, 1.5 Hz, H_9), 8.35 (2H, d, J = 8.5 Hz, H_2), 8.26 (1H, d, J = 2.6 Hz, H_{10}), 8.16 – 8.09 (2H, m, H_1, H_5), 7.83 (2H, d, J = 8.5 Hz, H_3), 7.43 (1H, d, J = 9.7 Hz, H_6), 2.82 (3H, s, H_4); ^{13}C-NMR δ_C (101 MHz; DMSO-d_6) 150.20, 149.95, 145.70, 142.75, 138.50, 137.91, 135.82, 132.81, 131.46, 127.50, 127.35 (2C), 127.09, 124.45 (2C), 113.48, 43.68; HPLC-MS, APCI$^+$: *m/z* $[M + H]^+$ = 351.1, calculated exact mass = 350.0950, purity: 96.5%, t_r = 2.617 min.

3-(4-(Methylsulfinyl)phenyl)-*N*-(1-(methylsulfonyl)piperidin-4-yl)imidazo[1,2-*b*]pyridazin-6-amine (43)

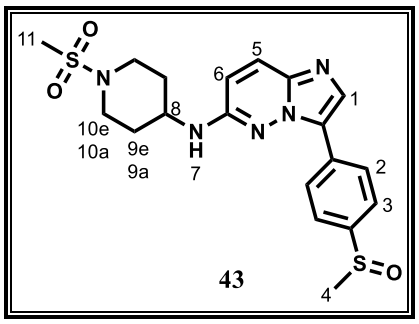

Purified by prep-TLC (developed once in 4% CH_3OH/DCM, then twice in 5% CH_3OH/DCM). Brown solid (0.022 g, 30%); R_f (CH_3OH : CH_2Cl_2 6 : 94) 0.36; ^{1}H-NMR δ_H (400 MHz; DMSO-d_6) 8.41 (2H, d, J = 8.6 Hz, H_2), 8.04 (1H, s, H_1), 7.87 – 7.74 (3H, m, H_3, H_5), 7.16 (1H, d, J = 6.5 Hz, H_7), 6.76 (1H, d, J = 9.7 Hz, H_6), 3.90 – 3.75 (1H, m, H_8), 3.68 – 3.55 (2H, m, H_{10e}), 3.07 – 2.97 (2H, m, H_{10a}), 2.94 (3H, s, H_{11}), 2.80 (3H, s, H_4), 2.26 – 2.13 (2H, m, H_{9e}), 1.69 – 1.52 (2H, m, H_{9a}); ^{13}C-NMR δ_C (101 MHz; DMSO-d_6) 153.21, 144.72, 138.10, 132.18, 131.40, 126.38, 126.27 (2C), 126.12, 124.54 (2C), 113.10, 48.00, 44.76 (2C), 43.62, 35.15, 30.82 (2C); HPLC-MS, APCI$^+$: *m/z* $[M + H]^+$ = 434.1, calculated exact mass = 433.1242, purity: 98.6%, t_r = 2.488 min.

6.1.2.13 Procedure for Synthesis of 3-(4-(methylsulfinyl)phenyl)-*N*-(4-(methylsulfonyl)phenyl)imidazo[1,2-*b*]pyridazin-6-amine (39)[3–6]

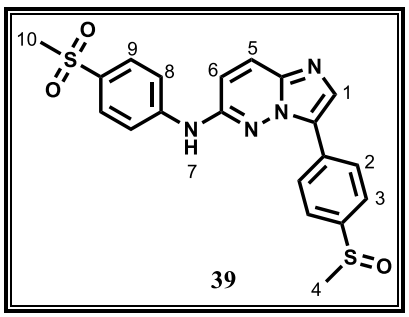

A mixture of 6-chloro-3-(4-(methylsulfinyl)phenyl)imidazo[1,2-*b*]pyridazine (**4a**) (0.130 g, 0.45 mmol), 4-(methylsulfonyl)aniline (0.0925 g, 0.54 mmol), $Pd_2(dba)_3$ (0.020 g, 0.022 mmol), (*R*)-BINAP (0.0168 g, 0.027 mmol) and K_2CO_3 (1.24 g, 9.00 mmol) in 1.8 mL anhydrous toluene was heated to 120 °C in a sealed tube and

stirred at this temperature for 17 hours. However, no significant amount of product was detected on HPLC-MS. At this point, anhydrous 1,4-dioxane (3.5 mL) was added and the reaction mixture stirred for another 17 hours where after a significant formation of the product was observed on HPLC-MS. The reaction mixture was then diluted with deionised water (40 mL) followed by extraction with DCM (70 mL). The solvents were removed *in vacuo* and the resulting residue taken up in DCM (70 mL), washed with a saturated aqueous solution of NaCl (40 mL × 3) and dried ($MgSO_4$). The solvent was then removed *in vacuo*. The obtained crude mixture was subjected to prep-TLC (developed in 5.5% CH_3OH/DCM) to afford the aminated target compound **39** as a brown solid (0.0251 g, 13%), m.p. 296.7 – 299.2 °C; R_f (CH_3OH : CH_2Cl_2 6 : 94) 0.25; ^{1}H-NMR δ_H (300 MHz; DMSO-d_6) 10.05 (1H, s, H_7), 8.30 (2H, d, J = 8.5 Hz, H_2), 8.13 – 8.04 (2H, m, H_1, H_5), 7.98 – 7.86 (6H, m, H_3, H_8, H_9), 7.07 (1H, d, J = 9.7 Hz, H_6), 3.19 (3H, s, H_{10}), 2.84 (3H, s, H_4); ^{13}C-NMR δ_C (100.6 MHz; DMSO-d_6) 150.7, 145.8, 145.2, 138.3, 135.9, 133.3, 132.5, 131.5, 128.8 (2C), 127.6, 127.4 (2C), 124.6 (2C), 118.4 (2C), 113.9, 44.5, 43.7; HPLC-MS, ESI$^+$/APCI$^+$: *m/z* [M + H]$^+$ = 427.0, calculated exact mass = 426.0820, purity: 98.0%, t_r = 2.650 min.

6.1.2.14 Procedure for Synthesis of 4-((3-(4-(methylsulfinyl)phenyl)imidazo[1,2-*b*]pyridazin-6-yl)amino)tetrahydro-2*H*-thiopyran 1,1-dioxide (41)[3–6]

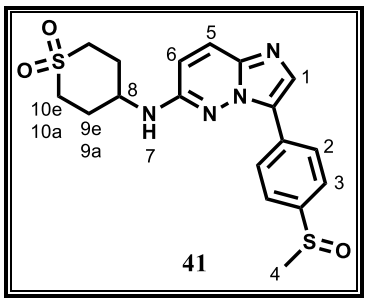

41

A suspension of 6-chloro-3-(4-(methylsulfinyl)phenyl)imidazo[1,2-*b*]pyridazine (**4a**) (0.0700 g, 0.24 mmol), 4-aminotetrahydro-2*H*-thiopyran 1,1-dioxide hydrochloride (0.0483 g, 0.26 mmol), $Pd_2(dba)_3$ (0.0176 g, 0.019 mmol), XPhos (0.0137 g, 0.029 mmol), sodium *tert*-butoxide (0.0461 g, 0.48 mmol) and triethylamine (TEA) (0.2 mL, 0.96 mmol) in 1.5 mL anhydrous 1,4-dioxane in a sealed tube was flashed with nitrogen for 30 minutes. The reaction mixture was then heated to 120 °C and stirred at this temperature for 17 hours. Only small quantities of the desired product were detected on HPLC-MS. At this point, the reaction mixture was charged with additional amounts of the amine hydrochloride (1.1 eq), $Pd_2(dba)_3$ (0.08 eq), TEA (8.0 eq), sodium *tert*-butoxide (2.0 eq) and 0.5 mL anhydrous 1,4-dioxane. The reaction mixture was again purged with nitrogen for 2 minutes after which it was heated to 120 °C and stirred for another 9 hours. The solvent was removed *in vacuo* and the resulting black residue taken up in DCM (50 mL), washed with saturated aqueous solutions of $NaHCO_3$ (30 mL × 3) and NaCl (30 mL × 3). The organic layer was dried ($MgSO_4$) where after the solvent was removed *in vacuo*. The crude mixture was then subjected

to prep-TLC (developed once in 5% CH_3OH/DCM, then twice in 6% CH_3OH/DCM) to afford the aminated target compound **41** as a brown solid (0.0142 g, 15%); m.p. 273.1 – 274.5 °C; R_f (CH_3OH : CH_2Cl_2 6 : 94) 0.38; ^{1}H-NMR δ_H (400 MHz; DMSO-d_6) 8.42 (2H, d, J = 8.5 Hz, H_2), 8.05 (1H, s, H_1), 7.87 – 7.76 (3H, m, H_3, H_5), 7.25 (1H, d, J = 6.7 Hz, H_7), 6.74 (1H, d, J = 9.7 Hz, H_6), 4.15 – 3.98 (1H, m, H_8), 3.46 – 3.27 (2H, m, H_{10e}), 3.25 – 3.14 (2H, m, H_{10a}), 2.80 (3H, s, H_4), 2.48 – 2.35 (2H, m, H_{9e}), 2.16 – 1.98 (2H, m, H_{9a}); ^{13}C-NMR δ_C (101 MHz; DMSO-d_6) 153.01, 144.71, 138.08, 132.05, 131.42, 126.51, 126.36 (2C), 126.18, 124.60 (2C), 113.00, 49.06 (2C), 46.84, 43.68, 29.08 (2C); HPLC-MS, APCI$^+$: *m/z* $[M + H]^+$ = 405.1, calculated exact mass = 404.0977, purity: 97.2%, t_r = 2.434 min.

6.1.2.15 Procedure for Synthesis of *N*-(1-methylpiperidin-4-yl)-3-(4-(methylsulfinyl)phenyl)imidazo[1,2-*b*]pyridazin-6-amine (42)[3–6]

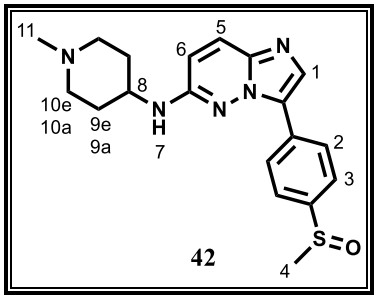

A suspension of 6-chloro-3-(4-(methylsulfinyl)phenyl)imidazo[1,2-*b*]pyridazine (**4a**) (0.0700 g, 0.24 mmol), $Pd_2(dba)_3$ (0.0176 g, 0.019 mmol), XPhos (0.0137 g, 0.029 mmol), and sodium *tert*-butoxide (0.0461 g, 0.48 mmol) in 1.5 mL of anhydrous 1,4-dioxane in a sealed tube was flashed with nitrogen for 20 minutes. 4-Amino-1-methylpiperidine (0.06 mL, 0.48 mmol) was then added and the reaction mixture heated to 100 °C and stirred at this temperature for 22 hours. The solvent was removed *in vacuo* and the resulting black residue taken up in DCM (50 mL), washed with saturated aqueous solutions of $NaHCO_3$ (30 mL × 3) and NaCl (30 mL × 3). The organic layer was dried ($MgSO_4$) after which the solvent was removed *in vacuo*. The resulting residue was subjected to flash column chromatography (0 – 14% CH_3OH/DCM). Further purification by prep-TLC (developed once in 20% CH_3OH/DCM, then once in 25% CH_3OH/DCM) furnished the target compound **20** as a brown solid (0.0121 g, 14%); R_f (CH_3OH : CH_2Cl_2 10 : 90) 0.076; ^{1}H-NMR δ_H (400 MHz; DMSO-d_6) 8.43 (2H, d, J = 8.6 Hz, H_2), 8.02 (1H, s, H_1), 7.87 – 7.66 (3H, m, H_3, H_5), 7.07 (1H, d, J = 6.7 Hz, H_7), 6.75 (1H, d, J = 9.7 Hz, H_6), 3.75 – 3.56 (1H, m, H_8), 2.92 – 2.72 (5H, m, H_4, H_{10e}), 2.24 (3H, s, H_{11}), 2.19 – 2.02 (4H, m, H_{9e}, H_{10a}), 1.65 – 1.43 (2H, m, H_{9a}); ^{13}C-NMR δ_C (101 MHz; DMSO-d_6) 153.28, 144.68, 138.05, 132.23, 131.26, 126.19 (3C), 125.99, 124.30 (2C), 113.18, 54.54 (2C), 48.56, 46.36, 43.66, 31.37 (2C); HPLC-MS, APCI$^+$: *m/z* $[M + H]^+$ = 370.1, calculated exact mass = 369.1623, purity: 99.9%, t_r = 0.230 min.

6.1.2.16 Procedure for Synthesis of *N*-(3-((diethylamino)methyl)-4-fluorophenyl)-3-(4-(methylsulfinyl)phenyl)imidazo[1,2-*b*]pyridazin-6-amine (44)[3–6]

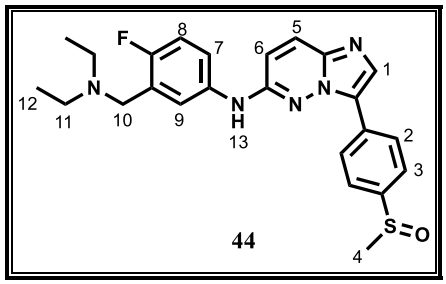

A mixture of 6-chloro-3-(4-(methylsulfinyl)phenyl)imidazo[1,2-*b*]pyridazine (**4a**) (0.070 g, 0.24 mmol), 3-((diethylamino)methyl)-4-fluoroaniline (0.0518 g, 0.26 mmol), $Pd_2(dba)_3$ (0.0088 g, 0.0096 mmol), BrettPhos (0.0077 g, 0.014 mmol), and Cs_2CO_3 in anhydrous 1,4-dioxane (1.7 mL) in a sealed tube was flashed with nitrogen for 25 minutes. The reaction mixture was then heated to 120 °C and stirred for 12 hours. Significant amounts of starting material, as monitored by HPLC-MS, were detected. At this point, an extra 0.04 eq of $Pd_2(dba)_3$ were added and the reaction mixture left to stir for another 4 hours under nitrogen atmosphere. The solvent was removed *in vacuo*. The resulting dark-brown residue was taken up in 100 mL DCM, washed with deionized water (50 mL × 2), saturated aqueous solutions of $NaHCO_3$ (50 mL × 2) and NaCl (50 mL × 2). After drying the organic layer ($MgSO_4$), the solvent was removed *in vacuo*. The obtained crude mixture was subjected to prep-TLC (developed in 5 : 94.5 : 0.5% CH_3OH/DCM/25% aq NH_4OH). The obtained target compound, **44**, was further purified by automated flash column chromatography (0 – 4% CH_3OH/DCM) followed by trituration in diethyl ether to give the title compound as a yellow solid (0.0158 g, 10%); m.p. 118.0 – 120.0 °C; R_f (CH_3OH : CH_2Cl_2 6 : 94) 0.1; ^{1}H-NMR δ_H (300 MHz; $CDCl_3$) 8.24 (2H, d, J = 8.5 Hz, H_2), 7.92 (1H, s, H_1), 7.84 – 7.63 (4H, m, H_3, H_5, H_9), 7.58 – 7.51 (1H, m, H_7), 7.33 (1H, s, H_{13}), 7.04 (1H, t, J = 9.1 Hz, H_8), 6.79 (1H, d, J = 9.5 Hz, H_6), 3.72 (2H, s, H_{10}), 2.81 (3H, s, H_4), 2.65 (4H, q, J = 7.0 Hz, H_{11}), 1.10 (6H, t, J = 7.1 Hz, H_{12}); HPLC-MS, ESI^+/$APCI^+$: *m/z* $[M + H]^+$ = 452.2, calculated exact mass = 451.1842, purity: 98.0%, t_r = 2.549 min.

6.1.2.17 Procedure for Synthesis of 2-((diethylamino)methyl)-4-((3-(4-(methylsulfinyl)phenyl)imidazo[1,2-*b*]pyridazin-6-yl)amino)phenol (45)[3–6]

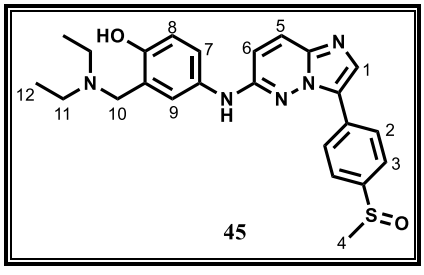

A suspension of 6-chloro-3-(4-(methylsulfinyl)phenyl)imidazo[1,2-*b*]pyridazine (**4a**) (0.100 g, 0.34 mmol), 4-amino-2-((diethylamino)methyl)phenol (0.0733 g, 0.38 mmol), $Pd_2(dba)_3$ (0.0250 g, 0.028 mmol), BrettPhos (0.0220 g, 0.04 mmol) and Cs_2CO_3 (0.222 g, 0.68 mmol) in anhydrous 1,4-dioxane (1.3 mL) in a sealed tube was purged with nitrogen for 30 minutes. The reaction mixture was then heated to 120 °C

and stirred under nitrogen for 18 hours after which the solvent was removed *in vacuo*. The resulting black residue was taken up in DCM (50 mL), washed with deionized water (30 mL × 2), saturated aqueous solutions of $NaHCO_3$ (30 mL × 2) and NaCl (30 mL × 1). After drying ($MgSO_4$) the organic layer, the solvent was removed *in vacuo* where after the crude mixture obtained was subjected to prep-TLC (developed in 8% CH_3OH/DCM) to deliver the aminated compound, **45**, as a brown solid (0.0275 g, 18%); R_f (CH_3OH : CH_2Cl_2 8 : 92) 0.12; R_f (CH_3OH : CH_2Cl_2 8 : 92) 0.12; ^{1}H-NMR δ_H (400 MHz; CD_3OD) 8.32 (2H, d, J = 8.5 Hz, H_2), 7.89 (1H, s, H_1), 7.80 (2H, d, J = 8.5 Hz, H_3), 7.74 (1H, d, J = 9.7 Hz, H_5), 7.54 (1H, d, J = 2.5 Hz, H_9), 7.33 (1H, dd, J = 8.6, 2.7 Hz, H_7), 6.91 (1H, d, J = 9.7 Hz, H_6), 6.75 (1H, d, J = 8.7 Hz, H_8), 3.82 (2H, s, H_{10}), 2.87 (3H, s, H_4), 2.71 (4H, q, J = 7.1 Hz, H_{11}), 1.15 (6H, t, J = 7.2 Hz, H_{12}); ^{13}C-NMR δ_C (100.6; CD_3OD) 153.3, 151.7, 143.3, 137.8, 132.3, 131.9, 129.9, 127.2 (2C), 124.9, 123.8 (2C), 121.9, 120.5 (2C), 116.7, 115.5, 114.0, 56.3, 46.4 (2C), 42.3, 10.2 (2C); HPLC-MS, ESI^+/$APCI^+$: *m/z* $[M + H]^+$ = 450.2, calculated exact mass = 449.1885, purity: 95.0%, t_r = 2.40 min.

6.1.2.18 General Procedure for Synthesis of Diarylated Imidazopyridazines (25 and 50)[1,7–9]

A suspension of 6-chloro-3-iodoimidazo[1,2-*b*]pyridazine (**3a**) (1.0 eq), an appropriate boronic acid (2.2 eq), and $Pd(PPh_3)_2Cl_2$ (0.10 eq) in anhydrous DMF (2.6 mL) was purged with nitrogen for 30 minutes. A 1 M aqueous solution of K_2CO_3 (2.1 eq) was then added. The reaction mixture was heated to 100 °C and left to magnetically stir at this temperature for 24 hours (**28**) and 15 hours (**3**). The reaction mixture was then diluted with DCM (60 mL), washed with deionized water (40 mL × 7), saturated aqueous solutions of $NaHCO_3$ (40 mL × 3), NH_4Cl (40 mL × 3), and NaCl (40 mL × 1). The organic layer was dried (Na_2SO_4), after which the solvent was removed *in vacuo*. The resulting crude mixture was subjected to prep-TLC purification to get the title compounds.

3,6-Bis(3-(methylsulfonyl)phenyl)imidazo[1,2-*b*]pyridazine (50)

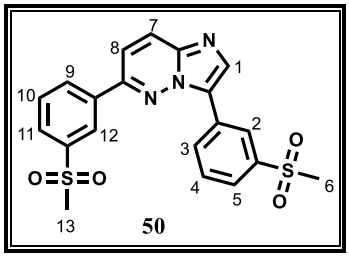

50

Purified by prep-TLC (developed in 4% CH_3OH/DCM). Crystallized in diethyl ether. Yellow solid (0.114 g, 62%); m.p. 228.7 – 230.8 °C; R_f (CH_3OH : CH_2Cl_2 4 : 96) 0.20; ^{1}H-NMR δ_H (400 MHz; $CDCl_3$) 9.17 (1H, s, H_2), 8.71 (1H, s, H_{12}), 8.55 – 8.21 (4H, m, H_1, H_5, H_7, H_{11}), 8.17 (1H, d, J = 7.6 Hz, H_3), 8.04 (1H, d, J = 7.4 Hz, H_9), 7.94 – 7.74 (3H, m, H_4, H_8, H_{10}), 3.24 (3H, s, H_6), 3.22 (3H, s, H_{13}); ^{13}C-

NMR δ_C (101 MHz; $CDCl_3$) 151.08, 142.30, 141.61, 136.18, 132.12 (3C), 131.56, 130.55, 130.11, 129.33 (2C), 127.04 (2C), 126.47, 126.20, 125.47, 117.29, 44.76, 44.53; HPLC-MS, $APCI^+$: *m/z* $[M + H]^+$ = 428.0, calculated exact mass = 427.0660, purity: 95.9%, t_r = 2.586 min.

3,6-Bis(4-(methylsulfinyl)phenyl)imidazo[1,2-*b*]pyridazine (25)

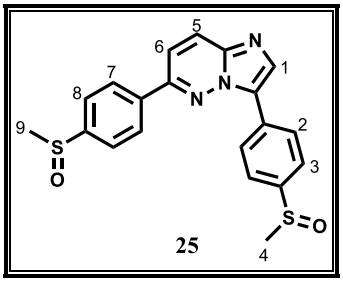

Purified by prep-TLC (developed twice in 5% CH_3OH/DCM). Crystallized in diethyl ether. Yellow solid (0.0665 g, 39%); m.p. 180.4 – 182.3 °C; R_f (CH_3OH : CH_2Cl_2 4 : 96) 0.21; ^{1}H-NMR δ_H (400 MHz; DMSO-d_6) 8.48 (2H, d, *J* = 8.8 Hz, H_7), 8.45 (1H, s, H_1), 8.39 (1H, d, *J* = 9.6 Hz, H_5), 8.35 (2H, d, *J* = 8.7 Hz, H_2), 7.99 (1H, d, *J* = 9.6 Hz, H_6), 7.91 (2H, d, *J* = 8.6 Hz, H_3), 7.89 (2H, d, *J* = 8.8 Hz, H_8), 2.84 (3H, s, H_9), 2.83 (3H, s, H_4); ^{13}C-NMR δ_C (101 MHz; DMSO-d_6) 151.04, 148.96, 145.89, 140.15, 137.75, 135.09, 131.10, 128.43 (2C), 127.23 (3C), 127.13, 124.91 (2C), 124.68 (2C), 116.98, 43.67 (2C); HPLC-MS, $APCI^+$: *m/z* $[M + H]^+$ = 396.0, calculated exact mass = 395.0762, purity: 98.5%, t_r = 2.563 min.

6.1.2.19 Procedure for Synthesis of 6-(3-(methylsulfinyl)phenyl)imidazo[1,2-*b*]pyridazine (6a)[1,7–9]

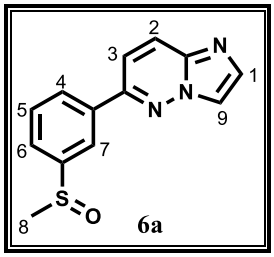

A suspension of 6-chloroimidazo[1,2-*b*]pyridazine (**2a**) (1.50 g, 9.8 mmol), 3-methylsulfinylphenylboronic acid (1.78 g, 9.8 mmol), and $Pd(PPh_3)_2Cl_2$ (0.344 g, 0.49 mmol) in anhydrous DMF (30 mL) was purged with nitrogen for 30 minutes. A 1 M aqueous solution of K_2CO_3 (1.42 g, 10.29 mmol) was then added. The reaction mixture was heated to 100 °C and magnetically stirred at this temperature for 3.25 hours. The black reaction mixture was then diluted with DCM (150 mL), washed with deionized water (75 mL × 8), saturated aqueous solutions of $NaHCO_3$ (75 mL × 3), NH_4Cl (75 mL × 1) and NaCl (50 mL × 5). After drying ($MgSO_4$) the organic layer, the solvent was removed *in vacuo* and the resulting crude mixture subjected to flash column chromatography (0 – 5% CH_3OH/DCM) to afford the phenylated intermediate, **6a** which was further crystallized in diethyl ether to obtain a yellow solid (1.20 g, 48%); ^{1}H-NMR δ_H (400 MHz; $CDCl_3$) 8.36 (1H, td, *J* = 1.8, 0.6 Hz, H_7), 8.25 (1H, d, *J* = 9.6 Hz, H_2), 8.15 (1H, dt, *J* = 7.7, 1.7 Hz, H_4), 8.10 (1H, d, *J* = 1.3 Hz, H_9), 7.89 (1H, d, *J* = 1.4 Hz, H_1), 7.78 (1H, dt, *J* = 7.8, 1.5 Hz, H_6), 7.74 (1H, td, *J* = 7.6, 0.6 Hz, H_5), 7.69 (1H, d, *J* = 9.5 Hz, H_3), 2.84 (3H, s, H_8); HPLC-MS, ESI^+: *m/z* $[M + H]^+$ = 258.1, calculated exact mass = 257.0623, t_r = 3.1 min.

6.1.2.20 Procedure for Synthesis of 3-bromo-6-(3-(methylsulfinyl)phenyl)imidazo[1,2-*b*]pyridazine (6b)[1,9]

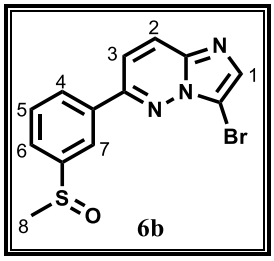

A brown solution of 6-(3-(methylsulfinyl)phenyl)imidazo[1,2-*b*]pyridazine (**6a**) (1.20 g, 4.7 mmol) in anhydrous DMF (4 mL) was purged with nitrogen for 30 minutes. NBS (0.912 g, 5.1 mmol) was added where after the reaction mixture was stirred at room temperature (23 °C) for 22 hours. The reaction mixture, containing a yellow precipitate at this point, was taken up in 100 mL DCM and washed with deionized water (75 mL × 8), saturated aqueous solutions of $NaHCO_3$ (75 mL × 2), NH_4Cl (75 mL × 2) and NaCl (75 mL × 1). The organic layer was dried ($MgSO_4$) after which the solvent was removed *in vacuo*. The obtained oily residue was crystallized and triturated with ethyl acetate for 30 minutes. The solid was filtered and washed with ethyl acetate to give **6b** as a yellow solid (0.939 g, 59%); ^{1}H-NMR δ_H (300 MHz; $CDCl_3$) 8.44 – 8.35 (2H, m, H_2, H_7), 8.29 – 8.23 (1H, m, H_4), 7.93 (1H, s, H_1), 7.90 – 7.73 (3H, m, H_3, H_5, H_6), 2.85 (3H, s, H_8); HPLC-MS, ESI$^+$: *m/z* $[M + H]^+$ = 336.0 & 338.0, calculated exact mass = 334.9728, t_r = 3.9 min.

6.1.2.21 Procedure for Synthesis of 3,6-bis(3-(methylsulfinyl)phenyl)imidazo[1,2-*b*]pyridazine (35)[1,7–9]

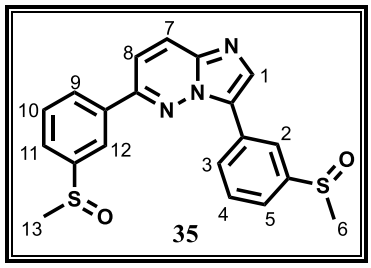

A suspension of 3-bromo-6-(3-(methylsulfinyl)phenyl)imidazo[1,2-*b*]pyridazine (**6b**) (0.100 g, 0.30 mmol), 3-methylsulfinylphenylboronic acid (0.0602 g, 0.33 mmol), and $Pd(PPh_3)_2Cl_2$ (0.0105 g, 0.015 mmol) in anhydrous DMF (2.0 mL) was purged with nitrogen for 30 minutes. A 1 M aqueous solution of K_2CO_3 (0.0435 g, 0.32 mmol) was then added. The reaction mixture was heated to 100 °C and magnetically stirred at this temperature for 20 hours. The reaction mixture was then diluted with DCM (60 mL), washed with deionized water (40 mL × 6), saturated aqueous solutions of $NaHCO_3$ (40 mL × 3), NH_4Cl (40 mL × 3) and NaCl (40 mL × 1). The organic layer was dried ($MgSO_4$), where after the solvent was removed *in vacuo*. The resulting crude mixture was subjected to prep-TLC (developed twice in 4% CH_3OH/DCM) to get **35** as an oil. Crystallization with diethyl ether gave **35** as a yellow solid (0.0481 g, 40%); R_f (CH_3OH : CH_2Cl_2 4 : 96) 0.17; ^{1}H-NMR δ_H (400 MHz; DMSO-d_6) 8.80 (1H, m, H_2), 8.48 – 8.42 (2H, m, H_1, H_{12}), 8.42 – 8.35 (2H, m, H_7, H_9), 8.33 (1H, dt, *J* = 7.6, 1.6 Hz, H_5), 8.03 (1H, d, *J* = 9.5 Hz, H_8), 7.94 – 7.88 (1H, m, H_{11}), 7.82 (1H, t, *J* = 7.7 Hz, H_{10}), 7.76 (1H, t, *J* = 7.7 Hz, H_4), 7.73 – 7.69 (1H, m, H_3), 2.88 (3H, s, H_6), 2.86 (3H, s, H_{13}); ^{13}C-NMR δ_C (101 MHz;

DMSO-d_6) 150.75, 148.34, 147.67, 140.06, 136.44, 134.81, 130.65, 130.14, 129.89, 129.73, 128.72, 127.15, 127.08, 125.63, 123.28, 122.60, 121.19, 116.75, 43.97, 43.82; HPLC-MS, APCI$^+$: *m/z* $[M + H]^+$ = 396.0, calculated exact mass = 395.0762, purity: 99.8% t_r = 2.525 min.

6.1.2.22 General Procedure for Synthesis of Aminated Analogues (46 - 49)[3–6]

A suspension of 3-bromo-6-(3-(methylsulfinyl)phenyl)imidazo[1,2-*b*]pyridazine (**6b**) (1.0 eq), an appropriate amine (1.3 eq), $Pd_2(dba)_3$ (0.2 eq), BrettPhos (0.12 eq) and Cs_2CO_3 (2.0 eq) in anhydrous 1,4-dioxane (2 mL) in a sealed tube was flashed with nitrogen for 20 minutes. The reaction mixture was then heated to 120 °C and stirred for 5 - 39 hours. The solvent was removed *in vacuo* after which the resulting black residue was taken up in DCM (60 mL), washed with saturated aqueous solutions of $NaHCO_3$ (40 mL × 3) and NaCl (40 mL × 1). The organic layer was dried (Na_2SO_4), after which the solvent was removed *in vacuo* and the crude mixture further purified.

6-(3-(Methylsulfinyl)phenyl)-*N*-(4-(methylsulfonyl)phenyl)imidazo[1,2-*b*]pyridazin-3-amine (46)

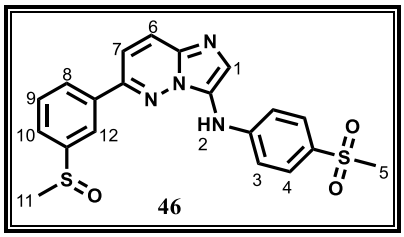

Purified by prep-TLC (developed thrice in 2.5% CH_3OH/DCM). Crystallized in diethyl ether. Brown solid (0.0121 g, 9%); m.p. 105.0 – 107.2 °C; R_f (CH_3OH : CH_2Cl_2 4 : 96) 0.23; ^{1}H-NMR δ_H (400 MHz; DMSO-d_6) 9.13 (1H, s, H_2), 8.32 – 8.25 (2H, m, H_6, H_{12}), 8.18 (1H, d, *J* = 7.7 Hz, H_8), 7.91 – 7.80 (3H, m, H_1, H_7, H_{10}), 7.78 – 7.68 (3H, m, H_3, H_9), 6.99 (2H, d, *J* = 8.4 Hz, H_4), 3.11 (3H, s, H_5), 2.80 (3H, s, H_{11}); ^{13}C-NMR δ_C (101 MHz; DMSO-d_6) 150.57, 149.91, 148.01, 136.65, 135.99, 130.46, 130.33, 129.64, 129.31 (2C), 127.66, 127.04, 126.95, 125.62, 122.61, 115.86, 114.13 (2C), 44.75, 43.63; HPLC-MS, APCI$^+$: *m/z* $[M + H]^+$ = 427.0, calculated exact mass = 426.0820, purity: 97.7%, t_r = 2.534 min.

6-(3-(Methylsulfinyl)phenyl)-*N*-(3-(methylsulfonyl)phenyl)imidazo[1,2-*b*]pyridazin-3-amine (47)

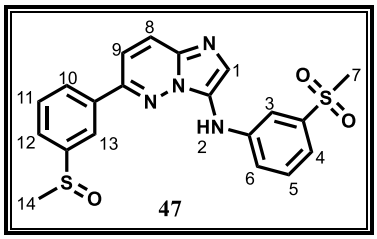

Purified by flash column chromatography (0 - 4% CH_3OH/DCM), trituration in diethyl ether. Brown solid (0.0127 g, 10%); m.p. 150.4 – 152.0 °C; R_f (CH_3OH : CH_2Cl_2 4 : 96) 0.19; ^{1}H-NMR δ_H (400 MHz; DMSO-d_6) 9.09 (1H, s, H_2), 8.38 (1H, d, J = 9.5 Hz, H_8), 8.29 (1H, s, H_{13}), 8.22 (1H, d, J = 7.9 Hz, H_{10}), 8.05 (1H, d, J = 9.6 Hz, H_9), 8.02 (1H, s, H_1), 7.86 (1H, d, J = 7.8 Hz, H_{12}), 7.77 (1H, t, J = 7.8 Hz, H_{11}), 7.50 (1H, t, J = 7.9 Hz, H_5), 7.45 (1H, s, H_3), 7.36 (1H, d, J = 7.6 Hz, H_6), 7.24 (1H, dd, J = 8.1, 2.3 Hz, H_4), 3.16 (3H, s, H_7), 2.81 (3H, s, H_{14}); ^{13}C-NMR δ_C (101 MHz; DMSO-d_6) 151.43, 148.10, 145.50, 142.26, 136.13, 134.94, 130.83, 130.55, 129.79, 128.30, 125.97, 125.83, 122.75 (2C), 119.50, 117.75 (2C), 112.76, 44.03, 43.62; HPLC-MS, APCI$^+$: *m/z* $[M + H]^+$ = 427.1, calculated exact mass = 426.0820, purity: 95.1%, t_r = 2.555 min.

***N*,6- Bis(3-(methylsulfinyl)phenyl)imidazo[1,2-*b*]pyridazin-3-amine (48)**

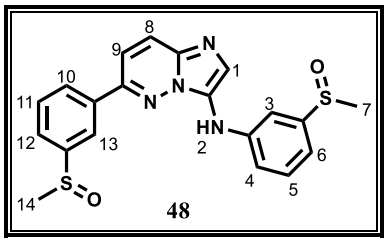

Purified by prep-TLC (developed in 4% CH_3OH/DCM). Crystallized in diethyl ether. Brick-red solid (0.0186 g, 15%); m.p. 110.0 – 113.5 °C; R_f (CH_3OH : CH_2Cl_2 4 : 96) 0.15; ^{1}H-NMR δ_H (400 MHz; DMSO-d_6) 8.90 (1H, s, H_2), 8.35 – 8.27 (2H, m, H_8, H_{13}), 8.23 (1H, d, J = 7.9 Hz, H_{10}), 8.00 – 7.90 (2H, m, H_1, H_9), 7.86 (1H, d, J = 7.8 Hz, H_{12}), 7.76 (1H, t, J = 7.7 Hz, H_{11}), 7.41 (1H, t, J = 7.9 Hz, H_5), 7.24 (1H, s, H_3), 7.07 (2H, m, H_4, H_6), 2.81 (3H, s, H_{14}), 2.69 (3H, s, H_7); ^{13}C-NMR δ_C (101 MHz; DMSO-d_6) 150.92, 148.05 (2C), 145.68, 136.37, 135.03, 130.50 (2C), 129.73, 128.59, 126.18, 125.77, 123.92, 122.72, 116.94, 116.61, 114.38, 109.29, 43.81, 43.62; HPLC-MS, APCI$^+$: *m/z* $[M + H]^+$ = 411.1, calculated exact mass = 410.0871, purity: 96.6%, t_r = 2.476 min.

6-(3-(Methylsulfinyl)phenyl)-*N*-(4-(methylsulfinyl)phenyl)imidazo[1,2-*b*]pyridazin-3-amine (49)

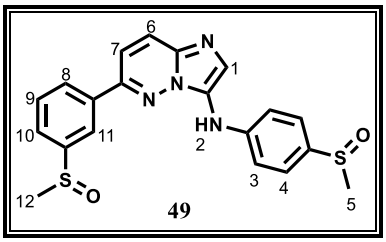

Purified by prep-TLC (developed twice in 6% CH_3OH/DCM), trituration in diethyl ether. Brown solid (0.0204 g, 17%); m.p. 161.6 – 163.7 °C; ^{1}H-NMR δ_H (400 MHz; DMSO-d_6) 8.83 (1H, s, H_2), 8.29 (1H, d, J = 1.8 Hz, H_{11}), 8.25 (1H, d, J = 9.6 Hz, H_6), 8.20 (1H, d, J = 7.8 Hz, H_8), 7.87 – 7.81 (3H, m, H_1, H_7,

H_{10}), 7.75 (1H, t, *J* = 7.8 Hz, H_9), 7.53 (2H, d, *J* = 8.6 Hz, H_3), 7.03 (2H, d, *J* = 8.4 Hz, H_4), 2.81 (3H, s, H_{12}), 2.69 (3H, s, H_5); ^{13}C-NMR δ_C (101 MHz; DMSO-d_6) 150.41, 147.99, 147.68, 136.69, 135.60, 135.32, 130.45, 129.64, 127.95, 126.83, 126.71, 125.84 (2C), 125.56, 122.63, 115.43, 114.92 (2C), 43.75, 43.63; HPLC-MS, APCI$^+$: *m/z* $[M + H]^+$ = 411.1, exact mass = 410.0871, purity: 99.9%, t_r = 2.450 min.

6.1.2.23 Procedure for Synthesis of 4-(6-chloroimidazo[1,2-*b*]pyridazin-3-yl)benzoic acid (7a)[1,7–9]

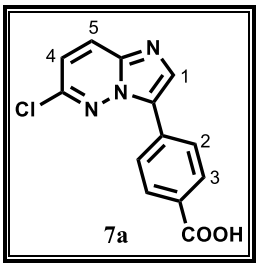

A suspension of 6-chloro-3-iodoimidazo[1,2-*b*]pyridazine (**3a**) (1.00 g, 3.6 mmol), 4-carboxylphenylboronic acid (0.657 g, 4.0 mmol) and $Pd(PPh_3)_2Cl_2$ (0.126 g, 0.18 mmol) in DMF (10 mL) was purged with nitrogen for 20 minutes. A 1 M aqueous solution of K_2CO_3 (0.522 g, 3.8 mmol) was added after which the reaction mixture was heated to 80 °C and left to stir for 27 hours. DMF was then removed under reduced pressure and the resulting yellow residue subjected to automated flash chromatography (silica, 0 – 8% CH_3OH/DCM) to afford the carboxylic acid intermediate, **7a**, as a yellow solid (0.555 g, 56%); ^{1}H-NMR δ_H (300 MHz; DMSO-d_6) 8.45 (1H, s, H_1), 8.34 (1H, d, *J* = 9.5 Hz, H_5), 8.26 (2H, d, *J* = 8.6 Hz, H_3), 8.09 (2H, d, *J* = 8.6 Hz, H_2), 7.48 (1H, d, *J* = 9.5 Hz, H_4); HPLC-MS, ESI$^+$/APCI$^+$: *m/z* $[M + H]^+$ = 274.0, calculated exact mass = 273.0305.

6.1.2.24 General Procedure for Synthesis of Carboxylic Acid Intermediates (7b - d)[1,7–9]

A suspension of 4-(6-chloroimidazo[1,2-*b*]pyridazin-3-yl)benzoic acid (**7a**) (1.0 eq), the appropriate substituted arylboronic acid (1.5 eq) and $Pd(PPh_3)_2Cl_2$ (0.05 eq) in DMF (3 mL/mmol of halogenated starting material) was flashed with nitrogen for 20 minutes. A 1 M aqueous solution of K_2CO_3 (1.05 eq) was then added. The reaction mixture was heated to 100 °C and left to stir for 22 hours. DMF was removed under reduced pressure and the resulting crude reaction mixture subjected to manual glass tube column chromatography (silica, 0 – 10% CH_3OH/DCM) to give carboxy-substituted intermediates **7b** and **7c**. For intermediate **7d**, a bromo-substituted starting material (see scheme 2.5 in chapter 2) was used as opposed to the chloro-substituted derivative. For this intermediate, the reaction mixture was stirred at 100 °C for 30 hours. DMF was removed *in vacuo* and the resulting residue subjected to manual glass tube column chromatography employing two separate sets of mobile phase solvent systems. Impurities were eluted from the column using a 50% EtOAc/hexane mobile phase after which

a 4% CH_3OH/DCM mobile phase was employed to elute the carboxy-substituted compound **7d**.

4-(6-(3-(Methylsulfinyl)phenyl)imidazo[1,2-*b*]pyridazin-3-yl)benzoic acid (7b)

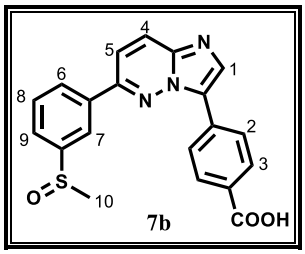

Manual glass tube column chromatography (silica, 0 - 10% CH_3OH/DCM). Yellow solid (0.159 g, 95%); ^{1}H-NMR δ_H (300 MHz; CD_3OD) 8.48 (1H, t, *J* = 1.5 Hz, H_7), 8.36 (2H, d, *J* = 8.8 Hz, H_3), 8.33 – 8.28 (2H, m, H_6, H_9), 8.24 (1H, s, H_1), 8.19 (2H, d, *J* = 8.8 Hz, H_2), 7.95 (1H, d, *J* = 9.6 Hz, H_4), 7.91 - 7.86 (1H, m, H_8), 7.84 (1H, d, *J* = 9.5 Hz, H_5), 2.92 (3H, s, H_{10}); HPLC-MS, ESI$^+$/APCI$^+$: *m/z* $[M + H]^+$ = 378.1, calculated exact mass = 377.0834.

4-(6-(3-(Trifluoromethyl)phenyl)imidazo[1,2-*b*]pyridazin-3-yl)benzoic acid (7c)

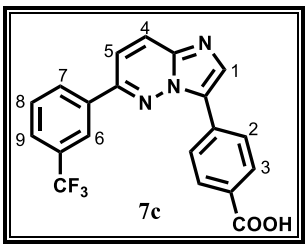

Manual glass tube column chromatography (silica, 1.5 - 4% CH_3OH/DCM). Yellow solid (0.152 g, 54%); ^{1}H-NMR δ_H (300 MHz; DMSO-d_6) 8.53 – 8.44 (3H, m, H_1, H_4, H_6), 8.43 – 8.35 (3H, m, H_3, H_5), 8.14 – 8.06 (3H, m, H_2, H_7), 7.96 (1H, d, *J* = 8.6 Hz, H_9), 7.87 (1H, t, *J* = 7.7 Hz, H_8); HPLC-MS, ESI$^+$/APCI$^+$: *m/z* $[M + H]^+$ = 384.0, calculated exact mass = 383.0882, t_r = 4.6 min.

4-(6-(3-(Methylsulfonyl)phenyl)imidazo[1,2-*b*]pyridazin-3-yl)benzoic acid (7d)

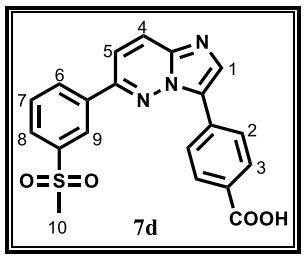

Manual glass tube column chromatography (silica, 50% EtOAc/hexane, then 4% CH_3OH/DCM). Yellow solid (0.108 g, 39%); ^{1}H-NMR δ_H (400 MHz; DMSO-d_6) 8.67 (1H, t, *J* = 1.7 Hz, H_9), 8.56 – 8.51 (1H, m, H_8), 8.49 (1H, s, H_1), 8.46 – 8.39 (3H, m, H_3, H_4), 8.17 – 8.10 (3H, m, H_2, H_6), 8.08 (1H, d, *J* = 9.5 Hz, H_5), 7.91 (1H, t, *J* = 7.9 Hz, H_7), 3.35 (3H, s, H_{10}); HPLC-MS, ESI$^+$/APCI$^+$: *m/z* $[M + H]^+$ = 394.1, calculated exact mass = 393.0783, t_r = 3.4 min.

6.1.2.25 Procedure for Synthesis of 4-(6-(3-(methylsulfinyl)phenyl)imidazo[1,2-*b*]pyridazin-3-yl)-*N*-((trimethylsilyl)methyl)benzamide (55)[10]

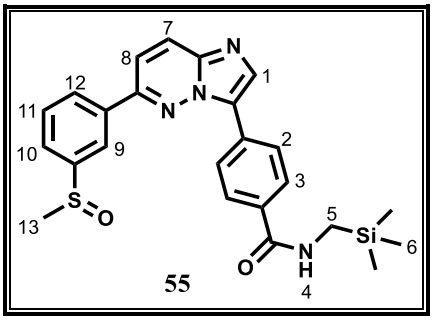

EDCI (0.162 g, 0.84 mmol) was added to a suspension of 4-(6-(3-(Methylsulfinyl)phenyl)imidazo[1,2-*b*]pyridazin-3-yl)benzoic acid (**7b**) (0.159 g, 0.42 mmol) and DMAP (0.103 g, 0.84 mmol) in DCM (4 mL). The resulting mixture was left to stir for 30 minutes under nitrogen before adding (trimethylsilyl)methylamine (0.100 mL, 0.75 mmol). The resulting reaction mixture was then left to stir for another 20 hours with no significant amount of the product being detected on HPLC-MS. The reaction appeared inhibited by poor solubility of the carboxylic acid starting material in DCM. DMF (0.6 mL) was, therefore, added and the reaction mixture stirred for another 40 hours after which a drastic improvement of conversion to the product was observed. The reaction mixture was then washed with saturated aqueous solutions of $NaHCO_3$ (1 ×), NH_4Cl (1 ×) and NaCl (1 ×). The organic layer was dried ($MgSO_4$) and concentrated *in vacuo* where after the obtained residue was subjected to prep-TLC (developed in 4% CH_3OH/DCM) to furnish **55** as a yellow solid (0.0191 g, 10%); m.p. 130.9 – 132.0 °C; R_f (CH_3OH : CH_2Cl_2 6 : 94) 0.45; ^{1}H-NMR δ_H (300 MHz; CD_3OD) 8.48 (1H, s, H_1), 8.42 – 8.19 (5H, m, H_3, H_4, H_7, H_8), 8.11 - 7.76 (6H, m, H_2, H_9, H_{10}, H_{11}, H_{12}), 3.00 (2H, s, H_5), 2.91 (3H, s, H_{13}), 0.17 (9H, s, H_6); ^{13}C-NMR δ_C (100.6 MHz; CD_3OD) 168.5, 152.0, 146.5, 137.3, 134.5, 132.0, 130.2, 129.7, 129.0, 127.3 (3C), 126.5 (2C), 125.4 (3C), 122.1, 118.0, 30.5, 22.6, -3.6 (3C); HPLC-MS, ESI$^+$/APCI$^+$: *m/z* $[M + H]^+$ = 463.1, calculated exact mass = 462.1546, purity: 96.7%, t_r = 2.820 min.

6.1.2.26 Procedure for Synthesis of 4-(6-(3-(methylsulfonyl)phenyl)imidazo[1,2-*b*]pyridazin-3-yl)-*N*-((trimethylsilyl)methyl)benzamide (57)[10]

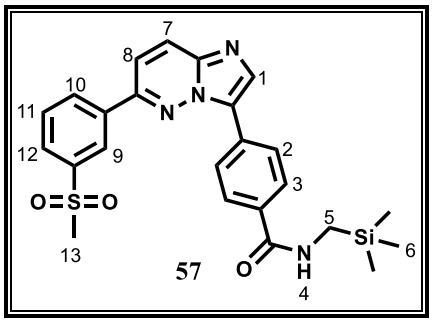

EDCI (0.105 g, 0.55 mmol) was added to a suspension of 4-(6-(3-(Methylsulfonyl)phenyl)imidazo[1,2-*b*]pyridazin-3-yl)benzoic acid (**7d**) (0.108 g, 0.27 mmol) and DMAP (0.067 g, 0.55 mmol) in DCM (3 mL). The resulting mixture was left to stir for 30 minutes under nitrogen before adding (trimethylsilyl)methylamine (0.200 mL, 1.4 mmol). The resulting reaction mixture was then left to stir for another 16 hours with no significant amount of the product being detected on HPLC-MS. DMF (0.5 mL) was added followed by 5.0 eq of (trimethylsilyl)methylamine. The reaction flask was then sealed and heated to 36 °C.

The reaction was allowed to proceed at this temperature for another 21 hours. The reaction mixture was diluted with DCM before washing with saturated aqueous solutions of $NaHCO_3$ (3 ×), NH_4Cl (2 ×) and NaCl (1 ×). The organic layer was dried (Na_2SO_4) and concentrated *in vacuo*. The obtained residue was subjected to manual glass tube column chromatography (1.5% CH_3OH/DCM) to deliver **57** as a yellow solid (0.0248 g, 19%); m.p. 209.8 – 211.0 °C; R_f (CH_3OH : CH_2Cl_2 6 : 94) 0.48; ^{1}H-NMR δ_H (300 MHz; $CDCl_3$) 8.56 (1H, t, J = 1.6 Hz, H_9), 8.35 (1H, d, J = 8.2 Hz, H_{12}), 8.26 – 8.15 (4H, m, H_1, H_3, H_7), 8.10 (1H, d, J = 8.3 Hz, H_{10}), 7.92 (2H, d, J = 8.5 Hz, H_2), 7.79 (1H, t, J = 7.8 Hz, H_{11}), 7.62 (1H, d, J = 9.5 Hz, H_8), 6.18 (1H, t, J = 5.5 Hz, H_4), 3.16 (3H, s, H_{13}), 3.03 (2H, d, J = 5.8 Hz, H_5), 0.18 (9H, s, H_6); HPLC-MS, $ESI^+/APCI^+$: *m/z* $[M + H]^+$ = 479.1, calculated exact mass = 478.1495, purity: 97.1%, t_r = 2.903 min.

6.1.2.27 Procedure for Synthesis of 4-(6-(3-(trifluoromethyl)phenyl)imidazo[1,2-*b*]pyridazin-3-yl)-*N*-((trimethylsilyl)methyl)benzamide (56)[10]

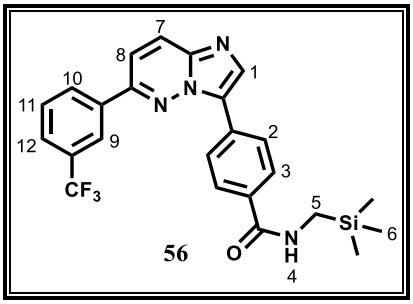

EDCI (0.153 g, 0.80 mmol) was added to a suspension of 4-(6-(3-(trifluoromethyl)phenyl)imidazo[1,2-*b*]pyridazin-3-yl)benzoic acid (**7c**) (0.152 g, 0.40 mmol) and DMAP (0.0977 g, 0.80 mmol) in DMF (4 mL). The resulting mixture was left to stir for 30 minutes under nitrogen before adding (trimethylsilyl)methylamine (0.270 mL, 2.0 mmol). The reaction mixture was then left to stir for another 20 hours. The reaction mixture was diluted with DCM and washed with saturated aqueous solutions of $NaHCO_3$ (2 ×), NH_4Cl (1 ×) and NaCl (2 ×). The organic layer was dried over Na_2SO_4, concentrated *in vacuo* after which the obtained residue was chromatographed using a manual glass tube column (1.0% CH_3OH/DCM). Further purification by trituration in diethyl ether afforded **56** as a yellow solid (0.028 g, 15%); m.p. 174.2 °C; R_f (CH_3OH : CH_2Cl_2 6 : 94) 0.41; ^{1}H-NMR δ_H (300 MHz; $CDCl_3$) 8.31 – 8.17 (6H, m, H_1, H_3, H_7, H_8, H_9), 7.92 (2H, d, J = 8.2 Hz, H_2), 7.81 (1H, d, J = 7.6 Hz, H_{10}), 7.72 (1H, d, J = 7.6 Hz, H_{12}), 7.69 – 7.60 (1H, m, H_{11}), 6.15 (1H, t, J = 5.8 Hz, H_4), 3.04 (2H, d, J = 5.7 Hz, H_5), 0.18 (9H, s, H_6); ^{13}C-NMR δ_C (100.6 MHz; $CDCl_3$) 167.1, 150.8, 136.3, 134.5, 133.3, 131.8 (q, J = 32.7 Hz), 130.9, 130.3, 129.8 (2C). 127.3 (2C), 126.9, 126.7 (2C), 126.4, 125.2, 123.9, 122.5, 116.0, 30.5, -2.5 (3C); HPLC-MS, $ESI^+/APCI^+$: *m/z* $[M + H]^+$ = 469.2, calculated exact mass = 468.1593, purity: 98.1%, t_r = 3.190 min.

6.1.3 Synthetic Methods for Aminopyrazines

6.1.3.1 Procedure for Synthesis of 5-bromo-3-(6-(trifluoromethyl)pyridin-3-yl)pyrazin-2-amine (7g)[11]

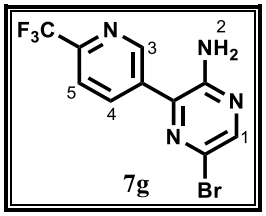

A yellow solution of 5-bromo-3-iodopyrazin-2-amine (**7f**) (1.00 g, 3.3 mmol) and 2-(trifluoromethyl)pyridine-5-boronic acid pinacol ester (0.991 g, 3.6 mmol) in 13 mL anhydrous 1,4-dioxane was degassed with nitrogen for 20 minutes. $Pd(PPh_3)_2Cl_2$ (0.116 g, 0.17 mmol) and a 1 M aqueous solution of K_2CO_3 (1.37 g, 9.9 mmol) were then added. The reaction mixture was heated to 110 °C and left to stir for 20 hours. The reaction mixture was diluted with water (70 mL) and extracted with EtOAc (100 mL × 3). The pooled organic layers were then washed with saturated aqueous NaCl (100 mL × 3). The organic layer was dried (Na_2SO_4) where after the solvent was removed *in vacuo*. The obtained residue was subjected to flash column chromatography (0 - 15% EtOAc/hexane) to deliver **7g** as a yellow solid (0.4564 g, 43%); ^{1}H-NMR δ_H (300 MHz; $CDCl_3$) 9.16 (1H, s, H_3), 8.30 (1H, d, J = 7.8 Hz, H_4), 8.20 (1H, s, H_1), 7.85 (1H, d, J = 8.2 Hz, H_5), 4.84 (2H, s, H_2); HPLC-MS, APCI$^-$: *m/z* $[M - H]^-$ = 317.0 & 319.9, calculated exact mass = 317.9728, t_r = 3.0 min.

6.1.3.2 Procedure for Synthesis of *tert*-butyl 4-(5-amino-6-(6-(trifluoromethyl)pyridin-3-yl)pyrazin-2-yl)-3,6-dihydropyridine-1(2*H*)-carboxylate (59)[11]

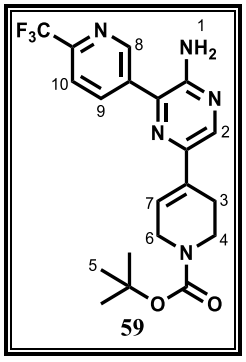

A suspension of 5-bromo-3-(6-(trifluoromethyl)pyridin-3-yl)pyrazin-2-amine (**7g**) (0.162 g, 0.51 mmol), 3,6-dihydro-2*H*-pyridine-1-*N*-boc-4-boronic acid pinacol ester (0.173 g, 0.56 mmol) and $Pd(PPh_3)_2Cl_2$ (0.0179 g, 0.026 mmol) in 3 mL anhydrous 1,4-dioxane was degassed with nitrogen for 20 minutes. A 1 M aqueous solution of K_2CO_3 (0.212 g, 1.53 mmol) was then added. The reaction mixture was heated to 110 °C and left to stir for 13 hours. The solvent was removed *in vacuo*. The remaining residue was taken up in DCM (70 mL) and washed with deionized water (40 mL × 1) and saturated aqueous NaCl (40 mL × 3). The organic layer was dried (Na_2SO_4) after which the solvent was removed *in vacuo*. The obtained residue was subjected to flash column chromatography (0 - 3% MeOH/DCM). Further purification by trituration in diethyl ether delivered **59** as a yellow solid (0.1289 g, 21%); m.p. 193 – 195 °C; R_f (CH_3OH : CH_2Cl_2 8 : 92) 0.49; ^{1}H-NMR δ_H (400 MHz; $CDCl_3$) 9.19 (1H, d, J = 2.0 Hz, H_8), 8.36 – 8.31 (1H, m, H_9), 8.16 (1H, s, H_2), 7.86 (1H, dd, J = 8.1, 0.8 Hz, H_{10}), 6.57 (1H, br s, H_7), 5.25 (2H, br s, H_1), 4.15 (2H, d, J = 3.1 Hz, H_6), 3.67 (2H, t, J = 5.7 Hz, H_4), 2.63 (2H, br s, H_3), 1.51 (9H, s, H_5);

^{13}C-NMR δ_C (101 MHz; $CDCl_3$) 154.79, 149.95, 149.50, 148.45 (q, *J* = 34.94 Hz), 143.74, 137.21, 135.57, 135.52, 132.05 (2C), 123.26 (2C), 120.65, 79.86, 43.68, 39.61, 28.47 (3C), 25.47; HPLC-MS, APCI$^-$: *m/z* $[M - H]^-$ = 420.1, calculated exact mass = 421.1726, purity: 99.9%, t_r = 2.919 min.

6.1.3.3 Procedure for Synthesis of *tert*-butyl 4-(5-amino-6-(6-(trifluoromethyl)pyridin-3-yl)pyrazin-2-yl)piperidine-1-carboxylate (60)[12]

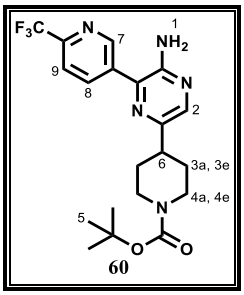

60

A suspension of *tert*-butyl 4-(5-amino-6-(6-(trifluoromethyl)pyridin-3-yl)pyrazin-2-yl)-3,6-dihydropyridine-1(2*H*)-carboxylate (**59**) (0.0602 g, 0.14 mmol), ammonium formate (NH_4HCO_2) (0.0631 g, 7.7 mmol) and 10% carbon-supported palladium (Pd/C) (0.0149 g, 0.14 mmol) in 2 mL anhydrous methanol in a sealed tube was evacuated. The reaction mixture was then left to stir at room temperature (24 °C) under an atmosphere of hydrogen captured in a balloon for 2.5 hours. The reaction mixture was filtered through a filter paper to remove the Pd/C catalyst after which the filtrate was concentrated *in vacuo*. The obtained residue was taken up in DCM (50 mL) and washed with deionized water (30 mL) and saturated aqueous NaCl (30 mL × 1). The organic layer was dried (Na_2SO_4) and concentrated under reduced pressure. The obtained residue was subjected to prep-TLC (silica, developed once in 2% CH_3OH/DCM) to give **60** which was crystallized in diethyl ether to furnish a yellow solid (0.054 g, 68%); m.p. 151 – 154 °C; R_f (CH_3OH : CH_2Cl_2 8 : 92) 0.46; ^{1}H-NMR δ_H (400 MHz; $CDCl_3$) 9.19 – 9.15 (1H, m, H_7), 8.32 (1H, d, *J* = 8.0 Hz, H_8), 7.95 (1H, s, H_2), 7.85 (1H, d, *J* = 8.0 Hz, H_9), 5.12 (2H, br s, H_1), 4.38 – 4.17 (2H, m, H_{4e}), 2.96 – 2.78 (3H, m, H_{4a}, H_6), 2.00 – 1.87 (2H, m, H_{3e}), 1.84 – 1.68 (2H, m, H_{3a}), 1.49 (9H, s, H_5); ^{13}C-NMR δ_C (101 MHz; $CDCl_3$) 154.76, 150.06, 149.96, 149.41, 148.52, 137.65, 137.27, 136.00, 135.69, 120.63, 119.99, 79.58, 43.91 (2C), 40.94, 31.39 (2C), 28.47 (3C); HPLC-MS, APCI$^-$: *m/z* $[M - H]^-$ = 422.1, calculated exact mass = 423.1882, purity: 99.6%, t_r = 2.824 min.

6.1.3.4 Procedure for Synthesis of 5-(piperidin-4-yl)-3-(6-(trifluoromethyl)pyridin-3-yl)pyrazin-2-amine (61)[13]

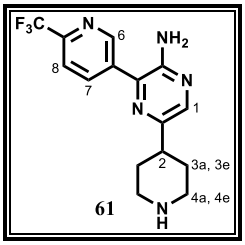

61

A solution of 4 M HCl in 1,4-dioxane (6.0 mL, 24 mmol) was added to *tert*-butyl 4-(5-amino-6-(6-(trifluoromethyl)pyridin-3-yl)pyrazin-2-yl)piperidine-1-carboxylate (**60**) (0.3170 g, 0.75 mmol). The reaction mixture was then stirred at room temperature (24 °C) for 30 minutes after which excess HCl and the solvent were removed *in vacuo*. The yellow

residue was dissolved in deionized water (30 mL) followed by basification to pH 12 by adding 4 M aqueous NaOH. The aqueous mixture was then extracted with DCM (40 mL × 3). The pooled organic layers were then washed with saturated aqueous NaCl (40 mL × 1) and dried ($MgSO_4$). The organic layer was concentrated *in vacuo* and subjected to prep-TLC (silica, developed once in 30% CH_3OH/DCM, developed once in 40% CH_3OH/DCM, developed once in 40% CH_3OH : 1% triethylamine : 59% DCM) to give **61** which was further crystallized in diethyl ether to give a yellow solid (0.0606 g, 25%); m.p. 127 – 129 °C; R_f (CH_3OH : CH_2Cl_2 8 : 92) 0.0; ^{1}H-NMR δ_H (400 MHz; CD_3OD) 9.10 (1H, d, J = 2.1 Hz, H_6), 8.44 (1H, ddt, J = 8.2, 2.1, 0.7 Hz, H_7), 7.96 (1H, d, J = 0.4 Hz, H_1), 7.93 (1H, dd, J = 8.2, 0.9 Hz, H_8), 3.22 – 3.13 (2H, m, H_{4e}), 2.85 (1H, tt, J = 11.8, 3.9 Hz, H_2), 2.77 (2H, td, J = 12.4, 2.9 Hz, H_{4a}), 1.96 – 1.88 (2H, m, H_{3e}), 1.80 (2H, dtd, J = 13.3, 12.0, 4.0 Hz, H_{3a}); ^{13}C-NMR δ_C (101 MHz; CD_3OD) 151.91, 149.46, 149.00, 146.83 (q, J = 34.70 Hz), 139.54, 137.32, 136.97, 134.48, 123.00, 120.23, 45.63 (2C), 40.49, 31.69 (2C); HPLC-MS, APCI$^-$: *m/z* $[M - H]^-$ = 321.8, calculated exact mass = 323.1358, purity: 97.1%, t_r = 0.566 min.

6.1.3.5 Procedure for Synthesis of 5-(1-(methylsulfonyl)piperidin-4-yl)-3-(6-(trifluoromethyl)pyridin-3-yl)pyrazin-2-amine (62)[14]

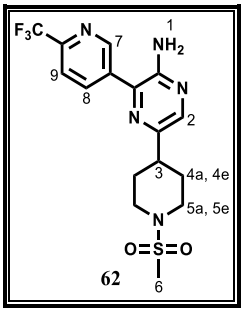

62

To a solution of 5-(piperidin-4-yl)-3-(6-(trifluoromethyl)pyridin-3-yl)pyrazin-2-amine (**61**) (0.0450 g, 0.14 mmol) and triethylamine (0.1 mL, 0.7 mmol) in 1 mL DCM cooled to 0 °C, methanesulfonyl chloride (0.012 mL, 0.15 mmol) was added dropwise. The reaction mixture was then left to warm to room temperature (23 °C) and stirred for 1 hour. The reaction mixture was diluted with 30 mL DCM and washed with deionized water (20 mL × 1), saturated aqueous solutions of $NaHCO_3$ (20 mL × 3), NH_4Cl (20 mL × 2) and NaCl (20 mL × 1). The organic layer was dried ($MgSO_4$) after which the solvent was removed *in vacuo*. The obtained residue was triturated in diethyl ether to deliver **62** as a white solid (0.0369 g, 66%); m.p. 193 – 196 °C; R_f (CH_3OH : CH_2Cl_2 8 : 92) 0.45; ^{1}H-NMR δ_H (600 MHz; $CDCl_3$) 9.16 (1H, d, J = 1.8 Hz, H_7), 8.34 – 8.30 (1H, m, H_8), 7.94 (1H, s, H_2), 7.87 (1H, d, J = 8.1 Hz, H_9), 5.61 (2H, br s, H_1), 4.01 – 3.93 (2H, m, H_{5e}), 2.95 – 2.74 (6H, m, H_3, H_{5a}, H_6), 2.14 – 2.04 (2H, m, H_{4e}), 2.02 – 1.92 (2H, m, H_{4a}); ^{13}C-NMR δ_C (151 MHz; $CDCl_3$) 149.54, 149.33, 148.79, 148.64, 148.55, 137.39 (2C), 135.22, 134.99, 120.76, 46.00 (2C), 40.10, 35.21, 30.93 (2C); HPLC-MS, APCI$^+$: *m/z* $[M + H]^+$ = 402.1, calculated exact mass = 401.1133, purity: 95.5%, t_r = 2.517 min.

6.1.3.6 Procedure for Synthesis of *tert*-butyl 4-(3-amino-6-(4-(methylsulfonyl)phenyl)pyrazin-2-yl)-3,6-dihydropyridine-1(2*H*)-carboxylate (63)

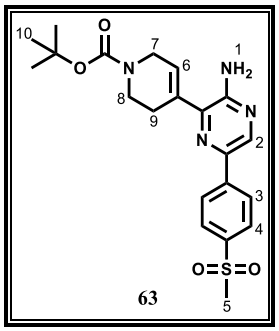

A suspension of 3-bromo-5-(4-(methylsulfonyl)phenyl)pyrazin-2-amine (**7h**) (0.6 g, 1.8 mmol), 3,6-dihydro-2*H*-pyridine-1-*N*-boc-4-boronic acid pinacol ester (0.6784 g, 2.2 mmol) and $Pd(PPh_3)_2Cl_2$ (0.0632 g, 0.09 mmol) in 6 mL anhydrous 1,4-dioxane was degassed with nitrogen for 20 minutes. A 1 M aqueous solution of K_2CO_3 (0.7463 g, 5.4 mmol) was then added. The reaction mixture was heated to 110 °C in a sealed tube and left to stir for 2 hours. The solvent was removed *in vacuo*. The remaining residue was taken up in DCM (70 mL) and washed with deionized water (50 mL × 4) and saturated aqueous NaCl (50 mL × 4). The organic layer was dried ($MgSO_4$) after which the solvent was removed *in vacuo*. The obtained residue was subjected to flash column chromatography (silica, 0 - 3% MeOH/DCM). Further purification by trituration in a mixture of EtOAc and diethyl ether delivered **63** as a maroon solid (0.617 g, 80%); m.p. 175 – 177 °C; R_f (CH_3OH : CH_2Cl_2 8 : 92) 0.44; ^{1}H-NMR δ_H (600 MHz; $CDCl_3$) 8.36 (1H, s, H_2), 8.10 (2H, d, J = 8.5 Hz, H_3), 8.01 (2H, d, J = 8.5 Hz, H_4), 6.39 (1H, br s, H_6), 5.63 (2H, br s, H_1), 4.17 (2H, d, J = 3.3 Hz, H_7), 3.71 (2H, t, J = 5.7 Hz, H_8), 3.08 (3H, s, H_5), 2.73 (2H, br s, H_9), 1.51 (9H, s, H_{10}); ^{13}C-NMR δ_C (151 MHz; $CDCl_3$) 154.74, 150.19, 141.55, 139.96, 139.50, 134.35 (2C), 133.96, 128.00 (2C), 126.96, 126.18 (2C), 80.14, 44.59 (2C), 43.11, 28.48 (3C), 27.39; HPLC-MS, APCI$^-$: *m/z* $[M - H]^-$ = 429.1, calculated exact mass = 430.1675, purity: 98.5%, t_r = 2.703 min.

6.1.3.7 Procedure for Synthesis of *tert*-butyl 4-(3-amino-6-(4-(methylsulfonyl)phenyl)pyrazin-2-yl)piperidine-1-carboxylate (64)

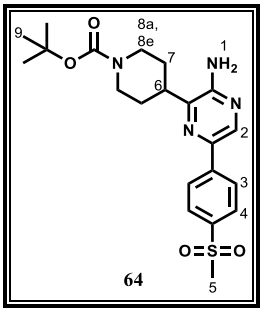

A suspension of *tert*-butyl 4-(3-amino-6-(4-(methylsulfonyl)phenyl)pyrazin-2-yl)-3,6-dihydropyridine-1(2*H*)-carboxylate (**63**) (0.5706 g, 1.3 mmol), NH_4HCO_2 (0.5850 g, 9.3 mmol) and 10% carbon-supported palladium (Pd/C) (0.1383 g, 1.3 mmol) in 15 mL anhydrous methanol in a sealed tube was evacuated. The reaction mixture was then left to stir at room temperature (24 °C) under an atmosphere of hydrogen captured in a balloon for 1 hour. The reaction mixture was filtered through a filter paper to remove the Pd/C catalyst after which the filtrate was concentrated *in vacuo*. The obtained residue was taken up in DCM (60 mL) and washed with deionized water (40 mL × 1) and saturated aqueous NaCl (40 mL × 4). The organic layer was dried ($MgSO_4$)

after which the solvent was removed to afford **64** as a cream white solid (0.3968 g, 71%); m.p. 180 – 183 °C; R_f (CH_3OH : CH_2Cl_2 8 : 92) 0.41; ^{1}H-NMR δ_H (400 MHz; $CDCl_3$) 8.34 (1H, s, H_2), 8.13 (2H, d, J = 8.7 Hz, H_3), 8.04 (2H, d, J = 8.5 Hz, H_4), 6.06 (2H, br s, H_1), 4.31 (2H, d, J = 13.3 Hz, H_{8e}), 3.11 (3H, s, H_5), 3.05 – 2.93 (3H, m, H_6, H_{8a}), 2.03 – 1.87 (4H, m, H_7), 1.52 (9H, s, H_9); ^{13}C-NMR δ_C (101 MHz; $CDCl_3$) 154.78, 149.59, 147.14, 141.40, 140.16, 139.52, 132.11, 128.02 (2C), 126.16 (2C), 79.76, 44.56, 43.67, 38.96 (2C), 29.40 (2C), 28.48 (3C); HPLC-MS, APCI$^-$: *m/z* $[M - H]^-$ = 431.1, calculated exact mass = 432.1831, purity: 99.6%, t_r = 2.806 min.

6.1.3.8 Procedure for Synthesis of 5-(4-(methylsulfonyl)phenyl)-3-(piperidin-4-yl)pyrazin-2-amine (65)[13]

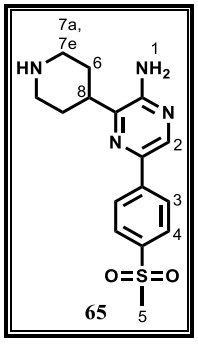

A solution of 4 M HCl in 1,4-dioxane (5.0 mL, 20 mmol) was added to a suspension of *tert*-butyl 4-(3-amino-6-(4-(methylsulfonyl)phenyl)pyrazin-2-yl)piperidine-1-carboxylate (**64**) (0.2654 g, 0.61 mmol) in 3 mL DCM. The reaction mixture was then stirred for 1 hour at room temperature (24 °C) after which excess HCl and the solvent were removed *in vacuo*. The white residue obtained was taken up in 60 mL EtOAc and basified to pH 11 by slowly adding 15% aqueous NaOH while vigorously stirring the mixture. The aqueous phase was removed using a separatory funnel. The organic layer was then dried (Na_2SO_4) where after the solvent was removed in vacuo. The obtained residue was triturated in EtOAc to afford **65** as a brown solid (0.1745 g, 86%); m.p. 125 – 128 °C; R_f (CH_3OH : CH_2Cl_2 8 : 92) 0.0; ^{1}H-NMR δ_H (400 MHz; DMSO-d_6) 8.52 (1H, s, H_2), 8.20 (2H, d, J = 8.7 Hz, H_3), 7.94 (2H, d, J = 8.6 Hz, H_4), 6.63 (2H, s, H_1), 3.21 (3H, s, H_5), 3.09 (2H, d, J = 12.2 Hz, H_{7e}), 3.03 – 2.93 (1H, m, H_8), 2.78 – 2.66 (2H, m, H_{7a}), 1.82 – 1.64 (4H, m, H_6); ^{13}C-NMR δ_C (101 MHz; DMSO-d_6) 153.24, 144.82, 142.82, 139.45, 137.98, 136.82, 127.88 (2C), 125.50 (2C), 46.18 (2C), 44.23, 37.80, 30.49 (2C); HPLC-MS, APCI$^+$: *m/z* $[M + H]^+$ = 333.1, calculated exact mass = 332.1307, purity: 99.8%, t_r = 0.249 min.

6.1.3.9 Procedure for Synthesis of 5-(4-(methylsulfonyl)phenyl)-3-(1-(methylsulfonyl)piperidin-4-yl)pyrazin-2-amine (66)[14]

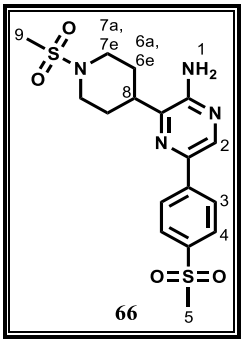

To a solution of 5-(4-(methylsulfonyl)phenyl)-3-(piperidin-4-yl)pyrazin-2-amine (**65**) (0.1745 g, 0.52 mmol) and triethylamine (0.36 mL, 2.6 mmol) in 1 mL DCM cooled to 0 °C, methanesulfonyl chloride (0.045 mL, 0.58 mmol) was added dropwise. The reaction mixture was then left to warm to room temperature (24 °C) and stirred for 1 hour. The reaction mixture was diluted with 30 mL DCM and washed with deionized water (20 mL × 1), saturated aqueous solutions of $NaHCO_3$ (20 mL × 3), NH_4Cl (20 mL × 2) and NaCl (20 mL × 1). The organic layer was dried ($MgSO_4$) after which the solvent was removed *in vacuo* to deliver **66** as a white solid; R_f (CH_3OH : CH_2Cl_2 8 : 92) 0.41; ^{1}H-NMR δ_H (300 MHz; DMSO-d_6) 8.56 (1H, s, H_2), 8.22 (2H, d, J = 8.6 Hz, H_3), 7.95 (2H, d, J = 8.5 Hz, H_4), 6.74 (2H, s, H_1), 3.89 – 3.78 (3H, m, H_{7e}, H_8), 3.22 – 3.21 (6H, m, H_5, H_9), 3.16 – 3.03 (2H, m, H_{7a}), 2.02 – 1.90 (2H, m, H_{6e}), 1.89 – 1.77 (2H, m, H_{6a}); HPLC-MS, APCI$^+$: *m/z* $[M + 2Na]^+$ = 489.1, calculated exact mass = 410.1082, purity: 95.2%, t_r = 2.434 min.

6.1.3.10 Procedure for Synthesis of 4-(3-amino-6-(4-(methylsulfonyl)phenyl)pyrazin-2-yl)benzoic acid (69)

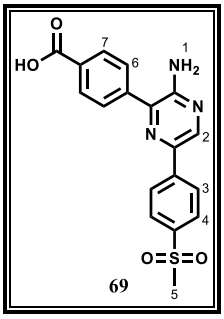

A suspension of 3-bromo-5-(4-(methylsulfonyl)phenyl)pyrazin-2-amine (**7h**) (0.3 g, 0.91 mmol), 4-carboxyphenylboronic acid (0.1820 g, 1.1 mmol) and $Pd(PPh_3)_2Cl_2$ (0.0319 g, 0.046 mmol) in 4 mL anhydrous 1,4-dioxane was degassed with nitrogen for 20 minutes. A 1 M aqueous solution of K_2CO_3 (0.3773 g, 2.7 mmol) was then added. The reaction mixture was heated to 110 °C in a sealed tube and left to stir for 2 hours. The solvent was removed in vacuo to obtain a deep brown residue which was directly subjected to flash column chromatography (silica, 0 - 12% CH_3OH/DCM). The brown solid obtained was triturated in EtOAc to deliver **69** as a brown solid (0.2671 g, 79%); m.p. 271 – 274 °C; R_f (CH_3OH : CH_2Cl_2 8 : 92) 0.16; ^{1}H-NMR δ_H (400 MHz; DMSO-d_6) 8.74 (1H, s, H_2), 8.26 (2H, d, J = 8.8 Hz, H_6), 8.09 (2H, d, J = 8.5 Hz, H_3), 7.98 (2H, d, J = 8.7 Hz, H_7), 7.93 (2H, d, J = 8.5 Hz, H_4), 6.66 (2H, s, H_1), 3.24 (3H, s, H_5); ^{13}C-NMR δ_C (101 MHz; DMSO-d_6) 153.32, 142.12, 141.57, 140.17 (2C), 139.92 (2C), 138.23, 137.79, 130.12 (2C), 128.79 (2C), 127.93 (2C), 125.92 (2C), 44.17; HPLC-MS, APCI$^+$: *m/z* $[M + H]^+$ = 370.1, calculated exact mass = 369.0783, purity: 99.9%, t_r = 2.496 min.

6.1.3.11 Procedure for Synthesis of di-*tert*-butyl 4,4'-(3-aminopyrazine-2,6-diyl)bis(3,6-dihydropyridine-1(2*H*)-carboxylate) (70)

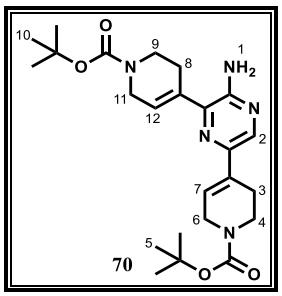

A suspension of 5-bromo-3-iodopyrazin-2-amine (**7f**) (0.3733 g, 1.2 mmol), 3,6-dihydro-2*H*-pyridine-1-*N*-boc-4-boronic acid pinacol ester (0.8467 g, 2.7 mmol) and $Pd(PPh_3)_2Cl_2$ (0.0842 g, 0.12 mmol) in 4 mL anhydrous 1,4-dioxane was degassed with nitrogen for 30 minutes. A 1 M aqueous solution of K_2CO_3 (0.9951 g, 7.2 mmol) was then added. The reaction mixture was heated to 110 °C in a sealed tube and left to stir for 4 hours. The solvent was removed *in vacuo*. The remaining brown residue was taken up in DCM (60 mL) and washed with deionized water (40 mL × 1) and saturated aqueous NaCl (40 mL × 3). The organic layer was dried (Na_2SO_4) after which the solvent was removed *in vacuo*. The obtained brown residue was subjected to flash column chromatography (silica, 0 - 4% CH_3OH/DCM). Further purification by prep-TLC (silica, developed once in 3% CH_3OH/DCM) gave **70** which was crystallized from a mixture of diethyl ether and pentane to obtain a faint yellow crystalline solid (0.374 g, 68%); m.p. 90 – 92 °C; R_f (CH_3OH : CH_2Cl_2 8 : 92) 0.41; ^{1}H-NMR δ_H (400 MHz; $CDCl_3$) 7.73 (1H, s, H_2), 6.59 (1H, br s, H_{12}), 6.50 – 6.32 (3H, m, H_1, H_7), 4.19 (2H, d, J = 3.1 Hz, H_{11}), 4.15 (2H, d, J = 3.5 Hz, H_6), 3.70 (2H, t, J = 5.6 Hz, H_9), 3.67 (2H, t, J = 5.6 Hz, H_4), 2.72 – 2.62 (2H, m, H_8), 2.57 – 2.48 (2H, m, H_3), 1.53 (9H, s, H_{10}), 1.51 (9H, s, H_5); HPLC-MS, APCI$^+$: *m/z* $[M + H]^+$ = 458.2, calculated exact mass = 457.2689, purity: 98.1%, t_r = 3.007 min.

6.1.3.12 Procedure for Synthesis of di-*tert*-butyl 4,4'-(3-aminopyrazine-2,6-diyl)bis(piperidine-1-carboxylate) (71)

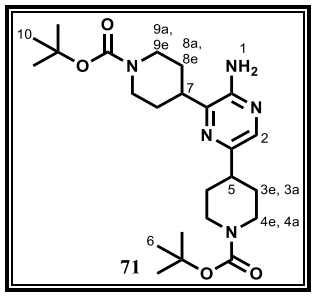

A suspension of di-*tert*-butyl 4,4'-(3-aminopyrazine-2,6-diyl)bis(3,6-dihydropyridine-1(2*H*)-carboxylate) (**70**) (0.135 g, 0.3 mmol), NH_4HCO_2 (0.1324 g, 2.1 mmol) and 10% carbon-supported palladium (Pd/C) (0.0319 g, 0.3 mmol) in 5.5 mL anhydrous methanol in a sealed tube was evacuated. The reaction mixture was then left to stir at room temperature (20 °C) under an atmosphere of hydrogen captured in a balloon for 4 hours. The reaction mixture was filtered through a filter paper to remove the Pd/C catalyst after which the filtrate was concentrated *in vacuo*. The obtained residue was taken up in DCM (50 mL) and washed with deionized water (25 mL × 1) and a saturated aqueous solution of NaCl (25 mL × 4). The organic layer was dried ($MgSO_4$) after which the solvent was removed. The obtained residue was subjected to prep-TLC (silica,

developed twice in 2% CH_3OH/DCM) to afford **71** as a white solid (0.084 g, 61%); m.p. 69 – 72 °C; R_f (CH_3OH : CH_2Cl_2 8 : 92) 0.43; ^{1}H-NMR δ_H (400 MHz; $CDCl_3$) 7.47 (1H, s, H_2), 6.55 (2H, s, H_1), 4.34 – 4.10 (4H, m, H_{4e}, H_{9e}), 3.04 – 2.89 (3H, m, H_7, H_{9a}), 2.88 – 2.69 (3H, m, H_{4a}, H_5), 1.93 – 1.75 (6H, m, H_{3e}, H_{8a}, H_{8e}), 1.73 – 1.58 (2H, m, H_{3a}), 1.48 (18H, s, H_6, H_{10}); ^{13}C-NMR δ_C (101 MHz; $CDCl_3$) 154.78, 154.73, 149.89, 147.51, 146.92, 125.37, 79.68, 79.64, 43.74 (4C), 40.64, 38.58, 31.03 (2C), 29.32 (2C), 28.46 (6C); HPLC-MS, APCI$^+$: *m/z* [M – boc + H]$^+$ = 362.2 and *m/z* [M – 2boc + H]$^+$ = 262.2, calculated exact mass = 461.3002, purity: 99.9%, t_r = 2.940 min.

6.1.3.13 Procedure for Synthesis of 3,5-di(piperidin-4-yl)pyrazin-2-amine (7i)[13]

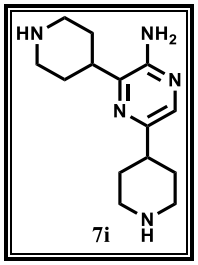

A solution of 4 M HCl in 1,4-dioxane (3.0 mL, 12 mmol) was added to a solution of di-*tert*-butyl 4,4'-(3-aminopyrazine-2,6-diyl)bis(piperidine-1-carboxylate) (**71**) (0.3612 g, 0.78 mmol) in 3 mL anhydrous 1,4-dioxane. The reaction mixture, containing a white precipitate at this point, was then stirred for 1.5 hours at room temperature (23 °C) after which excess HCl and the solvent were removed *in vacuo*. The white residue obtained was resuspended in 45 mL EtOAc and basified to pH 11 by slowly adding 15% aqueous NaOH while vigorously stirring the mixture. The aqueous phase was removed using a separatory funnel. The organic layer was concentrated *in vacuo* to afford **7i** as a white solid (0.1031 g, 50.7%) which was used in the next step without further purification; UPLC-MS, ESI$^+$: *m/z* [M + H]$^+$ = 262.1, calculated exact mass = 261.1953, t_r = 0.11 min.

6.1.3.14 Procedure for Synthesis of 3,5-bis(1-(methylsulfonyl)piperidin-4-yl)pyrazin-2-amine (72)[14]

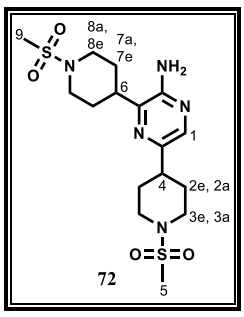

To a suspension of 3,5-di(piperidin-4-yl)pyrazin-2-amine (**7i**) (0.1031 g, 0.39 mmol) and triethylamine (0.54 mL, 3.9 mmol) in 3.5 mL DCM cooled to 0 °C, methanesulfonyl chloride (0.1 mL, 0.87 mmol) was added dropwise. The reaction mixture was then left to warm to room temperature (21.5 °C) and stirred for 12 hours. The reaction mixture was diluted with 50 mL DCM and washed with deionized water (15 mL × 1), saturated aqueous solutions of $NaHCO_3$ (15 mL × 2) and NaCl (15 mL × 2). The organic layer was dried ($MgSO_4$) after which the solvent was removed *in vacuo*. The obtained residue was subjected to prep-TLC (silica, developed twice in 1.5% CH_3OH/DCM) to deliver **72** as a white solid (0.038 g, 23%); m.p. 95 – 98 °C; R_f (CH_3OH : CH_2Cl_2 8 : 92) 0.54; ^{1}H-NMR δ_H (300 MHz;

$CDCl_3$) 8.31 (1H, s, H_1), 4.06 – 3.94 (4H, m, H_{3e}, H_{8e}), 3.22 – 3.08 (1H, m, H_6), 3.04 – 2.75 (11H, m, H_{3a}, H_4, H_5, H_{8a}, H_9), 2.21 – 1.86 (8H, m, H_{2a}, H_{2e}, H_{7a}, H_{7e}); purity: 98.7%, t_r = 2.417 min.

6.1.3.15 Procedure for Synthesis of 5-(4-(methylsulfonyl)phenyl)-3-(piperazin-1-yl)pyrazin-2-amine (67)

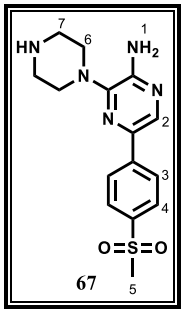

A mixture of 3-bromo-5-(4-(methylsulfonyl)phenyl)pyrazin-2-amine (**7h**) (0.05 g, 0.15 mmol), 1-boc-piperazine (0.0426 g, 0.23 mmol) and triethylamine (0.1 mL, 0.45 mmol) in a sealed tube was heated to 170 °C and left to stir for 4 hours. The reaction mixture, which was solid at this point, was suspended in 60 mL EtOAc and basified to pH 11 by slowly adding a solution of 15% aqueous NaOH while stirring vigorously (cloudy mixture clears after about 45 minutes). The aqueous phase was removed using a separatory funnel where after the organic layer was dried (Na_2SO_4). The solvent was removed *in vacuo* and the obtained residue triturated in ethyl acetate to furnish **67** as a brown solid (0.0787 g, 38.7%); m.p. 158 – 161 °C; R_f (CH_3OH : CH_2Cl_2 8 : 92) 0.03; ^{1}H-NMR δ_H (400 MHz; DMSO-d_6) 8.33 (1H, s, H_2), 8.17 (2H, d, J = 8.6 Hz, H_3), 7.92 (2H, d, J = 8.6 Hz, H_4), 6.27 (2H, s, H_1), 3.21 (3H, s, H_5), 3.11 – 3.06 (4H, m, H_6), 2.93 – 2.87 (4H, m, H_7); ^{13}C-NMR δ_C (101 MHz; DMSO-d_6) 149.15, 145.83, 142.85, 139.30, 135.36, 133.56, 127.83 (2C), 125.55 (2C), 49.57 (2C), 45.73 (2C), 44.22; HPLC-MS, APCI$^+$: *m/z* $[M + H]^+$ = 334.1, calculated exact mass = 333.1259, purity: 95.7%, t_r = 0.170 min.

6.1.3.16 Procedure for Synthesis of 5-(4-(methylsulfonyl)phenyl)-3-(4-(methylsulfonyl)piperazin-1-yl)pyrazin-2-amine (68)[14]

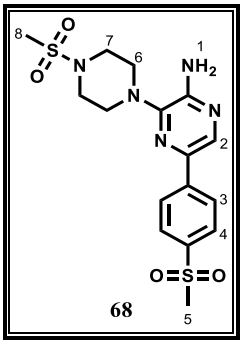

To a solution of 5-(4-(methylsulfonyl)phenyl)-3-(piperazin-1-yl)pyrazin-2-amine (**67**) (0.0564 g, 0.17 mmol) and triethylamine (0.12 mL, 0.85 mmol) in 1 mL DCM cooled to 0 °C, methanesulfonyl chloride (0.014 mL, 0.19 mmol) was added dropwise. The reaction mixture was then left to warm to room temperature (20 °C) and stirred for 30 minutes. The reaction mixture was diluted with 40 mL DCM and washed with deionized water (5 mL × 2), saturated aqueous solutions of $NaHCO_3$ (15 mL × 2), and NaCl (15 mL × 2). The organic layer was dried (Na_2SO_4) after which the solvent was removed *in vacuo*. The crude mixture was subjected to prep-TLC (silica, developed once in 5% CH_3OH/DCM) to deliver **68** which was crystallized in diethyl ether to give a yellow solid (0.0521 g, 74%); m.p. 239 – 242 °C; R_f (CH_3OH : CH_2Cl_2 8 : 92) 0.49; ^{1}H-NMR δ_H (400

MHz; DMSO-d_6) 8.39 (1H, s, H_2), 8.19 (2H, d, J = 8.6 Hz, H_3), 7.94 (2H, d, J = 8.6 Hz, H_4), 6.45 (2H, s, H_1), 3.40 – 3.34 (4H, m, H_6), 3.29 – 3.26 (4H, m, H_7), 3.22 (3H, s, H_5), 2.94 (3H, s, H_8); ^{13}C-NMR δ_C (101 MHz; DMSO-d_6) 149.13, 144.65, 142.61, 139.43, 135.40, 134.33, 127.84 (2C), 125.67 (2C), 47.65 (2C), 45.50 (2C), 44.20, 34.76; HPLC-MS, APCI$^+$: *m/z* [M + H]$^+$ = 412.1, calculated exact mass = 411.1035, purity: 99.9%, t_r = 2.447 min.

6.2 Biological Assays

6.2.1 *In Vitro* Asexual Blood Stage Antiplasmodial Assay

Compounds were screened against multidrug resistant (K1) and sensitive (NF54) strains of *P. falciparum in vitro* using the modified [^{3}H]-hypoxanthine incorporation assay.[15] *P. falciparum* was cultivated in a variation of the medium previously described,[16,17] consisting of RPMI 1640 supplemented with 0.5% ALBUMAX® II, 25 mM Hepes, 25 mM $NaHCO_3$ (pH 7.3), 0.36 mM hypoxanthine and 100 µg/mL neomycin. Human erythrocytes served as host cells. Cultures were maintained at 37 °C in an atmosphere of 3% O_2, 4% CO_2 and 93% N_2 in humidified modular chambers. Compounds were dissolved by sonication in DMSO (10 mg/mL) and diluted in hypoxanthine-free culture medium. Infected erythrocytes (100 µL per well with 2.5% hematocrit and 0.3% parasitemia) were added to each drug titrated in 100 µL duplicates over a 64-fold range. After 48 hours incubation, 0.5 µCi of [^{3}H]hypoxanthine in 50 µL medium was added and plates were incubated for an additional 24 hours. Parasites were harvested onto glass-fiber filters and radioactivity was counted using a Betaplate liquid scintillation counter (Wallac, Zurich). The results were recorded as counts per minute (cpm) per well at each drug concentration and expressed as a percentage of the untreated controls. Fifty percent inhibitory concentrations (IC_{50}) were estimated by linear interpolation.[18]

6.2.2 *In Vitro* Gametocytocidal Assay

6.2.2.1 Luciferase Reporter Assay

Two transgenic parasite lines (NF54-PfS16-GFP-Luc and NF54-Mal8p1.16-GFP-Luc) were used in the luciferase assays which facilitated stage-specific determination of gametocytocidal activity. Gametocytes were produced according to Reader *et al.*[19] On days 5 and 10 which respectively represent > 90% of early stage (I – III) and > 90% of late stage (IV and V) gametocytes, drug assays where set up. In both cases, 2 – 3% gametocytaemia and 1.5% haematocrit culture were used with a 48 hour drug pressure in a gas chamber (90% N_2, 5% O_2 and 5% CO_2) at 37ºC. To 20 µL parasite lysates, 50 µL of luciferin substrate (Promega Luciferase Assay System) was added at room temperature. Luciferase activity was determined

by detection of resulting bioluminescence at an integration constant of 10 seconds using the GloMax®-Multi+ Detection System with Instinct® Software. Methylene blue and dihydroartemisinin were used as controls.

6.2.2.2 ATP Assay

In the ATP assay, late stage gametocytes (IV and V, primarily stage V) were enriched using density gradient centrifugation and magnetic separation. Dilutions for the compounds were prepared in triplicate in 96-well plates. To each well, about 50,000 gametocytes in glucose-rich complete medium were added to make a final volume of 100 μL where after the plates were incubated at 37 °C in a humidified gas chamber (90% N_2, 5% O_2 and 5% CO_2) for 24 hours. The BacTiter-Glo™ assay (Promega) was then carried out in accordance with the manufacturer's guidelines at room temperature in the dark with assay substrate incubated for 10 minutes to detect ATP levels. The GloMax®-Multi+ Detection System with Instinct® Software was used to detect bioluminescence at an integration constant of 0.5 seconds. Methylene blue and dihydroartemisinin were used controls.

6.2.3 *In Vitro* Liver Stage Assay

Luminescence intensity in Huh7 cells, a human hepatoma cell line, infected with a firefly luciferase-expressing *P. berghei* line, *Pb*GFP-Luc_{con} was used to determine inhibition of liver stage infection as previously described.[20] A 1640 RPMI medium supplemented with 10% v/v fetal calf serum (FCS), 1% v/v non-essential amino acids, 1% v/v penicillin/streptomycin, 1% v/v glutamine and 10 mM 4-(2-hydroxyethyl)-1-piperazine-ethanesulphonic acid (HEPES), pH 7, and maintained at 37 °C with 5% CO_2 was used to culture the Huh7 cells. Dulbecco's Modified Eagle Medium (DMEM) (Gibco/Invitrogen) was used to harvest salivary glands from female *Anopheles stephensi* mosquitoes. The salivary glands were then homogenized in a grinder after which the resulting homogenate was filtered and centrifuged at 3000 RPM for 5 minutes. Phase-contrast microscopy was then used to count free sporozoites in a Neubauer chamber. DMSO was used to prepare 10 mM stock solutions of test compounds which were diluted with 1640 RPMI medium. A day before drug treatment and infection, Huh7 cells (1.2×10^4 per well) were seeded in 96-well plates. About 1 hour prior to infection with freshly obtained sporozoites, the medium in the cells was replaced by medium containing the appropriate concentration of each compound. The plates were centrifuged at 1700 RPM for 5 minutes following sporozoite addition. The AlamarBlue assay (Invitrogen, UK) was used to assess the effect of the compounds on the viability of Huh7 cells using the manufacturer's

protocol. A Tecan Infinite M200 spectrometer (Tecan Group, Switzerland) was used to measure fluorescence intensity at 530 nm excitation wavelength and 590 nm emission wavelength. A Luciferase Assay System Kit (Promega, Netherlands) was used to determine parasite load by measuring luminescence 48 hours post-infection according to the manufacturer's instructions. Briefly, phosphate buffer was used to wash out the 96-well plate after which cells were incubated with 75 µL of lysis buffer for 15 minutes in a shaker at 600 RPM. After the lysis, debris and membranes were then deposited by centrifuging the 96-well plate at 3000 RPM for 5 minutes. The supernatant (30 µL) was then transferred into a white 96-well plate and the luciferase activity was measured by adding 50 µL of Luciferase Assay substrate (1:50 dilution) (Luciferase Assay System Kit, Promega, Netherlands). A Tecan Infinite M200 spectrometer (Tecan Group, Switzerland) was used to measure luminescence intensity. To fit the normalized results of the dose-response curves, nonlinear regression analysis was employed, and IC_{50} values were determined using GraphPad Prism V 5.0.

6.2.4 *In Vitro* hERG Inhibition Assay

A QPatch hERG assay employing a four-point concentration-response format was used to carry out hERG inhibition studies by the UK-based Metrion Biosciences Ltd. The hERG gene was stably expressed in a CHO cell line which was grown and passaged under standard culture conditions. The external (e) and internal (i) recording solutions were of the following compositions (mM): NaCl – 140 (e) : 0 (i); KCl – 2 (e) : 70 (i); KF - 0 (e) : 60 (i); HEPES - 10 (e) : 10 (i); $MgCl_2$ - 1 (e) : 0 (i); $CaCl_2$ - 2 (e) : 0 (i); Glucose - 5 (e) : 0 (i); EGTA - 0 (e) : 5 (i); Mg_2ATP - 0 (e) : 5 (i) and pH – 7.4 (NaOH) (e) : 7.2 (KOH) (i). The external recording solution was regularly prepared and kept at 4 °C until required and was maintained at room temperature during recording. The internal recording solution was prepared and kept at – 20 °C until required.

The QPatch is a chip-based planar patch clamp which is automated. Using suction, cells added to each well are drawn across a small aperture creating a Giga-ohm seal between the membrane surface and a treated silicon surface. A small volume of bathing solution containing the test compound or control bathing solution is added to a reservoir on the chip which perfuses across the cell through quartz-lined microfluidic channels. The solution is removed by capillary action before the next sample is added. Using the industry +40/-40 voltage protocol, currents were triggered from a holding potential of -90 mV at a stimulus frequency of 0.1 Hz.

By cumulatively adding four escalating concentrations of the test compounds to an individual cell, the concentration response curves were established. This was done by firstly allowing the whole-cell configuration to be achieved followed by the addition of the vehicle (0.1% DMSO v/v in external recording solution) to each well in two bolus additions allowing a two-minute recording time between each addition. This was followed by the addition of four concentrations (0.3 – 10 μM) of test compounds in two bolus additions at 2-minute intervals. The effect on the hERG tail current amplitude was measured during the 4-minute recording time. The concentrations (0.3, 1, 3 and 10 μM) of the test samples were prepared in such a way to have a final concentration of 0.1% of DMSO v/v in the external recording solution. For each compound, the experiments at each concentration were done in triplicate and using a bioinformatics suite developed and running in Pipeline Pilot (Biovia, USA), the percent inhibition, as a reduction in mean peak current relative to the value measured at the end of the vehicle control period, was calculated. Such percent inhibition data were used to construct the concentration-response curves which enabled calculation of the IC_{50} values. For compounds which could not achieve 50% inhibition even at the highest tested concentration of 10 μM, extrapolated IC_{50} values for such are reported. In this regard, all IC_{50} values above 10 μM reported in this thesis were extrapolated and should be treated with caution.

6.2.5 *In Vitro* Cytotoxicity Assay[21]

Cytotoxicity was measured using the MTT-assay which measures cellular growth and survival calorimetrically. All growth and chemosensitivity was measured by the formation of tetrazolium salt. The test samples were assayed in triplicate on one occasion. Stock solutions of 2 mg/mL of test samples in DMSO were prepared with poorly soluble samples being tested as suspensions. The test samples were kept at -20 °C until required. In all experiments, emetine was used as a reference drug. 10-fold serial dilutions in complete medium to give 6 concentrations were made from an initial concentration of 100 μg/mL with the lowest concentration being 0.001 μg/mL. The cell viability was not affected by the highest concentration of the solvent to which the cells were exposed. The full dose-response curves plotted using a non-linear dose-response curve fitting analysis via GraphPad Prism V 4 software enabled the determination of the IC_{50} values.

6.2.6 Metabolic Stability Assay

The metabolic stability assay was performed in duplicate in a 96-well micro titre plate. The test compounds (0.1 μM) were incubated (37 °C) in mouse, rat and pooled human liver microsomes

(final protein concentration of 0.4 mg/mL; XenoTech, Lenexa, KS) suspended in 0.1 M phosphate buffer (pH 7.4) for 30 minutes, in the presence and absence of the cofactor NADPH (1 mM). The reactions were quenched by the addition of ice cold acetonitrile containing an internal standard (carbamazepine, 0.0236 µg/mL). The samples were centrifuged, and the supernatant was filtered and analysed by means of HPLC-MS/MS (Agilent Rapid Resolution HPLC, AB SCIEX 4500 MS). The relative loss of parent compound over time was monitored and plots were prepared for each compound of concentration versus time to determine the first order rate constant for compound depletion. This was used to calculate the degradation half-life, *in vitro* intrinsic clearance value and subsequently to predict the *in vivo* hepatic extraction ratio (E_H). Metabolite searches were not conducted during the metabolic stability assay.

6.3 Solubility Determination

6.3.1 Kinetic Solubility Employing HPLC

A miniaturised shake flask method was used to perform the solubility assay.[22] From 10 mM stock solutions of the test compounds in DMSO, calibration standards (10 - 220 µM in DMSO) were prepared. The 10 mM stock solutions were also used to spike (1:50) duplicate aqueous samples in phosphate buffered saline (pH 6.5). The DMSO was dried off in a GeneVac (MiVac, 90 min, 37 °C) after which the samples were incubated while shaking for 20 hours at 25 °C. Thereafter, the solutions were filtered, and their absorbance measured using HPLC-DAD (Agilent 1200 Rapid Resolution HPLC with a diode array detector). The calibration standards were used to plot the calibration curves, which were used to determine the solubility of the aqueous samples.

6.3.2 Kinetic (Turbidimetric) Solubility[23]

A phosphate buffered saline (PBS) solution comprising 0.14 M NaCl, 0.003 M KCl and 0.01 M phosphate buffer (pH 7.4) was prepared by dissolving one intact PBS buffer tablet in 1 L of water. Particulate contaminants were removed by filtering the solution through a 0.22 µm nylon filter and the pH verified using a pH meter. Stock solutions (10 mM) of test compounds were prepared by dissolving in DMSO. Using a 96-well plate, serial dilutions of the compounds in DMSO were prepared in triplicate starting from 8 mM to 0.25 mM (predilution plate). Secondary serial dilutions (5 – 200 µM) in DMSO and PBS buffer, also in triplicate, were prepared by pipetting 4 µL aliquots from the predilution plate to corresponding wells in the secondary plate containing 196 µL DMSO and PBS buffer (final volume of 200 µL in each

well). The serial dilutions in DMSO acted as controls to make sure the test compounds in solution did not absorb electromagnetic radiation at the test wavelength. The plate was covered and incubated for 2 hours in an oven maintained at 37 °C. The absorbance values of the wells were then measured by a UV-Visible Multiskan Go 1510-05438 spectrometer (Thermo Scientific). The values were then corrected by subtracting the absorbance of the blank wells containing only DMSO and 2% DMSO in PBS. The corrected absorbance values were plotted as a function of concentration using excel. A constant absorbance value of 0 at all concentrations indicates the compound is soluble at all concentrations. Insoluble compounds will precipitate and cause turbidity the absorbance of which was measured by a UV-Visible spectrometer. Solubility was taken to be that concentration above which the test compound precipitates from solution causing a sustained upward deviation of absorbance values from zero.

6.4 References

(1) Le Manach, C.; Gonzàlez Cabrera, D.; Douelle, F.; Nchinda, A. T.; Younis, Y.; Taylor, D.; Wiesner, L.; White, K. L.; Ryan, E.; March, C.; Duffy, S.; Avery, V. M.; Waterson, D.; Witty, M. J.; Wittlin, S.; Charman, S. A.; Street, L. J.; Chibale, K. Medicinal Chemistry Optimization of Antiplasmodial Imidazopyridazine Hits from High Throughput Screening of a SoftFocus Kinase Library: Part 1. *J. Med. Chem.* **2014**, *57*, 2789–2798.

(2) Delacourte, A.; Melnyk, P.; Burlet, S.; Lefur, N. Preparation of 7-Chloro-Quinolin-4-Amine Compounds and Uses Thereof for the Prevention or Treatment of Diseases Involving Formation of Amyloid Plaques and/or Where a Dysfunction of the App Metabolism Occurs. WO2011073322 A1, 2011.

(3) Driver, M. S.; Hartwig, J. F. A Second-Generation Catalyst for Aryl Halide Amination: Mixed Secondary Amines from Aryl Halides and Primary Amines Catalyzed by (DPPF)$PdCl_2$. *J. Am. Chem. Soc.* **1996**, *118*, 7217–7218.

(4) Guram, A. S.; Buchwald, S. L. Palladium-Catalyzed Aromatic Aminations with in Situ Generated Aminostannanes. *J. Am. Chem. Soc.* **1994**, *116*, 7901–7902.

(5) Paul, F.; Patt, J.; Hartwig, J. F. Palladium-Catalyzed Formation of Carbon-Nitrogen Bonds. Reaction Intermediates and Catalyst Improvements in the Hetero Cross-Coupling of Aryl Halides and Tin Amides. *J. Am. Chem. Soc.* **1994**, *116*, 5969–5970.

(6) Wolfe, J. P.; Wagaw, S.; Buchwald, S. L. An Improved Catalyst System for Aromatic Carbon−Nitrogen Bond Formation: The Possible Involvement of Bis(Phosphine) Palladium Complexes as Key Intermediates. *J. Am. Chem. Soc.* **1996**, *118*, 7215–7216.

(7) Miyaura, N.; Yamada, K.; Suzuki, A. A New Stereospecific Cross-Coupling by the Palladium-Catalyzed Reaction of 1-Alkenylboranes with 1-Alkenyl or 1-Alkynyl Halides. *Tetrahedron Lett.* **1979**, *20*, 3437–3440.

(8) Miyaura, N.; Suzuki, A. Palladium-Catalyzed Cross-Coupling Reactions of Organoboron Compounds. *Chem. Rev.* **1995**, *95*, 2457–2483.

(9) Le Manach, C.; Gonzàlez Cabrera, D.; Douelle, F.; Nchinda, A. T.; Younis, Y.; Taylor, D.; Wiesner, L.; White, K. L.; Ryan, E.; March, C.; Duffy, S.; Avery, V. M.; Waterson, D.; Witty, M. J.; Wittlin, S.; Charman, S. A.; Street, L. J.; Chibale, K. Medicinal

Chemistry Optimization of Antiplasmodial Imidazopyridazine Hits from High Throughput Screening of a SoftFocus Kinase Library: Part 2. *J. Med. Chem.* **2014**, *57*, 8839–8848.

(10) Montalbetti, C. A. G. N.; Falque, V. Amide Bond Formation and Peptide Coupling. *Tetrahedron.* **2005**, *61*, 10827–10852.

(11) Younis, Y.; Douelle, F.; González Cabrera, D.; Le Manach, C.; Nchinda, A. T.; Paquet, T.; Street, L. J.; White, K. L.; Zabiulla, K. M.; Joseph, J. T.; Bashyam, S.; Waterson, D.; Witty, M. J.; Wittlin, S.; Charman, S. A.; Chibale, K. Structure–Activity-Relationship Studies around the 2-Amino Group and Pyridine Core of Antimalarial 3,5-Diarylaminopyridines Lead to a Novel Series of Pyrazine Analogues with Oral in Vivo Activity. *J. Med. Chem.* **2013**, *56*, 8860–8871.

(12) Barsanti, P. A.; Aversa, R. J.; Jin, X.; Pan, Y.; Lu, Y.; Elling, R.; Jain, R.; Knapp, M.; Lan, J.; Lin, X.; Rudewicz, P.; Sim, J.; Taricani, L.; Thomas, G.; Xiao, L.; Yue, Q. Structure-Based Drug Design of Novel Potent and Selective Tetrahydropyrazolo[1,5-*a*]Pyrazines as ATR Inhibitors. *ACS Med. Chem. Lett.* **2015**, *6*, 37–41.

(13) Wuts, P. G. M.; Greene, T. W. *Greene's Protective Groups in Organic Synthesis*, 4th ed.; John Wiley & Sons: New York, 2007.

(14) Lakrout, S.; K'tir, H.; Amira, A.; Berredjem, M.; Aouf, N.-E. A Simple and Eco-Sustainable Method for the Sulfonylation of Amines under Microwave-Assisted Solvent-Free Conditions. *RSC Adv.* **2014**, *4*, 16027–16032.

(15) Desjardins, R. E.; Canfield, C. J.; Haynes, J. D.; Chulay, J. D. Quantitative Assessment of Antimalarial Activity in Vitro by a Semiautomated Microdilution Technique. *Antimicrob. Agents Chemother.* **1979**, *16*, 710–718.

(16) Dorn, A.; Stoffel, R.; Matile, H.; Bubendorf, A.; Ridley, R. G. Malarial Haemozoin/β-Haematin Supports Haem Polymerization in the Absence of Protein. *Nature.* **1995**, *374*, 269–271.

(17) Trager, W.; Jensen, J. Human Malaria Parasites in Continuous Culture. *Science.* **1976**, *193*, 673–675.

(18) Huber, W.; Koella, J. C. A Comparison of Three Methods of Estimating EC_{50} in Studies of Drug Resistance of Malaria Parasites. *Acta Trop.* **1993**, *55*, 257–261.

(19) Reader, J.; Botha, M.; Theron, A.; Lauterbach, S. B.; Rossouw, C.; Engelbrecht, D.; Wepener, M.; Smit, A.; Leroy, D.; Mancama, D.; Coetzer, T. L.; Birkholtz, L.-M. Nowhere to Hide: Interrogating Different Metabolic Parameters of Plasmodium Falciparum Gametocytes in a Transmission Blocking Drug Discovery Pipeline towards Malaria Elimination. *Malar. J.* **2015**, *14*, 213.

(20) Ploemen, I. H. J.; Prudêncio, M.; Douradinha, B. G.; Ramesar, J.; Fonager, J.; van Gemert, G.-J.; Luty, A. J. F.; Hermsen, C. C.; Sauerwein, R. W.; Baptista, F. G.; Mota, M. M.; Waters, A. P.; Que, I.; Lowik, C. W. G. M.; Khan, S. M.; Janse, C. J.; Franke-Fayard, B. M. D. Visualisation and Quantitative Analysis of the Rodent Malaria Liver Stage by Real Time Imaging. *PLoS ONE.* **2009**, *4*, e7881.

(21) Mosmann, T. Rapid Colorimetric Assay for Cellular Growth and Survival: Application to Proliferation and Cytotoxicity Assays. *J. Immunol. Methods.* **1983**, *65*, 55–63.

(22) Hill, A. P.; Young, R. J. Getting Physical in Drug Discovery: A Contemporary Perspective on Solubility and Hydrophobicity. *Drug Discov. Today.* **2010**, *15*, 648–655.

(23) Bevan, C. D.; Lloyd, R. S. A High-Throughput Screening Method for the Determination of Aqueous Drug Solubility Using Laser Nephelometry in Microtiter Plates. *Anal. Chem.* **2000**, *72*, 1781–1787.